Alma Mater Studiorum – Università di Bologna

DOTTORATO DI RICERCA IN

CHIMICA

Ciclo XXXI

Settore Concorsuale: 03/C2

Settore Scientifico Disciplinare: CHIM/04

HETEROGENEOUS CATALYSTS FOR THE VALORISATION OF RENEWABLE FEEDSTOCKS BY DEPOLYMERISATION OF LIGNINS

Presentata da: Iqra Zubair Awan

Coordinatore Dottorato **Supervisori**

Prof. Dr. Aldo Roda **Prof. Dr Fabrizio Cavani**

Esame finale anno 2019

HETEROGENEOUS CATALYSTS FOR THE VALORISATION OF RENEWABLE FEEDSTOCKS BY DEPOLYMERISATION OF LIGNINS

By

Iqra Zubair Awan

Approved by:

Prof. Dr Fabrizio Cavani

Chairman, Department of Industrial Chemistry

Alma Mater Studiorum-University of Bologna

Date Approved
26/10/2018

DECLARATION

I, Iqra Zubair Awan, hereby declare that the presented dissertation entitled *"Heterogeneous catalysts for the valorisation of renewable feedstocks by depolymerisation of lignins"* is my original work and has not been submitted previously, in the whole or partial form, in respect of any other award. The external sources used, have been properly acknowledged. I retain all the ownership rights to use it in future work and that I am free to register the copyright to my work.

Iqra Zubair

Signature of the candidate
Dated: 26/10/2018

I approved the above titled to be submitted for the PhD defense.

Fabrice Cavani

Signature of the Supervisor
Dated: 26/10/2018

ABSTRACT OF THE DISSERTATION

Lignin is a plant derived, amorphous, aromatic, polymer and a potential source of carbon feedstock for generation of fuels and bulk chemicals. Nonetheless, for so long the commercial use of lignin has not been favorably brought to the market due to its difficult processing as a raw material. Like the variety of depolymerization methods opted in the literature, this thesis contributes to the catalytic hydrodeoxygenation of lignin model molecules to obtain functional aromatics. The work is an attempted contribution to the improvement of quality of lignin obtained by organosolv pulping. We synthesized lignin model molecules in close resemblance to the native lignin in terms of structure and chemical reactivity. The hydrodeoxygenation of the model compound was carried out under mild conditions in the presence of mixed oxides catalysts obtained by the thermal decomposition of layered double hydroxide. The conversion and selectivity variation was manipulated by the detailed characterization (XRD, TG, TPR, SEM, EDX and N_2 physiosorption) of the solid catalysts. We observed that MeOH, as an efficient H-donor solvent can successfully cleave α-O-4 linkage, causing Meerwein–Ponndorf–Verley reduction and selective hydrodeoxygenation of the lignin model under mild condition, consequently generating products of solvolysis and successive hydrogenation. The depolymerized lignin products were characterized by GC (MS, FID).

Our original contribution to the subject through this thesis is the conversion of α-O-4 linkage of lignin model (4-(benzyloxy)-3-methoxybenzaldehyde) to the hydrogenated products (alcohols, phenols) under mild conditions (160-200°C) using mixed oxides from Ni-Cu-Fe and related LDH systems. The goal of the project was a heterogeneous catalyst-assisted step ahead in development of solvolysis of lignocellulosic biomass. To the best of our knowledge the mixed oxides obtained from this set of LDH cations, for this reaction and conditions with above mentioned model have never been reported in the literature.

KEYWORDS: Lignin model compounds, α-O-4 linkage, heterogeneous catalysis, layered double hydroxides, mixed oxides, hydrodeoxygenation

I dedicate this thesis to my great mentor Dr A. Q. Khan,
&
to my family
&
beloved country, Pakistan

ACKNOWLEDGMENTS

This PhD was the most challenging but tremendously rewarding period of my life. I would not have been able to come this far without the concerned attention of many. First and foremost, I wish to express my deepest gratitude and sincerest thanks to my co-supervisor Prof. Dr. Francesco Di Renzo, for being very generous with his time, wisdom, support and encouragement. I owe him special thanks for giving me funding and exposure through various platforms to help me achieve the best possible out of this learning opportunity. Under his expert advisory and jovial working environment, I learnt lessons for life. I was lucky to have him as my co-supervisor. Thank you! Dr Di Renzo.

I am also deeply indebted to my supervisor Prof. Dr. Fabrizio Cavani, who is an outstanding researcher. His extensive expertise in the field of catalysis, organic and green chemistry provided invaluable insights during discussions on the projects. I am really thankful to him for his humbleness and continuous support during my research work. I would also like to thank Prof. Dr. Stefania Albonetti, the EMJD SINCHEM program coordinator, for the many useful advices given, not merely on the research project but also for the administrative procedures-which, being an international student, were not so easy to pursue.

In our group, I would like to convey my special thanks to Prof. Dr. Didier Tichit, Prof. Dr. Francoise Quignard and Prof. Dr. Nathalie Tanchoux for sharing their knowledge and giving critical suggestions on my project during the group meetings. I am extremely grateful to Dr Alysson Duarte Rodrigues for his boundless efforts and prudent attention during the preliminary training, as well as sharing his tips and lab skills for the systematic research.

My endless gratitude for the project collaborators, Prof. Dr. Annalisa Martucci and Giada Beltrami in Physics and Earth Sciences department, University of Ferrara, for their crystallographic contribution and interpretation of the data. Danilo Bonincontro from University of Bologna for TPR, I owe you special thanks for being an amazing person.

I am also highly obliged for trainings and technical assistance provided by: Olinda Gimello (GC, HPLC, MALDI), Thomas Cacciaguerra (XRD, EDX, SEM), Cedrict Totee (NMR), Geraldine Layrac (TG, N_2 physiosorption), Gwendoline Grave (6-Pott autoclave), Prof. Dr. Lorenzo Stievano and Dr Moulay Sougrati (Mössbauer Spectroscopy), Prof. Nathalie Marcotte (UV-VIS), Jeremy Rodriguez (apparatus and chemicals), Mourad Guermache (IT), Isabelle Girard (Administration), Manon Gand and Kim Pla (orders and chemicals).Thank you very much, team MACS, ICGM, ENSCM. Your combined brainstorming efforts and discussion for this project made me understood the importance of teamwork and friendship.

In this diverse experience of staying far from my homeland, I would like to thank my friends in University of Bologna, SINCHEM team and ENSCM for their professionals and moral support in times of distress, particularly Lorenzo Grazia, Mattia Melloni, Giada Innocenti, Aisha Matayeva, Erica Lombardi, Francesco Puzzo, Atif Emre Demet, David Azria, Jason Richard, Quang-Nguyen Tran, Olena Vozniuk, Bilel Said, Elodie Wan, Melody Mathonnat, Julie Bossu, Daniel Aguilera, Lotfi Boudjema and Sonia Aguilera.

My deepest gratitude to the Awan family and friends especially my best friends Fatima Zahid and Ahsan Bilal, without whom I could not have done it. Lastly to Allah Almighty, who is the source of all good things that have, and will ever come to me.

Thank you!

Note: No editor has been used in the formatting or proofreading of this thesis.

TABLE OF CONTENTS

LIST OF ABBREVIATIONS

MALDI-TOF	Matrix-Assisted Laser Desorption Ionization-Time-of-flight
GC	Gas Chromatography
NMR	Nuclear Magnetic Resonance
HDO	Hydrodeoxygenation
LDHs	Layered Double Hydroxides
MS	Mass Spectrometry
BET	Brunauer–Emmett–Teller
EDX	Energy-Dispersive X-ray Spectroscopy
SEM	Scanning Electron Microscopy
FID	Flame Ionization Detector
TGA	Thermogravimetric analysis
DTA	Derivative Thermogravimetric Analysis
EA	Elemental Analysis
MMO	Mixed Metal Oxides
R&D	Research and Development
XRD	X-Ray Diffraction
GCMS	Gas Chromatograph Mass Spectrometry
NaOH	Sodium hydroxide
HCl	Hydrochloric acid
BTX	Benzene, Toluene, Xylene,
MCM-41	Mobil Composition of Matter No. 41
MPa	Megapascal
HZSM-5	Zeolite Socony Mobil–5
THF	Tetrahydrofuran
MJ/Kg^{-1}	Megajoules per kilogram
TPR	Temperature-Programmed Reduction
FTIR	Fourier-Transform Infrared Spectroscopy
XRF	X-ray Fluorescence
TEM	Transmission Electron Microscopy
ESR	Electron Spin Resonance
TPDD	Temperature-Programmed decomposition/desorption
DTA	Differential Thermal Analysis
HMF	Hydroxymethylfurfural

DFF	2,5-diformylfuran
PMO	Porous metal oxide
PE	2-phenoxy-1-phenethanol
n-BuLi	n-Butyllithium
LDA	Lithium diisopropylamide
$NaBH_4$	Sodium borohydride
$MgSO_4$	Magnesium Sulphate
Pd/C	Palladium/Carbon
LiCl	Lithium chloride
MPV	Meerwein-Ponndorf-Verley Reduction
REEs	Rare earth elements
GBL	γ-Butyrolactone

GENERAL INTRODUCTION TO THE PROJECT

Lignin is an attractive renewable source of diversified aromatic functionalities with low O/C ratio. However, the complexity and recalcitrant nature of the lignin structure has rendered it one of the most underexploited biopolymers. Several routes, such as oxidation, reduction, pyrolysis and acid/base catalysis have been proposed for the catalytic depolymerization of lignin. Due to the high cost of hydrogen, oxidative routes have been considered the most cost-effective but the oxidation reactions may bring challenges to the reactions by the formation of highly reactive free radicals and which may lead to recondensation of the depolymerised fragments. Reductive methods for the fractionations proposed in the literature are game-changing only if the cost issues (transport, high pressure control, storage) of hydrogen are resolved. This problem can be alleviated if addressed through a mechanism of transfer of hydrogen coming from a cheap hydrogen-donor source. In this context, a reductive route, hydrodeoxygenation (HDO) is considered one of the most simple and effective method for valorization of this rich reserve, eventually leading to the upgraded products. To address this problem several reports have proposed organic hydrogen donors (alcohols, formic acid) which not only aid in the partial/selective hydrodeoxygenation but also address the solubility issues of organosolv pulping. This opens up new pathways to simultaneous fractionation of biomass and lignin modification. Typically, Meerwein-Ponndorf-Verley reaction (MPV) is a chemoselective procedure to reduce carbonyl groups of aldehydes/ketones to their corresponding alcohols using a H-donating alcohol solvent but further surface-catalyzed mechanisms allow hydrogenation of simple C-O bonds. Alcohols are certainly potential H-donor solvents for their renewable nature and low cost but the selection of right alcohol is a requisite, due to the rigidity of stoichiometric formation of oxidation products of the hydrogen donor together with the desired hydrogenation products of substrate. Methanol complete oxidation results in easily separable CO_2 and renewable ethanol is already extensively used for organosolv pulping. The complicated variability of biomass lignin prompted the reliance on simplified, low molecular weight lignin model compounds to study the mechanism of depolymerization. These models mimic the linkages present in the real lignin polymer, are often intermediates of the lignin degradation streams and their separation by chromatographic techniques identification is possible using conventional analytical methods. Hence, we synthesized some α-O-4 and β-O-4 model molecules of lignin.

Rate and selectivity of catalytic hydrodeoxygenation largely depends on the type of catalysts used. Literature has favored the choice of heterogeneous catalysts, keeping in view the product recovery, toleration of wide temperature/pressure range and easy disposal. Single and mixed metal oxides (MMO) obtained from the transition series are interesting to impart redox properties to the system. The selection of Layered Double Hydroxides (LDHs) as a catalyst precursor for MMO is an attractive route to obtain oxides with high surface area, basic properties and homogeneous mixture of metal oxides. Taking into account the rich chemical properties of the transition metals, we modified a commonly known hydrotalcite ($Mg_6Al_2CO_3(OH)_{16}\cdot 4(H_2O)$) by replacing magnesium (Mg^{2+}) with less basic divalent nickel (Ni^{2+}) and copper (Cu^{2+}), a typical catalyst of lignin depolymerization and iron (Fe^{3+}) to induce further redox properties in the system. The synthesis of the catalyst precursor was done by conventional co-precipitation methods. Different types of Layered Double Hydroxides (LDHs) based on Cu,Ni/Fe-LDH have been synthesized by studying the effect of cation types, cation ratios, and the solubility domains of cations in the synthesis system. The structural, surface and morphological properties were studied by powder X-ray Diffraction (XRD), N_2 physiosorption, Thermal gravimetery (TG), Scanning Electron Microscopy (SEM) and Energy Dispersive X-Ray spectroscopy (EDX).

Syntheses of LDHs with any cation ratio were successful in Cu-Ni-Fe, Ni-Fe and Cu-Ni-Al systems. The pure Cu-Fe system resulted instead in precipitation of CuO or $Cu_2(OH)_3NO_3$, depending on the pH of the precipitation. None of these phases account for the presence of iron in the system. Iron, not visible through XRD, should exist in amorphous state. The independent precipitation of amorphous $Fe(OH)_3$ is due to the different precipitation domains of Fe^{3+} and Cu^{2+} prevents the formation of the expected mixed LDH phase. This phenomenon holds true for the calcined samples as well, where only at high calcination temperature ($\geq$600°C), crystallized iron-bearing phases are detected.

To further study this effect, we introduced Ni^{2+} in a Ni-Cu-Fe system to balance the solubility differences. This allowed to define a threshold amount of a second divalent cation (nickel in this case) allowing the formation of Cu-bearing LDHs up to (Cu/Ni) 1:1. It has been often reported that the Jahn Teller distortion in Cu^{2+} is the cause of no formation of Cu-Fe LDH. Indeed, Rietveld refinement of these mixed LDHs allowed us to observe an increase of the cation-oxygen distance of the Fe LDHs from 2.04 Å for pure Ni divalent to 2.06 for (Cu/Ni) 1:1 divalent ratio. This variation cannot be exploited by the smaller size of Cu^{2+} (0.69) with

respect to nickel (0.72) and can be justified instead by a disordered distribution of Cu octahedra elongated by Jahn-Teller effect. Despite its presence, the Jahn-teller effect of Cu^{2+} is a poor candidate for the difficult formation of Cu-Fe LDHs, as the same mechanism does not seem operative in the Cu-Al solid solution, in which pure Cu-Al LDHs are easily formed and the precipitated cation ratio corresponds to the initial synthesis. The actual challenge is the different solubility domains of Cu^{2+} and Fe^{3+} whereas Cu^{2+} can precipitate in the same conditions of Al^{3+}.

Formation of dispersed mixed metal oxides (MMO) are obtained as a result of progressive thermal dehydration and decarbonatation of LDH materials. The nature and distribution of oxide phases (NiO, CuO, spinel) were strictly dependent on the initial synthesis composition of LDH and the calcination temperatures. It was observed through x-ray diffraction that the Fe^{3+} was found missing in the samples which were subjected to moderate temperature of calcinations, concluding to the presence of an "amorphous" part in the mixed oxide. A cross check of analysis by EDX confirmed preferential crystallization (phase segregation) phenomena with the synthesis ratios initially employed. NiO was nearly completely segregated at 400°C and the following crystallization of CuO left trivalent-enriched amorphous materials, from which spinel phases crystallized at higher temperature (≥500°C). Late formation of crystalline Fe-bearing phases suggests a high stability of amorphous iron oxides. The percentage quantification of crystalline phases was done for all samples by Rietveld analysis. The amorphous part of the samples was measured by difference with the measured crystalline experiments with an internal standard. The catalytic activity of the catalysts was tested in batch liquid-phase reactors on the model molecules of lignin in the presence of different hydrogen-donor solvents (methanol, ethanol, 2-propanol) in the temperature range 160-200°C. This field of temperature is less severe than typical gas-phase hydrogen transfer reactions and nearer to the conditions of organosolv pulping of lignocellulosic biomass.

The use as a substrate of model molecules with aldehyde, methoxy and phenylether groups allowed modeling the effects of different catalysts on the reactivity of several functionalities of natural lignin. If aldehyde functions were easily hydrogenated by a typical MPV mechanism, the breaking of phenylether bonds, mimicking the most frequent β-O-4 bonds of lignin, was only partial and probably followed several pathways. Deeper hydrogenation was observed, possibly due to H_2 issued from methanol reforming, with the formation of hydroxycresol by hydrogenation of C-OH bonds. Traces of guaiacol were sometimes observed, suggesting that also hydrogenation of C-C bonds is possible in our conditions.

Conversion and selectivities heavily dependent on the nature of the catalyst and of the hydrogen-donor solvent. The yield of hydrogenation of the different bonds present in the model molecule could be calculated from product distribution. When methanol was used, nearly complete MPV hydrogenation of aldehyde groups was observed, whereas the breaking of ether bonds was less effective and just a quarter of the C-OH bonds formed by previous reactions could be hydrogenated. When ethanol was used, an inversion of reactivity trends was observed, with less effective MPV hydrogenation and much more effective breaking of C-O-C and C-OH bonds. The presence of copper seems critical to achieve high hydrogenation yields, as the oxides issued from the calcination of Ni-Fe LDH are much less effective than the ones formed in the Cu-Ni-Fe system.

CHAPTER 1

Introduction to Lignin Chemical Valorisation

Chapter Summary:

The substantially increasing demand of energy, the rising greenhouse gas emissions and the declining fossil fuels resources have necessitated the development of alternate renewable resources. In this perspective, a renewable resource like biomass offers significant potential in terms of carbon feedstocks to generate fuels and bulk chemicals with multiple benefits of sustainable development, environmental preservation and energy efficiency. Lignin, an inedible, diversified reservoir of aromatic functionalities with the lowest O/C ratio among the components of biomass, is a strikingly underexploited resource. However, lignin is a complex biopolymer formed of several propylphenol monolignol units (G, H, S) connected by diverse cross-linkages (β-O-4, α-O-4, β-5, β-β, 4-O-5, 5-5 or β-1) with a severe natural variability. The complexity of lignin has largely limited the development of processes for its industrial use. Due to this complexity, the study of lignin reactivity can be usefully addressed by relying on low molecular weight lignin model molecules which mimic the linkages present in native lignin and allow to understand how to cope with structural variations of raw lignin. In this chapter, examples of model molecules with various kinds of linkages and their depolymerisation strategies have been discussed. Typically, heterogeneous catalysis is a favored valorisation method because it can be carried out over a wide range of operating conditions, with easy separation and recyclability of the catalyst. In the current literature, catalytic pyrolysis, oxidative/reductive transformations and acid/base catalysis are being studied over various model molecules under a broad range of reaction conditions. The choice of a selected route may vary with the targeted products but a general overview of the cost and feasibility is often under debate. In this context, the reductive conversion could be extremely valuable to exploit and upgrade the abundantly available phenolics in the structure. Hydrogenation/hydrodeoxygenation is a well-founded method if alternate supply of the expensive hydrogen gas could be addressed. In this project, we focused on MPV and further hydrogenation reactions by early stage catalytic conversion of lignin α-O-4 model molecule by using alcohols as H-donor alcohol solvents at comparatively mild conditions. The ideal target is to improve the solvolysis of lignocellulosic biomass by the use of heterogeneous catalyst in order to obtain selectively hydrogenated lignin-derived products directly from organosolv processes of lignocellulose pulping.

Introduction

The perspective depletion of fossil fuels and the need to control emissions of greenhouse gases has provoked research in finding alternative renewable resources. Among them, lignocellulose is a largely underutilized form of natural biomass, not directly competing with food resources. However, the difference in structure, composition and complexity of biomass as compared to crude oil requires an extensive reevaluation and rethinking of feedstock processing strategies to render economically viable the proposed transition to a bio-based industry.[1,2]

Lignocellulosic biomass is essentially composed of three components: cellulose (38-50%), hemicellulose (23-32%) and lignin (15-25%). Cellulose is currently hydrolyzed to glucose and converted into valuable products such as ethanol biofuel and platform chemicals, such as levulinic and formic acids, gamma-valerolactone and derived products. Hemicellulose has potential applications for biofuel production and for the generation of valuable chemicals intermediates, such as furfural. Lignin is the most underutilized fraction of lignocellulose. The total lignin availability in the biosphere exceeds 300 billion tons and annually increases by around 20 billion tonnes.[3] Annually, 40-50 million tons of roughly isolated lignin are available as waste of pulp and paper industry and biorefineries. Only approximately 2% of the lignin available is commercially exploited while the remainder is burnt as a low-value fuel in the lignocellulose fractionation units.[4]

1.1 The potential of lignin

Lignin is an important component of secondary cell wall of plants, which forms a matrix between cellulose fibrils and provides mechanical strength and chemical protection to the plant. Lignin is a tridimensional amorphous polymer composed of three types of propylphenyl monolignols (Fig1.), differing by their degree of substitution: sinapyl alcohol (S), coniferyl alcohol (G) and p-coumaryl alcohol (H) units (see Fig.1.1).

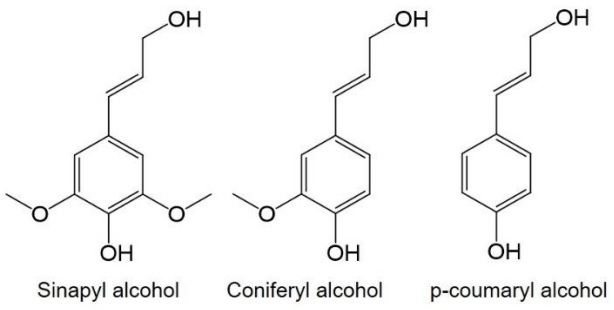

Figure 1.1 Monolignols, the building units of lignin

According to the source it derives from, lignin presents a high diversity of chemical structure, not only in terms of percentage of each monolignol, but also from the different ways the building blocks are connected to each other through various crosslinked C-O and C-C bonds including β-O-4, β-5, β-β, 4-O-5, 5-5 or β-1 to form a complex matrix (see Fig. 1.2).[5] Generally softwood has 45-48 wt % and hardwood has 60 wt % of β-O-4 aryl glycerol ether bonds. Softwood has approximately 5 wt% and hard wood has 0-2 wt % of dibenzodioxocin 5-5'-α, β-O-4' bonds. In addition, softwood has 3.5-8 wt % and hardwood has 6-9 wt % of diphenyl ether 5-O-4' linkages.[6,7] The presence of these propylphenolic groups is at the basis of the interest for lignin, as a large reservoir of aromatic hydrocarbons and fine and specialty chemicals.[8]

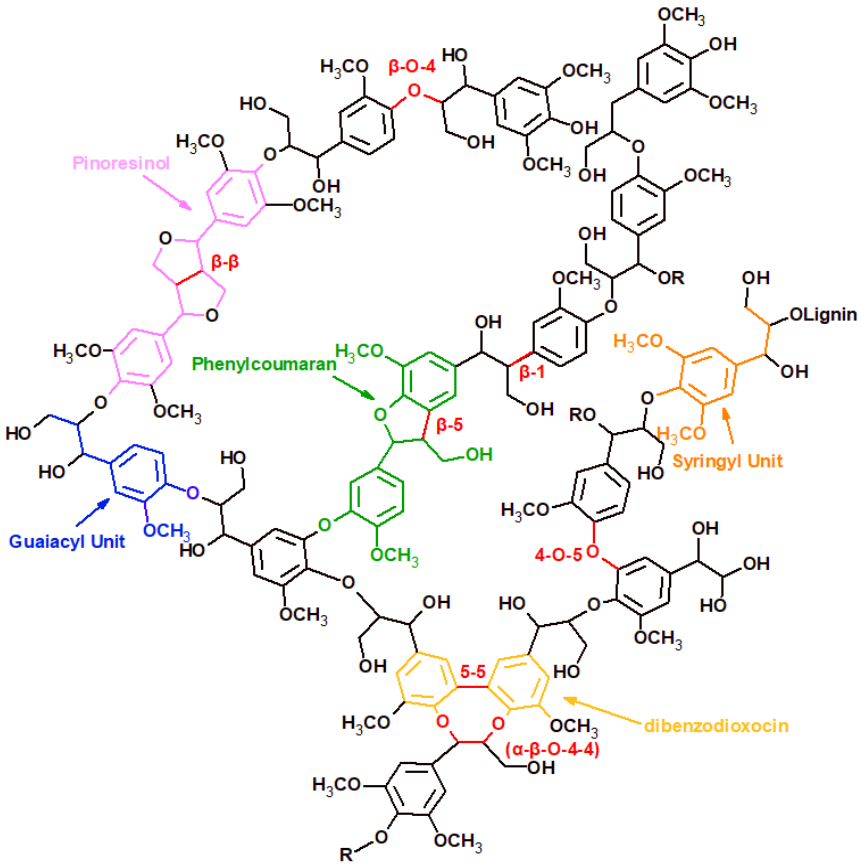

Figure 1.2 Idealized structure of lignin with the most representative functional groups

1.2 The challenges of lignin

Untransformed lignin finds property-based applications as component of epoxy glues for wood and packages, as fillers for bitumen and oil drilling fluids or as precursor of carbon fibres.[9] Considering the rich chemical functionalities of lignin, it is really promising to develop methods of depolymerisation for the production of phenolic monomers for the polymer, flavor and pharmaceutical industry.[10] Development of effective catalytic processes

is badly needed in lignin depolymerisation to orient the selectivity towards well-defined monomers, in order to minimize the separation costs, which can nullify the economic viability of depolymerisation.

In order to tailor processes for the chemical valorisation of lignin, a considerable challenge is to interpret the exact structural arrangement in the macromolecule. The structure of native lignin is only accessible by analysis of its hydrolysis products, which nature in turn depends on the separation process used. Moreover, the variability of lignin coming from different plant species hinders the developments of set protocols for lignin depolymerisation. To cope with lignin's chemical complexity, a multifaceted, translational approach is required that includes new analytical tools for structure characterization of substrates and products. The lignin depolymerisation technology is still in the early phases of R&D. Taking advantage of lignin as a reliable alternate source to fossil resources relies on the interest from game-changing investors, which will provide funding options when the depolymerisation technology will reach a sufficient level of maturity.[5]

1.3 Lignin model molecules

The complexity and variability of the structure of lignin has complicated the study of industrial lignin as a substrate. This fact has prompted the reliance on simplified, low molecular weight lignin model compounds to study lignin depolymerisation. The basic advantage of these models is that they mimic the linkages present in the real lignin polymer, which helps in a better understanding of the breaking mechanisms of specific bonds. Furthermore, similar molecules are often present in the lignin degradation streams, after the depolymerisation of lignin itself. The small compounds generated by fragmentation of lignin model compounds could be separated by chromatographic techniques, and further identification is possible using conventional analytical methods like GC-MS and NMR. Therefore, better and reliable characterization can be done because often only one type of linkage is present in the model molecule, which helps in understanding the reaction paths and the catalytic performance.

Catalytic systems can be studied in detail on oligomers and dimers aiming to understand the reactivity and selectivity of multifunctional group models. This is often the first step of research in lignin valorisation. Taking into account the solubility and polyfunctionality of native lignin, as well as the repolymerization with intermediate, demand a further step in the research planning. Different molecules are used as model compound for different bonds of native lignin (see Fig. 1.3).

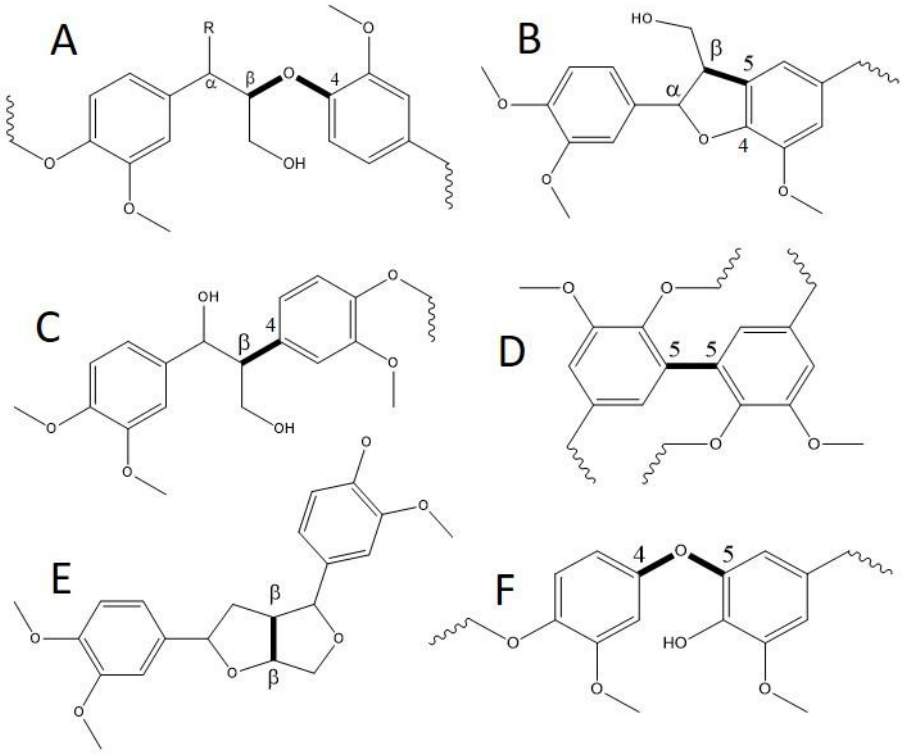

Figure 1.3 The main linkages in the lignin structure:β-O-4 (A), β-5 and α-O-4 (B), β-4 (C), 5-5 (D), β-β (E), 4-O-5 (F).

1.3.1 β-O-4 model molecules

It is the most abundant linkage found in lignin. The ether bond is readily cleaved; indeed, the cleavage of these bonds during alkaline pulping constitutes the principle pathways in which the lignin is depolymerised and generates monomers with a phenyl propane structure

The fragmentation of these linkages tends to lead to the generation of water-soluble oligomers containing phenolic hydroxyl groups.[11] The disruption of β-O-4 containing model molecules results in simpler analogs of the coumaryl, coniferyl, and sinapyl alcohols of monolignols (see Fig. 1.1). Secondary products obtained during the fragmentation include 3-hydroxypropaldehyde and arenes with various aldehyde or alkyl side chains.[12] Successive oxidation reactions of coniferyl alcohol form vanillin or lead to oxidation of the aromatic ring and form quinones (see Fig. 1.4 for possible lignin depolymerisation products).

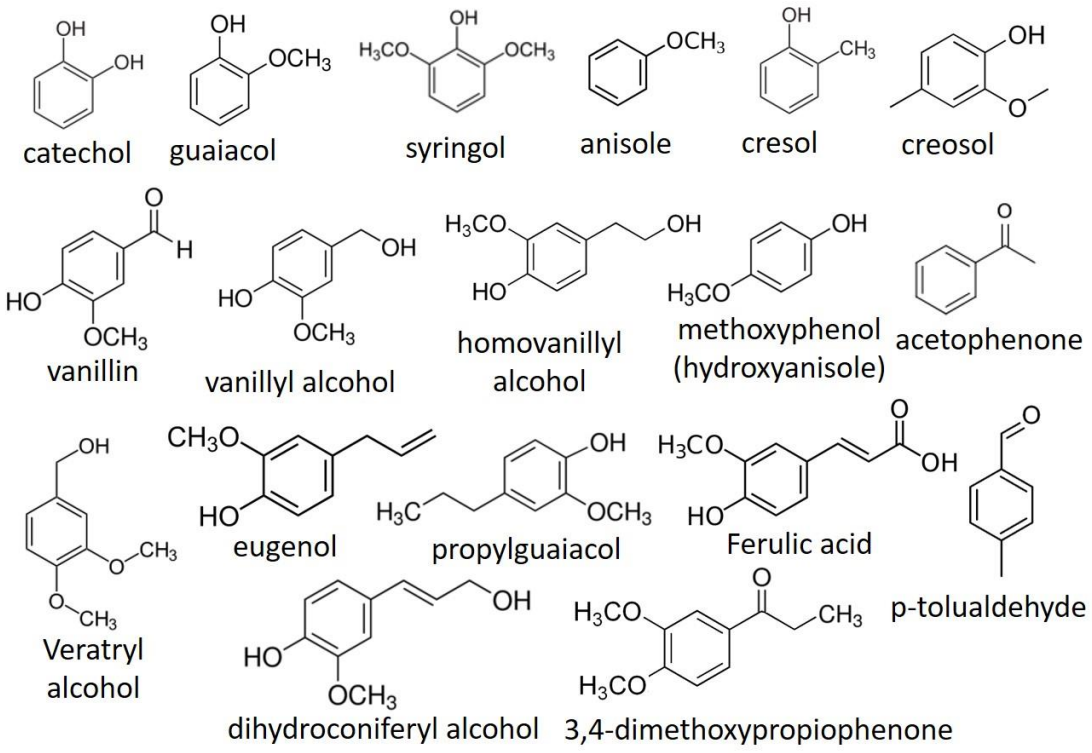

Figure 1.4 Common monomers to be familiar with in lignin chemistry.

1.3.2 C-C linkage model molecules

The C-C linkage in the lignin/model molecules are the hardest to break. Although carbon-carbon linkages are present in the native lignin polymer, additional carbon-carbon bonds can be formed during lignin pretreatment, such as in alkali-promoted condensation reactions during kraft pulping.[11] The development of catalysts capable of performing these disruptions (particularly the aryl-aryl linkages) is therefore a considerable challenge that has not yet been adequately addressed. Model compounds with these linkages usually involve dimeric arenes with varying methoxy and hydroxyl substituents on the arene, resembling dimers of p-coumaryl or coniferyl alcohols.

1.3.3 Phenylcoumaran model molecules

The β-5 linkage is often located in a five-membered oxygenated ring fused with an aromatic ring in a coumaryl structure. In the model molecules, the rupture of both these bonds often yields monomers such as vanillin and vanillic acid. Because of the inherent complexity in selectively disrupting both bonds, products resulting from the disruption of only one bond (*i.e.* the R-O-4 ether linkage) leaves compounds containing isolated β-5 linkage. In some instances, the β-5 bond remains intact and products resulting from the oxidation of the arene ring are observed.[7]

1.3.4 α-O-4 and 4-O-5 linkages model compounds

Compounds containing α-O-4 have also been observed in the lignin network however modern NMR experiments do not confirm the presence of non-cyclic α-O-4 moieties.[7]

The 4-O-5 aryl-aryl ether linkage is, however, present in lignin mainly as the result of demethoxylating oligomer-oligomer couplings and leads to branching of the polymer. Some model compounds have been studied in order to understand the chemistry of this particular linkage as well.

1.4 Lignin Depolymerisation Strategies

Catalysts are essential to facilitate energy and atom efficient lignin depolymerisation and to selectively deoxygenate the products for further applications. Considerable efforts have been devoted in this field but current methodologies are not satisfactory from the economical or environmental viewpoint. There are generally three main approaches for depolymerisation: thermochemical (pyrolysis), biochemical and chemical processes. In this chapter, we will deal essentially with the latter class of processes, under the aspects of hydrolysis, oxidation, and reduction. Pyrolysis refers to the thermal treatment of biomass/lignin in the absence of oxygen, with or without any catalysts at temperature between 300 and 600°C.[3,13] The cleavage of OH functional group linked to the aliphatic side chain, the breaking of alkyl side chain, aryl ether bonds and linkage between aromatic ring occur when temperature increases, forming a mixture of phenol, guaiacol, syringol and catechols. Cracking of the aromatic ring occurs at temperature above 500°C.[13,14] The process is poorly selective and is affected by several factors including feedstock type, heating rate and reaction temperature.[15] Biochemical methods have also been employed for the depolymerisation but, despite interesting selectivities and mild conditions required, time to grow the microorganisms/fungi and dilution of the system which can make the process slow and less efficient.[16] In the chemical conversion, ether bonds C-O-C are targeted. Comparing to thermochemical and biochemical processes, the chemical treatment of lignin has shown reliable results in terms of high selectivity and reaction control, with efficient valorisation of lignin into functionalized aromatics.

The development of selective and robust catalyst must be a core effort in a biorefinery program. While selecting the catalytic route, there are two main considerations to be taken into account:

1. Maximization of activity and selectivity of catalyst under the chosen conditions (as mild as possible) bearing in mind the bulky nature of biomass source and the reaction conditions

2. Repolymerisation and self-condensation capability of lignin under processing conditions, due to the formation of radicals and/or C-C bond through self-condensation reactions which eventually leads to a complex pool of re-condensed aromatics.[1]

The accountability of successful industrial scale production of chemicals is based on the selection of optimized reaction conditions, which include the chemical, engineering and financial aspects of a feasible reaction. In this chapter, we will overview the major pathways of lignin depolymerisation which can directly affect the reaction mechanisms controlling the nature and the yield of valuable products. For the chemical depolymerisation of lignin, a choice to be made among homogeneous and heterogeneous catalysis is on the top of the list.

1.4.1 Homogeneous catalysis for lignin depolymerisation

1.4.1.1 Base-Catalyzed Depolymerisation

Lignin depolymerisation through base-catalyzed hydrolysis is a well-known and straightforward route for the production of monomeric substituted phenols. The mineral bases used as catalysts, such as NaOH, KOH, and sometimes LiOH are cheap and commercially available but requires corrosion-resistant materials and treatment of waste sewage. Typically, reflux boiling of lignosulfonates in 12% NaOH solutions in nitrogen atmosphere provided up to 7% yields of high-value added vanillin.[17] The reaction proceeds with cleavage of alkyl-aryl ether bonds, including (β-O-4), which is considered to be the weakest bond in the lignin structure.[13,18] However, in the base-catalyzed lignin hydrolysis reactions, the selectivity and yield are chiefly dependent on temperature, concentration and nature of the base, time, pressure and lignin/solvent ratio.[19] Beauchet *et al.* worked on base-catalyzed depolymerisation reactions on less reactive Kraft lignin using NaOH as a base catalyst.[20] Total yield of identified monomers reached a maximum of 8.4 wt.% at 315°C. Although the base-catalyzed process was simple, it needed to be carried out at high temperature, and the control of selectivity was still difficult. The production of monomers is favored by high temperature and longer reaction time. The final yield is effectively decreased due to the formation of solid residues by the condensation reaction of intermediates and products. In base-catalyzed reactions, control of the rate of re-polymerization and condensation is the key challenge.[21] This fact is supported by the studies of Lercher and co-workers who carried out base-catalyzed liquid-phase hydrolysis of organosolv lignin at 300°C and 25MPa using NaOH as catalyst.[22] Syringol (4.1 wt%), hydroxyacetophenone(1.6 wt%) and guaiacol (1.1wt

%) were the major products of base-catalyzed hydrolysis and that oligomers form as secondary products. Oligomerization and polymerization of these highly reactive products, however, limit the amount of obtainable low-molecular-weight phenolic products. The inhibition of parasite oligomerization reactions is crucial to ensure a high yield of monomeric products. For analytical purposes this can be achieved by using a capping agent, as boric acid, to suppress addition and condensation reactions of initially formed products.[22]

1.4.1.2 Acid-Catalyzed Lignin Depolymerisation

Early attempts of acid-catalyzed lignin hydrolysis dates back to 1920's when Hagglund and Bjorkman distilled lignin with 12% HCl and observed severe repolymerization of the products.[23] The hydrolytic cleavage of α- and β-aryl ether linkages plays a main role in the acid-catalysed hydrolysis because aryl−aryl ether bonds, phenolic C−O bonds, and C−C bonds between aromatic lignin units are relatively more stable and difficult to break.

Better stabilisation of depolymerisation products was later obtained in aqueous solution of organic solvents, where acid-catalysed hydrolysis was combined with hydrodeoxygenation of the products by hydrogen transfer from hydroxyl-bearing solvents. Hewson and Hibbert studied an acid-catalysed treatment on maple wood meal by combinations of various acids and alcohols including HCl/ethanol and formic acid/ethylene glycol systems, with the purpose of separating the lignin into water-soluble and water-insoluble components.[24] The low range of temperature (78-200°C) was moderately effective for the degradation of complex lignin into monomers. Later, high temperature conditions have also been studied on acid catalysed reactions. For example, Barth and co-workers studied the effect of 13 wt.% formic acid in ethanol.[17] At temperature above 360°C the major products were methoxyphenol, catechol, and phenol.[17,25] The optimum reaction time was below 200 minutes. Formic acid/ethanol solutions in the presence of Pt/C catalyst allowed to reduce all carbonyl groups of the products and provided yields up to 7% propylguaiacol, 5% methylguaiacol and 3% homovanillyl alcohol.[26] In general, acid-catalysed depolymerisation required harsh reaction conditions, which could affect the cost and economic feasibility of the reaction.[13]

1.4.1.3 Oxidative Lignin Depolymerisation

Oxidative depolymerisation to vanillin has been the main historical industrial process of valorisation of lignin, justified by the high added value of vanillin as a flavor molecule.[27]

The cheap and effective oxidizing agent used is molecular oxygen, bubbled through basic solutions to couple oxidation reactions with alkaline hydrolysis.

Mathias and Rodrigues in 1995 described the classical state of the art, explaining that 60g/L solution of softwood Kraft lignin, treated at 120-130°C for 4-6h in the presence of 2N NaOH, could yield a maximum 13% (w/w) yield of vanillin.[28] In the same year, the Monsanto process at 160°C in 10% NaOH solution claimed a yield of vanillin of 19% when softwood sulfite liquor was oxidized through carefully controlled oxygen pressure.[29] It is interesting to observe that these yields were normalized on the assumed lignin content in the sulfite liquor. When the vanillin yield in the same commercial process was expressed on the basis of the lignosulfonate mass, the yield value was not higher than 7%.[30,31]

The original patent of Monsanto cited the optional use of Cu(II) salts as oxidants and catalysts. Copper salts were used when the Monsanto process was bought by Borregaard and cobalt and cerium salts were also tested.[30] Pacek *et al.* studied the Borregaard process under highly alkaline conditions, catalyzed by Cu^{+2} at 120, 140 and 160°C and pressures up to 10 bars in flow reactors.[31] They were able to determine that nearly 55% of the vanillin formed was issued from hydrolysis and 45% from oxidation. [6] Recently, Yamamoto *et al.* found that the use of $Bu_4NOH{\cdot}30H_2O$ (tetrabutylammonium hydroxide 30-hydrate) as reaction medium (instead of the commonly used aqueous NaOH solution) in aerobic oxidative degradation of lignin improved the yield of aromatic monomers.[32] At 120°C, total monomer yield of 6.5−22.5% was obtained with vanillin and vanillic acid as the main products.

1.4.2 Heterogeneous Catalysis for lignin depolymerisation

Homogeneous catalysis for the depolymerisation of lignin presents several drawbacks, notably in separation of catalyst from the reaction mixture and corrosiveness when strong mineral acid and bases are used.[33] Depolymerisation by heterogeneous catalysis offers promising strategies in spite of mass transfer limitations from bulk lignin to catalyst surface.[1] Heterogeneous catalysis means that catalysts and reagents form different physical phases. This type of catalysis is usually favored because it can be carried out over a wide range of operating conditions and offers easy separation and recyclability of the catalyst. The product recovery and purification are significant industrial facets of catalysis, on which the advantages of heterogeneous catalysis are based. As David Parker (ICI) said on 24th April 1988 during the 21st Irvine lectures at the University of Saint Andrews: “At the molecular level, there is a little to distinguish between homogenous and heterogeneous catalysis, but there are clear distinctions at the industrial level”. We will discuss in this chapter the

heterogeneous forms of catalysts applied to the fragmentation of lignin via pyrolysis, reduction and oxidation pathways.

1.4.2.1 Catalytic Pyrolysis

Liquefaction by pyrolysis has been developed to convert lignocellulosic biomass to bio-oil. It is a rapid heating of biomass at high temperatures (450-650°C) in the absence of oxygen to generate a mixture of non-condensable liquid, gas and oil mixtures.[34] The main target of biomass pyrolysis is the reduction of the oxygen content of biomass to make it suitable as fuel component. Lignin, as the biomass component with the lowest O/C ratio, has been extensively studied as a bio-oil precursor. Indeed, the activation energy of lignin pyrolysis is lower than the activation energy of cellulose pyrolysis.[35]

The requirement for high temperature of the pyrolysis processes is energy intensive and the final product is a mixture of a large number of components, mainly substituted aromatics. It is considered that the product distribution is the result of a number of reactions where non-volatile compounds are broken down into heavy volatile compounds at first and finally cracked into volatile alkyl aromatics and ultimately to coke and gas.[34]

The addition of catalyst to the pyrolysis reactor introduces some selectivity and directs the distribution of the product stream towards higher-value desired products. The proportion of each pyrolysis product is dependent on the process variables, particularly temperature and heating rate.[35] At lower temperature the first bonds cleaved are hydroxyl and ether groups attached to alpha or beta carbons to form condensable volatile products and water. Large fractions of methoxyphenols, such as substituted syringol and guaiacol, are present in the condensable volatile products as the methoxyl groups show more resistance than the ether linkages against thermal degradation. C-C bond is the strongest bond in all kind of transformations, its breaking only occurring at very high temperatures.[36]

Several kinds of catalysts have been tested for lignin pyrolysis. Zhan *et al.* studied the product distribution obtained from lignin at 400, 500 and 600°C on several catalysts with different pore structure and acidity; HZSM-5, MCM-41, TiO_2, ZrO_2 and Mg(Al)O.[37] It was concluded that HZSM-5 was the best catalyst for fast pyrolysis whereas the basic catalysts trigger reduction of the liquid, leading to oligomers and coke formation. Ohra-aho and Linnekoski studied the activity of HZSM-5, zeolite Y and Pd/C on Kraft lignin and pine wood lignin at 600°C. The catalyst with the larger influence on product distribution was the zeolite Y, which increased the extent of demethylation and demethoxylation of the monoaromatic products.[38] The yield of liquid and the selectivity of products can be monitored by tuning acidity and pore size of zeolites. Ma *et al*. compared the activity of several zeolites

with micropore size from 0.5 to 0.7 nm and Si/Al ratio from 7 to all silica.[39] Zeolite US-Y, the catalyst with the largest pores and the highest density of acid sites, allowed to increase the yield of liquid to 75% from 40% without a catalyst. Zeolite H-ZSM5 with smaller pores and a smaller number of stronger acid sites was able to increase the selectivity of phenol alkoxy species. The small size of pores is expected to prevent repolymerization and coke formation reactions.

Studies on model molecules have contributed to a better understanding of the mechanisms of lignin pyrolysis. For instance, Zhang *et al* have recently investigated the catalytic pyrolysis products of guaiacol over ZSM-5 between 400 and 650°C, showing that the mechanisms of pyrolysis are similar to the dehydration, decarbonylation and hydrogen transfer pattern of the geological formation of coal and hydrocarbons from lignocellulosic biomass.[40,41]

1.4.2.2 Reductive Transformations

The idea of reductive depolymerisation of lignin began in the late 1930s when the insoluble biomass isolated from tree sawdust was hydrogenated. The selective catalytic reduction of lignin has attained great attraction for the improvement of bio-oil over the past few years. For lignin reductions, typical reactions involve the removal of the extensive functionalities of the lignin subunits to form less substituted monomeric compounds, such as phenols, benzene, toluene, or xylene (BTX). These simple aromatic compounds can then be hydrogenated to alkanes for fuel applications or used as platform chemicals for the synthesis of bulk and fine chemicals using technology already developed by the petrochemical industry. The biomass or lignin model molecules are subjected to hydrogenating conditions for the production of high yield phenols and aromatics. Oxygen is generally removed in the form of H_2O and CO/CO_2 by means of different catalytic processes such as hydrogenation, C-O bond hydrogenolysis, dehydration, decarboxylation, decarbonylation.[1] Bifunctional catalyst having both acid and noble metal can give interesting results where they can simultaneously break ether bonds and deoxygenate the resulting monomers in the presence of H-donor solvent or H_2.

Harris *et al.* in 1938 studied the catalytic hydrogenation of hardwood lignin at 260°C for 18h in the presence of copper-chromium oxide catalyst and successfully achieved 70% conversion.[42]

Pepper *et al.* did extended comparative studies on the effectiveness of different metal catalysts (Raney Ni, Pd/C, Rh/C, Rh/Al_2O_3, Ru/C, Ru/Al_2O_3) for the hydrogenolysis of spruce wood lignin in dioxane/water at 195°C under 3.3 MPa H_2 pressure.[43] The best results were obtained on Rh/C, with a yield of identified monomers of 33%, the main products being

4-propylguaiacol and dihydroconiferyl alcohol.[44] The distribution of products was greatly influenced by catalyst loading and pH variations resulting in over-hydrogenated or degraded products.

In more recent years, many types of metal catalysts have been tested for hydrogenation of model molecules, commercial lignin or lignin-issued bio-oil (see Table 1). Metal catalysts are very effective in the improvement of the fuel properties of bio-oil, by decreasing its O/C ratio. Hydrodeoxygenation of substituted guaiacols and syringols, among the main components of bio-oil, was achieved on a variety of metal catalysts at 250-300°C under 40-50 bar H_2 with high yields of cycloalkanes, provided an acid function was also present.[45,46,47] The nature of the metal catalysts used spanned from noble metal palladium to Raney nickel and the acid function could be provided by addition of an inorganic acid, as H_3PO_4,[45] or by a heterogeneous co-catalyst, as silica-zirconia or Nafion.[46,47] At so high a temperature, also water has proven to be a good solvent for the reaction, allowing easy separation of the less polar hydrocarbon products at the end of the process.[45,47,48] The use of Rh/Ru nanoparticles and a Brønsted-acid ionic liquid ([bmim][TF2N], 1-Butyl-3-methylimidazolium bis(trifluoromethanesulfonyl)imide) as the solvent allowed to reach still higher yields of cycloalkanes at a much lower temperature of 130°C,[49] while a lower hydrogen pressure of 7 bar allowed only partial depolymerisation and hydrogenation of lignin, giving a low yield of arenes and cyclohexanes.[48]

Table 1.1 Some recent literature on the heterogeneous catalysis of hydrogenation of lignin and model molecules

Catalyst	**Solvent**	**Experimental Conditions**	**Substrate**	**Major Products**	**Ref**
Pd/C, H_3PO_4	H_2O	250°C, 50bars H_2	phenolic monomers	79% cycloalkanes	[45]
Ni/SiO_2-ZrO_2	Dodecane	300°C, 50bars H_2	Guaiacol	97% Cyclohexane	[46]
RaneyNi+ Nafion/SiO_2	H_2O	300°C, 40bars H_2	4-propylguaiacol	74% alkylcyclohexane	[47]
RhPt/ZrO_2	Tetradecane	400°C, 50bars H_2	Guaiacol	43% cyxlohexane	[54]
Rh/Ru Nanoparticles	[bmim][TF2N]	130°C, 40bars H_2	4-ethylphenol	99% ethylcyclohexane	[49]
Ru/Nb_2O_5	H_2O	250°C, 7 bars H_2	Birch lignin	21% arenes, 8% cycloalkanes	[48]
Ru/C	THF	250°C, 40bars H_2	Formaldehyde-treated beech lignin	77% phenolic monomers	[50]

Ni/C	THFA, dioxane	220°C, 20bars H_2	Beech lignin	14% phenolic monomers	[51]
Ni7Au3, NaOH	H_2O	160°C, 10bars H_2	Birch lignin	11% phenolic monomers	[52]
Zn/Pd/C	methanol	150°C, 20bars H_2	Vanillin	81% creosol	[53]
Ni/TiN	ethanol	150°C, 12bars H_2	Diphenyl ether	49% cyclohexanol, 46% benzene	[55]
Ni/SiO_2	Decalin	130°C, 30bars H_2	Dihydrobenzofuran	95% 2-ethylphenol	[56]
Pt/SiO_2	Gas phase	400°C, flowing H_2	Anisole	42% phenol, 33% cresols	[57]
Pt/HBeta	Gas phase	400°C, flowing H_2	Anisole	52% benzene, 28% toluene	[57]
Pd/C	dioxane	200°C, 1bar H_2	Miscanthus lignin	15% phenolic monomers	[58]
Raney Ni-H-USY	aqueous methanol	270°C, N2	Bamboo lignin	28% phenolic monomers	[59]
Ni/C	methanol	200°C, Ar	Birch lignin	49% phenolic monomers	[60]
$CoMo/Al_2O_3$	hexadecane	300°C, 69bars H_2	4-methylcathecol	25% methylcyclohexane, 20% cresol	[61]
Cu-Mg-Al mixed oxides	methanol	180°C, 40bars H_2	Organosolv lignin	63% phenolic monomers	[62]
MoOx/CNT	methanol	260°C, 30bars H_2	Birch lignin	47% phenolic monomers	[63]
CoMo, NiMo	tetradecane	400°C, 50bars H_2	Guaiacol	46% phenolic monomers	[54]
Mo_2N	Decalin	300°C, 50bars H_2	Guaiacol	47% phenol	[64]
FeS_2/C	Cyclohexane	300°C, 100bars H_2	Dibenzyl ether	98% toluene	[65]
MoO_3	Gas phase	320°C, flowing H_2	Guaiacol	31% phenol	[67]
MoO_3	Gas phase	320°C, flowing H_2	Anisole	44% benzene	[67]
Ni_2P/SiO_2 or Co_2P/SiO_2	Gas phase	300°C, flowing 20% H_2 in N_2	Guaiacol	48% benzene	[66]
WP/SiO_2	Gas phase	300°C, flowing 20% H_2 in N_2	Guaiacol	60% phenol	[66]

In the absence of an acid function, metal catalysts allowed effective depolymerisation of lignin at 250°C under 40 bar H_2 but the product was mainly a phenolic bio-oil with no significant hydrogenation of the aromatic rings.[50] Metal catalysts as different as Ru, Ni, Zn,

Pd, Ni_7Au_3 have been used with yields of phenolic monomers mainly depending on temperature and H_2 pressure.[50,51,52,53] Lin *et al*. studied the mechanism of hydrodeoxygenation of guaiacol, using mono and bimetallic Rh-based catalysts on zirconia and showed that RhPt significantly accelerated the hydrogenation to cycloalkanes by comparison to plain Rh or RhPd.[54] Studies on model molecules showed that ether bonds were easily cleaved also in mild hydrogenation conditions.[55,56]

The difference between simple metal catalysts and bifunctional metal-acid catalysts was highlighted by Zhu *et al.* in a mechanistic study of the hydrogenation of anisole (methoxybenzene) over a bifunctional metal-zeolite catalyst Pt/HBeta or a monofunctional catalyst Pt/SiO_2.[57] Anisole fed in gas phase at 400°C in flowing H_2 at atmospheric pressure was converted to phenolic monomers by demethylation and transalkylation on the metal catalyst and was hydrogenated to BTX (Benzene, Toluene, Xylene) on the bifunctional catalyst.

Molecular hydrogen was not the only possible agent of hydrodeoxygenation of lignin. Internal hydrogen transfer from alcohol groups has been suggested by Hartwig and co-workers to be active in breaking ether bonds of lignin.[58] In their paper, H_2 pressure of one atmosphere was used to reduce the weak amount of olefinic bonds present in the miscanthus lignin used. Hydrogen transfer from a hydrogen-donor solvent has been shown to be effective in the hydrodeoxygenation of lignin, 49% yield of phenolic monomers having been attained by treatment of birch lignin in methanol on Ni/C catalyst at 200°C in inert atmosphere.59,60

Non-metal catalysts were also tested in lignin hydrogenation, looking for a parallel with the highly stable classical sulfided CoMo and NiMo hydrotreatment catalysts of oil refineries. In a seminal study, Petrocelli and Klein investigated the hydrodeoxygenation of several model compounds over a sulfided $CoOMoO_3/\gamma\text{-}A1_20_3$ commercial catalyst at 300°C and 69 bars hydrogen pressure.[61] Compounds with aromatic methoxyl groups (4methylguaiaco1, eugenol, vanillin) underwent primary demethylation as their major reaction. Hydroxyl groups were removed readily at temperatures well below those required for thermal dehydroxylation. Catalytic cleavage of the inter-aromatic unit linkages of o-hydroxydiphenylmethane and phenyl ether was facile, while o,o'-biphenol was converted to single-ring products through dibenzofuran and 2-phenylphenol intermediates. In more recent years, yields of phenolic monomers as high as 47-63% were obtained by lignin depolymerisation at 180-260°C under 30-50 bar H_2 on catalysts as different as Cu-bearing basic mixed oxides issued from hydrotalcite decomposition or on molybdenum oxides on carbon nanotubes.[62,63] Molybdenum oxides and nitrides, as well as sulfides and phosphides of different metals, were tested in

mechanistic studies of hydrodeoxygenation of model molecules at temperature as high as 400°C and under H_2 pressure up to 100 bars or in flowing hydrogen atmosphere.[54,64,65,66,67] The main results of these studies were the suggestion of a scale of reactivity of the functional group of phenolic molecules, with ether bonds being more easily hydrogenated than methoxy groups, phenolic OH being the more resistant to hydrodeoxygenation. The interest of flow processes for the depolymerisation of lignin is evident, albeit the results on model molecules in the gas phase at high temperature are surely difficult to transpose to the reactivity of lignin of higher molecular weight.

1.4.2.3 Oxidative Transformations

Oxidative treatments of lignin are aimed to the production of high added value aromatics, especially aromatic aldehyde flavours. The increase of the O/C ratio in oxidative treatments render them inappropriate for the production of fuels but justifies some interest in total oxidation of lignin-containing paper mill wastes or selective oxidation of lignin-derived alcohols to aldehydes.[12,68,69,70] In this section, we will only examine applications of heterogeneous catalysis to selective oxidative fractionation of lignin or model oligomers.

Table 1.2 Some recent literature on the oxidation of lignin and lignin model oligomers by heterogeneous catalysis.

Catalyst	**Oxidant**	**Solvent**	**Experimental Conditions**	**Substrate**	**Major Products yield**	**Ref**
MeRhO3/polyvinyl pyridine	H_2O_2	CH_3COOH	Room T	β-O-4 phenolic dimer	28% guaiacol	[71]
Co-salen/SBA-15	H_2O_2	acetonitrile	150°C, microwaves	β-O-4 phenolic dimer	21% guaiacol	[72]
Cu,V-hydrotalcite	O_2 6bars	Pyridine	135°C	β-O-4 phenolic dimer	38% veratrylaldehyde	[73]
Graphene nitride	tert-butyl hydroperoxide	H_2O	120°C	β-O-4 phenolic dimer	45% benzylic acid	[74]
CeO_2	O_2 10bar	methanol	185°C	β-O-4 phenolic dimer	42% phenol, 40% methylbenzoate	[75]
Pd/CeO_2	O_2 1bar	methanol	185°C	β-O-4 phenolic dimer	41% phenol, 20% methylbenzoate	[75]

Pd/CeO_2	O_2 1bar	methanol	185°C	Organosolv lignin	5% vanillin, 2% hydroxybenzaldehyde	[52]
Pd/Al_2O_3	O_2 5bars	Aqueous 2M NaOH	140°C, flow reactor	Alkaline bagasse lignin	7% hydroxybenzaldehyde, 5% vanillin	[76]
$La(Co,Cu)O_3$ perovskite	O_2 5bars	Aqueous 2M NaOH	120°C	Steam-exploded cornstalk lignin	12% syringaldehyde, 5% vanillin	[78]
$La(Fe,Cu)O_3$ perovskite	O_2 5bars	Aqueous 2M NaOH	120°C	Steam-exploded cornstalk lignin	12% syringaldehyde, 4% vanillin	[77]
La-SBA-15	H_2O_2	Aqueous 2M NaOH	microwaves	Organosolv beech lignin	15% syringaldehyde, 9% vanillin	[79]

The formation of aromatic aldehydes by oxidative cleavage of model molecules containing β-O-4 bonds was studied on supported homogeneous catalysts using hydrogen peroxide as the oxidant. Crestini *et al.* used methyltrioxorhenium immobilized on poly(4-vinyl pyridine) or polystyrene at room temperature in acetic acid whereas Badamali *et al.* used Co(salen) complexes in SBA-15 mesoporous silica in acetonitrile with microwave heating, obtaining 21-28% yields of guaiacol.[71,72] Mottweiler *et al*. inspected Cu-V hydrotalcites for catalytic activity in the cleavage of the lignin model compound erythro-1-(3,4-dimethoxyphenyl)-2-(2-methoxyphenoxy)-l,3-propanediol with molecular oxygen as oxidant.[73] High yield of veratrylaldehyde was observed at 130°C but pyridine had to be used as solvent of the reaction.

Nitrogen-containing graphene materials were also tested for the oxidative cleavage of β-O-4 bonds by using tert-butyl hydroperoxide as the oxidant.[74] Also at the mild temperature of 120°C, over oxidation to benzylic acid was observed. Deng *et al.* tested several non-noble metal oxides as catalysts and reported that cerium oxide can efficiently catalyze the one-pot oxidative conversion of 2-phenoxy-1-phenylethanol in methanol under 10bars molecular oxygen.[75] The presence of a noble metal in CeO_2-supported palladium nanoparticles (Pd/CeO_2) allowed to reduce by a factor 10 the oxygen pressure needed for the reaction. With both catalytic system, over oxidation of tolualdehyde to methyl benzoate was observed. The same Pd/CeO2 catalyst was used in the same reaction conditions not on a model system but

on organosolv lignin. On such more demanding substrate, high yields of syringaldehyde and vanillin were obtained.[75]

Indeed, several heterogeneous catalysts have been successfully used in oxidative depolymerisation of several kinds of lignin in conditions similar to the ones of the Monsanto-Borregaard process for the synthesis of vanillin. Sales *et al*. employed Pd/ γ-Al_2O_3 catalysts for the oxidative conversion of alkaline lignin extracted from sugar cane bagasse in both batch slurry and continuous fluidized-bed reactors.[76] Good yields of syringaldehyde and vanillin were obtained in 2M aqueous NaOH solution at 120-140°C. The use of the perovskite-type mixed oxides $LaM_{1-x}Cu_xO_3$ (M=Co or Fe) has been proposed for the wet aerobic oxidation of cornstalk enzymatic lignin in 2M NaOH under 5 bars O_2. Yields of aromatic aldehydes comparable to the Monsanto process were reported and the catalysts were stable after a series of successive recycling.[77,78] The best yields in syringaldehyde and lignin from organosolv lignin were reported in a microwave-heated 2M NaOH solution by using hydrogen peroxide as the oxidant and La-SBA-15 as the catalyst.[79]

Pineda and Lee reported that oxidative protocols could sometime result in undesirable products because of free radicals-driven recondensation.[33] More complex multi-step reaction pathways have been proposed in order to use milder conditions for each step of the process. Samec and co-workers investigated a mild and chemoselective oxidation of α-alcohols β-O-4 glycerolaryl ethers at 80°C on Pd/C catalysts.[80,81] In this reaction, the benzylic alcohol groups were selectively oxydehydrogenated to the corresponding ketones attaining 60-93% of yield. Successive Pd-catalyzed β-O-4 bond cleavage of the obtained 2-aryloxy-1-arylethanols by hydrogen transfer from formic acid reached 92-98% yields of 3,4-dimethoxypropiophenone proposed as a platform molecule.

1.5 Economical aspects of lignin valorisation

Virtually all lignin presently available is a co-product of pulp and paper industry. However, the development of second-generation biorefineries is providing new industrial sources of isolated lignin. The concept of lignocellulose biorefinery is born with the perceived need of second generation biofuels to ensure sustainability while avoiding direct competition with food resources.[82,83] The installation of biorefinery plants based on new technologies of biomass fractionation opens the way to the integration of optimized lignin recovery in the plant design.[84,85] The introduction of more advanced plants is one of the aspects of the current trend of shifting the design of biorefineries away from the production of biofuels and towards the production of higher value-added chemicals able to replace present fossil-issued products.[86,87]

A significant hurdle in the development of profitable biorefineries is the adaptation to variability and seasonality of the biomass supply. Wood-issued lignin from the different processes of pulp and paper industry enjoys a constant supply and a stable price throughout the year, while other lignin sources, notably from cornstalks and wheat or rice straw, present a significant seasonal variability. In any case, the status of lignin as a co-product of the profitable cellulose industry provides it with a reasonable entry price, at the basis of its possible competition with oil-derived raw materials for the production of chemicals (see Table 1.3).

Table 1.3 Market values of medium-grade lignins compared to fossil oil, significant reagents and potential products[88,89,90,91,92]

Lignins, competitor and reagents	**$/ton**	**Products**	**$/ton**
Kraft lignin	260-500	Vanillin	15000-40000
Lignosulfonates	180-500	4-Hydroxybenzaldehyde	9500-11100
Soda lignin	200-300	Phenol	1400-1620
Organosolv lignin	280-520	Benzene	830-1280
Brent crude oil	490	Toluene	690-980
Methanol	460-490	Xylenes	690-1000
Hydrogen	~3900		

Clearly lignin, with a higher heating value of 21 MJ kg^{-1}, is a very poor fuel when compared with liquid hydrocarbons with a heating value of 45 MJ kg^{-1}. The same oxygen content which lowers the fuel performance of lignin necessary decreases the atomic yield of the production of any hydrodeoxygenation products. Albeit lignin, with a lower oxygen content than cellulose, can improve the yields of bio-oil production from biomass, it seems clear that production of valuable chemicals from lignin has to be based on the retention of useful functional groups already present in the raw material.

The retention of the aromatic rings by lignin hydrogenation to BTX has been developed at the pilot scale, despite the development of the process be hampered by the formation of chars which decreases the yield and poison the catalyst, as well as by the high selectivity to meta-xylene, the less valuable fraction of BTX.[93] The heavy burden of the cost of hydrogen strongly suggests that lignin be used for the production of oxygen-rich products rather than of fuels or base hydrocarbon chemicals.[94]

Indeed, the exploitation of substituted phenolics present in native lignin is at the basis of the production of high added-value flavors like vanillin and derivatives, a traditional staple of

biorefinery.[95] Other functionalized phenolics can provide valuable market outlets but the formation of many products, each with relatively low yields, made separation issues critical for the viability of biorefinery processes.[96,97]

It is clear that better economic returns require the development of technologies integrating easier fractionation of lignocellulosic biomass and more selective depolymerisation. A fuller exploitation of the lignin potential as a source of aromatics remains a worthy technological challenge.

Note: *This chapter of the manuscript has been published as a book chapter; I.Z. Awan, N. Tanchoux, F. Quignard, S. Albonetti, F. Cavani, F. Di Renzo, "Heterogeneous Catalysis as a tool for production of aromatic compounds from lignin" in S. Albonetti, S. Perathoner, E.A. Quadrelli (Eds.), Horizons in Sustainable Industrial Chemistry and Catalysis, Volume 178, 1st Edition, Elsevier (in press) ISBN: 9780444641274, Chapter13.*

References

[1] C. Xu, R.A.D. Arancon, J. Labidi, R. Luque, Lignin depolymerisation strategies: towards valuable chemicals and fuels, Chem. Soc. Rev. 43 (2014) 7485-7500.
[2] J.C. Serrano-Ruiz, R. Luque, A. Sepulveda-Escribano, Transformations of biomass-derived platform molecules: from high added-value chemicals to fuels via aqueous-phase processing, Chem. Soc. Rev. 40 (2011) 5266-5281.
[3] C. Li, X. Zhao, A. Wang, G.W. Huber, T. Zhang, Catalytic Transformation of Lignin for the Production of Chemicals and Fuels. Chem. Rev. 115 (2015) 11559-11624.
[4] C. Cheng, J. Wang, D. Shen, J. Xue, S. Guan, S. Gu, K.H. Luo, Catalytic Oxidation of Lignin in Solvent Systems for Production of Renewable Chemicals: A Review, Polymers 9 (2017) 240.
[5] F.G. Calvo-Flores, J.A. Dobado, J. Isac-García, F.J. Martín-Martínez (Eds.) Lignin and Lignans as Renewable Raw Materials: Chemistry, Technology and Applications, John Wiley & Sons, New York (2015) pp. 9-48.
[6] W. Boerjan, J. Ralph, M. Baucher, Lignin Biosynthesis. Annu. Rev. Plant Biology 54 (2003) 519-546.
[7] J. Zakzeski, P.C.A. Bruijnincx, A.L. Jongerius, B.M. Weckhuysen, The Catalytic Valorization of Lignin for the Production of Renewable Chemicals, Chem. Rev. 110 (2010) 3552-3599.
[8] S. Dutta, K.C.W. Wu, B. Saha, Emerging strategies for breaking the 3D amorphous network of lignin, Catal. Sci. Technol. 4 (2014) 3785-3799.
[9] R.J.A. Gosselink, M.H.B. Snijder, A. Kranenbarg, E.R.P. Keijsers, E. de Jong, L.L. Stigsson, Characterisation and application of NovaFiber lignin, Ind. Crops Prod. 20 (2004) 191–203.
[10] Z. Sun, B. Fridrich, A. de Santi, S. Elangovan, K. Barta, Bright Side of Lignin Depolymerisation: Toward New Platform Chemicals. Chem. Rev. 118 (2018) 614-678.
[11] F.S. Chakar, A.J. Ragauskas, Review of current and future softwood kraft lignin process chemistry, Ind. Crops Prod. 20 (2004) 131-141.

[12] J. Zakzeski, A. Debczak, P.C.A. Bruijnincx, B.M. Weckhuysen, Catalytic oxidation of aromatic oxygenates by the heterogeneous catalyst Co-ZIF-9, Appl. Catal. A 394 (2011) 79-85.
[13] H. Wang, M. Tucker, Y. Ji, Recent Development in Chemical Depolymerisation of Lignin: A Review, J. Appl. Chemistry 2013 (2013) 838645.
[14] M.P. Pandey, C.S. Kim, Lignin Depolymerisation and Conversion: A Review of Thermochemical Methods, Chem. Eng. Technol. 34 (2011) 29-41.
[15] D. Ferdous, A.K. Dalai, S.K. Bej, R.W. Thring, Pyrolysis of Lignins: Experimental and Kinetics Studies, Energy Fuels 16 (2002) 1405-1412.
[16] N.S. Reading, K.D. Welch, S.D. Aust, Free Radical Reactions of Wood-Degrading Fungi, in Goodell, D.D. Nicholas, T.P. Schultz (Eds.) Wood Deterioration and Preservation, 2003, American Chemical Society Symposium Series 845 (2003) pp. 16-31.
[17] J. R. Gasson, D. Forchheim, T. Sutter, U. Hornung, A. Kruse, T. Barth, Modeling the lignin degradation kinetics in an ethanol/formic acid solvolysis approach. Part 1. Kinetic model development, Ind. Eng. Chem. Res. 51 (2012) 10595–10606.
[18] Z.S. Yuan, S.N. Cheng, M. Leitch, C.B. Xu, Hydrolytic degradation of alkaline lignin in hot-compressed water and ethanol, Bioresour. Technol. 101 (2010) 9308−9313.
[19] N. Mahmood, Z. Yuan, J. Schmidt, C.C. Xu, Production of polyols via direct hydrolysis of kraft lignin: Effect of process parameters. Bioresour. Technol. 139 (2013) 13−20.
[20] R. Beauchet, F. Monteil-Rivera, J. M. Lavoie, Conversion of lignin to aromatic-based chemicals (L-chems) and biofuels (L-fuels), Bioresour. Technol. 121 (2012) 328–334.
[21] C. Li, X. Zhao, A. Wang, G.W. Huber, T. Zhang, Catalytic Transformation of Lignin for the Production of Chemicals and Fuels, Chem. Rev. 115 (2015) 11559-11624.
[22] V. Roberts, V. Stein, T. Reiner, A. Lemonidou, X. Li, J.A. Lercher, Towards quantitative catalytic lignin depolymerisation. Chem. European J. 17 (2011) 5939-5948.
[23] M. Phillips, The chemistry of lignin, Chem. Rev. 14 (1934) 103-170.
[24] W.B. Hewson, H. Hibbert, Studies on lignin and related compounds. LXV. Re-ethanolysis of isolated lignins, J. Amer. Chem. Soc. 65 (1943) 1173–1176.
[25] D. Forchheim, J. R. Gasson, U. Hornung, A. Kruse, T. Barth, Modeling the lignin degradation kinetics in an ethanol/formic acid solvolysis approach. Part 2. Validation and transfer to variable conditions, Ind. Eng. Chem. Res. 51 (2012) 15053-15063.
[26] W. Xu, S. J. Miller, P. K. Agrawal, C. W. Jones, Depolymerisation and hydrodeoxygenation of switchgrass lignin with formic acid, ChemSusChem 5 (2012) 667–675.
[27] G.H. Tomlinson, 2nd, H. Hibbert, Studies on Lignin and Related Compounds. XXV. Mechanism of Vanillin Formation from Spruce Lignin Sulfonic Acids in Relation to Lignin Structure, J. Amer. Chem. Soc. 58 (1936) 348-353.
[28] A.L. Mathias, A.E. Rodrigues, Production of vanillin by oxidation of pine kraft lignins with oxygen, Holzforschung 49 (1995) 273–278.
[29] B.C. Collis for Monsanto Chemicals, Manufacture of Vanillin from Lignin, CA515266 (1955).
[30] H.-R. Bjørsvik, F. Minisci, Fine Chemicals from Lignosulfonates. 1. Synthesis of Vanillin by Oxidation of Lignosulfonates, Org. Process Res. Dev. 3 (1999) 330-340.
[31] A.W. Pacek, P. Ding, M. Garrett, G. Sheldrake, A.W. Nienow, Catalytic Conversion of Sodium Lignosulfonate to Vanillin: Engineering Aspects. Part 1. Effects of Processing Conditions on Vanillin Yield and Selectivity, Ind. Eng. Chem. Res. 52 (2013) 8361-8372.
[32] K. Yamamoto, T. Hosoya, K. Yoshioka, H. Miyafuji, H. Ohno, T. Yamada. Tetrabutylammonium hydroxide 30-hydrate as novel reaction medium for lignin conversion. ACS Sustainable Chem. Eng. 5 (2017) 10111-10115.
[33] A.Pineda, A.F. Lee, Heterogeneously catalyzed lignin depolymerisation, Appl. Petrochem. Res. 6 (2016) 243-256.

[34 R.K. Sharma, N.N. Bakhshi, Catalytic upgrading of pyrolysis oil, Energy Fuels 7 (1993) 306-314.
[35] J. Cho, S. Chu, P.J. Dauenhauer, G.W. Huber, Kinetics and reaction chemistry for slow pyrolysis of enzymatic hydrolysis lignin and organosolv extracted lignin derived from maplewood, Green Chem. 14 (2012) 428-439.
[36] G.Jiang, D.J. Nowakowski, A.V. Bridgwater, Effect of the Temperature on the Composition of Lignin Pyrolysis Products, Energy Fuels 24 (2010) 4470-4475.
[37] Z.S. Zhan, C. Wang, K. Bi, X. Zhang, C. Yu, R. Dong, L. Ma, C. Pang, Py-GC/MS study of lignin pyrolysis and effect of catalysts on product distribution,. Int J Agric & Biol Eng 10 (5) (2017) 214-225.
[38] T. Ohra-aho, J. Linnekoski, Catalytic pyrolysis of lignin by using analytical pyrolysis-GC–MS. J. Anal. Appl. Pyrolysis 113 (2015) 186-192.
[39] Z. Ma, E. Troussard, J.A. van Bokhoven, Controlling the selectivity to chemicals from lignin via catalytic fast pyrolysis, Appl. Catal. A 423 (2012) 130-136.
[41] D.W. Van Krevelen. Graphical-statistical method for the study of structure and reaction processes of coal. Fuel 29 *(*1950*)* 269-284
[42] E.E. Harris, J. D'Ianni, H. Adkins, Reaction of Hardwood Lignin with Hydrogen. J. Am. Chem. Soc. 60 (1938) 1467-1470.
[43] J.M. Pepper, Y.W. Lee, Lignin and related compounds. I. A comparative study of catalysts for lignin hydrogenolysis, Can. J. Chem. 47 (1969) 723-727.
[44] J.M. Pepper, P. Supathna, Lignin and related compounds. VI. A study of variables affecting the hydrogenolysis of spruce wood lignin using a rhodium-on-charcoal catalyst, Can. J. Chem. 56 (1978) 899-902.
[45] C. Zhao, Y. Kou, A.A. Lemonidou, X.. Li, J.A. Lercher, Highly Selective Catalytic Conversion of Phenolic Bio-Oil to Alkanes, Angew. Chem. Int. Ed. 48 (2009) 3987-3990.
[46] X. Zhang, Q. Zhang, L. Chen, Y. Xu, T. Wang, L. Ma, Effect of calcination temperature of Ni/SiO_2-ZrO_2 catalyst on its hydrodeoxygenation of guaiacol. Chin. J. Catal. 35 (2014) 302-309.
[47] C. Zhao, Y. Kou, A.A. Lemonidou, X. Li, J.A. Lercher, Hydrodeoxygenation of bio-derived phenols to hydrocarbons using Raney Ni and Nafion/SiO2 catalysts. Chemical Communications, 46 (2010) 412-414.
[48] Y. Shao, Q. Xia, L. Dong, X. Liu, X. Han, S.F. Parker, Y. Cheng, L.L. Daemen, A.J. Ramirez-Cuesta, S. Yang, Y. Wang, Selective Production of Arenes via Direct Lignin Upgrading over a Niobium-Based Catalyst. Nat. Commun. 8 (2017) 16104.
[49] N. Yan, Y. Yuan, R. Dykeman, Y. Kou, P.J. Dyson, Hydrodeoxygenation of Lignin-Derived Phenols into Alkanes by Using Nanoparticle Catalysts Combined with Brønsted Acidic Ionic Liquids. Angew. Chem. Int. Ed. 49 (2010) 5549-5553.
[50] L. Shuai, M.T. Amiri, Y.M. Questell-Santiago, F. Héroguel, Y. Li, H. Kim, R. Meilan, C. Chapple, J. Ralph, J.S. Luterbacher, Formaldehyde Stabilization Facilitates Lignin Monomer Production during Biomass Depolymerisation. Science 354 (2016) 329−333.
[51] X. Si, F. Lu, J. Chen, R. Lu, Q. Huang, H. Jiang, E. Taarning, J. Xu, A Strategy for Generating High-Quality Cellulose and Lignin Simultaneously from Woody Biomass. Green Chem. 19 (2017) 4849−4857.
[52] H. Konnerth, J. Zhang, D. Ma, M.H.G. Prechtl, N. Yan. Base Promoted Hydrogenolysis of Lignin Model Compounds and Organosolv Lignin over Metal Catalysts in Water. Chem. Eng. Sci. 123 (2015) 155−163.
[53] T.H. Parsell, B.C. Owen, I. Klein, T.M. Jarrell, C.L. Marcum, L.J. Haupert, L.M. Amundson, H.I. Kenttamaa, F. Ribeiro, J.T. Miller M.M. Abu-Omar, Cleavage and hydrodeoxygenation (HDO) of C-O bonds relevant to lignin conversion using Pd/Zn synergistic catalysis. Chemical Science, 42 (2013) 806-813.

[54] Y.-C. Lin, C.-L. Li, H.-P. Wan, H.-T. Lee, C.-F. Liu, Catalytic Hydrodeoxygenation of Guaiacol on Rh-Based and Sulfided CoMo and NiMo Catalysts. Energy Fuels 25 (2011) 890-896.
[55] V. Molinari, C. Giordano, M. Antonietti, D. Esposito, Titanium Nitride-Nickel Nanocomposite as Heterogeneous Catalyst for the Hydrogenolysis of Aryl Ethers. J. Am. Chem. Soc. 136 (2014) 1758−1761.
[56] R. Shu, Y. Xu, P. Chen, L. Ma, Q. Zhang, L. Zhou, C. Wang, Mild Hydrogenation of Lignin Depolymerisation Products Over Ni/SiO2 Catalyst, Energy Fuels 31 (2017) 7208-7213.
57] X. Zhu, L.L. Lobban, R.G. Mallinson, D.E. Resasco, Bifunctional transalkylation and hydrodeoxygenation of anisole over a Pt/HBeta catalyst, J. Catal. 281 (2011) 21-29.
[58] F. Gao, J.D. Webb, H. Sorek, D.E. Wemmer, J.F. Hartwig. Fragmentation of Lignin Samples with Commercial Pd/C under Ambient Pressure of Hydrogen. ACS Catal. 6 (2016) 7385−7392.
[59] Y. Jiang, Z. Li, X. Tang, Y. Sun, X. Zeng, S. Liu, L. Lin. Depolymerisation of Cellulolytic Enzyme Lignin for the Production of Monomeric Phenols over Raney Ni and Acidic Zeolite Catalysts. Energy Fuels 29 (2015) 1662−1668.
[60] Q. Song, F. Wang, J. Cai, Y. Wang, J. Zhang, W. Yu, J. Xu. Lignin Depolymerisation (LDP) in Alcohol over Nickel-Based Catalysts via a Fragmentation–Hydrogenolysis Process. Energy Environ. Sci. 6 (2013) 994–1007.
[61] F.P. Petrocelli, M.T. Klein, Chemical modeling analysis of the yields of single-ring phenolics from lignin liquefaction, Ind. Eng. Chem. Prod. Res. Dev. 24 (1985) 635-641.
[62] K. Barta, G.R. Warner, E.S. Beach, P.T. Anastas. Depolymerisation of Organosolv Lignin to Aromatic Compounds over Cu-Doped Porous Metal Oxides. Green Chem. 16 (2014) 191-196.
[63] L.-P. Xiao, S. Wang, H. Li, Z. Li, Z.-J. Shi, L. Xiao, R.-C. Sun, Y. Fang, G. Song, Catalytic Hydrogenolysis of Lignins into Phenolic Compounds over Carbon Nanotube Supported Molybdenum Oxide. ACS Catal. 7 (2017) 7535−7542.
[64] I.T. Ghampson, C. Sepúlveda, R. Garcia, B.G. Frederick, M.C. Wheeler, N. Escalona, W.J. DeSisto, Guaiacol transformation over unsupported molybdenum-based nitride catalysts. Appl. Catal. A 413-414 (2012) 78-84.
[65] N. Ji, X. Wang, C. Weidenthaler, B. Spliethoff, R. Rinaldi, Iron(II) Disulfides as Precursors of Highly Selective Catalysts for Hydrodeoxygenation of Dibenzyl Ether into Toluene. ChemCatChem, 7 (2015) 960-966.
[66] H.Y. Zhao, D. Lia, P. Bui, S.T. Oyama, Hydrodeoxygenation of guaiacol as model compound for pyrolysis oil on transition metal phosphide hydroprocessing catalysts. Appl. Catal. A 392 (2011) 305-310.
[67] T. Prasomsri, M. Shetty, K. Murugappan, Y. Roman-Leshkov. Insights into the catalytic activity and surface modification of MoO3 during the hydrodeoxygenation of lignin-derived model compounds into aromatic hydrocarbons under low hydrogen pressures. Energy Environ. Sci. 7 (2014) 2660-2669.
[68] S. Bhargava, H. Jani, J. Tardio, D. Akolekar, M. Hoang, Catalytic Wet Oxidation of Ferulic Acid (A Model Lignin Compound) Using Heterogeneous Copper Catalysts, Ind. Eng. Chem. Res. 46 (2007) 8652-8656.
[69] A. Jha, K.R. Patil, C.V. Rode, Mixed Co–Mn Oxide-Catalysed Selective Aerobic Oxidation of Vanillyl Alcohol to Vanillin in Base-Free Conditions. ChemPlusChem 78 (2013) 1384-1392.
[70] V.R. Mate, M. Shirai, C.V. Rode, Heterogeneous Co_3O_4 catalyst for selective oxidation of aqueous veratryl alcohol using molecular oxygen. Catal. Commun. 33 (2013) 66-69.

[71] C. Crestini, M.C. Caponi, D.S. Argyropoulos, R. Saladino, Immobilized methyltrioxo rhenium (MTO)/H_2O_2 systems for the oxidation of lignin and lignin model compounds. Bioorg. Med. Chem. 14 (2006) 5292-5302.
[72] S.K. Badamali, R. Luque, J.H. Clark, S.W. Breeden, Co(salen)/SBA-15 Catalysed Oxidation of a β-O-4 Phenolic Dimer Under Microwave Irradiation. Catal. Commun. 12 (2011) 993–995.
[73] J. Mottweiler, M. Puche, C. Räuber, T. Schmidt, P. Concepcion, A. Corma, C. Bolm, Copper- and Vanadium-Catalyzed Oxidative Cleavage of Lignin using Dioxygen. ChemSusChem 8 (2015) 2106-2113.
[74] Y. Gao, J. Zhang, X. Chen, D. Ma, N. Yan, A Metal-Free, Carbon-Based Catalytic System for the Oxidation of Lignin Model Compounds and Lignin. ChemPlusChem 79 (2014) 825-834.
[75] W. Deng, L. Lin, S. Liu, Oxidative conversion of lignin and lignin model compounds catalyzed by CeO2-supported Pd nanoparticles. Green Chemistry, 17 (2015) 5009-5018.
[76] F.G. Sales, L.C.A. Maranhão, N.M. Lima Filho, C.A.M. Abreu, Experimental evaluation and continuous catalytic process for fine aldehyde production from lignin. Chem. Eng. Sci. 62 (2007) 5386-5391.
[77] J. Zhang, H. Deng, L. Lin, Wet Aerobic Oxidation of Lignin into Aromatic Aldehydes Catalysed by a Perovskite-type Oxide: LaFe1-xCuxO3 (x=0, 0.1, 0.2). Molecules, 14 (2009) 2747-2757.
[78] H. Deng, L. Lin, S. Liu, Catalysis of Cu-Doped Co-Based Perovskite-Type Oxide in Wet Oxidation of Lignin to Produce Aromatic Aldehydes. Energy Fuels 24 (2010) 4797–4802.
[79] X. Gu, K. Cheng, M. He, Y. Shi, Z. Li, La-Modified SBA-15/H2O2 systems for the Microwave Assisted Oxidation of Organosolv Beech Wood Lignin. Maderas Cienc. Tecnol.14 (2012) 31-42.
[80] M. Dawange, M.V. Galkin, J.S.M. Samec, Selective Aerobic Benzylic Alcohol Oxidation of Lignin Model Compounds: Route to Aryl Ketones. ChemCatChem 7 (2015) 401-404.
[81] M.V. Galkin, C. Dahlstrand, J.S.M. Samec, Mild and Robust Redox-Neutral Pd/C-Catalyzed Lignol b-O-4' Bond Cleavage through a Low-Energy-Barrier Pathway. ChemSusChem 8 (2015) 2187-2192.
[82] G.W. Huber, S. Iborra, A. Corma, Synthesis of Transportation Fuels from Biomass: Chemistry, Catalysts, and Engineering. Chem. Rev. 106 (2006) 4044-4098.
[83] G. Centi, P. Lanzafame, S. Perathoner, Analysis of the alternative routes in the catalytic transformation of lignocellulosic materials. Catal. Today 167 (2011) 14-30.
[84] F. Schüth, R. Rinaldi, N. Meine, M. Käldström, J. Hilgert, M.D. Kaufman Rechulski, Mechanocatalytic depolymerisation of cellulose and raw biomass and downstream processing of the products. Catal. Today 234 (2014) 24-30.
[85] A.J. Ragauskas, G.T. Beckham, M.J. Biddy, R. Chandra, F. Chen, M.F. Davis, B.H. Davison, R.A. Dixon, P. Gilna, M. Keller, P. Langan, A.K. Naskar, J.N. Saddler, T.J. Tschaplinski, G.A. Tuskan, C.E. Wyman, Lignin Valorization: Improving Lignin Processing in the Biorefinery. Science 344 (2014) 1246843.
[86] D. Esposito, M. Antonietti, Redefining biorefinery: the search for unconventional building blocks for materials. Chem. Soc. Rev. 44 (2015) 5821-5835.
[87] R. Rinaldi, R. Jastrzebski, M.T. Clough, J. Ralph, M. Kennema, P.C.A. Bruijnincx, B.M. Weckhuysen, Paving the Way for Lignin Valorisation: Recent Advances in Bioengineering, Biorefining and Catalysis. Angew. Chem. Int. Ed. 55 (2016) 8164 –8215.
[88] L. Hodasova, M. Jablonski, A. Skulcova, A. Haz, Lignin, potential products and their market value. Wood Res. 60 (2015) 973-986.
[89] M.R.D. Valladares, Global Trends and Outlook for Hydrogen, IEA Hydrogen Technology Collaboration Program, 2017, 20 pp.

[90] https://www.methanex.com/our-business/pricing, consulted December 2017
[91] https://www.statista.com, consulted December 2017
[92] A.J.J. Straathof, A. Bampouli, Potential of commodity chemicals to become bio-based according to maximum yields and petrochemical prices. Biofuels, Bioprod. Bioref. 11 (2017) 798-810.
[93] F. Cavani, S. Albonetti, F. Basile, Aromatics from Biomasses: Technological Options for Chemocatalytic Transformations, in F. Cavani, S. Albonetti, F. Basile, A. Gandini (Eds.), Chemicals and Fuels from Bio-Based Building Blocks, Wiley-VCH, Weinheim (2016) pp. 33-50.
[94] J.-P. Lange, Catalysis for biorefineries – performance criteria for industrial operation. Catal. Sci. Technol. 6 (2016) 4759-4767.
[95] G. Rødsrud, M. Lersch, A. Sjöde, History and future of world's most advanced biorefinery in operation. Biomass Bioener. 46 (2012) 46-59.
[96] S. Venkatesan, Adsorption, in S. Ramaswamy, H.-J. Huang, B.V. Ramarao (Eds.), Separation and Purification Technologies in Biorefineries. Wiley, New York (2013) 101-148.
[97] A.A. Kiss, J.-P. Lange, B. Schuur, D.W.F. Brilman, A.G.J. van der Ham, S.R.A. Kersten, Separation technology. Making a difference in biorefineries. Biomass Bioen. 95 (2016) 296-309.

Literature Review

CHAPTER 2

Layered Double Hydroxides (LDHs) as Precursors of Mixed Metal Oxide Catalysts

Chapter Summary:

Layered Double Hydroxides (LDHs) or anionic clays form an inorganic family of natural or synthetically occurring 2-D lamellar hydroxides with tunable composition with multivalent-cations (M^{2+}, M^{3+}) in the main layers and counter-balancing anions (A^{n-}) in the interlayer region. LDHs have received profound attention by virtue of their properties like high surface area, low cost synthesis, tailor-ability and recyclability. This family of materials has demonstrated applications in the fields of catalysis, drug delivery, sensors and anion exchangers. Their applications in catalysis are either as direct catalysts, precursors of mixed oxides, or catalyst supports. In most reaction conditions, LDH-derived mixed metal oxides (MMO), obtained by the thermal decomposition, are more active and stable than the parent LDH. A temperature-dependent calcination imparts surface properties to the mixed metal oxides catalytic systems. Both basic and redox mixed oxide catalysts have been reported in the literature for the conversion of biomass-derived molecules. This chapter explains the aim of modifying a classical, basic, dopable, member of this family, hydrotalcite [$Mg_6Al_2CO_3(OH)_{16}\cdot 4(H_2O)$], to produce a tailored redox catalyst. Among cost-effective transition metals, Ni-Cu-Fe system was chosen, since copper (Cu^{2+}) is a typical candidate catalyst for the depolymerisation of lignin, nickel (Ni^{2+}) is less basic as compared to Mg^{2+} in the hydrotalcite and iron (Fe^{3+}) replacing Al^{3+} induces further redox properties to the system. Benchmark catalysts systems have been synthesized to understand existing Jahn Teller distortion in the Cu-Fe system, which is critically described. The nature and distribution of mixed oxide phases are strictly dependent on the type of cation and on calcination temperatures. Interestingly, the MMO phases are not always like expected from the composition of the systems; instead they underwent phase segregations leaving an amorphous phase when calcination temperature is not high enough. This phenomenon, as reported in the literature, varies with the type and ratio of cations used. MMO catalysts have been widely used for the conversion of biomass and derived molecules with selectivity and conversions characteristically dependent on the composition of the catalysts. Hence, a careful selection with respect to cation ratio, nature and size of cations has been carried out. Moreover, keeping in view the experimental studies, a general literature overview of synthesis conditions of LDHs, their derived oxides and their applications is presented. Prospects and objectives of the project have also been summarized.

Background

Layered Double Hydroxides (LDHs) is the class of natural or synthetic two-dimensional lamellar hydroxides consisting of at least two kinds of metallic cations in the main layers with charge-compensating exchangeable anions in the interlayer domains, with a general formula $[M_{1-x}^{2+} M_x^{3+} (OH)_2]^{x+} [A_{x/n}]^{n-} \cdot mH_2O$ where M^{2+} (Mg^{2+}, Ni^{2+}, Cu^{2+}, Zn^{2+}, Ca^{2+}) and M^{3+} (Fe^{3+}, Al^{3+}) are divalent and trivalent metal ions, respectively, and A^{n-} (Cl^-, NO^{3-}, and CO_3^{2-}) is the interlayer anion. They are often called anionic clays, double layered hydroxides, mixed metallic hydroxides or hybrid layered structures. Layered Double Hydroxides are often also commonly called hydrotalcite-like materials due to their similarity with a naturally occurring mineral called Hydrotalcite (a hydrated, talc-like, hydroxy carbonate of magnesium and aluminium), first discovered in 1842 in Sweden.[2] Thus Hydrotalcite is a special instance of Layered Double Hydroxide (LDHs). The normal formula of Hydrotalcite was suggested as $(Mg_6Al_2(OH)_{16}CO_3.4H_2O))$ by E. Manasse in 1915.[3] Later, the name was allotted to call a large group of LDH naturally occurring minerals.[86]

A typical LDH material with CO_3^{-2} counter-anions has cell parameters a = b = 3.07 Å, c = 23.23 Å, α = β = 90°, and γ = 120°. Layer stacking is highly ordered in either polytypes with a hexagonal cell (2H symmetry) or polytypes with a rhombohedral (3R symmetry)[1]

Figure 2.1 A naturally occurring Hydrotalcite[76]

Hydrotalcite-like compounds drastically drew attention in the early 1970's when a patent by BASF reported them to be the optimal precursors for the preparation of hydrogenation catalysts.[4] Since then, great efforts have been put to better understand their structural characterization and their anionic exchange properties and to develop novel synthesis and preparation methods to get the best possible advantage in heterogeneous catalysis,

pharmaceutical applications and electrochemical and magnetic properties. LDHs are distinguished for their ability to incorporate and disperse more than one transition metal cation, which may impart redox properties to the system. Their significant characteristics, such as anion mobility, surface basicity[5], sorption[6] and anion exchange[7] make them efficient sensors[8], catalysts[9,10], electrodes[11] and biomaterials[114]. Therefore, keeping in view the economic and environmental aspects, LDHs have received tremendous attention by virtue of their simple handling, low cost, tuna-bility and tailor-ability, easy separation and recyclability.[12] This is clear from the increasing trend of publications on layered double hydroxides as catalysts (see Fig. 2.2)

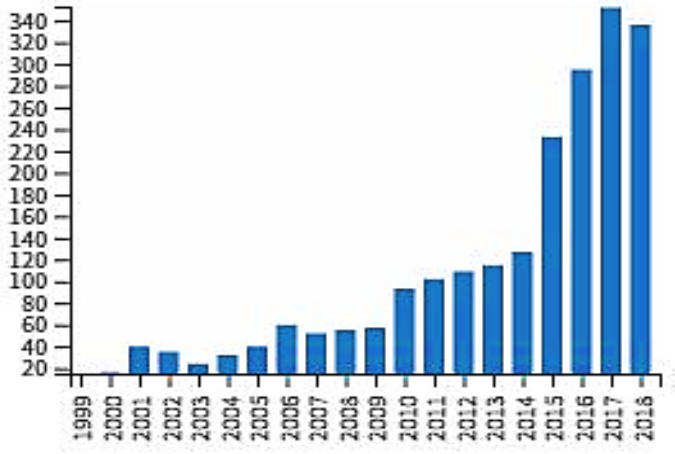

Figure 2.2 Annual Publications on Layered Double Hydroxides as catalysts(data obtained from Web of Science Core collection dated as of 05.09.2018)

A part of this research project is based on the structural modifications and the acquired properties of the LDH materials; therefore the structural description and the properties of the synthesis will be introduced here and discussed in detail in the later chapters.

2.1 General Structural Aspects

LDHs compounds are characterized on the basis of their structural similarity to brucite ($Mg(OH)_2$), in which layers, where the octahedral units of Mg^{2+} share edges to form stacked sheets in order to build $Mg(OH)_2$ layers. These infinite stacked sheets/main layers are held one above the other with two different symmetries, rhombohedral or hexagonal, by the hydrogen bonding between the surrounding hydroxyl ions. As depicted in the general formula of LDH, $[M_{1-x}^{2+}M_x^{3+}(OH)_2]^{x+}\ [A_{x/n}]^{n-}\cdot mH_2O$, it is evident that the octahedral units of the main layers can host a variety of divalent (M^{2+} = Mg^{2+}, Fe^{2+}, Mn^{2+}, Zn^{2+}) and trivalent cations (Al^{3+}, Fe^{3+}, Cr^{3+}, Mn^{3+}) with a varying ratio of charge compensating M^{2+}/M^{3+}. An isomorphous substitution of M^{2+} by M^{3+} dispenses net positive charge to the layer which is electrically neutralized by the incorporation of an adequate number of anions (CO_3^{2-}, NO_3^-,

Cl^-, SO_4^{2-}, etc.) into the interlayer domains between the stacked sheets. The free space in the interlayer region is occupied by water of crystallization (see Fig. 2.3) Hence it is obvious that the charge density is proportional to the trivalent metal ratio 1/x= M^2/ (M^2+M^3). Detailed information on the structure of the conventional LDH is provided by Reichle[13] and Mills.[85]

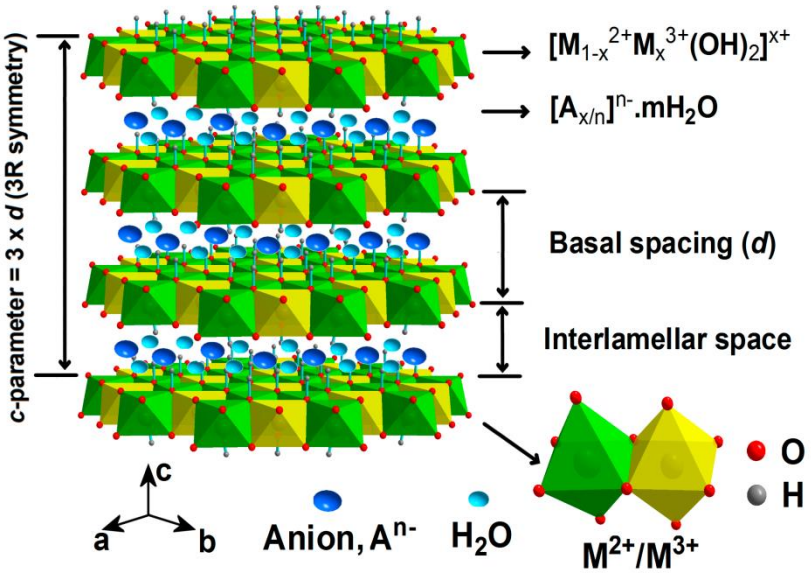

Figure 2.3 Schematic view of LDH structure[14]

2.1.1 Selection of Cations

A wide variety of metallic cations (M^{2+}/M^{3+}) can be integrated into the interlayers of the synthetic LDH system chosen on the basis of the intended applications. The structural properties of LDHs vary with the nature of cations used, by the position of anions and water in the interlayer region and by the type of stacking of the brucite-like sheets.[2] Therefore, selection of the appropriate cations for the LDH system governs the stabilized structure with the exception of some structural changes.[15] It is suggested that only those cations having not too different radius than Mg^{2+} can be fitted well into the octahedral sites of main layers to successfully form LDHs.[2] The ionic radii of cations in LDH are usually indicated as being in the range of 0.65-0.80Å for divalent cations and 0.62 - 0.69 Å for for trivalent ones with the main exception, Al^{3+}: 0.50 Å. (Table 1). The 6-fold symmetry of the oxygen atoms surrounding the cation imposes a minimum ratio of 0.414 between the radius of the cation and the radius of oxygen. With a radius 1.35 Å of O^{2-}, Al^{3+} is at this lower limit. Smaller cations such as Be^{2+} or cations with higher ionic radii (Ca^{2+}, Cd^{2+} and Sc^{3+}, La^{3+}) seem to be incompatible with the formation of true brucite-like layers.[15] Ordering of the cations in the layers in superstructures are a multiplication of the simplest brucite-sheet unit (ab) in which edges are equal to [$M(OH)_6$] octahedron. Insertion of the largest radii cations as Ca^{2+} in the

layers imposes a higher coordination than six. Therefore the octahedron is broken and Ca^{2+} is directly coordinated with water molecules in the layer. Thus the symmetry around the cation is changed and lowered from D3d to C3v.[15]This leads to distortion of the lattice yielding pseudo-hexagonal superstructures like hydrocalumite $[Ca_4Al_2(OH)_{12}]^{2+}[Cl_2(H_2O)_4]^{2-}$. [133,134] This is a unique kind of layered material family unlike the conventional layered double hydroxide. Indeed, only traces of Ca^{2+} in natural and synthetic LDHs have been reported by Allmann[115, 85]and Drits[16].

Table 2.1 Ionic radius (Å) of some cations in decreasing order

M^{2+}	Ca	Cd	Mn	Fe	Zn	Co	Ni	Cu	Mg	Be
	0.98	0.97	0.80	0.76	0.74	0.74	0.72	0.69	0.65	0.30
M^{3+}	In	Ti	V	Cr	Mn	Fe	Co	Ni	Ga	Al
	0.81	0.76	0.74	0.69	0.66	0.64	0.63	0.62	0.62	0.50

2.1.2 Cation Ratio

As a role of thumb, a general accepted range for the divalent verses trivalent ratio in a well crystalline LDH, spans from $0.2 \leq x \leq 0.33$.[2] In some cases, LDHs are described by the M^{2+}/M^{3+} fraction, generally with integer value (R= 2, 3, 4) equivalent to the relative amount of cations present in the coprecipitation mixture. (Fig. 2.4) There have been literature reports for preparation of synthetic LDH outside this range but the phase purity is questionable.[21, 116]

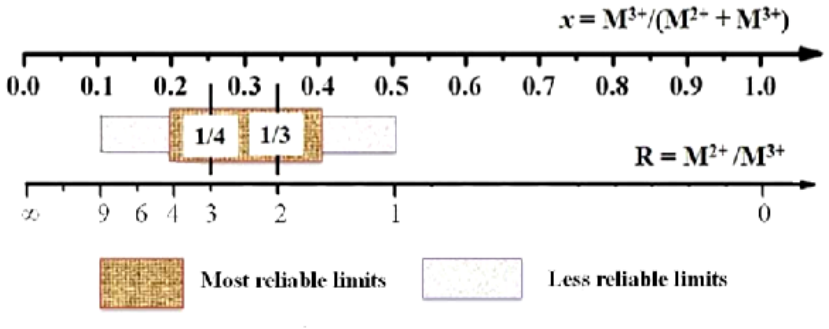

Figure 2.4 Comparison of trivalent metal fraction x scale and divalent vs. Trivalent ratio R scale and corresponding limits for LDH compositions.[15]

The upper limit of the ratio is associated to the degree of electrostatic repulsion between adjacent trivalent cations in the layer which can be minimized when $x < 1/3$. The lower limit corresponds to an insufficient amount of corresponding anions to keep open the interlayer domains, leading to the collapse of the interlayer structure.

2.1.3 The choice of anions

The choice of anions is practically vast and not limited by the ionic size. However the stoichiometric amount plays a vital role in counter-balancing the net positive charge corresponding to the trivalent cations. Nevertheless, some structural alterations or contaminations might come through the way. Typically, in choosing anion other than carbonate (CO_3^{2-}) in the synthesis, carbonate can be anyway found in the product, as the contamination of LDH with atmospheric CO_2 on aqueous solution is a frequent occurrence. The use of inorganic anions (NO_3^{2-} [2], Cl^-, CO_3^{2-}, SO_4^{2-} [23]), heteropolyacids $(PMo_{12}O_{40})^{3-}$ [24], $(PW_{12}O_{40})^{3-}$ [25] and organic acids[26] such as oxalic, succinic, malonic, sebacic acid in the interlayer domains has been reported. As suggested by Wang et *al*. nitrate and chloride tend to have special effects when to be incorporated in the LDH system.[104] This is because LDH are generally formed at low pH and carbonate incorporation in the system is normally prevented. Thus, LDH having nitrate, sulphate and chloride have their own layered spacing.[102] The thickness of the interlayer is determined both by the size of the anions and by the bonds between anions layers and hydration water. Typically, for a given anion, the interlayer distance decreases at higher content of trivalent cation.

2.2 Preparation of LDH

Several methods have been developed for the synthesis of LDH. These include urea method, sol gel method, coprecipitation, microwave irradiation method and alkali method. Among these, coprecipitation method is the most common. In this method, a slow addition of stoichiometric amounts of divalent and trivalent metal cation solutions is added in a water-containing reactor. An alkaline solution is continuously added dropwise to the reactor to maintain the selected pH of the system constant. Coprecipitation starts with the condensation of metal aqueous complexes to form a stacked brucite-like structure, in which the metallic cations are uniformly distributed with anions existing in the interlayer region. The obtained slurry is then aged for several hours at moderate temperature to promote nucleation/agglomeration of the particles which are obtained as microcrystalline platelets upon filtration and drying.[82] The rate of addition and physical parameters of ageing determine the crystallinity of the LDHs.[82] Some typical factors to be taken into consideration are:

1. pH of the reaction medium
2. Concentration of metallic salts
3. Temperature of the reactor
4. Flow rate of the reactants
5. Aging of the precipitates

6. Concentration of alkaline solution[15]

It must be noted that LDH materials are stable in alkaline and neutral solution although they are soluble at pH below 4.0[27], which means that at pH around 9-10, LDHs are stable solid compounds.

2.3 Characterization of LDHs

The characterization of LDH is principally done by X-Ray Diffraction (XRD). Diffraction methods are used to determine the crystalline properties of LDH compounds by study of the structure of the crystallites, phases present and the unit cell parameters. Further analysis through crystallographic techniques can also give clues about the structural defects.

The degree of crystallinity and quantitative determination of each cation in the phase is confirmed by the Energy Dispersive X-ray (EDX) which allows the comparison of the initial (synthesis) with final (precipitated fraction) atomic ratio of the material formed, be it crystalline LDH or other phase or also amorphous material.

The Thermogravimetry (TG) can give quantitative information on successive changes upon thermal decomposition of the LDH compound. This allows determining calcination temperatures needed to obtain mixed metal oxides from LDH. N_2 Adsorption/Desorption technique (BET) gives significant information about the pore size, surface area and pore volume of the materials. Temperature Programmed Reduction (TPR) can also be employed to study the redox properties of calcined LDH.[28] The morphology of the crystallites can be examined by Scanning Electron Microscopy (SEM). Other techniques, like Fourier-transform infrared spectroscopy (FTIR)[29], X-ray fluorescence (XRF), Transmission electron microscopy (TEM)[78], X-ray absorption spectroscopy (XAS)[79] and electron spin resonance (ESR)[80], as well as Raman spectroscopy[81], have also been less frequently reported.

2.4 Which metals to choose for LDH?

Changes brought by the wide variety of composition and calcination conditions can crucially affect crystallite size, nature and distribution of cations in the LDHs. Thus, the catalytic properties and performance of the LDH-obtained mixed oxides can significantly vary. Additionally, if reducible cations are employed in the metallic framework with intercalating anions of different sizes and functions, a distinctive approach of design of redox bifunctional catalysts can be achieved.[30]

There are generally two main categories of functional materials used in redox catalysis. Noble metals for example palladium (Pd), platinum (Pt), ruthenium (Ru) and rhodium (Rh) and base transition metals (3d-type, first series) such as chromium (Cr), copper (Cu), cobalt

(Co) and nickel (Ni) and their respective oxides. Despite frequent superior performances of the noble metals, the choice among them is worth consideration due to the limited reserves of noble metals and their easy poisoning. Transition base metals are generally cheap, thus do not require strict control during the reaction processes. Oxides of the transition metal-based precursors have seen to be promising catalysts for oxidation and hydrogenation reactions owing to their easy preparation and handling.[31] One of the main targets in the preparation of mixed oxides is a homogenous and high dispersion of cations, avoiding any phase separation (segregation).[32] To date, coprecipitation has been considered the most reliable and effective method for the synthesis of LDH precursors. This method favors the synergetic effect of the starting materials and homogenously mixed precursors can be achieved.

2.4.1 The choice of redox metallic System (Ni-Cu-Fe)

Classical hydrotalcite, $Mg_6Al_2CO_3(OH)_{16}\cdot 4(H_2O)$ is an effective basic catalyst and has been widely used for a range of applications such as alkylation of ketones and phenols, aldol condensation, Michael additions, Claisen-Schmidt condensation, transesterification of vegetable oils for biodiesel production [37,135-139,145] Regarding the calcined products of the hydrotalcites, several authors reported concerns on the chemical composition which has significant impact on the acid/base properties of the catalysts and hence their catalytic activity is under debate.[137,140]

2.4.1.1 Iron (Fe^{3+}) as catalyst

Leclercq *et al.* reported a poor performance (conversion of 35% after 22 h of reaction) of mixed oxides from a commercial Mg/Al hydrotalcite for the transesterification of rapeseed oil with methanol/oil molar ratio of 75 at 60°C.[141] Macala *et al.* studied the introduction of a transition metal such as Fe, Cr, and Ga in a MgAl hydrotalcite system to improve the catalytic activity of the obtained mixed oxides.[142] Their studies showed that Fe-doped materials performed the best for transesterification reaction. For the transesterification of soybean oil, a conversion of 38% after 40 min on-stream at 80°C using 1 wt % of catalyst was obtained.

2.4.1.2 Nickel as a hydrogenation Catalyst

The use of nickel as a hydrogenation catalyst for lignin monomers has been reported by Qi.[143] Also Pepper *et al.* reviewed the outstanding performance of Ni for the catalytic hydrogenation

of lignin and its model substances. [144] Another study by Usman *et al.* indicated the use of nickel supported on highly ordered mesoporous silica for the hydrogenation of edible vegetable oil achieving 81% conversion. The catalyst was stable, reused, and resistant to leaching and poisoning. [146]

2.4.1.3 The role and interest in Cu based LDHs

Copper is a non-noble and cheap transition metal which induces redox effects in the catalyst by favoring electron donation or supply in the reaction system. It can dramatically affect the surface properties of the catalysts as claimed by Dupin and co-workers, who synthesized LDH-derived mixed oxides with different proportions of Ni, Cu, Mg and Al to achieve acid-base and redox properties in the catalyst. Both acidity and basicity of the catalysts was dependent on the ratio between the reducible metals Ni/Cu.[121]Thus its tailor-able and wide range of properties make it a desirable catalyst for the industry. A long list of reactions are efficiently catalyzed by copper.

Copper-containing catalysts are frequently utilized in organic chemistry to catalyze reactions of C-C bonds, C-heteroatoms such as, Ullmann reactions, [117] C–O cross-coupling reaction, [118] C (aryl)-O. C (aryl)-N, and C (aryl)-S Bond Formation,[119] Diels-Alder reactions[120] etc. Furthermore, copper is also known for assisting in reduction reactions such as electrochemical reduction of CO_2 to C_2H_4[122], photochemical reduction of CO_2 to CO[123] and MOF-Derived Cu@Cu_2O nanocatalyst for oxygen reduction and cycloaddition reactions[124].

Cu-containing LDH, taking advantage of known redox properties of copper have been exploited in many applications. Velu *et al*. conducted oxidative steam reforming of methanol over CuZnAl(Zr)-LDH derived oxides for the selective production of Hydrogen from fuel cells. With Cu:Zn:Al 37.6 : 50.7 : 11.7 (wt%) around 100% conversion was achieved at 503K without any detectable CO in the outflow stream.[105] Zhao *et al.* explained the characteristic structural and chemical features of NiAl, 1%CuNiAl, 3%CuNiAl, 5%CuNiAl LDH-based mixed oxides for the SO_2 abatement concluding that 5% CuNiAl had the best performance because increasing the copper content enriches Cu^{2+}-O^{2-} which infers oxygen vacancy sites.[110]

2.5 Synthesis Limitations of Copper-LDH

It has been early reported that all divalent cations from Mn^{2+} to Mg^{2+} form LDHs except Cu^{2+} which can only form LDH in the presence of a substantial amount of another divalent cation.[2] The ratio between Cu^{2+} and the second divalent cation should be equal or lower than one. The

higher copper content distorts the structural symmetry in LDH and brings to the formation of phases such as malachite and gerhardtite.[17] This effect is attributed to the Jahn Teller distortion in Cu^{2+} system due to the lifting of degeneracy of the d^9 state, which decreases the symmetry of the octahedra to the extent that the structural stability is lost (see Fig. 2.5).[18] Cu^{2+} in octahedral coordination is not stable electronically.

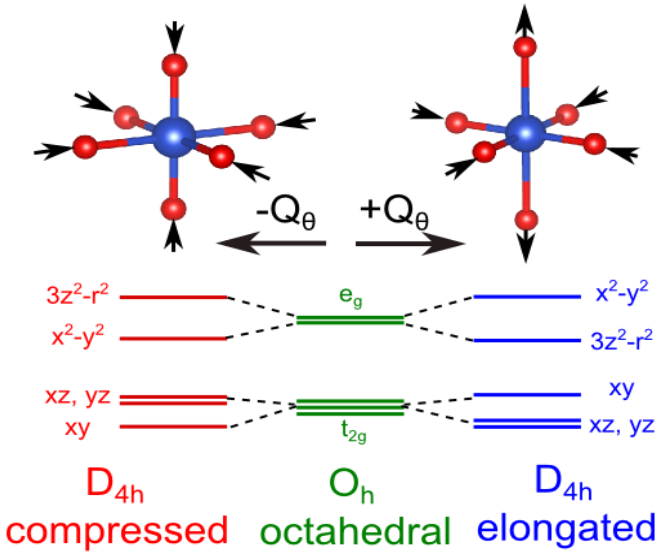

Figure 2.5 Lifting of the d^9 degeneracy by Jahn Teller distortion in Cu^{2+}.[87]

Despite the synthesis of Cu LDH has been early reported to be difficult,[2] many examples are known of experimental synthesis of Cu-Al based LDH, where Cu^{2+} is the only divalent and Al^{3+} serves as a trivalent. Apart from natural presence as Woodwardite, ($Cu_4Al_2(SO_4)(OH)_{12}.3(H_2O)$), successful procedure for synthetic analogue of woodwardite has also been reported with application in affinity for Rare earth elements (REEs).[88] Lwin *et al*. prepared series of catalyst precursors from atomic ratios Cu/Al 0.25-1, mainly forming Hydrotalcite-like and malachite phases.[100] The ratio of phases present and their crystallinity was controlled by the Cu-concentration in the system. Remarkably, another synthesis of Cu-Al (1:4) has been reported by Fogg *et al*. indicating that Cu-Al can be synthesized over a wide range of cationic fractions.[99] Likewise, application of Cu-Al LDH-derived mixed oxide catalysts include, H_2 production by water gas shift reactions[89], from methanol steam reforming [90] and catalytic decomposition of ethanol and other alcohols in a fuel stream [90, 91] Cu-Al LDH/racBinol ligand has been proposed for selective oxidation of alcohols at room temperature.[92] Similarly ternary hydrotalcite (CuAl-M^{2+} metal cation) systems have also been investigated. For instance, Rives *et al.* reported the catalytic hydroxylation of phenol over

CuCoAl with ((Cu+Co/Al)=3) [93] and CuNiAl with ((Cu+Ni/Al)= 2, 3).[94] Vaccari and co-workers studied the combination of CuAl with Zn with a highest performing atomic ratio of (Cu+Zn/Al) =2 for the water gas shift reaction. [95]

2.5.1 Studies on formation Mechanism of LDH and effect on peculiar synthesis of Cu LDH:

The ineffective synthesis dealing with the structural constraints in a Cu-Fe LDH have been reported many times[2, 19, 20.] Cu-LDH has been considered a special problem due to the structural differences of cupric hydroxide, which does not form layered structures, at difference from other divalent hydroxides.[102] Though, a complex Cu-Al LDH ($Cu_{0.67}Al_{0.33}(OH)_2(SO_4)_{0.15}(CO_3)_{0.015}\cdot 0.5H_2O$) had been reported by the addition of mixed solution of aluminium sulfate and sodium hydroxide to a cupramine complex solution.[101] Grosso *et al*. screened the catalysts precipitation conditions for the synthesis of Cu-Cr LDH system, although not pure LDH phase was obtained.[103] Taking into account this, it can be said that every precursor catalysts system has own preference which must be explored to optimize the properties. Another explanation has been advanced, dealing with the choice of anions selected for the incorporation into the layered system.

It is known that the LDH formation mechanism is a two-step process.[48, 77] In stage one, the formation of hydrous oxide takes place followed by the formation of LDH in a second stage, in which the LDH crystallization occurs either by diffusion of M^{3+} inside the hydrous M^{2+} oxide[47] or through the diffusion of M^{2+} cations into the M^{3+} rich phase. [45, 46] It is very important to understand the bottom line of this phenomena which has been well explained by Ruby and co-workers in terms of formation mechanism of Ni-Fe and Mg-Fe layered structures (see Fig. 2.6).[48] After the precipitation of Fe^{3+}(stage 1), the formation of a precursor begins on Fe^{3+} oxyhydroxide surface. The LDH phase is formed (stage 2) when slow diffusion of Fe^{3+} into the $Ni(OH)_2$, $Mg(OH)_2$ layered structures precursors occurs.[48] This fact that refrains a Cu-Fe LDH system because as explained in the above example, LDH is not merely composed of M^{2+}+M^{3+} cations however the structural properties are drastically affected by the choice of cations used. $Cu(OH)_2$ does not possess a layered structure, thus in a Cu-Fe system, precursor required for stage 2 is absent consequently no LDH is formed.

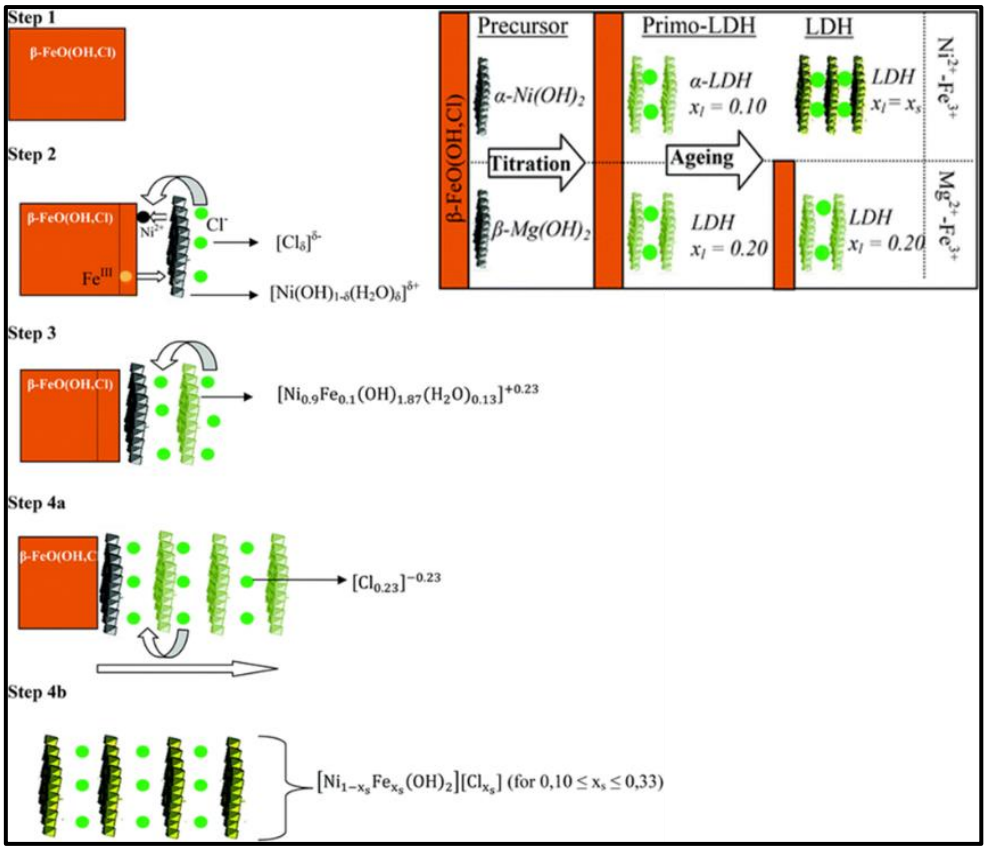

Figure 2.6 Mechanism of formation of Ni^{2+}. Mg^{2+}-Fe^{3+} LDH phase[48]

However, this is not the case in Cu-Al, which is explained by virtue of M^{2+}/Al system example.[77] At the beginning of the precipitation, sequential hydrolysis and polycondensation of Al^{3+} takes place producing amorphous aluminium hydroxide structures. These particles of $Al(OH)_3$ combine into sphere-like aggregates, which are later transformed into a lamellar boehmite acting as precursors, where Mg^{2+} can diffuse to produce a Mg/Al LDH structure. The unbalance in charge invites carbonates into the interlayer region and thus sheet stacking continues.

Furthermore, another hypothesis has been based on a detailed study on distribution of NO_3^{1-} and H_2O in the interlayer and the strong supramolecular interaction between host and guest.[19] by Shi *et al.* suggested that this Jahn Teller effect on LDH structure is linked to the intermolecular effect of water on supramolecular Cu-Fe LDH. Based on the density functional theory it was proposed that Cu_3Fe-LDHs-.$_yH_2O$ geometry can be optimized by the controlled distribution of NO_3^{1-} and water of hydration.

For Cu^{2+}/ $M^{2+} \leq 1$, Cu^{2+} cations are far apart in the interlayer, which maintains an adequate distance for undistorted octahedra in the brucite-like sheet. If the ratio of Cu^{2+}/ $M^{2+} \geq 1$, the Cu^{2+} cations in octahedral position impose a distorted symmetry energetically favoured in comparison to the LDH structure.[2]

Against these, sometimes contradictory literature reports, we will present our results and discuss the effect of hydroxide solubilities on the synthesis of Cu-LDH in a further chapter.

2.6 From LDH to Mixed Metal Oxides (MMO)

The mixed metal oxides produced by the calcinations of LDH are generally more active as catalyst than the parent LDH[33], depending on the phases obtained as a function of the calcination temperatures used.[34] Metal oxides became an important class of catalysts in the mid 1950's when found to effectively catalyze some important redox and acid-base reactions. Recently, solid acid/base mixed metal oxide catalysts have widely been utilized and reported for applications in refining and petrochemical industry.[83] They are in good competition for replacing the homogenous catalysts to decrease the E-factor which, in a nutshell, is explained as "weight of waste/weight of product" by Sheldon.[35,36] Later, a lot of attention was given to the impact and influence of the chemical processes on the environment, which, in the case of homogeneous catalysis, is drastically affected.

2.6.1 Single and Mixed Metal Oxides

Mixed metal oxides are often preferred for their catalytic applications as compared to single metal oxides. The properties of surface metal ions and oxides can be tailored for their oxidation/reduction degree by being electron deficient and electron rich. Choice of transition metals is promising to achieve ease of continuity in the redox cycle. The advantage of using several transition metals is that electron transfer between metal cations with different redox potential can facilitate the regeneration of the catalyst in the reaction cycle.

Regardless of the redox properties of MMO, the properties of metal ions are significantly modified by matrix, concentration and the presence of co-cations associated with the system.[93] In some cases, the metal cations may act in a cooperative manner to catalytically promote the stepwise chemical process. Hence, the choice of cations in the mixed metal oxides is often considered keeping in mind the catalytic applications it will be used for.

2.6.1.1 Rehydration of Mixed Metal Oxides

A property of LDH-derived MMO is their ability to reverse to their initial precursor (lamellar hydroxide) when the mixed $M^{2+}(M^{3+})O$ oxide, obtained at moderate calcination temperature (450°C) is immersed in a solution of the anion to be intercalated [37,39] This phenomenon is known as the memory effect. For instance, Abello *et al*. studied a rehydration/memory effect in both gas and liquid phases on Mg/Al (3:1) LDH-derived mixed oxides (MgO, $Mg(Al)O_x$) obtained by sintering at 450°C for 15h. Vapour phase rehydration was done at room

temperature for 15h (40mL/min) under water-saturated argon gas flow to reattain the hydrotalcite structure. Liquid phase rehydration was carried out by treating MMO in decarbonated water (1g sample/100mL H_2O) at room temperature for 1h along with mechanical stirring (500rpm).[37] Similarly, synthetic hydrocalumite, a Ca/Al-LDH calcined at 500-900°C produced crystalline mayenite ($Ca_{12}Al_{14}O_{33}$) and lime (CaO), which were completely reversed to their original precursor structure at room temperature in deionized water.[125] Likewise, Mascolo was able to synthesize Li/Al-LDH directly from alumina xerogel and dissolved $LiOH.H_2O$.[126] Some other examples in the literature have long established the foregoing facts. [39]

2.6.2 Reaction Mechanism of Mixed Oxides

O^{2-} anions line the surface of oxide due to their large size in comparison to the cations (M^{n+}). This disturbs and eventually loses the coordination and symmetry of cations (M^{n+}) on the surface. The water vapors in the reaction system compensate for the surface unsaturation by the formation of surface hydroxyl groups ($M_2O + H_2O \rightarrow 2MO$). These hydroxyl groups are conjugated acids of lattice oxide ions O^{2-} which are strong bases and conjugated bases of water molecules.[36]

In addition, single and complex mixed metal oxides from the transition series are interesting by virtue of the unfilled 3d electron shell which creates non-stoichiometric phenomena. The transition of electron and formation of vacancies impart redox properties to the system as stated above. For instance, a change in the partial pressure of oxygen during the reaction may decide the fate of reaction to be oxidation or reduction. When the partial pressure of oxygen (pO_2) is low, oxygen is lost, which generates electrons, promoting n-type conductivity as $O_0 \leftrightarrow (1/2)\ O_2 + V_O^{\bullet\bullet} + 2e^-$. In case of high oxygen pressure, oxygen is incorporated into an oxygen vacancy and takes two electrons from the valence band, leading to a holes that contributing to the p-type conduction, as $(1/2)\ O_2 + V_O^{\bullet\bullet} \leftrightarrow O_0 + 2h^{\bullet}$.[36]

The selection of Layered Double Hydroxides (LDHs) as catalyst precursors is an attractive route to obtain oxides with high surface area, basic properties and homogenous mixture of mixed metal oxides. Oxides formed as a result of calcinations of LDH materials are small in crystal size, thermally stable and can recover their properties to form LDH parent material when contacting the product of the thermal treatment with water solution containing various ions.[2]

Valente and co-workers enquired the applications of Mg–Me–Al (Me: Cu, Fe, Ni, Zn) mixed oxides as bifunctional catalysts for conversion of 4-methylpentan-2-ol in a gas-phase.[40-43] The

extent of basicity and acidity can be controlled by the compositional ratio of metals, their type and valency.[40]

2.7 Calcination of LDH

LDHs calcination results in the formation of a mixture of phases. The nature of these phases is primarily dependent on the initial synthesis composition of LDH and the thermal treatments. Formation of homogeneous mixed metal oxides (MMO) solid solution is obtained as a result of progressive temperature increase in LDH materials which ultimately breaks the house of cards assembly of the structure. The thermal decomposition of the LDH material is associated with the structural composition of the layers such as the nature of cations employed, the interlayer anions, and the heating parameters (oxidative, reductive or inert atmosphere) used for calcinations. The first step in the calcination is the dehydration, where the loss of physically bound water molecules on the external crystallite surface takes place, followed by loss of water of crystallization in the interlayer region. This occurs between 100 and 250°C [44]. In the later step, hydroxyl groups coordinating with anions in the interlayer region are lost as water vapor. The LDH material is completely collapsed as the anions in the interlayer regions are lost at high temperature (>450°C) as shown from one of the examples here.

1. **Removal of water from precursor** (≈ 100-250°C)

$$[M^{2}_{1-x}M^{3}_{x}(OH)_2]^{x+}(A^{n-})_{x/n}.mH_2O\ (LDH) \longrightarrow [M^{2}_{1-x}M^{3}_{x}(OH)_2]^{x+}(A^{n-})_{x/n}$$

2. **Dehydroxylation** (350-450°C)

$$[M^{2}_{1-x}M^{3}_{x}(OH)_2]^{x+}(A^{n-})_{x/n} \longrightarrow [M^{2}_{1-x}M^{3}_{x}O]^{x+}(A^{n-})_{x/n}$$

3. **Decarbonation (Anion)** (420-470°C)

$$[M^{2}_{1-x}M^{3}_{x}O]^{x+}(A^{n-})_{x/n} \longrightarrow M^{2}_{1-x}M^{3}_{x}O_1 + {}_{x/2}(BO_y)$$

4. **Formation of mixed oxides** (450°C)

$$M^{2}_{1-x}M^{3}_{x}O_1 + {}_{x/2}(BO_y) \longrightarrow M^{2}O + M^{2}M^{3}O_4 + BO_y \qquad [9]$$

The loss of hydroxyl groups and interlayer anions, as well as the structural decomposition are often interpreted quantitatively by thermal gravimetry (TG) and Temperature-programmed decomposition/desorption (TPDD) analysis of the gases evolved inveterate the order of the decomposition sequence.[112, 113]

2.7.1 Oxides by Sintering of LDH

Sintering is a thermal treatment of powder catalysts at a temperature below the melting point for the purpose of increasing their strength by bonding the particles together. When subjected

to high temperature, the crystallites form new point of contact in such a way that the original inter-particles boundaries disappear, giving rise to new crystallization mosaics. Small catalyst particles with high surface area and a high reaction temperature are in general factors that increase the reactivity of a catalyst (see Fig. 2.7). However, these factors are also the circumstances under which sintering occurs.[132] For a porous catalytic surface, the pores may collapse due to sintering, resulting in loss of surface area and structural changes. However, the process is inevitable to carry out in order to stabilize the catalysts to be used in high temperature reactions.[73] In the field of catalysis, the term calcinations sometimes implicitly includes some sintering beyond its main effects of decomposition of carbonates, hydroxyls or other labile compounds in the precursor of the catalyst. Some examples from literature have been taken into account to highlight the effect of temperature on the oxide phases formed (Table 2.2).

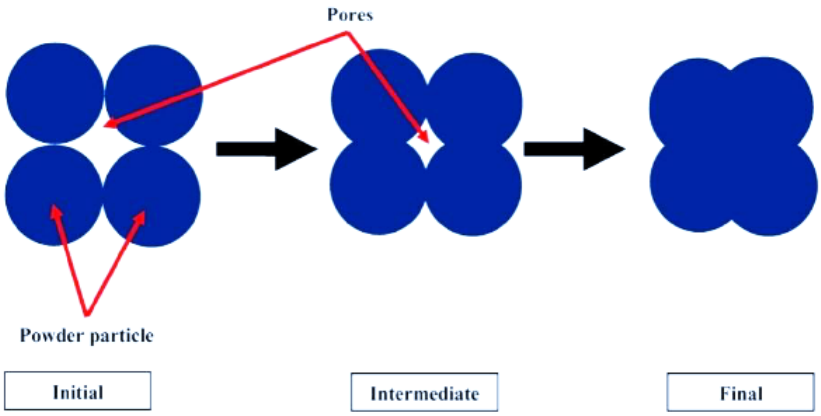

Figure 2.7 Powder particle sintering stages [131]

Table 2.2: Synthesis and calcination conditions reported for the preparation of mixed metal oxides from LDH

Precursor Catalyst	**M^{2+}/M^{3+}**	**Synthesis pH**	**Calcination Temp (°C)/ time(h)**	**Oxides formed**	**Surface area of mixed oxide (m^2g^{-1})**	**Ref**
Pd doped/ MgAl LDH	3	10	550/4	$Pd/MgO/Al_2O_3$	-	[49]
CuCoAl LDH	(5, 2, 1/2, 1/5)	6.5	450/5	Co_3O_4, CuO, CuCo	-	[50]
MgZnAl LDH	3	8	550/4	MgO	167	[40]

MgFeAl LDH	3	8	550/4	MgO	237	[40]
MgCuAl LDH	3	8	550/4	MgO, CuO	200	[40]
LaMgAl LDH	3	10	450/9	La_2O_3/MgO	301	[51]
Mg/Fe LDH	3	-	400 and 500/-	MgO	-	[52]
Ni/Fe LDH	3	-	400 and 500/-	NiO	-	[52]
Zn/Al LDH	2	-	450/14	$ZnAl_2O_4$, ZnO	38	[53]
Ni/Al LDH	3	-	650/-		-	[54]
Cu_{40}MgAl LDH	-	9.5-10	460/6	MgO/CuO	125	[55]
NiMgAl LDH	3	10	450/4	θ-Al_2O_3, $MgAl_2O_4$, k-Al_2O_3, MgO, NiO, Al_2O_3, $(Ni_{0.198}Al_{0.802})(Al_{1.198}Ni_{0.802})O_4$, $Mg_{0.36}Al_{2.44}O_4$	753	[38]
CoFe LDH	1/2	9.4	927/1	CoO, Co_3O_4 and $CoFe_2O_4$	< 5	[56]
CuMgFe LDH	3/3/2	10.5±0.2	450/5	CuO,$CuFe_2O_4$,Fe_2MgO_4, $MgCu_2O_3$	65.6	[96]
Mg/Al LDH	3	9.5	800/7	MgO,	236.3	[97]
CuFeMg LDH	4	7-8	600/5	MgO, $CuFe_2O_4$, Fe_2O_3	50.32	[98]
Ni/Co/Al	2	10	400/4	NiO,CoO,Co_3O_4	163	[108]
MgAl/Ga (5 wt %)	3	10	460/18h	MgO	-	[20]
Cu/Zn/Al	3	-	450	CuO, ZnO, $CuAl_2O_4$	143	[109]

The literature suggests that the variability of the surface area could subject to the synthesis conditions developed and phases formed.

2.7.1.1 Fractional crystallization in the preparation of Mixed Metal Oxides

Regardless of the nature of cations used, more importantly the calcination temperature effectively determines the qualitative and quantitative phase composition of the catalyst.[61] For instance, Babey and co-workers claimed that Co-Fe system as in $[Co_2Fe(OH)_6]$ (NO_3), nH_2O may have several possibilities of evolution upon decomposition. i) Below 900°C, the oxide product could form a single phase mixed oxide of different oxidation states of Co such type Co^2 $(Co^3, Fe^3)O_4$ ii) at 950°C, a possibility of formation of a normal spinel phase Co_3O_4 and inverse spinel $CoFe_2O_4$by demixtion of the original iron cobaltite.[57, 58] Vaccari and co-workers explained the synthesis of different mixed oxides of Ni/Al in the temperature range 350<T<800°C. The authors reported three different types of oxides. i) A NiO phase,

containing a small amount of Al^{3+} ions between 350-750°C. ii) a spinel-type phase ($NiAl_2O_4$) above 900°C. iii) An alumina-type phase (doped with small amounts of Ni^{2+} ions), grafted on the spinel-type phase.[59] Ferreira *et al*. studied structure and morphology of spinels; $FeCo_2O_4$ and $CoFe_2O_4$ produced by annealing between 300°C and 800°C. At 300°C, a heterogeneous chemical composition of spinel $CoFe_2O_4$ was observed until 500°C. At 900°C a single $CoFe_2O_4$ spinel was obtained whereas $FeCo_2O_4$ only appears above 900°C.[127] Ulibarri and colleagues studied the Cd/Al/Fe- LDH-derived calcined products with CdO crystallizing at 300°C, Spinel as $CdAl_2O_4$, $Cd_{1-x}Fe_{2+x}O_4$ and $Cd_xFe_{2.66}O_4$ observed at 800°C.[84] Leont'eva *et al.* reviewed nature and composition of some commonly known LDH-derived mixed oxides (Mg/Al, Ni/Al) focusing on the characterization techniques used for their determination.[60] Fornasari *et al.* also well studied the crystallographic parameters of the oxide and spinel phases formed by Ni/Mg/Al LDH as a function of composition and calcination temperature.[106]

As already cited for the Cd/Al/Fe system,[84] an interesting feature of the mixed metal oxides is the fractional crystallization of metal cations in the system. Fractional crystallization usually occurs when the temperature of calcination is relatively low and some cations form crystalline oxide phases more easily than other cations, leaving these last ones in the amorphous material formed by the dehydration and deanionisation of the LDH. A number of reports on mixed oxides from LDH have reported this fact.[2,9,44,84,128,129,135,147] In such cases, the authors mentioned to use other characterization techniques such as XPS[59], Raman[61], XANES spectroscopy[44] beyond elemental analysis to verify the presence of cations in the material not corresponding to phases determined by XRD.

Trifirò et *al.* studied the calcinations of Ni-Cr and Ni-Al LDHs.[59] They observed that, in bothcases, NiO was the only crystalline phase formed at 450°C, whereas $NiCr_2O_4$ appeared only at 600°C and $NiAl_2O_4$ appeared at 750°C. Rives *et al*. calcined the LDH with several amounts of Cu/Ni/Al (M^{2+}/M^{3+}=2) at 500°C leading to the formation of NiO and CuO crystallized phases but leaving Al in an amorphous material. However, increase in temperature to 850°C produced well crystallized NiO, CuO and $NiAl_2O_4$ with ratios depending on the amount of cations present in the system.[130]Bernal et *al.* observed a similar trend in Co-Fe system calcined at 1200°C where CoO, Co_3O_4 and $CoFe_2O_4$ (spinel), were detected, where spinel being the only phase, for large Fe contents.[56] Thermal decomposition of Cr^{3+}/Mg LDH calcined at 500°C leads to formation of MgO with traces of $MgCrO_4$ magnesium chromate whereas $MgCr_2O_4$ only appear at 750°C and becomes an important phase at 1000°C.[63]

2.8 Examples of LDH as efficient catalysts/supports for biomass (derived) molecules Conversion

Since the last decade, a great deal of research has been ongoing for environmentally benign heterogeneous catalytic processes for the depolymerisation of biomass and derived molecules. In this context, biomass and derived intermediates (platform molecules), such as 5-(hydroxymethyl) furfural (HMF), glycerol, furfural, levulinic acid, benzyl alcohol, cinnamaldehyde, glucose, fructose, etc. have been catalytically upgraded by layered double hydroxides. LDHs and their derived mixed metal oxides have been proven to be active and selective catalysts due to metal dispersion, environmental friendliness and easy recovery. Their bifunctional redox and/or controlled acid-base properties have listed them among the effective materials.

2.8.1 LDH as catalyst supports

Liang *et al.* reported a synthesis of bimetallic Au-Pd nanoparticles on a unique support of LDH derived Mg-Al mixed oxides (Au-Pd/MAO) to produce metal nanoparticles with high degree of coordinative unsaturation of metal atoms.[65] Au-Pd/MAO gave highly efficient aerobic solvent-free oxidation of benzyl alcohol and glycerol with a turnover frequency of 91000 h^{-1} at 160°C with molecular O_2 air pressure. Au-Pd/MAO was also found to have 98.5% conversion with a selectivity for tartronic acid (TARAC, 36.6%) in aerobic oxidation of glycerol. Similarly, Takagaki employed hydrotalcite supported ruthenium (Ru/HT) catalyst for the selective oxidative synthesis of 2, 5-Diformylfuran (DFF) from HMF in the presence of molecular oxygen under mild conditions of 120°C.[66] Another biomass-derived molecule, glycerol, was investigated for the oxidation to dicarboxylic acids (tartronic acids and oxalic acid) in the presence of cobalt-based catalysts.[67] Cobalt catalysts supported on $Mg_3Al(OH)_y(CO_3)z$ showed 100% conversion of glycerol with a selectivity of 64% tartronic acid and 24% oxalic acids under mild conditions of 55-70°C at 1MPa oxygen pressure. Several parameters, such as cobalt content, temperature, concentration-time profiles and possible reaction pathways were also discussed. Likewise, Yuan et *al.* studied the effect of series of catalysts such as MgO, H-beta zeolite, Al_2O_3, HZSM-5, and LDH precursors-supported platinum catalysts for the hydrogenolysis of glycerol to 1,2-propanediol in a base-free aqueous solution. [68] Results show that, due to strong alkalinity and high dispersion of Pt on the hydrotalcite precursor, LDH precursors-supported platinum catalyst showed the most favorable performance for the desired reaction, i.e. 93 % of selectivity and 92.1% of 1,2-propanediol at low pressure in base-free aqueous solution. Xia and co-workers have also

reported an extraordinary conversion and selectivity of glycerol to 1,2-propanediol by a series of bimetallic Pd/Cu ($PdxCu_{0.4}Mg_{5.6}{-}xAl_2(OH)_{16}CO_3$ crystals) solid base catalysts.[70] On $Pd_{0.04}Cu_{0.4}/Mg_{5.56}Al_2O_{8.56}$, at 180°C, 2MPa pressure of H_2 in an ethanol solution for 10h, 88% conversion and 99.6% of selectivity were achieved. The catalyst has been reported to be stable upto five recycles. Similarly, Yuan *et al.* worked on catalytic hydrogenolysis of glycerol by a homogenously dispersed copper on a solid base ($Cu_{0.4}/Mg_{5.6}Al_2O_{8.6}$-CP, with 80.1% copper dispersion) obtained by thermal reductive decomposition at 300°C of $Cu_{0.4}Mg_{5.6}Al_2(OH)_{16}CO_3$ LDH.[69] At 180°C, in the presence of 3MPa H_2 in 20 hours, the base catalysts offered 80% conversion of glycerol with a selectivity of 98.2% of 1, 2-propanediol.

2.8.2 LDH as catalysts

Castiglioni *et al.* investigated the physical and catalytic properties of mixed oxides obtained from Cu/Zn/Al LDH as a function of surface area and porosity for the selective vapor phase hydrogenation of maleic anhydride as an alternative to Cr-containing catalysts.[111] The study shows that Cu/Zn/Al in 25:25:50 ratio is a best compromise, allowing low temperature and high yield conversion to γ-Butyrolactone (GBL). Yan *et al.* synthesized a series of selective Cu (Cr, Al, Fe)-catalysts derived from hydrotalcite precursors for the hydrogenation of biomass-derived furfural and levulinic acid.[64] Cu–Fe oxides were the most effective catalysts under optimized conditions reported. Up to 90% yield of furfuryl alcohol at 160°C in 5 hours and 51% yield of 2-methylfuran at 220°C in 14 hours were achieved in the selective hydrogenation of furfural and 91% yield of c-valerolactone was achieved in the hydrogenation of levulinic acid at 200°C in 10 hours. Hansen et *al.* discussed the one-pot reduction of HMF in the presence of supercritical methanol via hydrogen transfer method at 300°C by a copper-containing porous metal oxide (Cu–PMO) obtained by the calcinations of a hydrotalcite.[71] Zhang *et al*. studied the copper catalysts (Cu_XAl) derived from LDH for selective transfer hydrogenation of furfural (FFR) to furfuryl alcohol (FA) and 2-methyl furan (MF) using methanol as a hydrogen donor solvent.[107] High yield of 94 mol % has been reported at 200°C in methanol. The copper catalyst was further treated with H_2/N_2 at 500°C forming the metallic Cu^{2+} species which catalyzed conversion of FRR to MF at 240°C yielding 94.1% mol. Also the activated Cu^{2+} gave remarkable performance in converting HMF to 2, 5-dimethylfuran (DMF). Yan and fellows summarized several methods of LDH synthesis and biomass degradation processes by their corresponding oxides.[72] Considerable selectivity, reactivity, metal dispersion, and improved methods of catalysts recovery have been discussed.

2.9 Examples of LDH as efficient catalysts for depolymerisation of lignin and its models

The layered double hydroxides have been known for long as effective depolymerisation catalysts for lignin, either as precursors in the formation of direct catalysts or as active supports for multifunctional catalysts.[62] Huang *et al*. investigated the role of varying percentage of Cu in a Cu-Mg-Al mixed oxides system obtained from LDH for the depolymerisation of soda lignin in supercritical ethanol.[55] The 20 wt % Cu catalyst was considered optimum for the process which produced 36% monomers at 340°C for 4h without the formation of char. Barta et *al.* investigated disassembling of the organosolv lignin using the mixed oxides catalysts obtained from 20% Cu-doped hydrotalcite and supercritical methanol acting as H-transfer reagent.[74] The catalyst was reported to have completely hydrogenated the phenyl ether bonds along with the hydrogenation of aromatic rings at supercritical methanol conditions (300°C). The same group of Barta et *al.* later also conducted catalytic depolymerisation on solvent-extracted lignin from candlenut biomass using methanol and H_2 in the presence of porous metal oxide catalyst (PMO) derived from a Cu-doped hydrotalcite-like precursor.[75] Cu-PMO produced mixture of aromatic compounds in high yields from low molecular weight lignin without formation of char. Lignin conversion of >90% and high yields of methanol-soluble products (>70%) with optimized catalyst and biomass loading was achieved at 180°C.[75]

2.10 Prospective

A variety of binary and ternary LDHs-derived mixed oxides can be synthesized by changing the cation ratios and physical parameters of synthesis to carry out selective catalysis aimed at desired products. Tailor-made properties can offer outstanding conversion and selectivity performance. More investigation needs to be done to apprehend the formation mechanism and properties of amorphous state of cations in the catalysts. These studies have merely been reported in the literature since the characterization of amorphous phase is arduous. In this present study, we have carried out attempts to quantify the amorphous phase present in LDH samples with different compositions, synthesized under the same condition and calcined at different temperatures. Furthermore, a detailed study on the amorphous material and its characteristic role in catalytic reactions has been performed.

References

[1] R.L. Frost, M.L. Weier, M.E. Clissold, P.A. Williams, Infrared spectroscopic study of natural hydrotalcites carrboydite and hydrohonessite. Spectrochim Acta A Mol Biomol Spectrosc. 59, 14 (2003) 3313-3319.

[2] F. Cavani, F. Trifirò, A. Vaccari, Hydrotalcite-type anionic clays: Preparation, properties and applications. Catal. Today. 11, 2 (1991) 173-30.

[3] E. Manasse, Idrotalcite e piroaurite. Atti della Societa Toscana di Scienze Naturali, 24 (1915) 92–105.

[4] F.J. Brocker, L. Kainer, German Patent 2,024,282 (1970) to BASF AG, and UK Patent 1,342,020 (1971) to BASF AG.

[5] F. Prinetto, G. Ghiotti, R. Durand, D. Tichit, Investigation of acid−base properties of catalysts obtained from layered double hydroxides. J. Phys. Chem. B, 104, 47 (2000) 11117–11126.

[6] S. Miyata, T. Hirose, Adsorption of N_2, O_2, CO_2, and H_2 on hydrotalcite-like system: Mg^{2+}-Al^{3+}-$(Fe\ (CN)_6)_4$. Clays Clay Miner. 26, 6 (1978) 441-447.

[7] S.P. Newman, W. Jones, Synthesis, characterization and applications of layered double hydroxides containing organic guests. New J. Chem. 22 (1998) 105-115.

[8] S.B. Khan, A.M. Asiri, K. Akhtar, M. AbdulRub, Development of electrochemical sensor based on layered double hydroxide as a marker of environmental toxin. J Ind Eng Chem. 30 (2015) 234-238.

[9] Z.P. Xu, J. Zhang, M.O. Adebajo, H. Zhang, C. Zhou, Catalytic applications of layered double hydroxides and derivatives. Appl. Clay Sci. 53, 2 (2011) 139-150.

[10] D. Tichit, C. Gerardin, R. Durand, B. Coq, Layered double hydroxides: precursors for multifunctional catalysts. Top Catal. 2006. 39, 1 (2006) 89-96.

[11] M. Sarfraz, I. Shakir, Recent advances in layered double hydroxides as electrode materials for high-performance electrochemical energy storage devices. J. Energy Storage. 13 (2017) 103-122.

[12] T. Nishimura, N. Kakiuchi , M. Inoue, S. Uemura, Palladium(ii)-supported hydrotalcite as a catalyst for selective oxidation of alcohols using molecular oxygen. Chem. Commun. 14 (2000) 1245-1246.

[13] W.T. Reichle, Synthesis of anionic clay minerals (mixed metal hydroxides, hydrotalcite). Solid State Ionics. 22, 1 (1986) 135-141.

[14] T. Li, H.N. Miras, Y.F. Song, Polyoxometalate (POM)-Layered Double Hydroxides (LDH) Composite Materials: Design and Catalytic Applications. Catalysts, 7 (2017) 260.

[15] A.D. Roy, C. Forano, J.P. Besse, Layered double hydroxides: synthesis and post-synthesis modification in V. Rives (Ed.) in Layered Double Hydroxides: Present and Future, Nova Science Publishers, New York (2001) 1-39.

[16] V.A. Drits, T.N. Sokolova, G.V. Sokolova, V.I. Cherkashin, New members of the hydrotalcite-manasseite group. Clays Clay Miner. 35, 6 (1987) 401-417.

[17] J. Li, S. Zhang, Y. Chen, T. Liu, C. Liu, X. Zhang, M. Yi, Z. Chu, X. Han, A novel three-dimensional hierarchical CuAl layered double hydroxide with excellent catalytic activity for degradation of methyl orange. RSC Adv. 7, 46 (2017) 29051-29057

[18]J. Liu, P. Yao, Z-M. Ni, Y. Li, W. Shi, Jahn-Teller Effect of Cu-Mg-Al Layered Double Hydroxides. Acta Phys.-Chim. Sin. 27, 9 (2011) 2088-2094.

[19]W. Shi, J. Hu, Z-M. Ni, Y. Li, J. Liu, Influence of Interlayer Water Content on Supermolecular Interaction of Copper-Iron Layered Double Hydroxides. Acta Physico-Chimica Sinica, 28, 8 (2012) 1869-1876.

[20]O. D. Pavel, R. Zavoianu, E. Angelescu, The effect of modifying cations on the catalytic activity of hydrotalcite-like compounds in 1, 4-addition reactions. Rev. Roum. Chim. 61, 8-9 (2016) 671-681.

[21]A.M. Fogg, V.M. Green, H.G. Harvey, D. O'Hare, New Separation Science Using Shape-Selective Ion Exchange Intercalation Chemistry. Adv. Mater., 11, 17 (1999) 1466-1469.
[22] S. Marappa, S. Radha, P.V. Kamath, Nitrate-Intercalated Layered Double Hydroxides – Structure Model, Order, and Disorder. Eur. J. Inorg. Chem. 12 (2013) 2122-2128.
[23] V.R.L. Constantino, T.J. Pinnavaia, Basic Properties of $Mg^{2+}_{1-x}Al^{3+}_{x}$ Layered Double Hydroxides Intercalated by Carbonate, Hydroxide, Chloride, and Sulfate Anions. Inorganic Chemistry, 34, 4 (1995) 883-892.
[24] Y. Li, X. Yang, Y. Wang, Preparation of the 12-Molybdophosphoric Acid-Layered Double Hydroxides Nanocomposite Hybrid and its Electrocatalytic Reduction of Halate Ions. Analytical Letters, 45, 13 (2012) 1910-1918.
[25] Y. Jia, Y. Fang, Y. Zhang, H.N. Miras, Y.F. Song, Classical Keggin Intercalated into Layered Double Hydroxides: Facile Preparation and Catalytic Efficiency in Knoevenagel Condensation Reactions. Chem. Eur. J. 21, 42 (2015) 14862-14870.
[26] S. Carlino, The intercalation of carboxylic acids into layered double hydroxides: a critical evaluation and review of the different methods. Solid State Ionics. 98, 1 (1997) 73-84.
[27] J.T. Kloprogge, L. Hickey, R.L. Frost, The effects of synthesis pH and hydrothermal treatment on the formation of zinc aluminum hydrotalcites. J. Solid State Chem. 177, 11 (2004) 4047-4057.
[28] D.P. Debecker, E.M. Gaigneaux, G. Busca, Exploring, tuning, and exploiting the basicity of hydrotalcites for applications in heterogeneous catalysis. Chem. Eur. J. 15, 16 (2009) 3920-3935.
[29] A. Jaiswal, M.C. Chattopadhyaya, Synthesis and characterization of novel Co/Bi-layered double hydroxides and their adsorption performance for lead in aqueous solution. Arab. J. Chem. 10 (2017) S2457-S2463.
[30] D. Tichit, F. Fajula, Layered double hydroxides as solid base catalysts and catalyst precursors. Stud Surf Sci Catal. 125 (1999) 329-340.
[31] D. Tichit, A.Vaccari, Editorial. Appli. Clay Sci., 13, 5 (1998) 311-315.
[32] A. Monzon, E. Romeo, A. Marchi, Hydrogenation catalysis by mixed oxides prepared from LDHs in V. Rives (Ed.) in Layered Double Hydroxides: Present and Future, Nova Science Publishers, New York (2001) 323-382.
[33] R. Chitrakar, A. Sonoda, Y. Makita, T. Hirotsu, Calcined Mg–Al layered double hydroxides for uptake of trace levels of bromate from aqueous solution. Ind. Eng. Chem. Res., 50, 15 (2011) 9280–9285.
[34] X. Zhao, F. Zhang, S. Xu, D. G. Evans, X. Duan, From layered double hydroxides to ZnO-based mixed metal oxides by thermal decomposition: transformation mechanism and UV-blocking properties of the product. Chem. Mater. 22, 13 (2010) 3933–3942.
[35] R.A. Sheldon, The E Factor: fifteen years on. Green Chem. 9, 12 (2007) 1273-1283.
[36] J.C. Védrine, Heterogeneous catalysis on metal oxides. Catalysts, 7, 11 (2017) 341.
[37]S. Abelló, F. Medina, D. Tichit, J.P. Ramírez, J.C. Groen, J.E. Sueiras, P. Salagre, Y. Cesteros, Aldol Condensations Over Reconstructed Mg–Al Hydrotalcites: Structure–Activity Relationships Related to the Rehydration Method. Chem Eur J. 11, 2 (2005) 728-39.
[38] D. Bharali, R. Devi, P. Bharali, R.C. Deka, Synthesis of high surface area mixed metal oxide from the NiMgAl LDH precursor for nitro-aldol condensation reaction. New J. Chem. 39, 1 (2015) 172-178.
[39] G. Mascolo, M.C. Mascolo, On the synthesis of layered double hydroxides (LDHs) by reconstruction method based on the "memory effect". Microporous Mesoporous Mater. 214, (2015) 246-248.
[40] J.S.Valente, J.H. Cortez, M.S. Cantu, G. Ferrat, E.L. Salinas, Calcined layered double hydroxides Mg–Me–Al (Me: Cu, Fe, Ni, Zn) as bifunctional catalysts. Catal. Today. 150, 3 (2010) 340-345.

[41] A.M. Robinson, J.E. Hensley, J.W. Medlin, Bifunctional Catalysts for Upgrading of Biomass-Derived Oxygenates: A Review. ACS Catal. 6, 8 (2016) 5026–5043
[42] L. Faba, E. Díaz, S. Ordóñez, Improvement of the stability of basic mixed oxides used as catalysts for aldol condensation of bio-derived compounds by palladium addition. Biomass Bioenergy, 56 (2013) 592-599.
[43] K.K. Ramasamy, M. Gray, H. Job, C. Smith, Y. Wang, Tunable catalytic properties of bi-functional mixed oxides in ethanol conversion to high value compounds. Catal. Today. 269 (2016) 82-87.
[44] V. Rives, Characterisation of layered double hydroxides and their decomposition products. Mater. Chem. Phys, 75, 1-3 (2002) 19-25.
[45] J.W. Boclair, P.S. Braterman, Layered double hydroxide stability. 1. Relative stabilities of layered double hydroxides and their simple counterparts. Chem. Mater. 11,2 (1999) 298-302.
[46] A. Seron, F. Delorme, Synthesis of layered double hydroxides (LDHs) with varying pH: A valuable contribution to the study of Mg/Al LDH formation mechanism. J. Phys. Chem. Solids 69, 5-6 (2008) 1088-1090.
[47] A.A. Eliseev, A.V. Lukashin, A.A. Vertegel, V.P. Tarasov, Y.D. Tret'yakov, A study of crystallization of Mg–Al double hydroxides. Dokl Chem. 387, 4-6 (2002) 339-343.
[48] B.Grégoire, C.Ruby, C.Carteret, Hydrolysis of mixed Ni^{2+}–Fe^{3+} and Mg^{2+}–Fe^{3+} solutions and mechanism of formation of layered double hydroxides. Dalton Trans. 42, 44 (2013) 15687-15698.
[49] Z. Wu, Q. Zhu, C. Shen, T.Tan, Monodispersed Pd Nanoparticles Supported on Mg–Al Mixed Metal Oxides: A Green and Controllable Synthesis. ACS Omega, 1, 4 (2016) 498–506.
[50] W. Gao, Y. Zhao,H. Chen, H. Chen,Y. Li, S. He, Y. Zhang, M. Wei, D. G. Evans, X. Duan, Core–shell Cu@(CuCo-alloy)/Al2O3 catalysts for the synthesis of higher alcohols from syngas. Green Chem. 17, 3 (2015) 1525-1534.
[51] N. Balsamo, S. Mendieta. M. Oliva, G. Eimer, M. Crivello, Synthesis and Characterization of Metal Mixed Oxides from Layered Double Hydroxides. Procedia Mat. Sci. 1, (2012) 506-513.
[52] R. Elmoubarki, F.Z. Mahjoubi, A. Elhalil, H. Tounsadi, M. Abdennouri, M. Sadiq, S. Qourzal, A. Zouhri, N. Barka, Ni/Fe and Mg/Fe layered double hydroxides and their calcined derivatives: preparation, characterization and application on textile dyes removal. J. of Mat. Res. & Tech. 6, 3 (2017) 271-283.
[53] W. Kagunya, Z. Hassan, W. Jones, Catalytic Properties of Layered Double Hydroxides and Their Calcined Derivatives. Inorg. Chem. 35, 21 (1996) 5970-5974.
[54] N.S. Puttaswamy, P.V. Kamath, Reversible thermal behaviour of layered double hydroxides:a thermogravimetric study. J. of Mat. Chem. 7, 9 (1997) 1941-1945.
[55] X. Huang, C. Atay, T. I. Korányi, M. D. Boot, E. J. M. Hensen, Role of Cu–Mg–Al Mixed Oxide Catalysts in Lignin Depolymerisation in Supercritical Ethanol. ACS Catal. 5, 12 (2015) 7359-7370.
[56] M.E.P. Bernal, R.J.R. Casero, V. Rives, Preparation and properties of Co-Fe mixed oxides obtained by calcination of layered double hydroxides. Ceramics-Silikáty. 48, 4 (2004) 145-154.
[57] S. Babay, A. Bulou, A. M. Mercier, M. Toumi, The decomposition of the layered double hydroxides of Co and Al: Phase segregation of a new single phase spinel oxide. Spectrochimica Acta Part A: Mol. & Biomol. Spectroscopy. 141, 15 (2015) 80-87.
[58] M. Takahashi, M.E.Fine, Magnetic behavior of quenched and aged $CoFe_2O_4$–Co_3O_4 alloys. J. Appl. Phys. 43, 10 (1972) 4205-4216.
[59] F. Trifirò, A. Vaccari, O. Clause. Nature and properties of nickel-containing mixed oxides obtained from hydrotalcite-type anionic clays. Catal. Today. 21, 1 (1994) 185-195.

[60] N.N. Leont'eva, S.V. Cherepanova, V.A. Drozdov, Thermal decomposition of layered double hydroxides Mg-Al, Ni-Al, Mg-Ga: Structural features of hydroxide, dehydrated, and oxide phases. J. Struct. Chem. 55, 7 (2014) 1326-1341.
[61] F. Kovanda, T. Rojka, J. Dobešová, V. Machovič, P. Bezdička, L. Obalová, T. Grygar, Mixed oxides obtained from Co and Mn containing layered double hydroxides: Preparation, characterization, and catalytic properties. J. Solid State Chem.179, 3 (2006) 812-823.
[62] W.Y. Hernández, J. Lauwaert, P.V.D. Voort, A. Verberckmoes, Recent advances on the utilization of layered double hydroxides (LDHs) and related heterogeneous catalysts in a lignocellulosic-feedstock biorefinery scheme. Green Chem, 19, 22 (2017) 5269-5302.
[63] F.M. Labajos, V. Rives, Thermal Evolution of Chromium (III) Ions in Hydrotalcite-like Compounds. Inorg. Chem. 35, 18 (1996) 5313-5318.
[64] K. Yan, J. Liao, X. Wu, X. Xie, A noble-metal free Cu-catalyst derived from hydrotalcite for highly efficient hydrogenation of biomass-derived furfural and levulinic acid. RSC Adv. 3, 12 (2013) 3853-3856.
[65] L. Wang, W. Zhang, S. Zeng, D. Su, X. Meng, F. Xiao, Mg-Al Mixed Oxides Supported Bimetallic Au-Pd Nanoparticles with Superior Catalytic Properties in Aerobic Oxidation of Benzyl Alcohol and Glycerol. Chin. J. Chem. 30, 9 (2012) 2189-2197.
[66] A. Takagaki, M. Takahashi, S. Nishimura, K. Ebitani, One-Pot Synthesis of 2,5-Diformylfuran from Carbohydrate Derivatives by Sulfonated Resin and Hydrotalcite-Supported Ruthenium Catalysts. ACS Catal. 1, 11 (2011) 1562-1565.
[67] X. Jin, M. Zhao, C. Zeng, W. Yan, Z. Song, P.S. Thapa, B. Subramaniam, R.V. Chaudhari, Oxidation of Glycerol to Dicarboxylic Acids Using Cobalt Catalysts. ACS Catal. 6, 7 (2016) 4576-4583.
[68] Z. Yuan, P. Wu, J. Gao, X. Lu, Z. Hou, X. Zheng, Pt/solid-base: a predominant catalyst for glycerol hydrogenolysis in a base-free aqueous solution. Catal Letters. 130, 1-2 (2009) 261-265.
[69] Z. Yuan, L. Wang, J. Wang, S. Xia, P. Chen, Z. Hou, X. Zheng, Hydrogenolysis of glycerol over homogenously dispersed copper on solid base catalysts. Appl Catal B. 101, 3 (2011) 431-440.
[70] S. Xia, Z. Yuan, L. Wang, P. Chen, Z. Hou, Hydrogenolysis of glycerol on bimetallic Pd-Cu/solid-base catalysts prepared via layered double hydroxides precursors. Appl. Catal., A. 403, 1 (2011) 173-182.
[71]T.S. Hansen, K. Barta, P.T. Anastas, P.C. Ford, A. Riisager, One-pot reduction of 5-hydroxymethylfurfural via hydrogen transfer from supercritical methanol. Green Chem. 14, 9 (2012) 2457-2461.
[72] K. Yan, Y. Liu, Y. Lu, J. Chai, L. Sun, Catalytic application of layered double hydroxide-derived catalysts for the conversion of biomass-derived molecules. Catal. Sci. & Tech. 7, 8 (2017) 1622-1645.
[73] G. Kuczynski (Ed.) Sintering and catalysis. Springer Science & Business Media. Plenum Press Newyork, USA 10 (2012).
[74] K. Barta, T.D. Matson, M.L. Fettig, S.L. Scott, A. V. Iretskii, P.C. Ford, Catalytic disassembly of an organosolv lignin via hydrogen transfer from supercritical methanol. Green Chem. 12, 9 (2010) 1640-1647.
[75] K. Barta, G.R. Warner, E.S. Beach, P.T. Anastas, Depolymerisation of organosolv lignin to aromatic compounds over Cu-doped porous metal oxides. Green Chem. 16, 1 (2014) 191-196.
[76] MINDAT [Web Database] consulted on 05.09.2018.
[77] Y. Yang, X. Zhao, Y. Zhu, F. Zhang, Transformation mechanism of magnesium and aluminum precursor solution into crystallites of layered double hydroxide. Chem. Mater., 241 (2011) 81-87.

[78] K. Ruengkajorn, V. Erastova, J.C. Buffet, H.C. Greenwell, D. O'Hare Aqueous Immiscible Layered Double Hydroxides: Synthesis, Characterisation and Molecular Dynamics Simulation. Chem. Commun. 54, 35 (2018) 4394-4397.
[79] C. Barriga, W. Jones, P. Malet, V. Rives, M.A. Ulibarri, Synthesis and Characterization of Polyoxovanadate-Pillared Zn−Al Layered Double Hydroxides: An X-ray Absorption and Diffraction Study. Inorg. Chem., 37, 8 (1998) 1812–1820.
[80] C.A.S. Barbosa, A.M.D.C. Ferreira, V.R.L. Constantino, Synthesis and Characterization of Magnesium-Aluminum Layered Double Hydroxides Containing (Tetrasulfonated porphyrin)cobalt, Eur. J. Inorg. Chem. 2005, 8 (2005) 1577-1584.
[81] B. Balcomb, M. Singh, S. Singh, Synthesis and Characterization of Layered Double Hydroxides and Their Potential as Nonviral Gene Delivery Vehicles. ChemistryOpen. 4, 2 (2015) 137-145.
[82] A.P. Tathod, O.M. Gazit, Fundamental Insights into the Nucleation and Growth of Mg−Al Layered Double Hydroxides Nanoparticles at Low Temperature. Cryst. Growth Des. 16, 12 (2016) 6709–6713.
[83]S. Badoga, R.V. Sharma, A.K. Dalai, J. Adjaye, Hydrotreating of Heavy Gas Oil on Mesoporous Mixed Metal Oxides (M–Al_2O_3, M = TiO_2, ZrO_2, SnO_2) Supported NiMo Catalysts: Influence of Surface Acidity. *Ind. Eng. Chem. Res.* 53, 49 (2014) 18729–18739.
[84] M.R. Pérez, C. Barriga, J.M. Fernández, V. Rives, M.A. Ulibarri, Synthesis of Cd/(Al+Fe) layered double hydroxides and characterization of the calcination products. J. Solid State Chem. 180, 12 (2007) 3434-3442.
[85] S.J. Mills, A.G. Christy, J. M. Génin, T. Kameda, F. Colombo, Nomenclature of the hydrotalcite supergroup: natural layered double hydroxides. Mineralogical Mag, 76, 5 (2012) 1289-1336.
[86]J.D. Dana, E.S. Dana, 16b.06,0.1.01, Sjogrenite-Hydrotalcite in the Dana's New Mineralogy: The System of Mineralogy 8th edition (1944) 501.
[87]Wikipedia contributors. Jahn–Teller effect. In Wikipedia, The Free Encyclopedia. consulted on September 15, 2018, from [https://en.wikipedia.org/w/index.php?title=Jahn%E2%80%93Teller_effect&oldid=859286236].
[88] S. Consani, T.B. Zunic, A.M. Cardinale, W. Sgroi, G. Giuli, C. Carbone, A Novel Synthesis Routine for Woodwardite and Its Affinity towards Light (La, Ce, Nd) and Heavy (Gd and Y) Rare Earth Elements. Materials. 11, 1 (2018) 130.
[89] D. Li, Y. Cai, Y. Ding, R. Li, M. Lu, L. Jiang, Layered double hydroxides as precursors of Cu catalysts for hydrogen production by water-gas shift reaction. Int J Hydrogen Energy. 40, 32 (2015) 10016-10025.
[90] S.R. Segal, K.B. Anderson, K.A. Carrado, C.L. Marshall, Low temperature steam reforming of methanol over layered double hydroxide-derived catalysts. Applied Catalysis A: General. 231, 1-2 (2002) 215-226.
[91] S.R. Segal, K.A. Carrado, C.L. Marshall, K.B. Anderson, Catalytic decomposition of alcohols, including ethanol, for in situ H_2 generation in a fuel stream using a layered double hydroxide-derived catalyst. Appl. Catal. A. 2481-2 (2003) 33-45.
[92] M.L. Kantam, R. Arundhathi, P.R. Likhar, D. Damodara, Reusable Copper-Aluminum Hydrotalcite/rac-BINOL System for Room Temperature Selective Aerobic Oxidation of Alcohols. Advanced Synthesis & Catalysis, 351, 16 (2009) 2633-2637.
[93] V. Rives, A. Dubey, S. Kannan, Synthesis, characterization and catalytic hydroxylation of phenol over CuCoAl ternary hydrotalcites. Phys Chem Chem Phys. 3, 21 (2001) 4826-4836.
[94] A. Dubey, V. Rives, S. Kannan, Catalytic hydroxylation of phenol over ternary hydrotalcites containing Cu, Ni and Al. J. Mol. Catal. A, Chem. 181, 1-2 (2002) 151-160.

[95] C. Lucarell, C. Molinari, R. Faure, G. Fornasari, D. Gary, N. Schiaroli, A. Vaccari, Novel Cu-Zn-Al catalysts obtained from hydrotalcite-type precursors for middle-temperature water-gas shift applications. Appl. Clay Sci. 155 (2018) 103-110.
[96] Y. Chen, J. Yan, D. Ouyang, L. Qian, L. Han, M. Chen, Heterogeneously catalyzed persulfate by CuMgFe layered double oxide for the degradation of phenol. Appl. Catal., A. 538 (2017) 19-26.
[97] G. Carja, R. Nakamura, H. Niiyama, Copper and iron substituted hydrotalcites: properties and catalyst precursors for methylamines synthesis. Appl. Catal., A. 236, 1-2 (2002) 91-102.
[98] W. Gao, Y. Zhao, J. Liu, Q. Huang, S. He, C. Li, M. Wei, Catalytic conversion of syngas to mixed alcohols over CuFe-based catalysts derived from layered double hydroxides. Catal Sci Technol. 3, 5 (2013) 1324-1332.
[99] A.M. Fogg, G.R. Williams, R. Chester, D. O'Hare, A novel family of layered double hydroxides—$[MAl_4(OH)_{12}](NO_3)_2 \cdot xH_2O$ (M= Co, Ni, Cu, Zn). J. Mater. Chem. 14, 15 (2004) 2369-2371.
[100] Y. Lwin, A. B. Mohamad, Z. Yaakob, W.R.W. Daud, XRD and TPR studies of Cu-Al hydrotalcite derived highly dispersed mixed metal oxides. React Kinet Catal L., 70, 2 (2000) 303-310.
[101] I.Y. Park, K. Kuroda, C. Kato, Preparation of complex copper aluminum double hydroxide phases from copper (II) ammine complex solutions. Solid State Ion. 42, 3-4 (1990) 197-203.
[102] M. Rajamathi, P.V. Kamath, Ageing behaviour of unary hydroxides in trivalent metal salt solutions: Formation of layered double hydroxide (LDH)-like phases. Bull. Mater. Sci. 23, 5 (2000) 355-359.
[103]R.P.J Grosso, S.L. Suib, R.S. Weber, P.F. Schubert, Main effects in the syntheses of copper/chromium layered double hydroxides. Chem. Mater. 4, 4 (1992) 922-928.
[104] J. Wang, Y. Tian, R. C. Wang, A. Clearfield, Pillaring of layered double hydroxides with polyoxometalates in aqueous solution without use of preswelling agents. Chem. Mater. 4, 6 (1992) 1276-1282.
[105] S. Velu, K. Suzuki, M.P. Kapoor, F. Ohashi, T. Osaki, Oxidative steam reforming of methanol over CuZnAl(Zr)-oxide catalysts for the selective production of hydrogen for fuel cells: catalyst characterization and performance evaluation. J Catal, 194, 2 (2000) 373-384.
[106] G. Fornasari, M. Gazzano, D. Matteuzzi, F. Trifirò, A. Vaccari, Structure and reactivity of high-surface-area Ni/Mg/Al mixed oxides. Appl. Clay Sci. 10, 1-2 (1995) 69-82.
[107] J. Zhang, J. Chen, Selective transfer hydrogenation of biomass-based furfural and 5-hydroxymethylfurfural over hydrotalcite-derived copper catalysts using methanol as a hydrogen donor. ACS Sustain Chem Eng. 5, 7 (2017) 5982-5993.
[108] T.P. Sulmonetti, S.H. Pang, M.T. Claure, S. Lee, D.A. Cullen, P.K. Agrawal, C.W. Jones, Vapor phase hydrogenation of furfural over nickel mixed metal oxide catalysts derived from layered double hydroxides. Appl. Catal., A. 517 (2016) 187-195.
[109] S.M. Mascarós, R.M. Navarro, L.G. Sainero, U. Costantino, M. Nocchetti, J.L.G. Fierro, Oxidative methanol reforming reactions on CuZnAl catalysts derived from hydrotalcite-like precursors. J. Catal 198, 2 (2001) 338-347.
[110] L. Zhao, X. Li, J. Zhao, Correlation of structural and chemical characteristics with catalytic performance of hydrotalcite-based CuNiAl mixed oxides for SO_2 abatement. Chem Eng J. 223 (2013) 164-171.
[111] G.L. Castiglioni, A. Guercio, A. Vaccari, R. Lancia, Porosity-activity relationships in selective vapour phase hydrogenation of maleic anhydride on Al-containing catalysts. J Porous *Mat*. 2, 1 (1995) 79-84.
[112] P. Bera, M. Rajamathi, M.S. Hedge, P.V. Kamath, Thermal behaviour of hydroxides, hydroxysalts and hydrotalcites. Bull. Mater. Sci. 23, 2 (2000) 141-145.

[113] V. Rives, Comment on “Direct Observation of a Metastable Solid Phase of Mg/Al/CO_3 -Layered Double Hydroxide by Means of High-Temperature in Situ Powder XRD and DTA/TG”. Inorg. Chem. 38, 2 (1999) 406–407.
[114] G. Mishra, B. Dash, S. Pandey, Layered double hydroxides: A brief review from fundamentals to application as evolving biomaterials. Appl. Clay Sci. 153 (2018) 172-186.
[115] R. Allmann, N. Refinement of the hybrid layer structure, Jhb. Miner. Mh. 3 (1977) 136-144.
[116] G. Mascolo, O. Marino, A new synthesis and characterization of magnesium-aluminium hydroxides. Mineral Mag. 43, 329 (1980) 619-621.
[117] C. Sambiagio, S.P. Marsden, A.J. Blacker, P.C. McGowan, Copper catalysed Ullmann type chemistry: from mechanistic aspects to modern development. Chem. Soc. Rev. 43, 10 (2014) 3525-3550.
[118] Y. Liu, S.K. Park, Y. Xiao, J. Chae, Copper (ii)-catalyzed C–O coupling of aryl bromides with aliphatic diols: synthesis of ethers, phenols, and benzo-fused cyclic ethers. Org. Biomol. Chem. 12, 26 (2014) 4747-4753.
[119] S.V. Ley, A.W. Thomas, Modern synthetic methods for copper-mediated C (aryl)-O. C (aryl)-N, and C (aryl-S Bond Formation. Angew. Chem. Int. Ed. 42 (2003) 5400-5449.
[120] S. Reymond, J. Cossy, Copper-Catalyzed Diels−Alder Reactions. Chem. Rev. 108, 12 (2008) 5359-5406.
[121] L. Dussault, J.C. Dupin, H. Martinez, E. Dumitriu, A. Auroux, C. Guimon, Influence of the metal nature (Ni, Cu, Mg) on the surface acid–base properties of mixed oxides elaborated from LDH. Surf. Interface Anal. 38 (2006) 234–237.
[122] S. Kusama, T. Saito, H. Hashiba, A. Sakai, S. Yotsuhashi, Crystalline Copper (II) Phthalocyanine Catalysts for Electrochemical Reduction of Carbon Dioxide in Aqueous Media. ACS Catal, 7, 12 (2017) 8382-8385.
[123] W.J. Liu, H.H. Huang, T. Ouyang, L. Jiang, D. C. Zhong, W. Zhang, T.B. Lu, A Copper (II) Molecular Catalyst for Efficient and Selective Photochemical Reduction of CO_2 to CO in a Water-Containing System. Chem. Eur. J 24, 18 (2018) 4503-4508.
[124] A. Kim, N. Muthuchamy, C. Yoon, S.H. Joo, K.H. Park, MOF-Derived Cu@ Cu_2O Nanocatalyst for Oxygen Reduction Reaction and Cycloaddition Reaction. Nanomaterials, 8, 3 (2018) 138.
[125] J. Tian, Q. Guo, Thermal Decomposition of Hydrocalumite over a Temperature Range of 400–1500°C and Its Structure Reconstruction in Water, J Chem. (2014) 454098.
[126] G. Mascolo, Synthesis of anionic clays by hydrothermal crystallization of amorphous precursors. Appl. Clay Sci. 10, 1-2 (1995) 21-30.
[127] T.A.S. Ferreira, J.C. Waerenborgh, M.H.R.M. Mendonça, M.R. Nunes, F.M. Costa, Structural and morphological characterization of FeCo2O4 and CoFe2O4 spinels prepared by a coprecipitation method. Solid State Sci. 5, 2 (2003) 383-392.
[128] J.S. Valente, F. Figueras, M. Gravelle, P. Kumbhar, J. Lopez, J.P. Besse. Basic properties of the mixed oxides obtained by thermal decomposition of hydrotalcites containing different metallic compositions. J. Catal. 189, 2 (2000) 370-381.
[129] M. Kaneyoshi, W. Jones, Formation of Mg-Al layered double hydroxides intercalated with nitrilotriacetate anions. J. Mater. Chem. 9, 3 (1999) 805-811.
[130] V. Rives, S. Kannan, Layered double hydroxides with the hydrotalcite-type structure containing Cu^{+2} , Ni^{+2} and Al^{+3}, J. Mater. Chem 10 (2000) 489-495.
[131] C. Mangkonsu, I. Kunio, R.B. Othman, The Effect of Sintering Temperatures on the Microstructure and Properties of BTCP. Aust. J. Basic & Appl. Sci. 8, 5 (2014) 492-497.
[132] P.J.F. Harris, The sintering of platinum particles in an alumina-supported catalyst: Further transmission electron microscopy studies. J. Catal. 97, 2 (1986) 527-542.
[133]M. Sacerdoti, E. Passaglia, Hydrocalumite from Latium, Italy: its crystal structure and relationship with related synthetic phases. Neues Jb Miner Monat (1988) 462–475.

[134] S.N. Britvin, Structural diversity of layered double hydroxides. In Minerals as Advanced Materials Springer, Berlin, Heidelberg (2008)123-128.
[135] A. Corma, S. Iborra, J. Primo, F. Rey, One-step synthesis of citronitril on hydrotalcite derived base catalysts. Appl Catal. A, 114, 2 (1994) 215–225.
[136] M.J. Climent, A. Corma, S. Iborra, J. Primo, Base catalysis for fine chemicals production: claisen-schmidt condensation on zeolites and hydrotalcites for the production of chalcones and flavanones of pharmaceutical interest. J Catal. 151, 1 (1995) 60–66.
[137]W.M. Antunes, C.D.O. Veloso, C.A. Henriques, Transesterification of soybean oil with methanol catalyzed by basic solids. Catal. Today, 133 (2008) 548-554.
[138] C.N. Pérez, C.A. Pérez, C.A. Henriques, J.L.F Monteiro, Hydrotalcites as precursors for Mg, Al-mixed oxides used as catalysts on the aldol condensation of citral with acetone. Appl. Catalysis A. 272, 1-2 (2004) 229–240.
[139]C.O. Veloso, C.A. Henriques, A.G. Dias, J.L.F. Monteiro, Condensation of glyceraldehyde acetonide and acetone over basic catalysts. Catal. Today. 107-108 (2005) 294–301.
[140] J.L. Shumaker, C. Crofcheck, S.A. Tackett, E.S. Jimenez, T. Morgan, T., Y. Ji, M. Crocker, T.J Toops, Biodiesel synthesis using calcined layered double hydroxide catalysts. Appl. Catal B. 82, 1-2 (2008) 120–130.
[141] E. Leclercq, A. Finiels, C. Moreau, Transesterification of rapeseed oil in the presence of basic zeolites and related solid catalysts. J Am. Oil Chem. Soc. 78, 11 (2006) 1161–1165.
[142] G.S. Macala, A.W. Robertson, C.L. Johnson, Z.B. Day, R.S. Lewis, M.G. White, A.V. Iretskii, P.C. Ford Transesterification catalysts from iron doped hydrotalcite-like precursors: solid bases for biodiesel production. Catal. Lett. 122, 3-4 (2008) 205–209.
[143]S.C. Qi, L. Zhang, H. Einaga, S. Kudo, K. Norinaga, I.J. Hayashi, Nano-sized nickel catalyst for deep hydrogenation of lignin monomers and first-principles insight into the catalyst preparation. J. Mater. Chem. A, 5, (2017) 3948-3965.
[144] J.M. Pepper, W.F. Steck, R. Swoboda, J.C. Karapall, Hydrogenation of lignin using nickel and palladium catalysts. In J. Marton (Ed.) Lignin structure and reactions, Advances in Chemistry, Vol. 59 American Chemical Society (1966) 238-248.
[145] P.M. Veiga, S.B.S. Zilacleide, C. M. S. Polato, M.F. Portilho, C.O. Veloso, C.A. Henriques, Influence of the Incorporation of Transition Metals on the Basicity of Mg, Al-Mixed Oxides and on Their Catalytic Properties for Transesterification of Vegetable Oils. Catalysts, (2013) 685063.
[146] M.A. Usman, T.O. Alaje, V.I. Ekwueme, E.A. Awe, Investigation of the Catalytic Performance of a Novel Nickel/Kit-6 Nanocatalyst for the Hydrogenation of Vegetable Oil, ISRN Chemical Engineering. (2012) (526852).
[147] P.S. Braterman, Z.P. Xu, F. Yarberry Layered Double Hydroxides in S.M. Auerbach, K.A. Carrado, P.K. Dutta (Eds.) Handbook of Layered Materials. Marcel Dekker, Inc., New York (2004) 373-474.

Experimental Methodology

CHAPTER 3

Techniques for Catalyst Characterization

Chapter Summary:

This chapter summarizes applications of all the analytical techniques, methods and their specifications, used for the structural and morphological studies carried out on catalysts. The characterization of as-synthesized and mixed metal oxides were done by X-ray diffraction (XRD), N_2 physiosorption, Energy Dispersive Powder X-ray Spectroscopy (EDX), scanning electron microscopy (SEM), thermogravimetry (TG) and temperature programmed reduction (TPR).

3.1 Calcination of Catalysts

The dried Layered Double Hydroxides (LDH) samples were calcined at different temperatures, 300-800°C for 6 hours at heating rate of 2°C/min in the presence of air to transform them into mixed metal oxides. Prior to the calcinations, the thermogravimetric analysis of the LDH was done to obtain the appropriate temperatures required to form complete oxides.

3.2 Characterization of Catalysts:

3.2.1 Powder X-Ray Diffraction (PXRD)

For the structural identification of the materials (Fig. 3.1), powder X-ray diffraction (XRD) patterns of the synthesized catalyst were recorded at a room temperature on a Bruker AXS D8 Advance diffractometer operated at 40KV-40mA using monochromatic CuKα (1.5402 Å) radiation at 4-80˚and step size of 0.020˚and phases were identified by using the International Centre for Diffraction Data (ICDD) database. The parameters refined were zero shift (2θ), background, cell parameters and peak shapes. Scherrer method was used for the calculation of crystallite size of a multiphasic sample from the full width at half maximum intensity measurements.

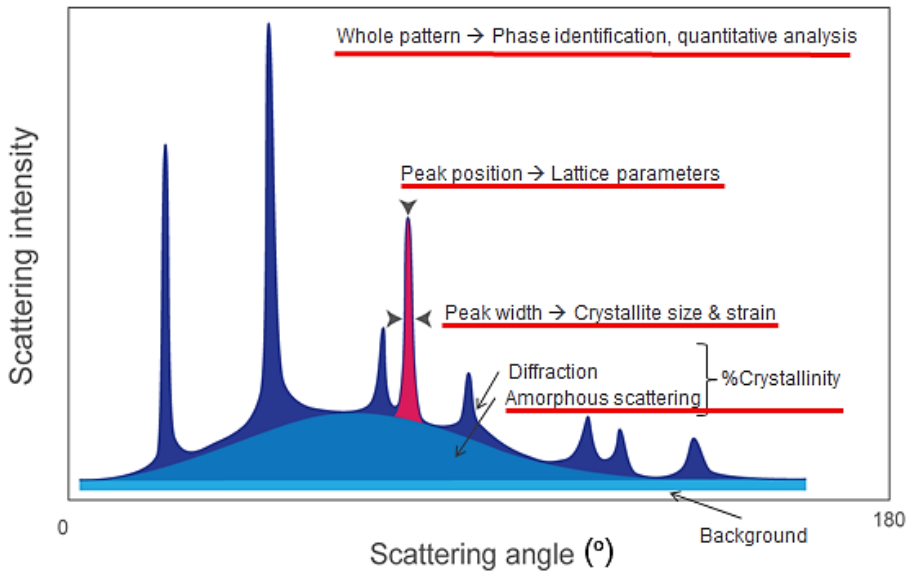

Figure 3.1 Obtainable information from a XRD diffractogram [8]

As indicated in the figure (Fig. 3.1), XRD can be used to obtain a broad range of information on structure of the material. Considering the unique patterns produced by each solid, it can surely be called as a fingerprint of the material. Structural defects and information on

presence of amorphous state is also perceptible. The miller indices obtained from the diffractogram provide information on the cell parameters and crystallinity and hence detailed characterization of the material becomes easier.

3.2.1.1 Internal Standard Method for Relative Abundance of oxide phases

The quantitative phase analysis was carried out using the method suggested by Gualtieri.[1] Initially the internal standard; anatase (TiO_2) nanopowder <25nm particle size sample purchased from Sigma Aldrich, was collected individually and assumed as zero. A finally grinded mixture of sample and 10wt% of the internal standard was carefully weighted by analytical balance and homogenized by mixing with mortar. The prepared samples were run on the XRD using the specifications described above.

3.2.2 Nitrogen Physiosorption

The textural characterization and surface area was studied using conventional adsorption/desorption of N_2 as the adsorbate at 77 K by a multipoint method; carried out using Micrometrics Tristar-3000 automated gas adsorption system. Prior to the nitrogen adsorption, the samples were degassed for 12 hours under vacuum at 50°C for uncalcined sample and 250°C for calcined samples by Micrometrics VacPrep 061 auto-degassing station to remove any adsorbed species and moisture. The Brunauer- Emmett-Teller (BET) method was used to calculate the specific surface area, pore size distribution and pore volume of the catalyst.

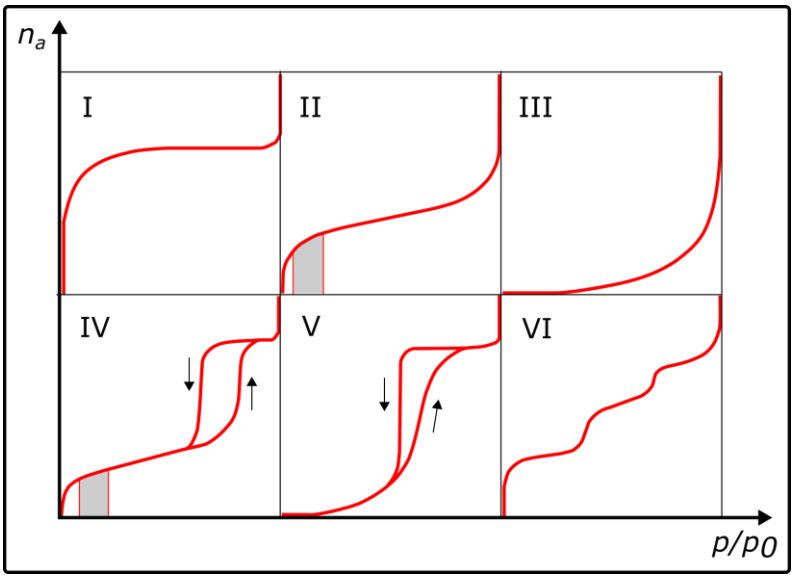

Figure 3.2 IUPAC classification of adsorption isotherms[2]

The isotherms have been generally categorized into 6 groups among which 4 are most common (Fig. 3.2).[2] Merely, the shape of the isotherm provides many clues about the porosity of the catalysts for instance i) Type I isotherms are allotted to microporous solids with small external surfaces ii) Type II isotherm is associated with a non-porous/macroporous adsorbent material. Iii) Type III and V are uncommon types of isotherms which represent weak interaction of adsorbent-adsorbate. iv) Type IV isotherms are related to the mesoporous industrial adsorbents. v) Type VI isotherm indicates a multilayer stepwise adsorption on a uniform non-porous surface.[2]

3.2.3 Scanning Electron Microscope (SEM)

A Hitaichi S-4800 Scanning Electron Microscopy (SEM) at an accelerating voltage of 5.0kV and magnification 10k/100k mixed BSE and SE electron was used to analyse the microscopic morphology of the synthesized materials.

The high resolution images generated from SEM, typically linked with EDX provide information on topography, morphology, elemental maps and spatial variations in chemical compositions of materials. (Fig 3.4) SEM is also used to analyze surface fractures, microstructures, examine surface contaminations along with phase discrimination. (Fig. 3.3)

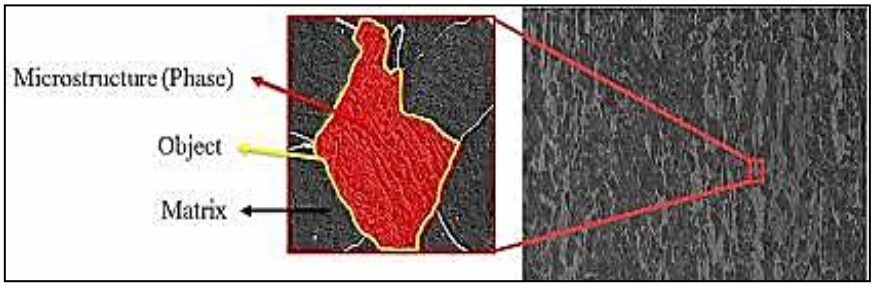

Figure 3.3 SEM images of a microstructure[3]

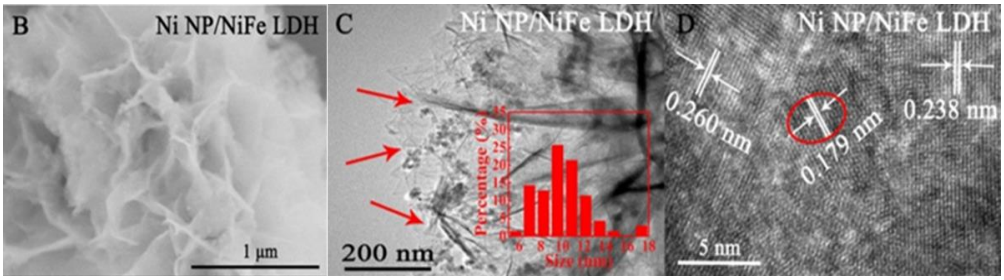

Figure 3.4 The structural details of LDH materials obtained from SEM images[4]

3.2.4 Thermogravimetry (TG)

The thermal analysis (TG and DTG) to study the progressive thermal decomposition of the materials was carried out using Perkin Elmer STA 6000/8000; approximately 25mg of catalyst in Al_2O_3 crucible was heated in the presence of air (60mL/min) from 40-900°C with the linear heating rate of 5°C/min.

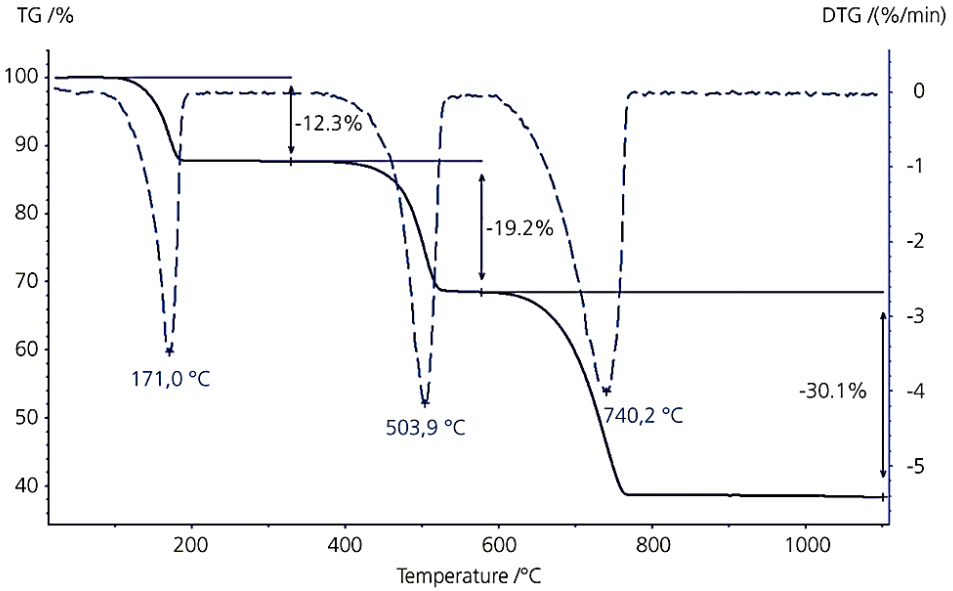

Figure 3.5 TG and DTG curves of sample giving percentage decomposition information of physical and chemical changes as a function of temperature[5]

TGA provides information on the thermal stability of the material which is decisive for determining the maximum temperature under which the catalyst can be used in a stable state. As indicated in Fig. 3.5, it can also be utilized for quantitative composition analysis such as temperature dependent weight loss in sample, determining the water content or the residual solvents in the material, evaporation rate as a function of temperature.

3.2.5 Energy Dispersive X-Ray (EDX)

The composition of the as-synthesized precursor catalysts was done by using Energy Dispersive X-Ray analysis (EDXA) by QUANTA 200F with Detector Oxford Instruments X-Max ^{N} SDD/ working condition at 15kV/1 µm3 area, BSE electron in which samples were at vacuum (0.38torr) at room temperature.

EDX is used for the chemical characterization of elements in a material, an estimation of their relative abundance and presence of any contaminants. (Fig. 3.6) EDX is a helpful tool for the identification of amorphous phase in the sample which otherwise is not detected by other techniques such as XRD.

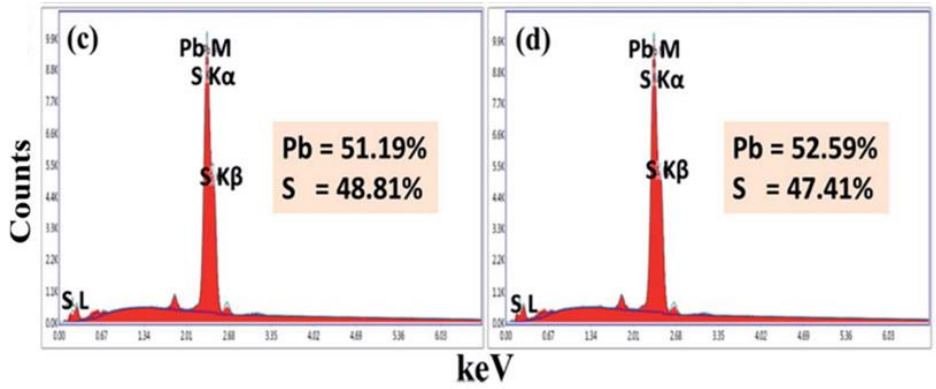

Figure 3.6 Energy-dispersive X-ray spectroscopy (EDX) analysis for elemental abundance in PbS sample[6]

3.2.6 Temperature Programmed Reduction (TPR)

The H_2-TPR was carried out on Micromeritics Autochem II 2920 instrument equipped with thermal conductivity detector (TCD). Sample were pre-treated in Helium (He) flow at 450°C for 45min, analysed in 5% Hydrogen (H_2) at the rate of 30mL/min with heating ramp of 10°C/min to 800°C (isotherm 40min).

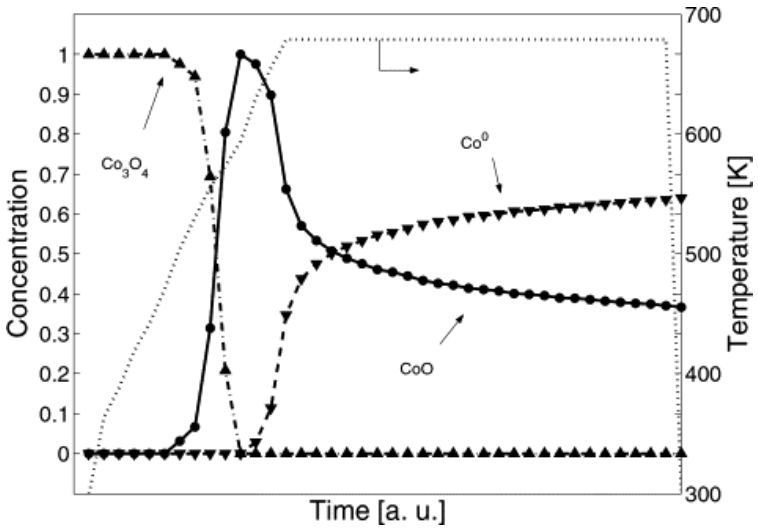

Figure 3.7 TPR of cobalt species during TPR of Fischer-Tropsch Catalysts[7]

TPR profile is a key technique used for the characterization in heterogeneous catalysis to determine the ideal reduction conditions. The surface chemistry of the mixed oxides can be studied over a range of temperature. In Fig. 3.7 Co_3O_4 can be observed changing its state and reducing to Co^0.

The oxidized catalysts is subjected to the set temperature in the presence of the flowing gas hydrogen. This tool accurately investigates the catalyst reproducibility. Furthermore, a TPR-

MS can also provide qualitative and quantitative data on the reduction of gas mixture in the presence of mixed oxides catalysts.

References

[1] A.F. Gualtieri, A guided training exercise of quantitative phase analysis using Expgul Gsas Tutorials and Examples (2003).
[2] K.S. Sing, Reporting physisorption data for gas/solid systems with special reference to the determination of surface area and porosity (Recommendations 1984). Pure Appl. Chem. 57, 4 (1985) 603-619.
[3] S.M. Azimi, D. Britz, M. Engstler, M. Fritz, F. Mücklich, Advanced Steel Microstructural Classification by Deep Learning Methods. Sci. Rep. 8, 1 (2018) 2128.
[4] X. Gao, X. Long, H. Yu, X. Pan, Z. Yi, Ni Nanoparticles Decorated NiFe Layered Double Hydroxide as Bifunctional Electrochemical Catalyst. J. Electrochem. Soc. 164, 6 (2017) H307-H310.
[5]https://www.netzsch-thermal-academy.com/en/advanced-materials-testing/methods/thermogravimetric-analysis/ consulted in October 2018
[6] C.V. Gopi, J.H. Bae, M.V. Haritha, S.K. Kim, Y.S. Lee, G. Sarat, H.J. Kim, One-step synthesis of solution processed time-dependent highly efficient and stable PbS counter electrodes for quantum dot-sensitized solar cells. RSC Adv. 5, 130 (2015) 107522-107532.
[7] B. Øyvind, R. Magnus, S. SØlvi, H. Anders, Identification of cobalt species during temperature programmed reduction of Fischer-Tropsch catalysts. Stud Surf Sci Catal. 163 (2007) 255-272.
[8] https://nptel.ac.in/courses/115103030/3 consulted in October 2018

CHAPTER 4

Synthesis of the LDH Catalyst Precursors

Chapter Summary:

The chapter deals with the detailed experimental procedures and coprecipitation conditions employed for the synthesis of the catalyst precursors. Three major types of parameters have been studied and explained: 1) under same physical parameters, a complete shift in crystalline phase as a ratio of copper cations (x ≤0.75) in a Ni-Cu-Fe system. A nickel-diluted system rendered an impossible formation of LDH phase, confirming the Jahn Teller effect in copper complex as stated in chapter II. 2) Attempts for synthesis of a well crystalline Cu-Fe LDH at pH ranging from acidic (4.5) to strongly basic (12.5). No evidence on formation of the desired phase could be achieved. 3) An investigation on atypical copper chemistry by replacing iron with aluminium, in both; a divalent (Cu-Al) and trivalent (Ni-Cu-Al) LDH system. However, the effect of Teller distortion in Cu-Al case does not seem operative; Cu-Al and Ni-Cu-Al were obtained in a very well crystalline LDH materials. A brief discussion on a difference of solubilities of the cations has been reported.

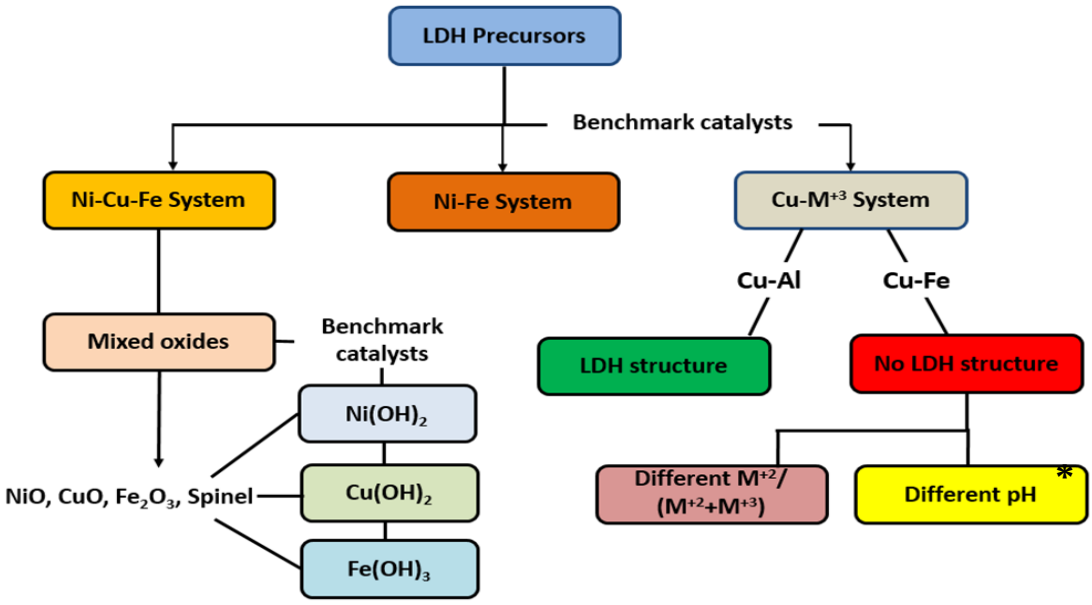

Roadmap of catalysts synthesis and structural investigations

*Possible synthesis of Cu-Fe LDH suggested by computational methods: Shi, W., Hu, Jun., Ni, Z.M., Li, Y., Liu, J. Acta Phys. Chim. Sin. 28, 8 (2012) 1869-1876.

Experimental

4.1 Reagents and Apparatus

Nickel nitrate hexahydrate ≥98.5% ($Ni(NO_3)_2.6H_2O$), copper nitrate trihydrate ≥99% ($Cu(NO_3)_2.3H_2O$), Iron nitrate nonahydrate ≥99.95% ($Fe(NO_3)_3.9H_2O$), aluminium chloride hexahydrate ≥99% ($AlCl_3.6H_2O$), and sodium hydroxide ≥97% *(*NaOH) of high Purity grade from Sigma Aldrich and sodium carbonate ≥99% (Na_2CO_3) from Prolabo were purchased and used as received without further purification. Deionized water was used throughout the experiments.

4.1.1 Apparatus

The synthesis of Layered Double Hydroxides (LDH) was done with Metrohm 877 Titrino plus potentiometric titrator coupled with a flow pump to control the rate of addition of the cationic solution. A hydroxide solution was added dropwise to maintain stable pH. The post-synthesis washing of the catalyst precursors was done with a conventional centrifuge (see Fig. 4.1)

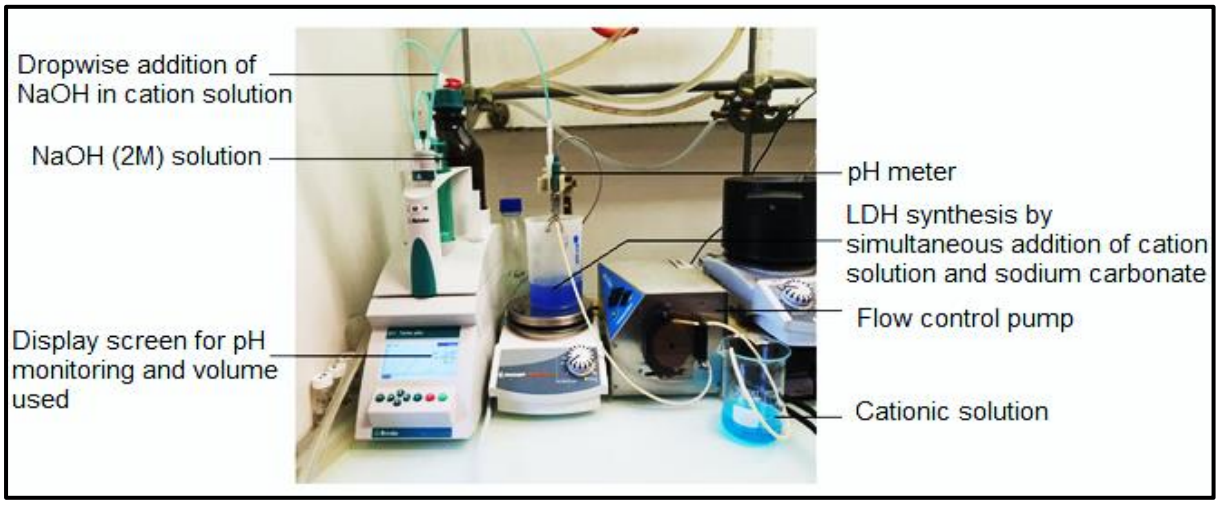

Figure 4.1 A typical apparatus used for coprecipitation of layered double hydroxides

4.1.2 Procedure

For the preparation of precursor layered double hydroxides , a range of $((M_1^{2+}+M_2^{2+})/M^{3+}=x$ =0.6-0.75) nitrates of the respective cations were taken. Four different types of Layered Double Hydroxides (LDH) based on NiFe-LDH, CuFe-LDH, NiCuFe-LDH and CuAl-LDH systems were synthesized at different pH and cation ratios with the coprecipitation method describ by Tichit and co-workers.[1]

For the explanation of synthesis method, consider NiCuFe-LDH as an example. 0.5M solution of nickel nitrate nonahydrate ($Ni(NO_3)_2.6H_2O$) and 0.5M solution of copper nitrate trihydrate($Cu(NO_3)_2.3H_2O$) were prepared separately in 100mL of deionized water and stirred at room temperature. This solution was later added to a 0.3M solution of iron nitrate nonahydrate ($Fe(NO_3)_3.9H_2O$). The cationic solution was added dropwise into 50mL of caustic solution of 0.25M Na_2CO_3 at the rate of 0.4mL/sec with constant stirring at 700 rpm. To keep constant pH during the coprecipitation, the addition of alkaline solution NaOH (2M) was done in a controlled manner by pH-STAT Titrino (Metrohm). The resulting suspension was aged for 15 hours at 80°C under constant stirring in the mother liquor; centrifuged at 5000rpm for 10minutes; washed (x3) with deionized water; and dried firstly under vacuum for 3 hours and kept at 80°C for 12h to dry. Fig. 4.2 shows an outline of the procedure of LDH synthesis and agglomeration of the particles.

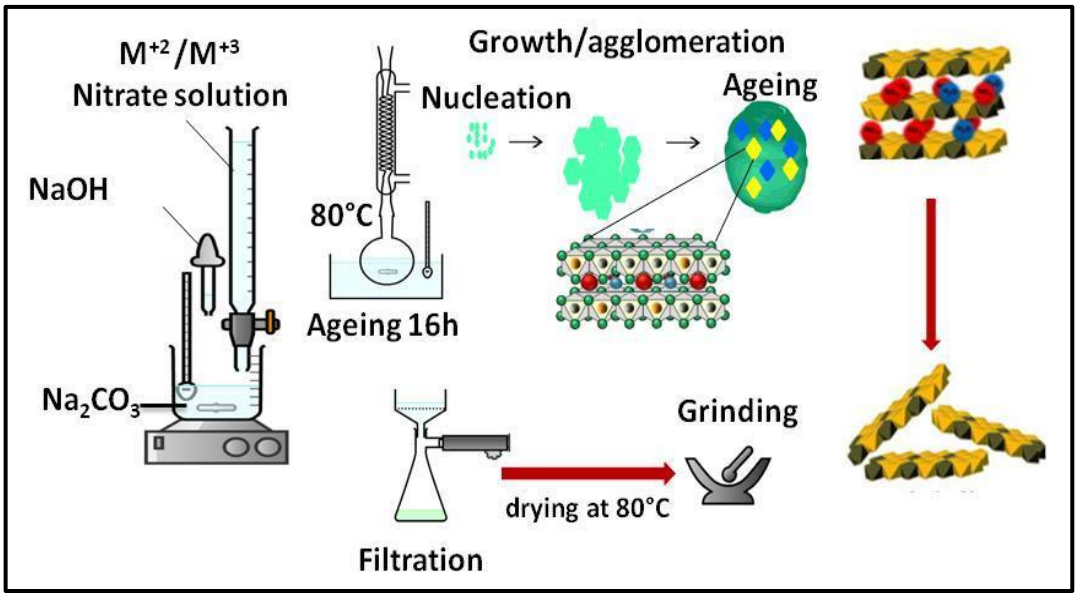

Figure 4.2 Schematic diagram of LDH synthesis and particle growth by coprecipitation

There can be no single protocol for the synthesis of LDH, every combination of M^{2+}/M^{3+} having its own particular characteristics. Preparation of a pure LDH is often hindered by severe limitations.[8] The synthesis parameters could strongly influence the structural modifications in the LDH structure.[6] Therefore, we tried to cover various aspects of favourable synthesis conditions to study the Cu-Fe system such as pH, cation ratio and nature of cations.

4.2 CASE I: Series of catalyst precursors with different copper content for attempted synthesis of Cu-Fe LDH

Objective: The limitations of synthesis of Cu-Fe LDH have been attributed in the literature to a significant structural distortion caused by the copper content in the LDH. In the present study, we tried to evaluate the tolerable amount of copper in the LDH system to keep the symmetry intact. In other words, the amount of another divalent cation to support the LDH structure has been estimated. Series of Cu-Ni-Fe preparations with Fe:x=0.25 starting from Cu: x= 0 to 0.75 show a prominent transition from LDH phase to CuO.

Table No 4.1 A shift in crystalline phase as dilution of Ni^{2+} (divalent cation) by Cu^{2+} in a Ni-Cu-Fe LDH system

Catalyst Precursor	Synthesis Atomic Ratio			Crystalline Phase	Final Atomic Ratio (EDX)		
	Ni	Cu	Fe		Ni	Cu	Fe
IZA 22	0.75	-	0.25	LDH	0.75	-	0.25
IZA147	0.70	0.05	0.25	LDH	0.72	0.04	0.26
IZA20	0.375	0.375	0.25	LDH	0.37	0.38	0.25
IZA 27	0.25	0.50	0.25	LDH+CuO	0.28	0.44	0.28
IZA23	-	0.75	0.25	CuO	-	0.65	0.35

*The table is in increasing order of copper percentage in the system.
*All syntheses were carried out at room temperature at pH 10.

4.2.1 Result and Discussion

X-ray Diffraction: In figure 4.3, it is shown that a well crystallized Ni-Fe LDH system is incorporated with copper in such a way that at each step of catalysts precursor synthesis, the copper content is increased; decreasing nickel and keeping iron constant, to maintain the overall divalent/trivalent ratio uniform throughout the series. This was done to investigate the potential threshold amount of another divalent cation required to synthesize a well fitted Cu-Fe LDH structure. Overall, the XRD shows a transition between LDH and CuO.

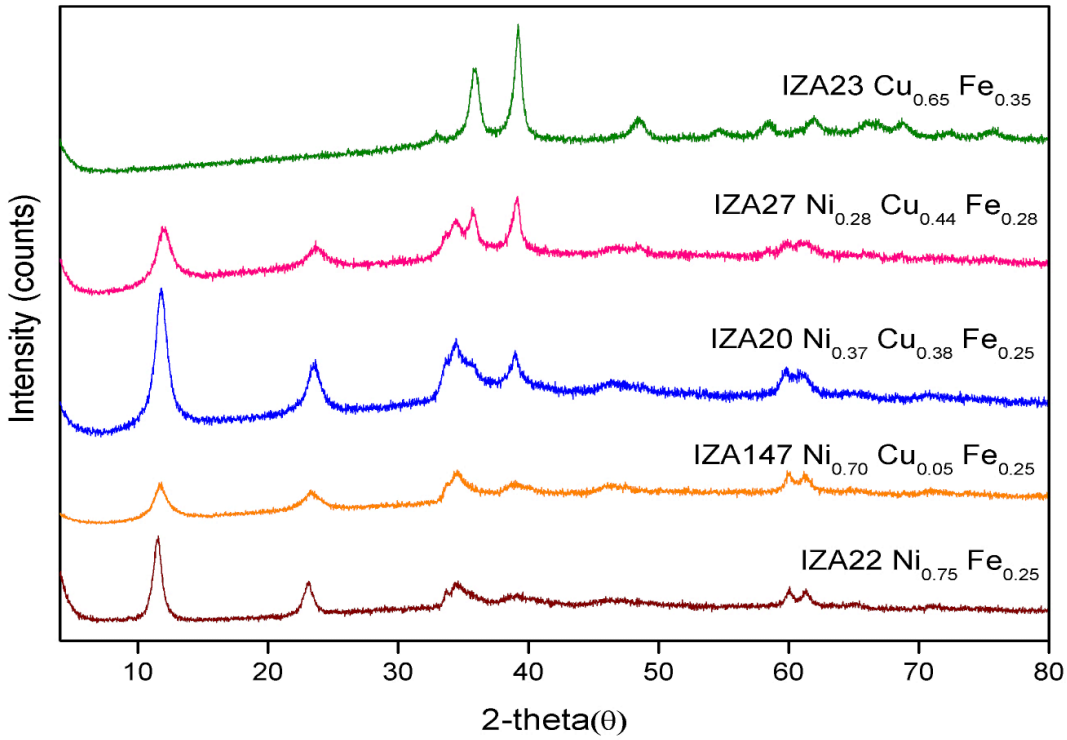

Figure 4.2 Series of Ni-Cu-Fe catalyst precursors changing crystallinity as a result of dilution of Ni^{2+} by Cu^{2+} at pH 10.

The cell parameters of LDHs and the distribution of phases (LDH and tenorite) obtained from Rietveld refinement are reported in Table 4.2, together with the crystallite size estimated from Scherrer analysis of the peaks (003) for LDH and (111) for tenorite.

Table No 4.2 Cell parameters of LDH, distribution of phases from Rietveld analysis and crystallite size by Scherrer method for catalyst precursors in the Ni-Cu-Fe LDH system

Samples	**Elemental composition**	**LDH Cell Parameters (Trigonal, R-3)**		**Phases percent**		**crystallite size (nm)**		**SBET ($m^2 g^{-1}$)**
		a=b	c	LDH	CuO	LDH	CuO	
IZA23	$Cu_{0.65}Fe_{0.35}$				100		51	109
IZA27	$Ni_{0.28}Cu_{0.44}Fe_{0.28}$	3.1153	23.002	84	16	6	44	
IZA20	$Ni_{0.37}Cu_{0.38}Fe_{0.25}$	3.1054	22.903	100		8		109
IZA147	$Ni_{0.7}Cu_{0.05}Fe_{0.25}$	3.0837	22.842	100		7		119
IZA22	$Ni_{0.75}Fe_{0.25}$	3.0607	23.023	100		14		88

As observed in the Ni-Fe sample IZA22, an appropriate LDH structure with sharp and symmetric reflections for (003), (006), (012), (110), (113) and broad peaks for (015) (018) planes is present. As a limited amount of copper is introduced in the system in IZA147, the diffraction peaks are broadened and intensities have shown variation with prominent peak shoulders (101) (009) appearing at 2θ (34.0°) and (35.5°) respectively. The broadening of the XRD peaks corresponds to a significant decrease of the particle size, as evaluated by the

Scherrer method, and an increase of the surface area, as evaluated by the BET method. The particle size further decreases when more copper replaces Ni in IZA20 and IZA27.

The cell parameter *c* of LDHs is strongly affected by the content of the interlayer space and its small irregular variations (less than 1%) from one sample to another are probably justified by changes of hydration state in sample dried at 80°C but not kept later in inert atmosphere. The cell parameter *a* is instead virtually independent from the hydration state and, at constant iron content, variations following the Vegard's law can be expected with the substitution of Ni by Cu. It can be observed that the *a* parameter steadily increases with the copper content, increasing by nearly 2 % from the value of all-Ni IZA22 to the value of IZA 27, containing more copper than Ni. As the ionic ratio of Cu^{2+}, 0.69 Å, is smaller than the ionic ratio of Ni, 0.72 Å, it is clear that the variation of the *a* parameter follows a trend opposite to the relative size of the cations. It would be tempting to attribute this effect to a deformation of the Cu^{2+} octahedra induced by the Jahn-Teller effect.

In case of IZA27, when the copper content of the sample is approximately 1.6 times more than the nickel in the system, the typical LDH diffraction peak intensity at (003) tends to lower down whereby CuO peak of reflection (111) at 2θ (35.2°) appears. The pattern explains that the purity of the LDH structure has been affected by the structural distortion caused by the unendurable copper content that could be present in an LDH in the absence of another divalent cation.

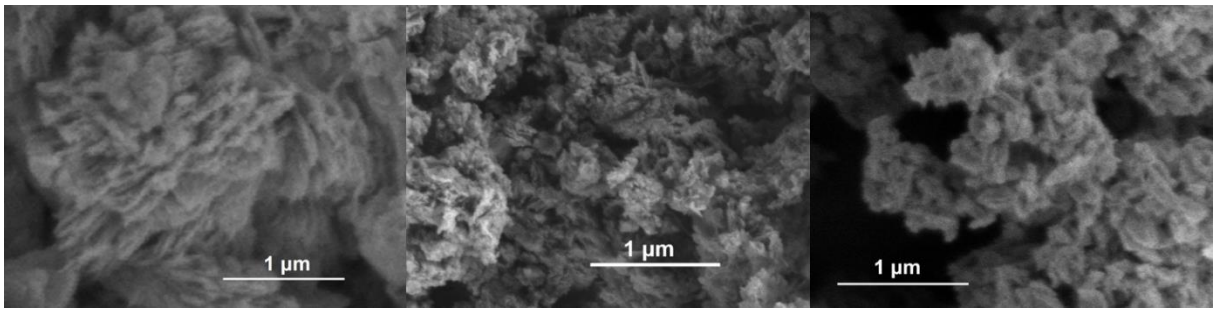

Figure 4.4 Scanning micrographs of Ni-Cu-Fe precipitates with different Cu/Ni ratios. From left to right $Ni_{0.75}Fe_{0.25}$ (IZA22), $Cu_{0.44}Ni_{0.28}Fe_{0.25}$ (IZA27), $Ni_{0.75}Fe_{0.25}$ (IZA23).

As soon as nickel is no more present in the Cu-Fe system (IZA23), layered structure could not be observed anymore. The diffraction pattern depicted presence of CuO phase showing intense peaks of (110), (111), (202), (020), (202) (113), (311), (220) and (004). It is also important to remark that no iron-containing phase is visible in the XRD of IZA23. Iron has to be present as an amorphous material, possibly identifiable with smaller lamellae present in the micrographs of IZA23 together with the larger CuO platelets.

The transition of copper oxide to LDH is thus supported by appropriate amount of nickel which enables to reduce the distorted effect of copper in a LDH system and provides structural stability to the layers.

This fact has already been illustrated by Cavani *et al.* who reported that the ratio between the Cu^{2+} and the second metal M^{2+} ion must be equal or lower than one.[2] Furthermore, the individual Cu-Fe LDH system faces decreased chemical stability, weaken hydrogen bonding, and decreased electrostatic interactions between host and the guest layer has been proposed by Lui.[3] Nonetheless, the gradual shift in the phase compositions in Ni-Cu-Fe system with $M^{2+}/ (M^{2+}+M^{3+}) =0.75$ had never been studied before.

Conclusion: Despite the close similarity in the ionic radius of Cu^{2+} (0.69 Å) to Mg^{2+} (0.72 Å) (a typical hydrotalcite cation), Cu-Fe LDH could only be synthesized by virtue of another divalent cation. For Cu/Ni ratio higher than 1 in Ni-Cu-Fe system reasonably stable LDH structure could not be formed.

4.3 CASE II: Series of Cu-Fe catalyst precursors at different pH

Objective: As per the definition of coprecipitation itself, the precipitation of the M^{2+} and M^{3+} occur in a desired proportion as fixed in the start of the reaction. Therefore, the formation of hydroxides is primarily determined by the pH because of the required enough concentration of OH^- ions to be present in the system which must react in order to produce $M^{2+}_{(1-x)} M^{3+}_x(OH)_2X_{x/m}.nH_2O$.[6]

Effects of pH on various systems have been studied. For instance Seron *et al.* described the mechanism of Mg/Al LDH formation at varying pH from 10 to 13.2.[9] Interesting diffusion of Al-rich species into Mg until the complete formation of LDH, has been observed. Similar phenomena were studied by C. Ruby and co-workers, investigating the Ni^{2+}-Fe^{3+} and Mg^{2+} and Fe^{3+} hydrolysis along with the mechanism of LDH formation with respect to phases obtained at pH values 6, 8, 10, 12.5.[10] In this way, Cu-Fe LDH synthesis attempts at varying pH could provide some reliable clues on the mechanism of formation of this system. Beside this, another important factor of coprecipitation is the choice of pH at which the reaction has to be conducted. If the cation M^{2+} and M^{3+} are far apart in pH range of precipitation, the precipitation may not be fruitful for the synthesis of a multi-valent system. One of the cations may precipitate leaving the other one as amorphous. Therefore, we tried a range of pH from acidic to basic to evaluate the presence of different phases at each pH under similar conditions.

Result and Discussion

Trials for synthesis of a well crystalline Cu-Fe LDH at various pH (4.5, 8, 10, 12.5) was done but no success could be achieved under the attempted conditions. (Fig. 4.5)

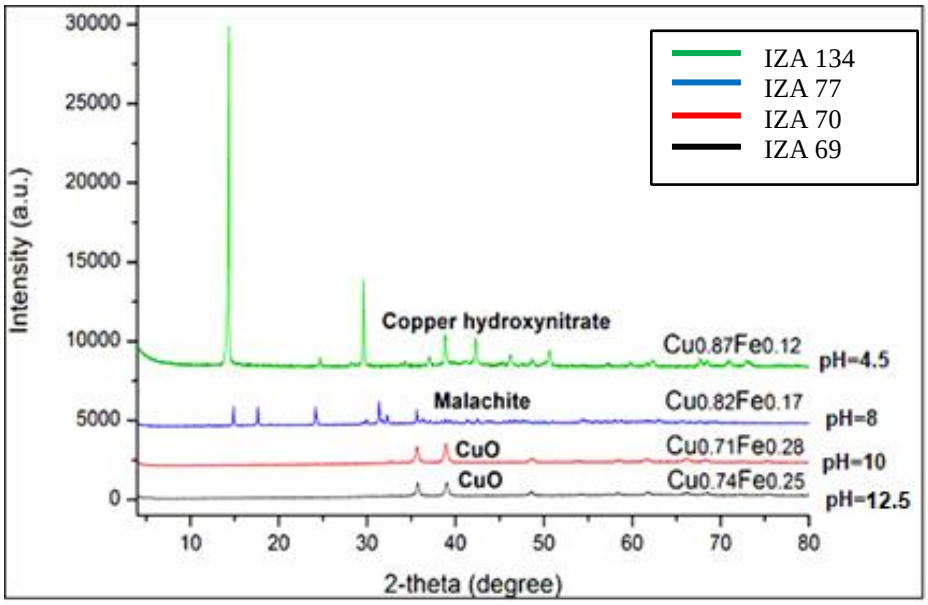

Figure 4.5 Phases formed in Cu-Fe system at different pH with same cation ratio

Table 4.3 Synthesis attempts of Cu-Fe LDH at various pH

Catalyst Precursor	Synthesis Atomic Ratio		pH	Crystalline Phase	Final Atomic Ratio (EDX)		Scherrer grain size (nm)
	Cu	Fe			Cu	Fe	
IZA 134	0.75	0.25	4.5	$Cu_2(OH)_3NO_3$	0.87	0.12	37
IZA 77	0.75	0.25	8	$Cu_2CO_3(OH)_2$	0.82	0.17	56
IZA 70	0.75	0.25	10	CuO	0.71	0.28	111
IZA 69	0.75	0.25	12.5	CuO	0.74	0.25	94

*All syntheses were carried out at room temperature

X-ray Diffraction: At pH > 8, CuO tenorite nanocrystals were formed. At pH 8, crystallization at room atmosphere often lead to carbonation and formation of malachite ($Cu_2(CO_3)(OH)_2$). A better crystallization of copper hydroxynitrate ($Cu_2(OH)_3NO_3$) is observed at lower pH but a significant difference in initial and final cation ratio is confirmed

by the EDX. Iron at lower pH does not seem to be incorporated in the solid and clearly has been lost in solution or as subcolloidal particles not centrifugated. On the other hand, at higher pH, the precipitated cation ratio corresponds well to the initial synthesis ratio however preventing copper precipitation as a hydroxy(carbonate/nitrate).[5] However, no iron-bearing phase is observable by XRD and iron has to be present in colloidal amorphous particles. This fact indicates that a best compromise between pH in a multi-cation system is crucial in order to form desired multiple-cation phases.[13]

4.4 CASE III: Series of Catalyst Precursors by replacement of Iron by Aluminium

Objective: After verification of the impossibility of formation of LDH in Cu-Fe system, several reports of successful synthesis of a Cu-trivalent cation LDH in Cu-Al system aroused our attention. Consequently, we chose Al^{3+} cation to replace Fe^{3+}. Three different categories of syntheses were done as follows:

1. A comparison of Cu-Fe and Cu-Al system (to study possible formation of LDH)
2. A comparison of Ni-Fe and Ni-Al system (to investigate the difference of parameters when Ni^{2+} is incorporated with aluminium)
3. Intermediate copper content syntheses of Ni-Cu-Fe and Ni-Cu-Fe (to find range of Cu^{2+} effecting the symmetry and effect of content of M^{3+} in the system)

Table 4.4 Attempted syntheses of LDH in Cu-Fe and Cu-Al systems

Catalyst Precursor	Synthesis pH	Synthesis Atomic Ratio			Crystalline Phase	Final Atomic Ratio (EDX)		
		Cu	Fe	Al		Cu	Fe	Al
IZA31	10	0.67	0.33	-	$Cu_2(OH)_3NO_3$	0.47	0.53	-
IZA120	10	0.66	-	0.33	LDH	0.74	-	0.26

4.4.1 Results and Discussion

X-ray Diffraction: In the IZA 120, Cu-Al system, a proper LDH phase is obtained. On the other hand, Cu-Fe shows formation of copper hydroxynitrate $Cu_2(OH)_3(NO_3)$ (gerhardtite, a mineral dedicated to Charles Frédéric Gerhardt, professor at the University of Montpellier and discoverer of the synthetic analogue of the mineral. To him is dedicated the present Institut Charles Gerhardt in Montpellier) and no crystalline phase of iron is detected. (Fig. 4.6)

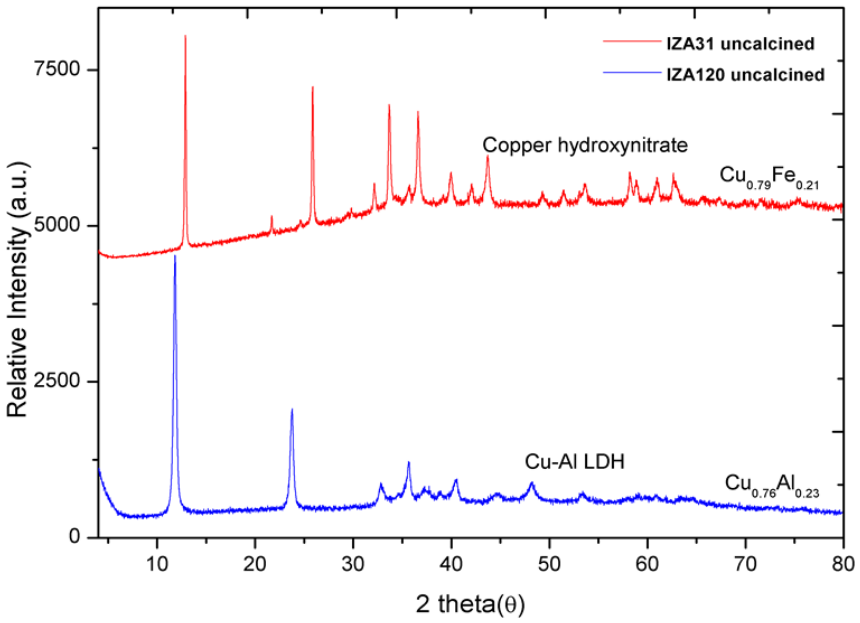

Figure 4.6 Diffractograms comparing precipitate formed in Cu^{2+}/M^{3+} (Cu-Fe, Cu-Al) systems

This indicates a contradiction in results obtained by XRD and EDX. Hence, the undetected iron by XRD is though present in the system, perhaps as nanocrystalline iron hydroxide, $Fe(OH)_3$.

Ramesh *et al.* have explained the formation of gerhardtite by suggesting that some hydroxyl groups of copper hydroxide layers are replaced by nitrate ions which are directly coordinated to the sheets.[7] Thus, copper occupies two different distorted octahedral sites in the copper hydroxynitrate structure. The symmetry of the synthetic copper hydroxynitrate, reported in Table 4.4, differs from the symmetry of the orthorhombic natural gerhardtite. The synthetic material shares the basal plane of gerhardtite but presents a monoclinic cell with half the volume of the cell of the natural material.

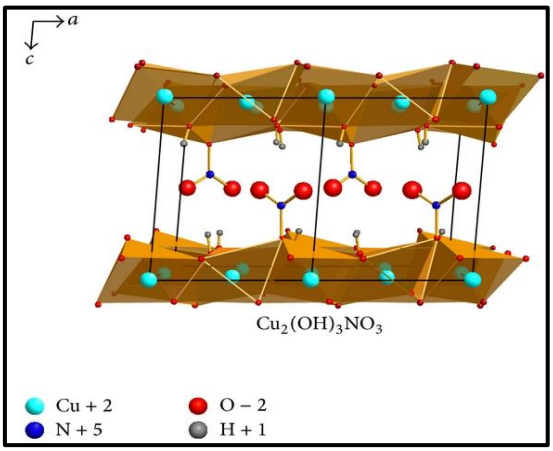

Figure 4.7 Crystal structure of copper hydroxynitrate-$Cu_2(OH)_3NO_3$.[7]

Table 4.5 Cell parameters of Cu-Fe and Cu-Al LDH system

Catalyst Precursor	Composition			Structure	a (Å)	b(Å)	c(Å)	β	γ
	Cu	Fe	Al						
IZA 31	0.47	0.53	-	$Cu_2(OH)_3NO_3$	5.5956	6.0767	6.9299	94.607	90
IZA 120	0.74	-	0.26	LDH	2.970	-	22.446	90	120

Figure 4.8 Colour of uncalcined precursors at a variation of trivalent cation

Table 4.6 Replica of Ni-Fe and Cu-Ni-Fe LDH system with aluminium replacing iron

Catalyst Precursor	Synthesis Atomic Ratio				Crystalline Phase	Final Atomic Ratio (EDX)			
	Ni	Cu	Fe	Al		Ni	Cu	Fe	Al
IZA 127	0.75	-		0.25	LDH	0.74	-	-	0.25
IZA 22	0.75	-	0.25	-	LDH	0.75	-	0.25	-
IZA 126	0.37	0.37	-	0.25	LDH	0.38	0.39	-	0.23
IZA20	0.38	0.38	0.25	-	LDH	0.37	0.38	0.25	-
IZA 124	0.65	0.02	0.33	-	LDH	0.62	0.02	0.35	-
IZA 125	0.65	0.02	-	0.33	LDH	0.65	0.02	-	0.32

*All syntheses were carried out at room temperature at pH 10.

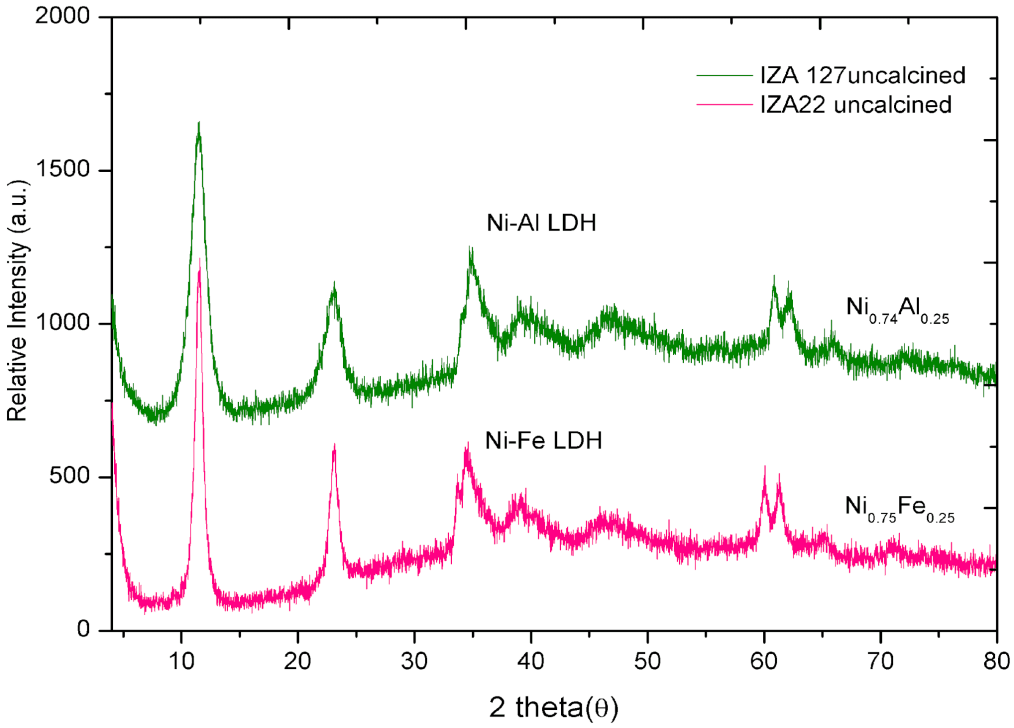

Figure 4.9 Diffractograms comparing Ni-Fe and Ni-Al LDH system

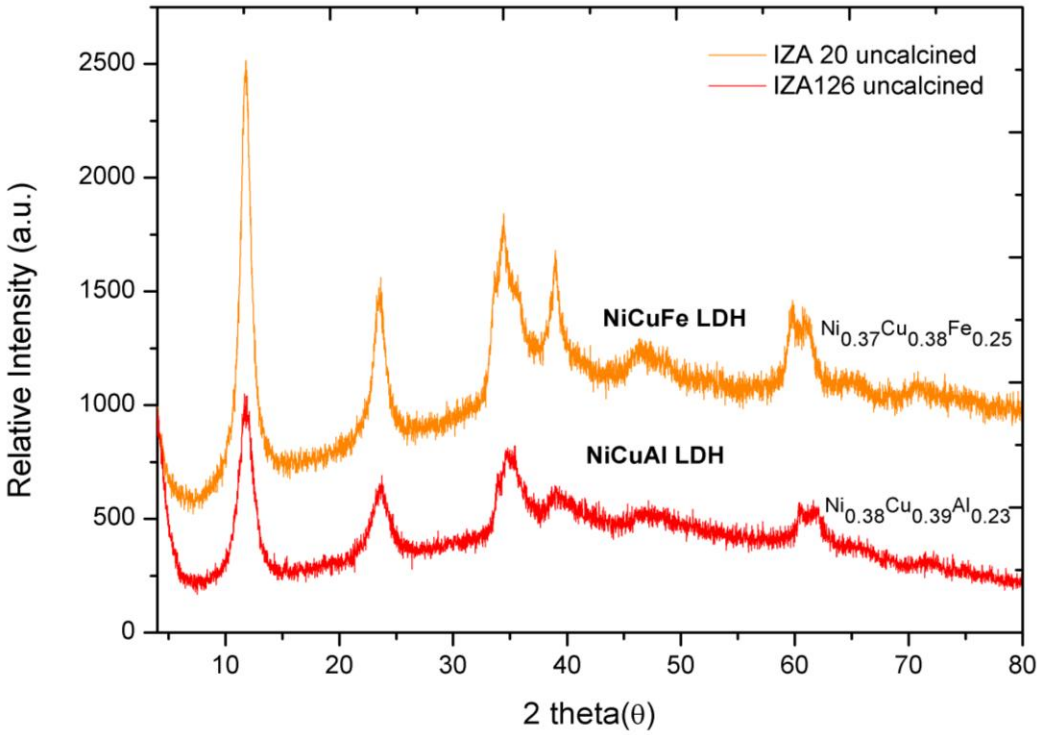

Figure 4.10 Diffractograms comparing of Cu-Ni-Fe and Cu-Ni-Al LDH system

Table 4.7 Cell parameter variation in catalysts as a function of cation nature and ratio

Catalyst Precursor	Composition				a(Å)	b(Å)	c(Å)	β	γ	Cell Volume ($Å^3$)
	Ni	Cu	Fe	Al						
IZA22	0.75	-	0.25	-	3.0738	-	23.132	90	120	189.28
IZA 127	0.74	-	-	0.25	3.06243	-	23.5122	90	120	191.74
IZA 31	-	0.47	0.53	-	5.5956	6.0767	6.9299	94.607	90	234.8
IZA120	-	0.74	-	0.26	2.970	-	22.446	90	120	171.47
IZA 20	0.37	0.38	0.25	-	3.0907		22.913	90	120	189.55
IZA126	0.38	0.39	-	0.23	3.07368		22.9836	90	120	182.71
IZA124	0.62	0.02	0.35	-	3.0809		22.841	90	120	187.75
IZA125	0.65	0.02	-	0.32	3.0051		22.770	90	120	178.08

The cell parameters of the LDHs vary with the composition. The *a* parameter, which can be expected to be not affected by the degree of hydration, decreases from the Ni-Fe LDH (IZA22) to the Ni-Al LDH (IZA127), in good agreement with the ratio of the ionic radii of iron and aluminium cations. In a similar way, the cell parameter *a* strongly decreases from the Ni-Al LDH (IZA127) to the Cu-Al LDH (IZA120), following a Vegard's law with the decrease of the ionic radius from nickel to copper cations. This logical result is in contrast with the increase of the cell parameter with the copper content previously observed in the Ni-Cu-Fe samples with variable copper content. An alternative explanation of the anomalous behavior of the series of the Ni-Cu-Fe samples is that the amount of trivalent in the LDH is not always the one expected from the chemical analysis. A decrease of the fraction of iron in the LDH structure at the increase of the Cu content would justify an anti-Vegard trend and could be attributed to the formation of amorphous Fe-rich material, that we have already detected in the Cu-rich end-term of the Ni-Cu-Fe series.

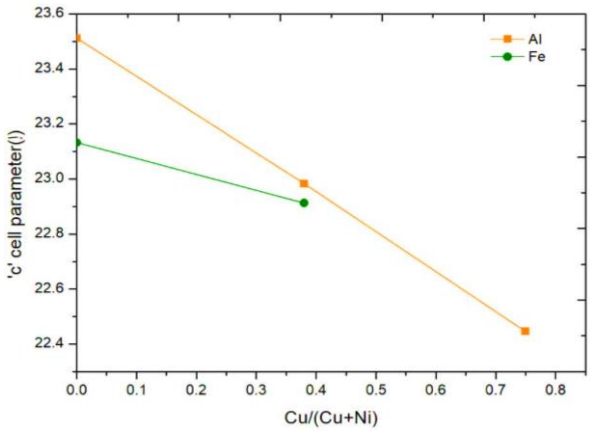

Figure 4.11 Variation of 'c' cell parameter in Ni-Cu (Fe, Al) LDH systems

The *c* cell parameter of Cu-Ni (Fe, Al) LDH systematically decreases with the Cu fraction, both for Al or Fe as trivalent cation in either ratio ($M^{2+}/M^{2+}+M^{3+}$ = 0.66, 0.75). The variations of the c parameter with composition cannot be usually explained by the cation size. The Fe-bearing samples present a lower parameter than the Al-bearing ones, despite a larger cation radius of Fe^{3+} (0.64 Å) than Al^{3+} (0.50 Å). The decrease of cell parameter with the copper content could be justified by the cation radius of Cu^{2+} (0.69 Å), smaller than the cation radius of Ni^{2+} (0.72 Å), but a 5% decrease of the *c* parameter largely exceeds what would be justified by the decreased cation radius and clearly depends on a change of the interlayer spacing.

The results show that *c* cell parameter is characteristically dependent on the trivalent cation in agreement with results reported for Co/M^{3+} system by Ramirez.[14] As the M^{3+} systematically increases, the coulombic forces of attraction between the negatively charged interlayer anions and the positively charged sheets of the LDH increase, causing a decrease in *c* cell parameter.[11,] Zhao *et al.* also suggested a similar fact in Mg^{2+}/Al^{3+} LDH system, when irrespective of the synthesis method opted, the crystallite size in the *c* direction decrease when Mg^{2+}/Al^{3+} ratio is increased. The presence of excessive trivalent cations probably accelerates the stacking of the sheets.[12] In our case, the increase of trivalent content from IZA22 to IZA124 and from IZA127 to IZA125 clearly justifies the decrease of the *c* parameter, while the effect of the copper content on the *c* parameter still needs to be explained.

4.5 Synthesis of Single hydroxides

In order to study a comparison between mixed oxides obtained from layered double hydroxides and single hydroxides, identical synthesis conditions (pH 10) were opted for the preparation of single hydroxides. The PXRD shows that IZA238 iron hydroxides was a multiphase sample with nearly equivalent amounts of goethite ((α-FeO(OH)), orthorhombic system, and Fe_2O_3. Similarly, Nickel hydroxide was prepared (IZA239), albeit a splitting of the 001 peak was observed at 2θ (18.8-19.1°), probably indicating some heterogeneity in the interlayer hydration. IZA240, an attempted synthesis of $Cu(OH)_2$, shows a crystallization of CuO tenorite rather than copper hydroxide as shown in the Fig 4.12. This is clearly due to the well-known metastability of $Cu(OH)_2$ towards CuO.[15] These hydroxides were then calcined at different temperatures and used in catalysis as benchmarks catalysts, as explained in a next chapter.

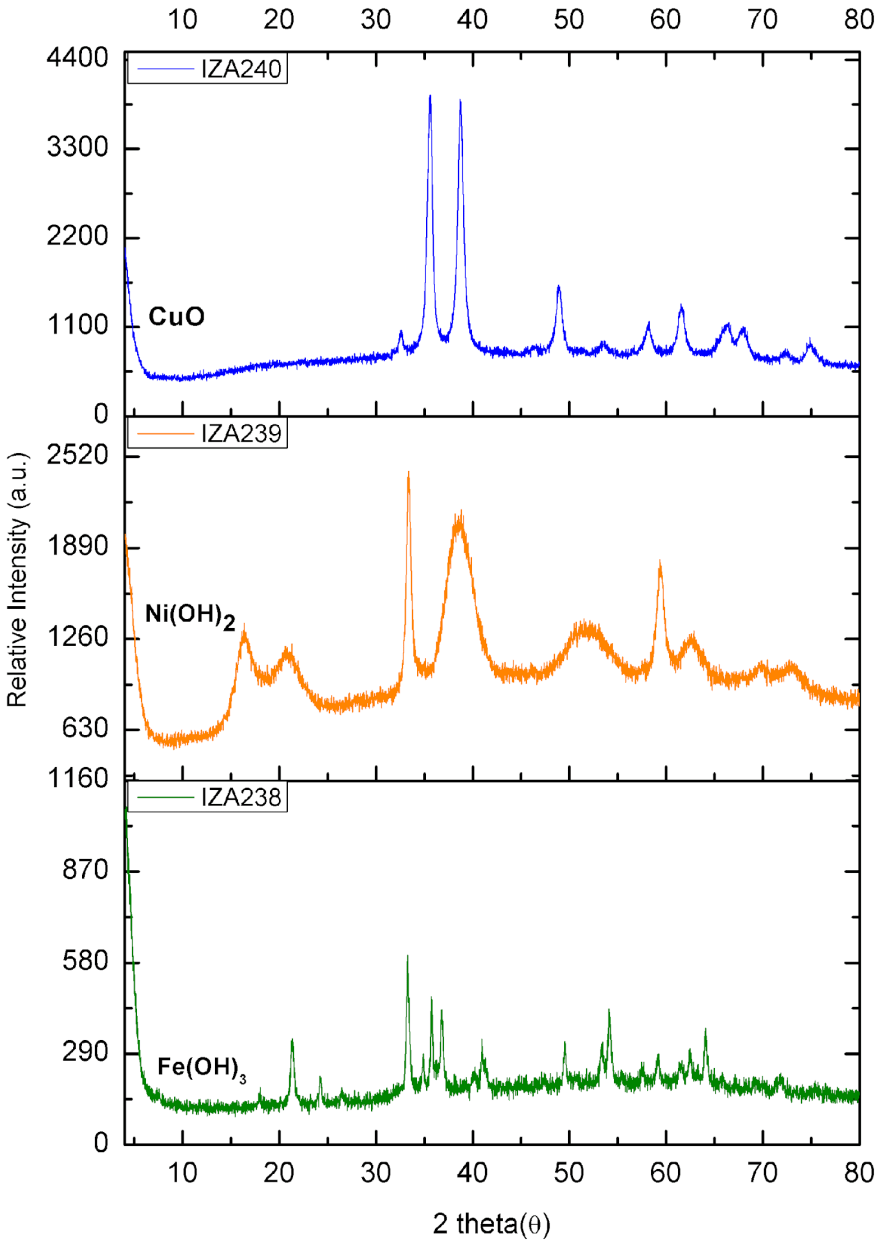

Figure 4.12 Diffractograms of single hydroxides prepared under identical conditions as of corresponding LDH

Table 4.8 Synthesis of single hydroxides

Catalyst	Cation used	Identified Phases	Phase %	a(Å)	b(Å)	c(Å)	β	Cell Volume(Å^3)
IZA 238	Fe^{3+}	Fe_2O_3	44.73	5.0385	-	13.773	-	302.81
		(α-FeO(OH)	55.26	4.6117	9.954	3.0187	-	138.57
IZA 239	Ni^{2+}	$Ni(OH)_2$	100	3.1237	-	4.739	-	40.05
IZA 240	Cu^{2+}	CuO	4.6842	-	3.4279	5.1448	99.175	81.553

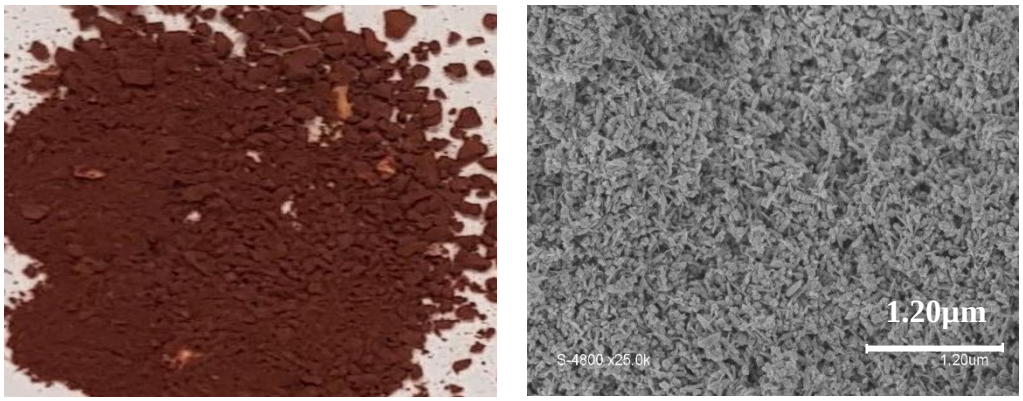

IZA 238 uncalcined ($Fe(OH)_3$) +Fe_2O_3

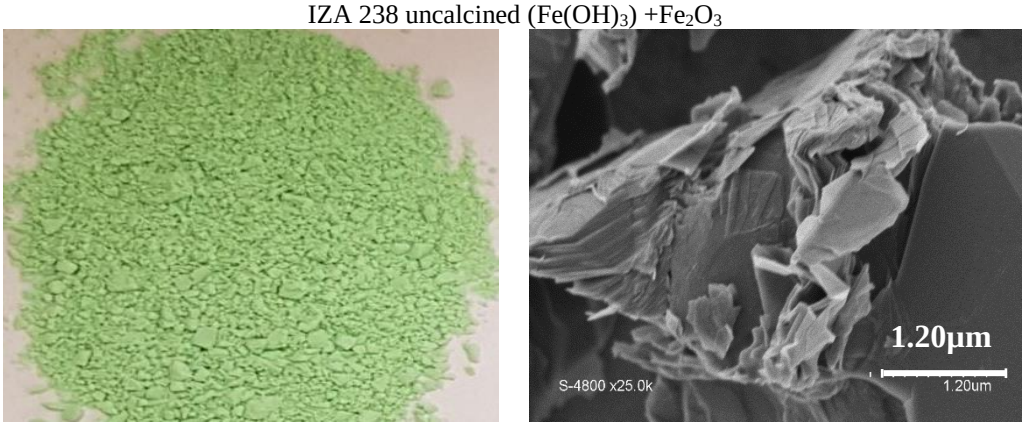

IZA239 uncalcined ($Ni(OH)_2$)

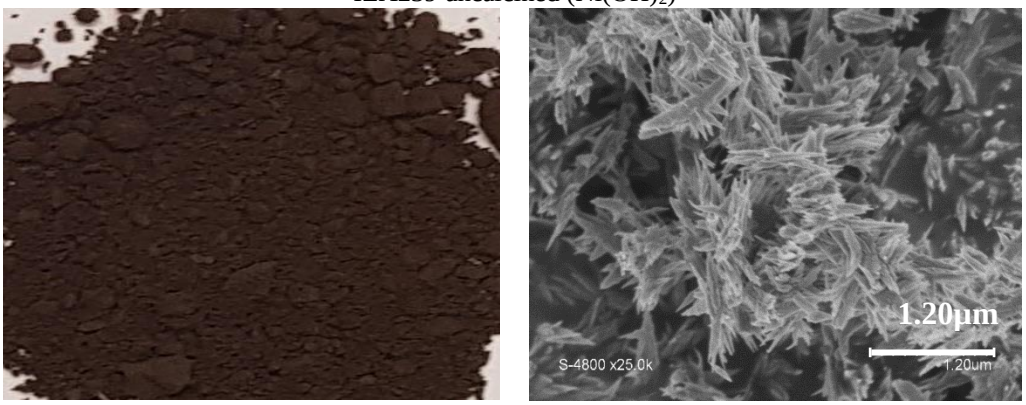

IZA 240 uncalcined (CuO)

Figure 4.13 Change in colour of uncalcined precursor catalysts (Left) and SEM images (right) as a variation of cations

4.5.1 Titration Curves provide useful clues on the mechanism of formation of LDH

It is widely accepted that the mechanism of formation of LDH is a multistep mechanism, in which an initial layered phase is formed by the less soluble cation and other components are incorporated in further local dissolution-recrystallization steps. The experimental study of the precipitation of each component during titration by NaOH of acid solutions provides useful information on the possible sequence of steps in the formation of LDHs. We have measured these curves by monitoring the evolution of pH in the same apparatus and the same methods used for the synthesis of the LDHs. The resulting curves are reported in Figure 4.14

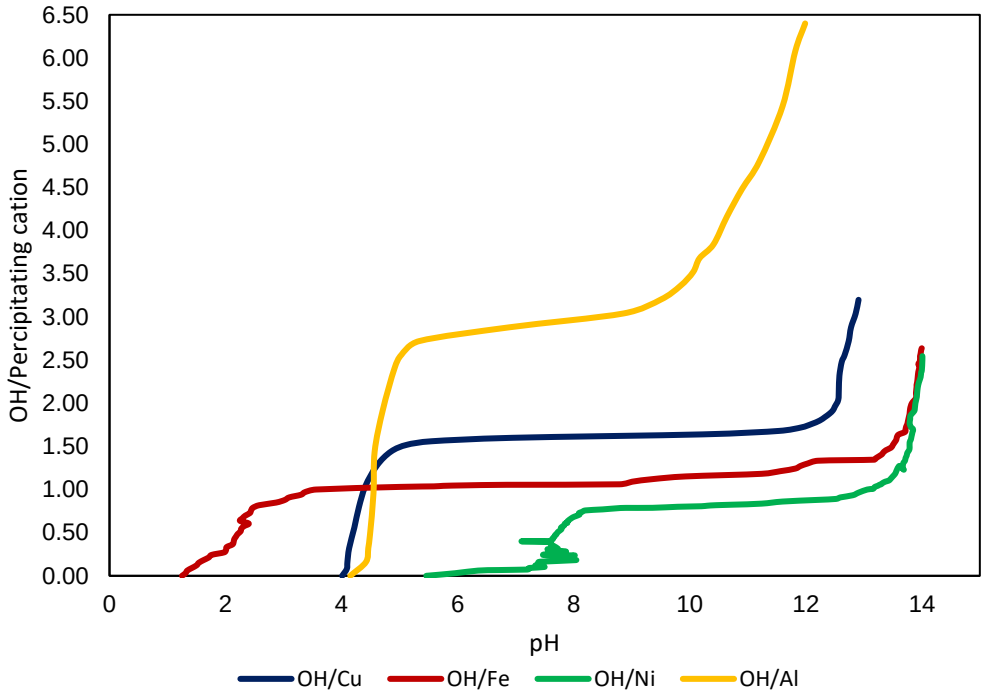

Figure 4.14 Titration curves for nitric acid solutions of Ni^{2+}, Cu^{2+}, Fe^{3+} and Al^{3+}

As shown in Figure 4.14, the solubility domains of the cations are diverse. For individual cation precipitation curves, at room temperature, an initial visible plateaus for each metallic cation can be observed at the pH of the parent solution.The initial plateau corresponds to the precipitation of an earlier precursor, which provides a pH buffer when NaOH is added. The end of this plateau is the onset of a sharp increase of pH, indicating that the precipitation of the initial precursor is no more taking place. The ratio OH/cation at the end of the plateau provides an information on the composition of the first precipitated precursor.

In case of Fe, the first plateau ends at OH/cation ratio 1, indicating the uptake of one hydroxyl ion (OH^-) by precursor Fe^{3+} precipitating out as goethite (FeOOH). This can be expressed as:

$$Fe(NO_3)_3 + H_2O + OH^- \longrightarrow FeOOH + 2H^+ + 3NO_3^{-1}$$

The successive step of pH is interrupted by small plateau at pH 9.01 and 12.04 indicating minor precipitation steps.

For Cu^{2+} the initial precipitation plateau ends at OH/cation 1.5. In the presence of nitrate, this value corresponds to the formation of copper hydroxynitrate $Cu_2(OH)_3NO_3$ (gerhardtite). The acid dissociation constant (pKa) of $Cu^{2+}(aq)$ is nearly 7 therefore at pH lower than 6, the formation of $Cu(OH)_2$ is not possible in the aqueous solution.[4]

The phase experimentally observed at the end of the precipitation is CuO, which is normally formed by dehydration of $Cu(OH)_2$. The formation of $Cu(OH)_2$ would require further consumption of OH^-, which is not observed. It is possible to postulate a direct mechanism of formation of CuO from gerhardtite, which would respect the charge balance and could be favoured at high pH by the extraction of protons:

$$Cu_2(OH)_3NO_3 \longrightarrow 2CuO + H_2O + 2H^+ + NO_3^{-1}$$

In the case of Ni, the precipitation plateau ends at a value OH/cation slightly lower than 1. Such a value has been interpreted as due to the formation of layered salts of non-stoichiometric hydroxo-aquo species of general formula $[Ni(OH)_{1-\delta}(H_2O)_\delta]^{\delta+}$.[10] These species could be weathered at high pH, forming $Ni(OH)_2$ by releasing protons and anions.

The case of aluminium is somewhat different. The initial precipitation plateau ends sharply at OH/cation 3, clearly indicating the precipitation of a trihydroxide $Al(OH)_3$. However, at difference of the other cations, the steps of pH increase is less sharp and the pH rises again slowly for pH higher than 9. The amphoteric nature of aluminium oxides and hydroxides, with isoelectric point near to 7, allows aluminate species $Al(OH)_4$ to be formed at higher pH from the dissolution of the previously precipitated hydroxide.

The titration curves give us information on the mechanism of formation of LDHs if it can be assumed that the initial formation of a lamellar phase is needed as a seed for the formation of the mixed layered structure. In this case, we can consider that, in the case of the Fe-Cu system, early precipitation of goethite takes place. This non-lamellar phase can hardly evolve by further incorporation of copper ions. In this case, copper will form an independent hydroxynitrate phase which will be the only one later detectable by XRD, due to the low crystallinity of the nanogoethite formed.

It can be observed that a different situation occurs in the Ni-Fe system. The early formation of layered Ni oxyhydoxy salts at the beginning of the alkalinisation of the solution provides seeds on which iron species can be incorporated, allowing the formation of LDH. In the presence of an incipient mixed phase, also Cu^{2+} ions will be incorporated in the growing LDH. In this case, the limit of formation of pure LDH will depend on the competition between incorporation of Cu^{2+} in the Ni-Fe LDH and the independent precipitation of gerhardtite.

The situation will be radically different when Al is present instead of Fe. In this case, the need of large amounts of NaOH for the precipitation of $Al(OH)_3$ leaves place to early

formation of Ni or Cu lamellar precursors, in which the Al^{3+} cations can be easily incorporated, with the formation of classical LDHs.

Such an explanation of the limit of formation of Cu-Fe LDH solves the conundrum of the difference between Cu-Fe and Cu-Al systems, without requiring the intervention of the structural instability allegedly brought by Jahn-Teller effect, which intervention in the presence of Fe and not of Al was especially difficult to justify.

References

[1] I.C. Marcu, N. Tanchoux, F. Fajula, D. Tichit, Catalytic conversion of ethanol into butanol over M–Mg–Al mixed oxide catalysts (M= Pd, Ag, Mn, Fe, Cu, Sm, Yb) obtained from LDH precursors. Catal. Lett. 143, 1 (2013) 23-30.

[2]F. Cavani, F. Trifirò, A. Vaccari, Hydrotalcite-type anionic clays: Preparation, properties and applications. Catal. Today. 11, 2 (1991) 173-30.

[3] J. Liu, P. Yao, Z.M. Ni, Y. Li, W. Shi, Jahn-Teller Effect of Cu-Mg-Al Layered Double Hydroxides. Acta Phys. - Chim. Sin. 27, 9, (2011) 2088-2094.

[4] G.A. Parks, The isoelectric point of solid oxides, hydroxides, and aqueous hydroxo complex systems. Chem. Rev. 65 (1965) 177-198.

[5] L. Hidmi, M. Edwards, Role of temperature and pH in Cu $(OH)_2$ solubility. Environ. Sci. Technol. 33, 15 (1999) 2607-2610.

[6] A.D Roy, C.C. Forano K.E. Malki, J.P. Besse, Anionic Clays: Trends in Pillaring Chemistry. In: M. L. Occelli, H. E. Robson. (Eds.) Expanded Clays and Other Microporous Solids. Springer, Boston, MA (1992).

[7] T.N. Ramesh, T.L. Madhu, Thermal Decomposition Studies of Layered Metal Hydroxynitrates (Metal: Cu, Zn, Cu/Co, and Zn/Co), Int J Inorg Chem, (2015) 536470.

[8] W.T. Reichle, Synthesis of anionic clay minerals (mixed metal hydroxides, hydrotalcite). Solid State Ionics, 22, 1 (1986) 135-141.

[9] A. Seron, F. Delorme, Synthesis of layered double hydroxides (LDHs) with varying pH: A valuable contribution to the study of Mg/Al LDH formation mechanism. J. Phys. Chem. Solids 69, 5-6, (2008) 1088-1090.

[10] B. Grégoire, C. Ruby, C. Carteret, Hydrolysis of mixed Ni^{2+}–Fe^{3+} and Mg^{2+}–Fe^{3+} solutions and mechanism of formation of layered double hydroxides. Dalton Trans. 42, 44 (2013) 15687-15698.

[11] G. Mascolo, O. Marino, A new synthesis and characterization of magnesium-aluminium hydroxides. Mineral Mag. 43,329 (1980) 619-621.

[12] Y. Zhao, F. Li, R. Zhang, D. G. Evans, X. Duan, Preparation of layered double-hydroxide nanomaterials with a uniform crystallite size using a new method involving separate nucleation and aging steps. Chem. Mater. 14, 10 (2002) 4286-4291.

[13] J.W. Boclair, P.S. Braterman, Layered double hydroxide stability. 1. Relative stabilities of layered double hydroxides and their simple counterparts. Chem. Mater. 11, 2 (1999) 298-302.

[14] J.P. Ramirez, G. Mul, F. Kapteijn, J.A. Moulijn, A spectroscopic study of the effect of the trivalent cation on the thermal decomposition behaviour of Co-based hydrotalcites. J. Mater. Chem. 11, 10 (2001) 2529-2536.

[15] Y. Cudennec, A. Lecerf, The transformation of Cu(OH)2 into CuO, revisited. Solid State Sciences 5 (2003) 1471–1474.

CHAPTER 5

Synthesis of Lignin Model Molecules

Chapter Summary:

Despite the rich functionalities and accessibility to lignin, the complexity of this biopolymer has only rendered its use limited as an industrial substrate. This fact has prompted the use of low molecular weight lignin model molecules which mimic the linkages present in the native lignin. The easier analysis (compared to lignin) of the reaction products of simple model molecules allows collecting reliable information on the effect of catalysts and reaction conditions and it is a prerequisite of advanced studies on lignin reactivity. Advantageously, to avoid structural variation, model molecules can be easily and repeatedly synthesized and well characterized on a lab-scale. In this chapter, the synthesis protocols of lignin α-O-4 and β-O-4 model molecules have been stated. Gas Chromatography Mass Spectrometry (GCMS), Nuclear Magnetic Resonance (NMR), Matrix-Assisted Laser Desorption Ionization-Time of Flight (MALDI-TOF) and Elemental Analysis (EA) were used for the characterization of the models. After a brief introduction to the characterization techniques and methods of analysis; purity and analytical limitations for model molecules sensitive to high temperatures have also been reported.

Introduction to Lignin Model Molecules

Model molecules are the smallest representative units of lignin that mimic the linkages present in the native lignin. The diversity in lignin type coming from different sources and its separation methods from the lignocelluloses impart specific properties to it, which make the study of lignin very complex. However model molecules can be easily and repeatedly synthesized at a lab-scale using synthesis procedures available in literature to avoid structural variation. Keeping in view this point, we headed to the synthesis of different α-O-4 and β-O-4 lignin model molecules (see Fig. 5.1).

5.1 Synthesis Schemes of lignin model compounds

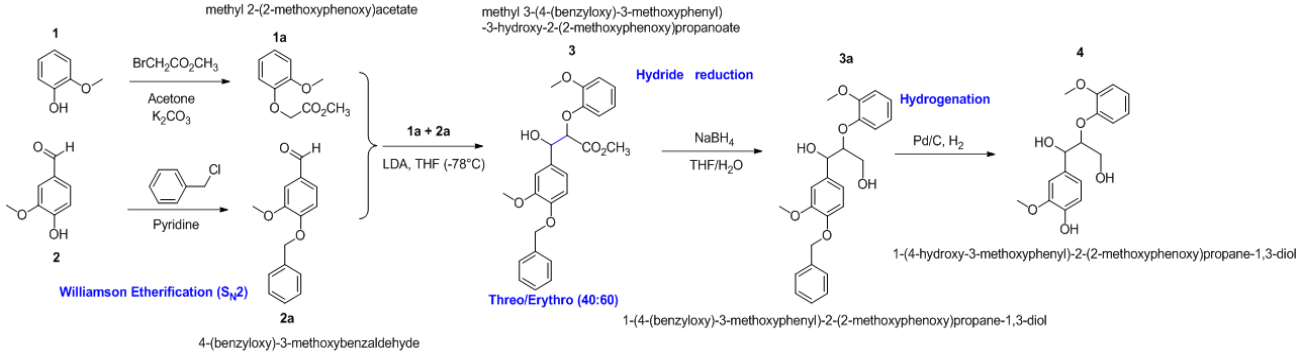

Figure 5.1 Synthesis Scheme of self-synthesized α-O-4 and β-O-4 lignin model molecules

5.1.1 Materials and Methods

Guaiacol (98%), vanillin (99%), Methyl α-bromoacetate (97%), Potassium carbonate (99%), Benzyl bromide (98%), Tetrahydrofuran (99.9%), Sodium borohydride (96%), Diisopropylamine (99.5%), n-ButylLithium (1.6M in hexane), Dioxane (99.5%), Palladium on carbon catalyst (10% wt), Ethyl acetate(99.5%) and Ethanol(99.8%) from Fluka, Dry acetone (100%) and Hydrochloric acid (35%) from VWR and Magnesium sulphate(99%) from Carlo Erba were purchased and used as received without further purification. carbon dioxide (99.99%), 5700 kPa cylinder, was purchased from Air Liquide.

5.1.1.a Synthesis of methyl 2-(2-methoxyphenoxy)acetate (1a)[1]

A solution of guaiacol (9mL, 9.9 g, 79.8mmol) in dry acetone (100mL) and methyl α-bromoacetate (10.85mL, 13.5g, 88.2mmol) was added in anhydrous potassium carbonate (13.73g, 99.3mmol) at room temperature and the resulting mixture was refluxed for 2 hours at 54°C. When the desired product (monitored by TLC) was formed, the mixture was filtered

and washed with ethyl acetate (50 mL approx.); concentrated in the rotator evaporator and dried under vacuum to give a colourless product, yield= 86.7% (Fig. 5.2). GCMS highest peaks: [m+z] (Relative abundance) = 77(100), 95(69.3), 122(53.3), 123(59.2), 196 (66.8); ^{1}H NMR (400MHz, $CDCl_3$): δ 3.71 (s, CH_3), 4.63 (s, CH_2-CO), 6.81-8.23 (m, 4H, Ph-H). ^{13}C NMR (100MHz, $CDCl_3$): δ 52.22 (CH3-COO), 55.88 (CH3-O), 66.50 (CH_2-O), 112.11-122.63 (C-Ar); (M+ n/z) 196.0; elemental analysis $C_{10}H_{12}O_4$ (calculated %) C 60.75, O 34.1, H 5.94. The product was stored under vacuum at -5°C. (Refer to the GCMS, NMR, MALDI data at the end of the chapter)

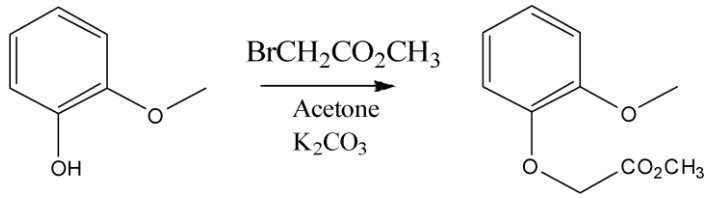

Figure 5.2 Williamson etherification scheme for synthesis of methyl 2-(2-methoxyphenoxy)acetate (1a)

5.1.2 α-O-4 Model Molecule

5.1.1b Synthesis of 4-(benzyloxy)-3-methoxybenzaldehyde (2a)[2]

A mixture of Vanillin (10g, 65.7mmol) in benzyl bromide (15.27g, 89.2mmol), potassium carbonate (4.04g, 29.2mmol) and acetone (150mL) were refluxed for 12 hours at 54°C and then water (approx. 150mL) was added to quench the reaction. The precipitated product was recrystallized with water and ethanol (2:1), 50mL. A cloudy white solution appeared that was centrifuged and washed with water (x3) at 5000 rpm at 0°C for 15 minutes each. The crystals were then filtered and dried in a vacuum desiccator overnight, yield = 72% (Fig. 5.3). GCMS highest peaks: [m+z] (Relative abundance) = 51(7.2), 65(23.4), 91(100), 92(8.55), 242(4.28); ^{1}H NMR (400MHz, $CDCl_3$: δ 3.82 (s, CH_3), 4.63 (s, CH_2-O), 6.76-6.94 (m, 8H, Ph-H), 7.20 (s, CHO). ^{13}C NMR (100MHz, $CDCl_3$): δ 56.09 (CH3-O), 70.90 (CH_2-O), 109.39-128.74 (C-Ar), 190.23 (CHO).; (M+ n/z) 242.1; elemental analysis $C_{15}H_{14}O_3$ (calculated %) C 72.06, O 18.52, H 5.23. The compound, if not stored properly, was oxidizing; with its colour changing to yellowish. Therefore, strict measures were taken to retain the molecule purity. (Refer to the GCMS, NMR, MALDI data at the end of the chapter)

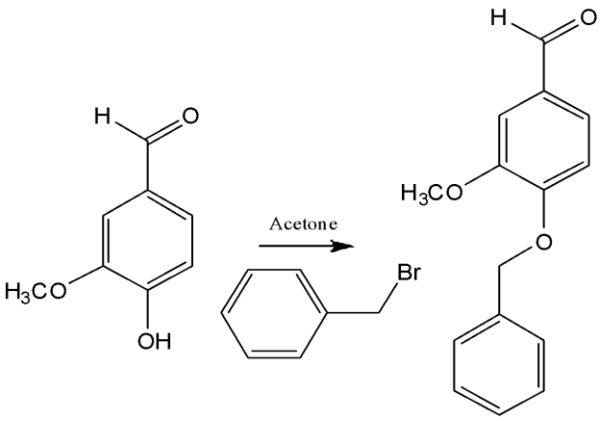

Figure 5.3 Williamson etherification scheme for synthesis of 4-(benzyloxy)-3-methoxybenzaldehyde(2a)

Figure 5.4 Precipitated, clear colourless needles of 4-(benzyloxy)-3-methoxybenzaldehyde

5.1.1.c Synthesis of methyl 3-(4-benzyloxy)-3-methoxyphenyl)-3-hydroxy-2-(2-methoxyphenoxy)propanoate(3)[3]

A two-necked 250mL round bottom flask with a magnetic stirrer and a thermocouple was flushed with argon gas. (2.875mL, 20.3mmol) of diisopropylamine was added in 50mL of THF. This reaction mixture was cooled to 0°C and a (14.6mL, 155mmol) of n-ButylLi was added very slowly in 30 min. This mixture was then cooled to -78°C with dry ice. After stirring for 1 hour, a separate solution of compound 1a (4.266g, 21.7mmol) in 50mL of THF was added slowly in 2 hours (approx. 0.75mL per minute) by maintaining the temperature at -78°C. After stirring of additional 20min, a solution of compound 2a (3.18g, 13.14mmol) in 50mL of THF was added dropwise in 1 hour (approx. 1mL per minute).

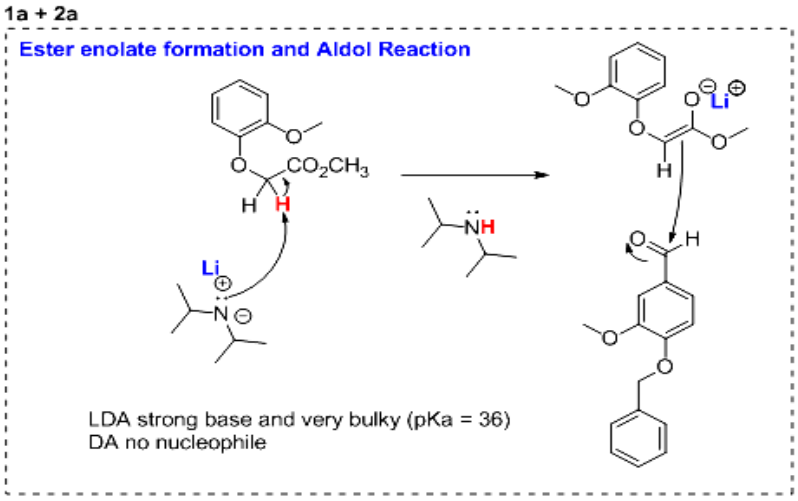

Figure 5.5 Mechanism reaction of compounds1a and 2a

The reaction mixture was allowed to stir for 90min at -78°C and 120mL of distilled water was added for quenching. The aqueous phase was extracted by solvent extraction by Ethyl acetate 540mL (180 x 3). The separated organic phase was washed with HCl (14.07mL in 160mL), water 160mL and brine 200mL. It was then dried with $MgSO_4$ to absorb the excess of water left in the organic phase. The mixture was then concentrated under reduced pressure and dried for 3 hours in vacuum to obtain a yellowish-orange product, a combination of two diastereomers threo/erythro. Yield=74% (Fig. 5.6)^{1}H NMR (400MHz, $CDCl_3$: δ 3.77 (s, CH_3), 3.82 (s, CH_3), 3.88 (CH_3-COO), 3.94 (s, OH), 4.91 (CH-COO), 5.07 (s, CH_2-O), 5.18 (CH-OH), 7.19-7.38 (m, 12H, Ph-H). ^{13}C NMR (100MHz, $CDCl_3$): δ 52.2 (**C**H_3-O), 55.9 (**C**H_3-O), 70.92 (**C**H_3-COO), 74.8 (**C**H-O), 70.9 (**C**H-OH), 90.59 (**C**H_2-O), 110-128 (**C**-Ar).; (M+ n/z), 438.17; elemental analysis $C_{25}H_{26}O_7$ (calculated %) C 64.68, O 29.13, H 5.96. The product was stored in fridge at -5°C under vacuum and analyzed by MALDI and NMR.

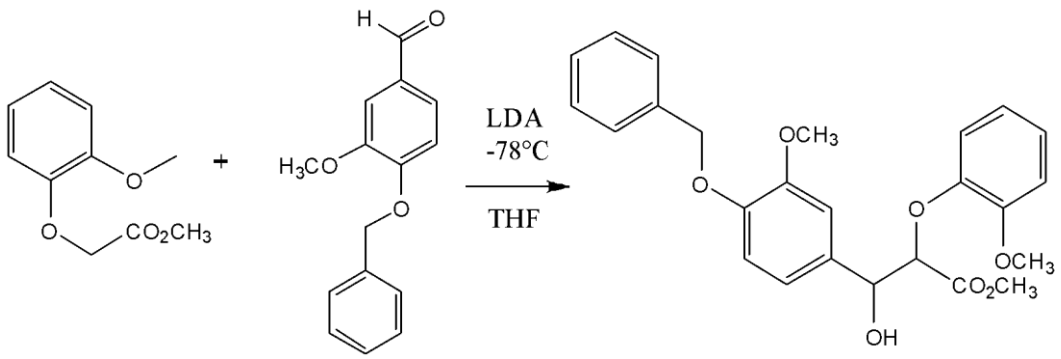

Figure 5.6 Aldol reaction scheme for synthesis of methyl 3-(4-benzyloxy)-3-methoxyphenyl)-3-hydroxy-2-(2-methoxyphenoxy)propanoate (3)

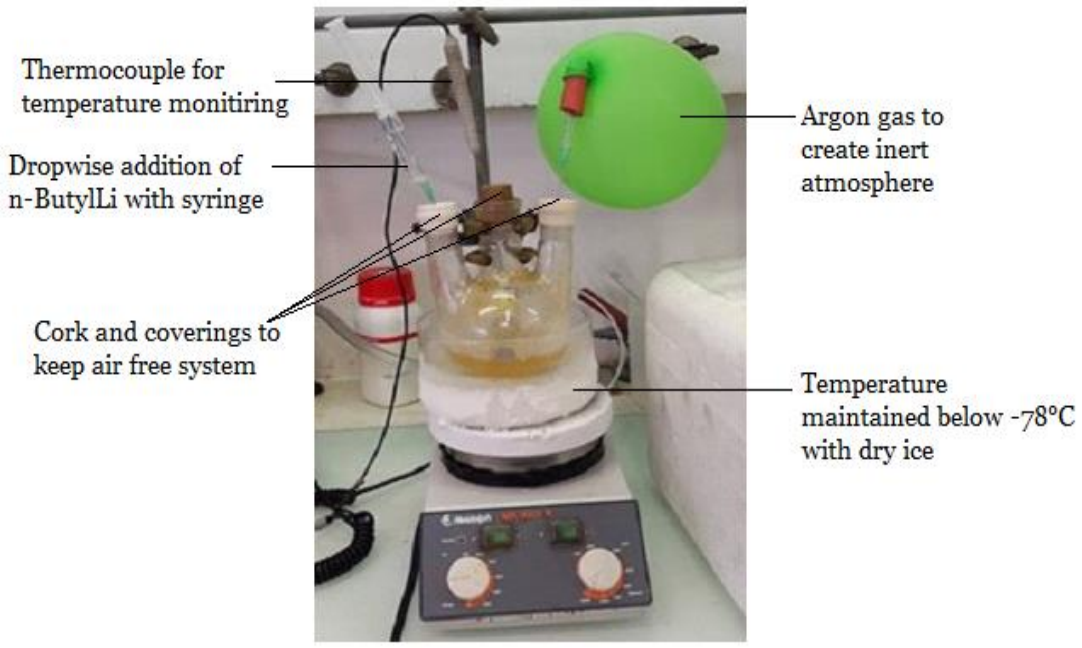

Figure 5.7 System setup for the synthesis of compound 3

5.1.1c.1 Purification of Compound 3

The synthesis and purity of compound 3 was monitored by the TLC during the reaction. After the completion of the reaction, the left over unreacted reactants were observed in the reaction stream which was separated by column chromatography with silica (70-200microns) packed column using as eluent a mixture of THF and hexane (1:1) respectively. (see Fig. 5.8)

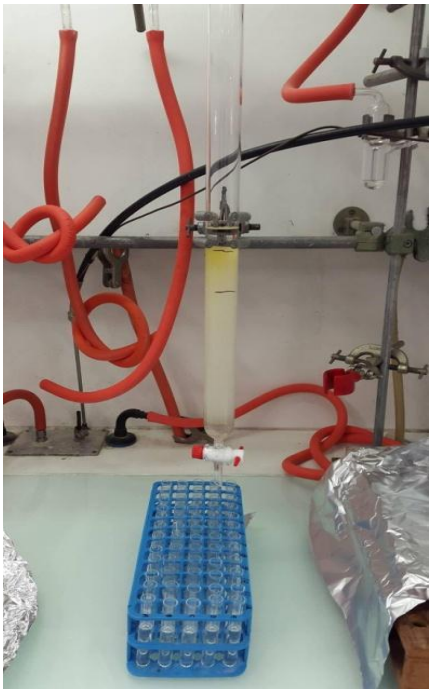

Figure 5.8 Column chromatography to purify compound 3 from the unreacted compound 1a and 2

5.1.1.d Synthesis of 1-(4-(benzyloxy)-3-methoxyphenyl)-2-(2-methoxyphenoxy)propane-1,3- diol (3a)[4]

A solution of (0.646g, 1.47mmol) of methyl 3-(4-(benzyloxy)-3-methoxyphenyl)-3-hydroxy-2-(2-methoxyphenoxy)proponoate (3) in 12.99mL of THF/H_2O (7.692mL/4.308mL=3:1) was prepared. 0.6g of $NaBH_4$ (15.8mmol) was added with continuous stirring in three turns (0.2g each/2 hours).The mixture was left stirring until 48 hours at room temperature. 25mL of water was added and the aqueous solution was extracted with ethyl acetate (200mL).

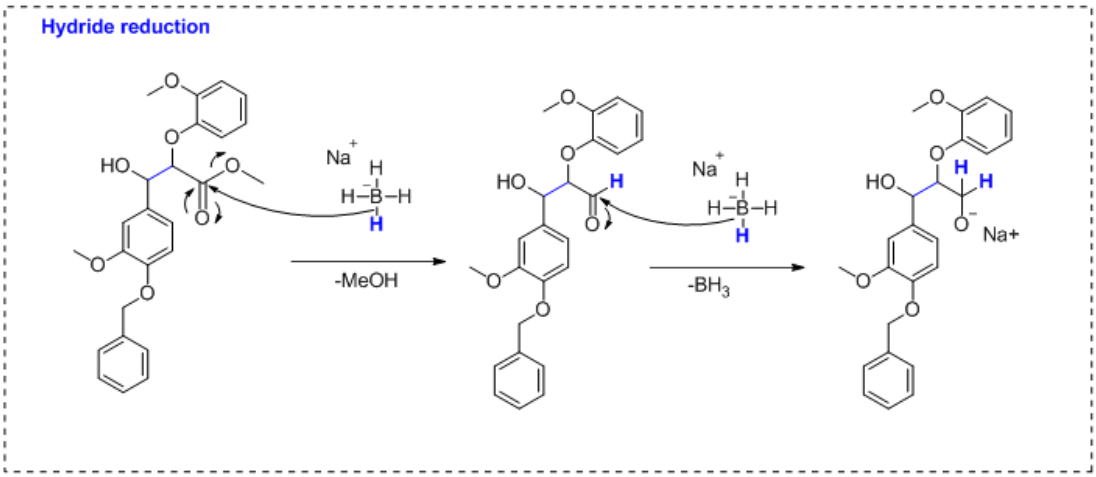

Figure 5.9 Mechanism of hydride reduction and protonation

The organic phase was washed and dried with $MgSO_4$, filtered and concentrated to give the product. Yield=36% (Fig 5.10) (M+ n/z), 410.17; elemental analysis $C_{24}H_{26}O_6$ (calculated %) C 68.67, O 23.46, H 5.94. The characterization done by MALDI-TOF can be found at the end of the chapter.

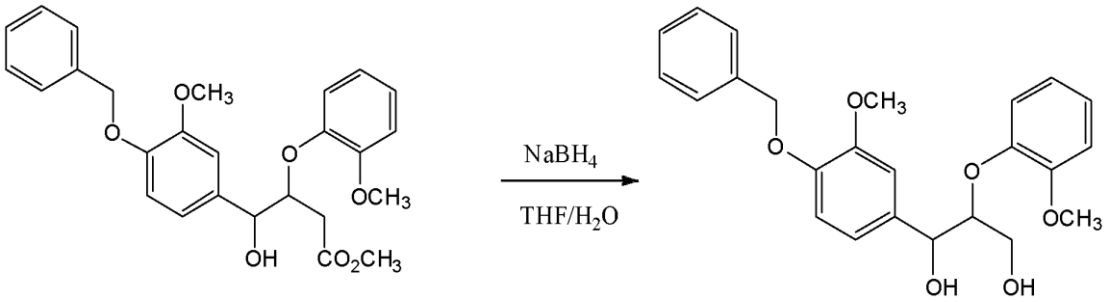

Figure 5.10 Hydride reduction scheme for synthesis of 1-(4-(benzyloxy)-3-methoxyphenyl)-2-(2-methoxyphenoxy)propane- 1,3- diol (3a)

Due to impurities in the molecule, the NMR results were not conclusive enough, so we performed the MALDI-TOF analysis to see the molecular ion.

5.1.1.e Synthesis of 1-(4-hydroxy-3-methoxyphenyl)-2-(2 methoxyphenoxy)propane-1,3-diol (4)[5]

(0.16g, 0.39mmol) of 1-(4-(benzyloxy)-3-methoxyphenyl)-2-(2-methoxyphenoxy)propane-1,3-diol was added in 8.57mL of Dioxane and 0.04g of 10wt% Palladium/Carbon catalyst with continuous stirring. H_2 was purged into the system and the consumption of the starting material was monitored with TLC. The catalyst was added with the same rate until all the starting material was consumed. The catalyst was filtered and dioxane was evaporated to get the product. Yield= 64% (Fig. 5.11). (M+ n/z), 320.13; elemental analysis $C_{17}H_{20}O_6$ (calculated %) C 62.81, O 28.43, H 5.98. Result of MALDI-TOF spectrum has been attached at the later part of the chapter.

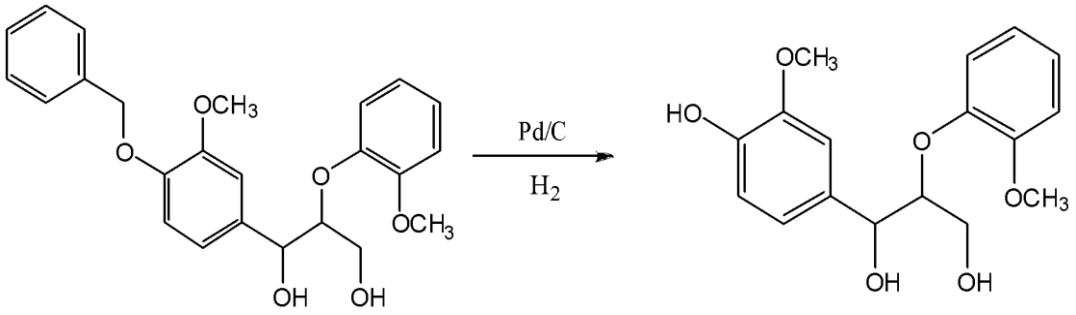

Figure 5.11 Hydrogenation scheme for synthesis of 1-(4-hydroxy-3-methoxyphenyl)-2-(2 methoxyphenoxy)propane-1,3- diol (4)

Due to impurities in the molecule, the NMR results were not conclusive enough, so we performed the MALDI-TOF analysis to see the molecular ion for this compound as well.

5.2 Characterization of Model Molecules

The characterization of the model molecules was done by various techniques however it was observed that some techniques were valid up to a certain point. For example, when GCMS of compound 3 was done, it broke apart into the component reactants and only their peaks could be seen in the MS spectrum however when the same molecule was analyzed by NMR and MALDI-TOF, the compound was easily detected. Thus temperature sensitive molecules could only be analyzed by NMR or MALDI-TOF and elemental analysis.

- GCMS
- NMR
- MALDI-TOF
- Elemental Analysis

5.2.1 Gas Chromatography-Mass Spectrometry

A Gas Chromatography (GC) coupled with Mass spectrometry (MS), GCMS, is an analytical technique for the qualitative and/or quantitative analysis of low molecular weight single components or mixtures that are sufficiently volatile but thermally stable at high temperatures. A sample dissolved in an appropriate solvent is injected into the GC where it is evaporated and taken through the column by the carrier gas, helium (mobile phase). The components of the mixture are separated on the basis of their interaction with the column coating (stationary phase). The helium gas containing the sample is transferred to a heated transfer line with a connecting ion source at the end where separated components of mixture are converted to ions. A typical method of ionisation is Electrospray ionization (ESI). A sample molecular ion (M^+) is formed as a result of loss of electron by the beam of electrospray. The high energy transferred to the molecules fragments leads them to produce smaller units (ions) with characteristic relative abundance that confirms the distinctive molecular species as a 'fingerprint' (Fig. 5.12). As these ions travel to the mass analyser (commonly quadrupoles), the positively charges ions are separated and travel to the detector. An amplified signal from the detector is sent to the computer and individual spectral peaks yield the molecular weight of the compound (Fig. 5.13). Thus GCMS is a reliable technique for the separation of component mixture, their purities and a confirmation test. However, for the sake of quantification, GCMS has limitations.[6]

5.2.1.1 GCMS Analysis of Lignin Models

The analysis of the model molecules was done by Shimadzu GCMS-QP 2010 plus using Zebron ZB-5HT column of dimensions: length 15m, thickness 0.10µm, diameter 0.25mm, using the following method. For GC; Column oven temperature 40°C; Injection temperature 250°C; Constant flow of Helium 1.21mL/min, Split ratio 30. For MS, ESI mode of ionization with ion source temperature 200°C; Interface temperature 250°C; (m/z 33-750).

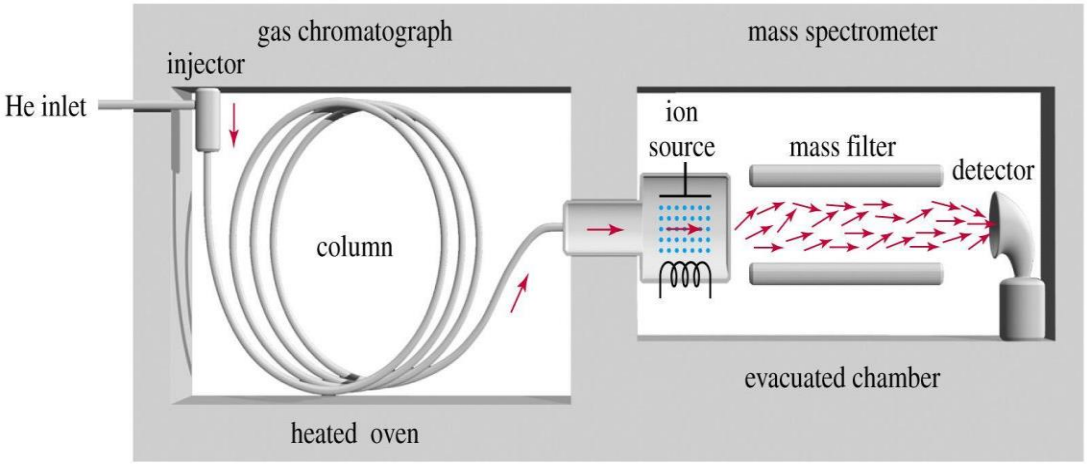

Figure 5.12 Block diagram of a gas chromatograph-mass spectrometer.[7]

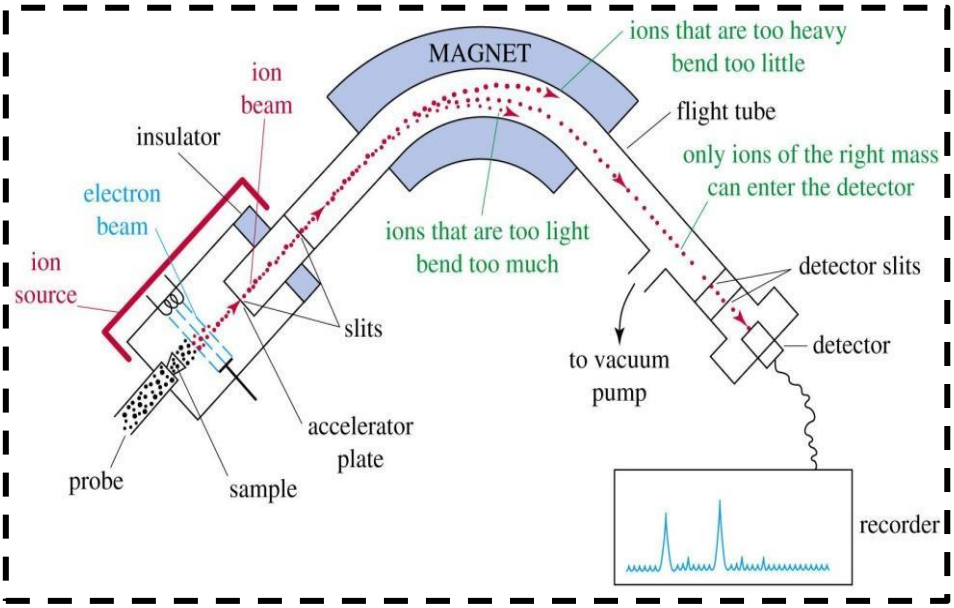

Figure 5.13 Working Principle of GCMS.[7]

5.2.1.2 GC-MS Identification of Model Molecules

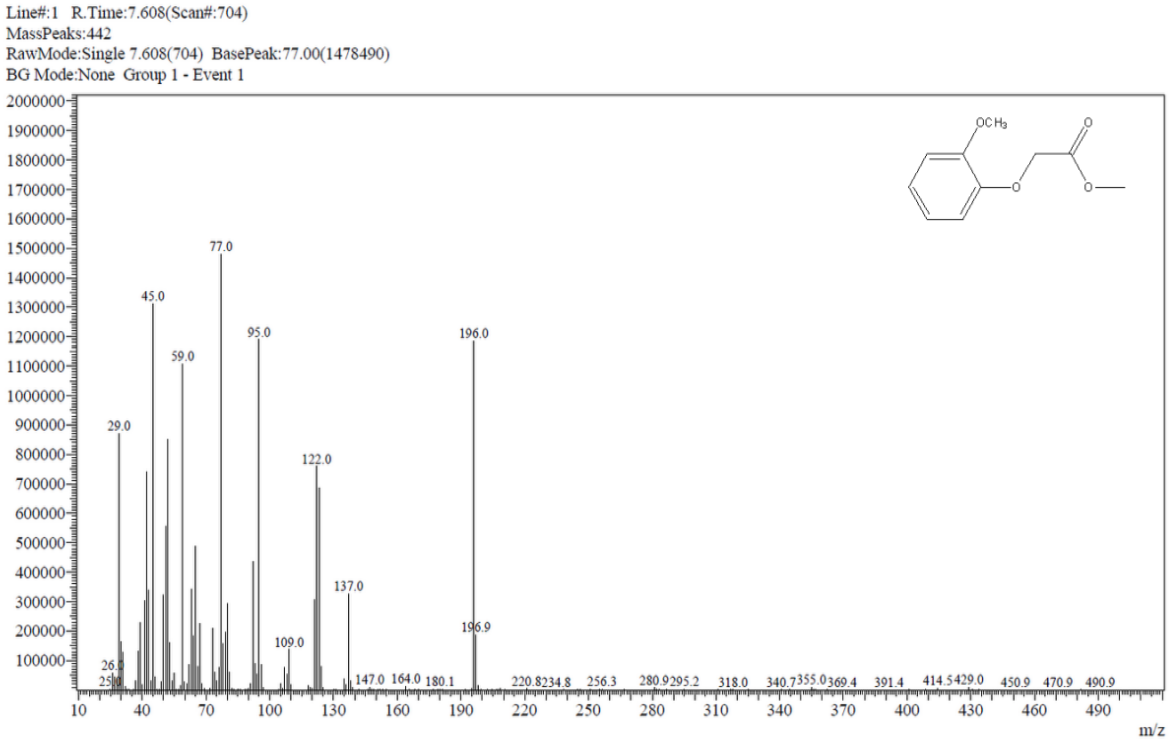

Figure 5.14 MS spectrum of MS spectrum of methyl 2-(2-methoxyphenoxy)acetate (1a)

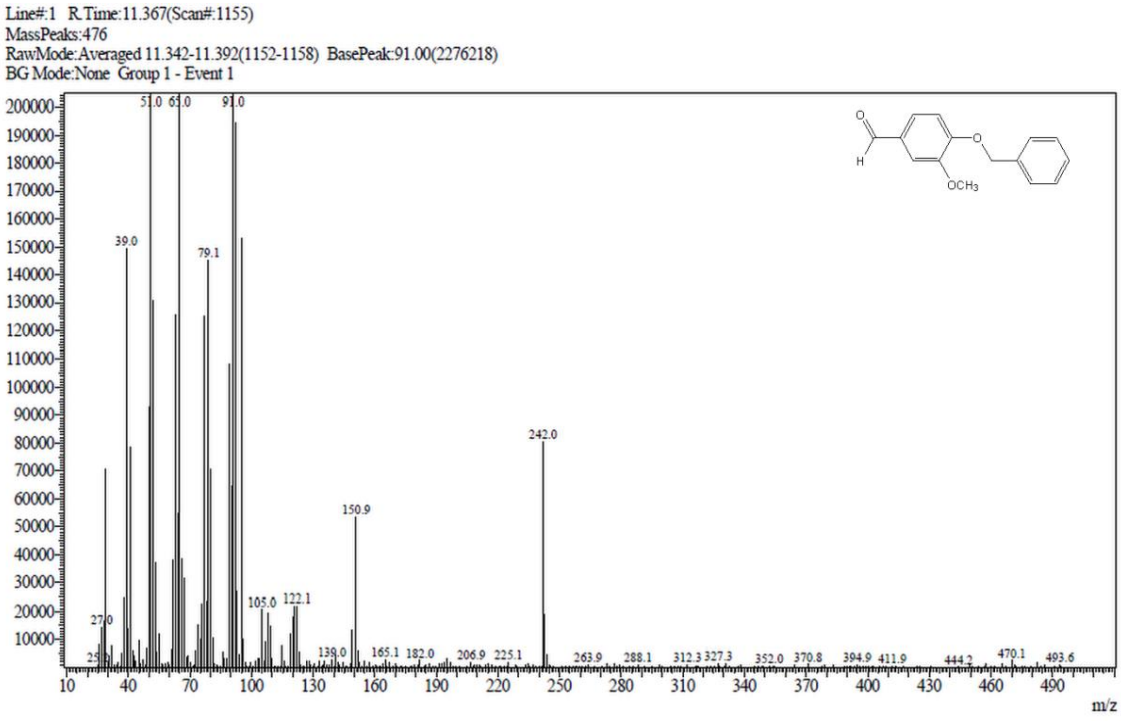

Figure 5.15 MS spectrum of 4-(benzyloxy)-3-methoxybenzaldehyde (2a)

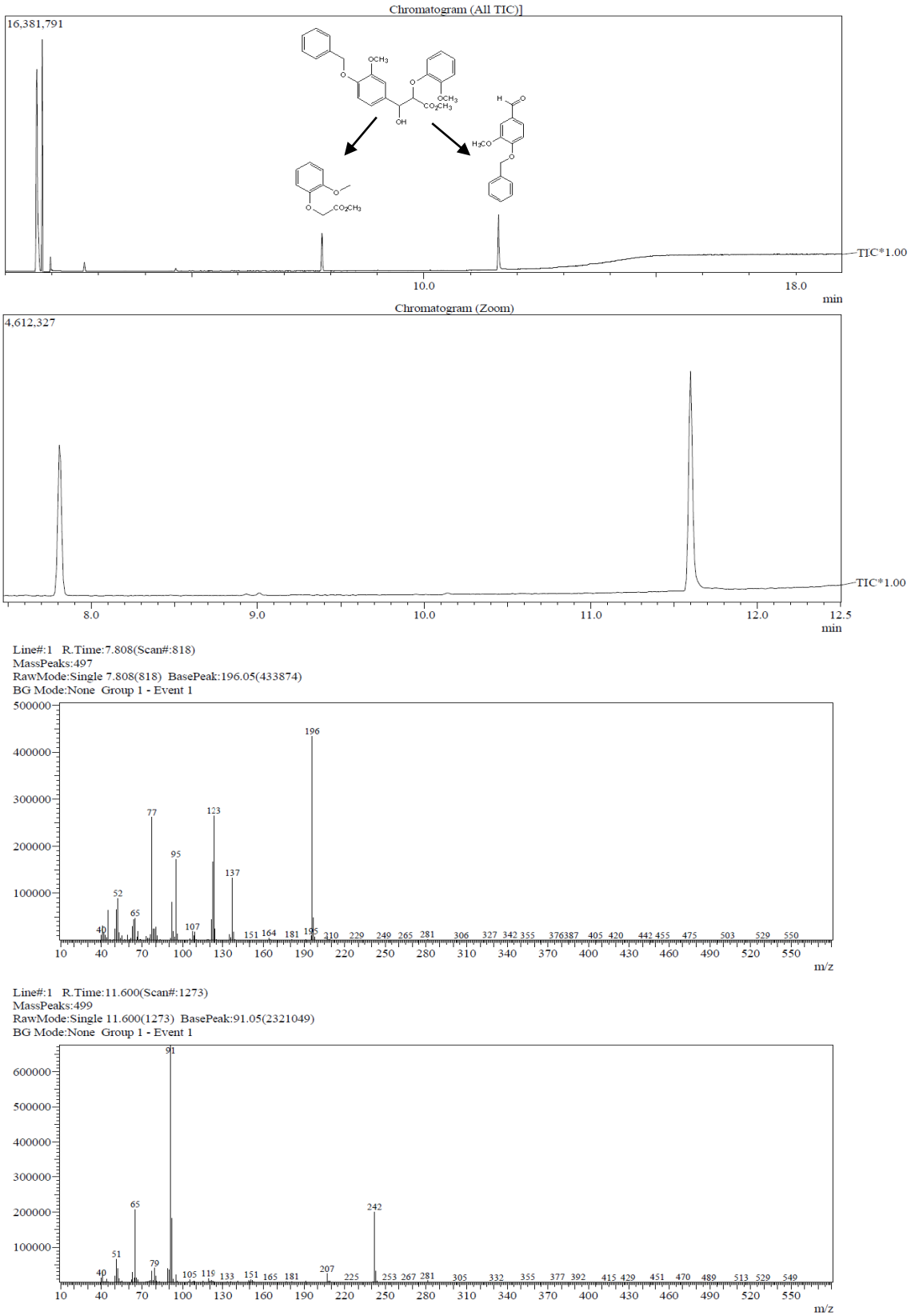

Figure 5.16 MS spectrum of methyl 3-(4-benzyloxy)-3-methoxyphenyl)-3-hydroxy-2-(2-methoxyphenoxy)propanoate(3)

5.2.2 Matrix-Assisted Laser Desorption Ionization-Time of Flight (MALDI-TOF) Analysis

MALDI Technique is an advanced tool for analysis of heavy molecular weight compounds that are sensitive to high temperatures. Its principle is similar to Mass Spectrometry the molecules are vaporized and converted into charged ions and the mass to charge ratio is calculated. But, contrarily to GCMS, MALDI relies on soft ionization method i.e. the addition of one or more known ions to the sample molecule. The addition however can be either cationic (positive mode) or anionic (negative mode). This gentle ionization technique saves the sample integrity to a significant level. Another advantage of the MALDI technique is the production of singly charged ions, which simplify the interpretation of data. Therefore, MALDI has been considered a reliable instrument for analysis of high molecular weight compounds and proteins.

Practically, the sample is uniformly mixed with the matrix on a conductive plate. The matrix, together with the sample is vaporized and comes in interaction with the Ultra violet radiation. This produces charged ions of different sizes on the sample plate which fly towards the detector due to a potential difference between two points. As the potential difference between two points is constant for all ions, lighter ions tend to travel faster through the drift space to reach the detector. (Fig. 5.14) Consequently, the time spent by each ion in the vacuumed space is different, depending on their mass (Time of flight). Hence, this system is known as MALDI-TOF MS Spectrum.

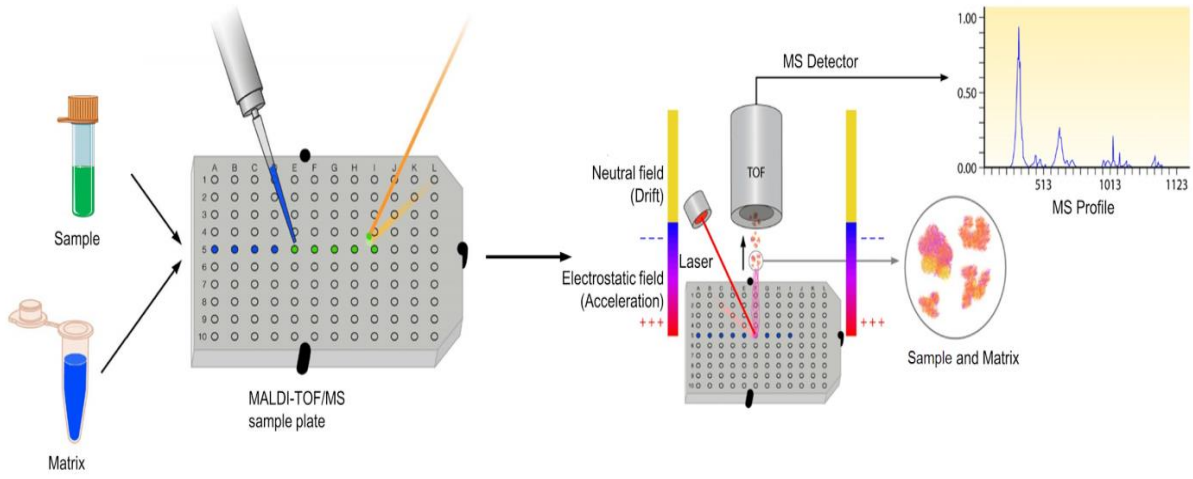

Figure 5.17 Schematic Diagram showing the working principle of MALDI-TOF MS.[8]

5.2.2. MALDI-TOF Analysis of Lignin Models

Full scan mass spectra MALDI-TOF-MS were performed on a MALDI-TOF/TOF Bruker RapifleX mass spectrometer, using a nitrogen laser for MALDI (=337 nm). Mass spectra of 3000 shots were accumulated for the spectra at a 25 kV acceleration voltage and reflectron lens potentials at 26.3 KV. Mixture of peptides was used for external calibration. The samples were dissolved at 40 mg/mL in a mixture of water: acetone (50:50 vol %). The matrix used was DHB (2,5-dihydroxybenzoic acid). It was dissolved at 10 mg/mL in a mixture of acetone and water (50:50 vol %). The cationization agent was LiCl (10 mg/mL in methanol). 10 µL of matrix solution, 4 µL of sample and 1 µL of salt were mixed. 1 µL of this mixed solution was hand spotted on a MALDI target and left to dry before analysis.

5.2.2.1 MALDI-TOF Identification of Model Molecules

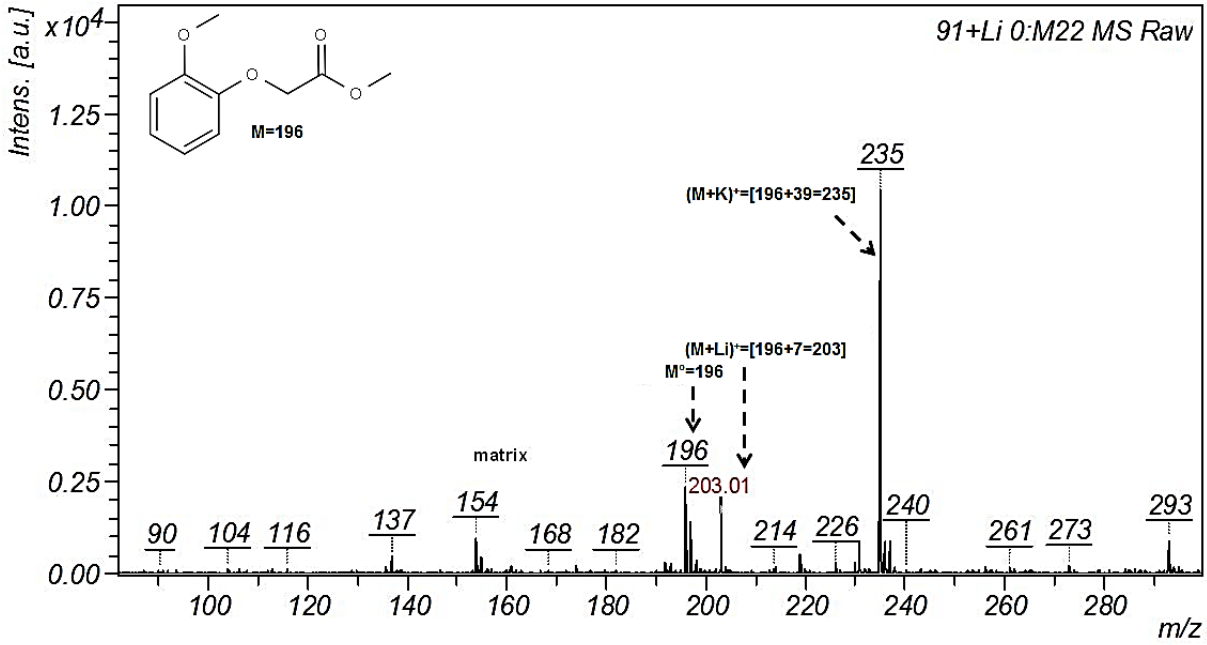

Figure 5.18 Spectrum MALDI-TOF of methyl 2-(2-methoxyphenoxy)acetate (1a)

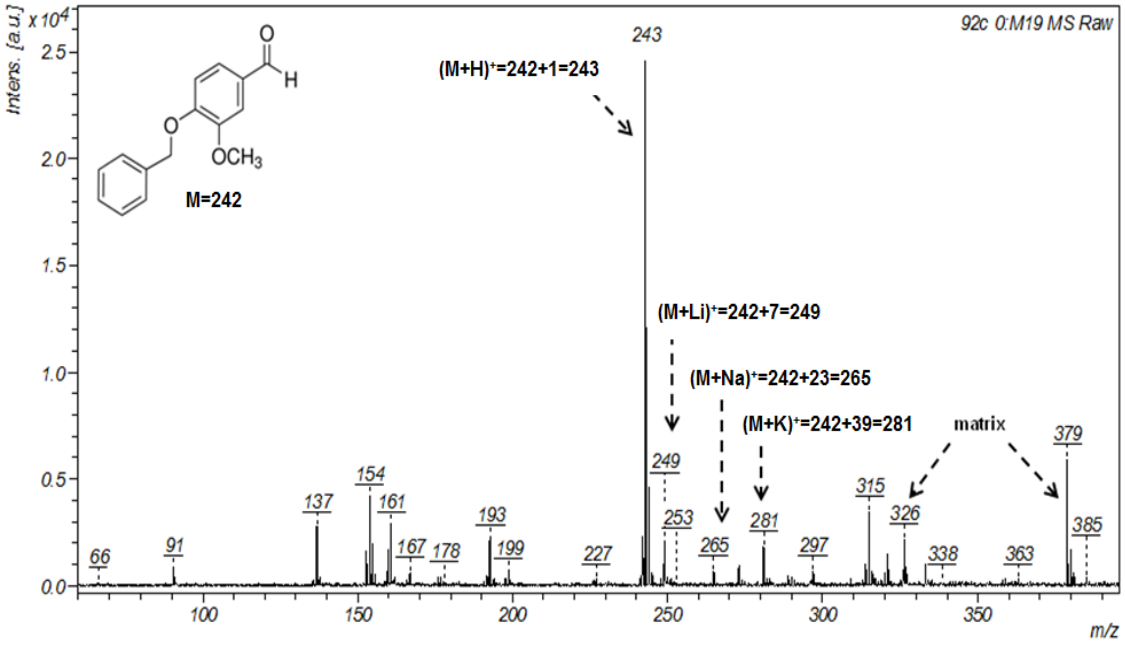

Figure 5.19 Spectrum MALDI-TOF of 4-(benzyloxy)-3-methoxybenzaldehyde (2a) in positive ionization mode

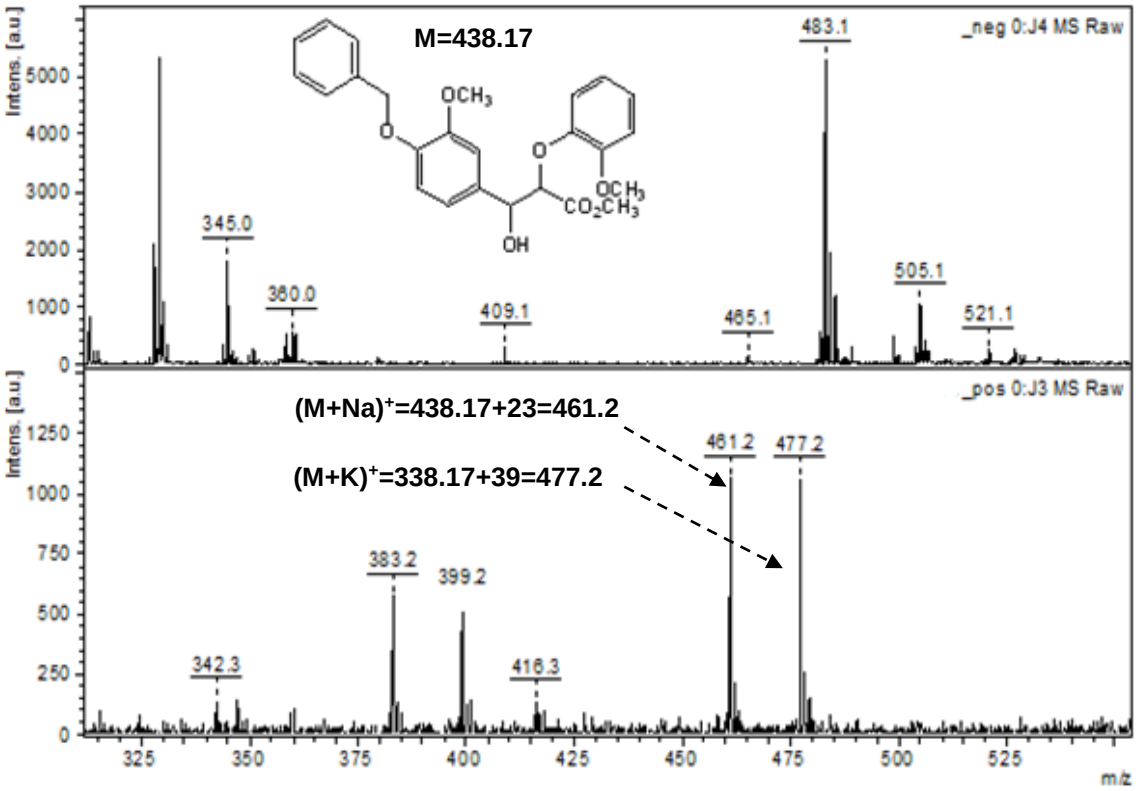

Figure 5.20 Spectrum MALDI TOF of methyl 3-(4-benzyloxy)-3-methoxyphenyl)-3-hydroxy-2-(2-methoxyphenoxy)propanoate (3) in negative (top) and positive (bottom) ionization mode

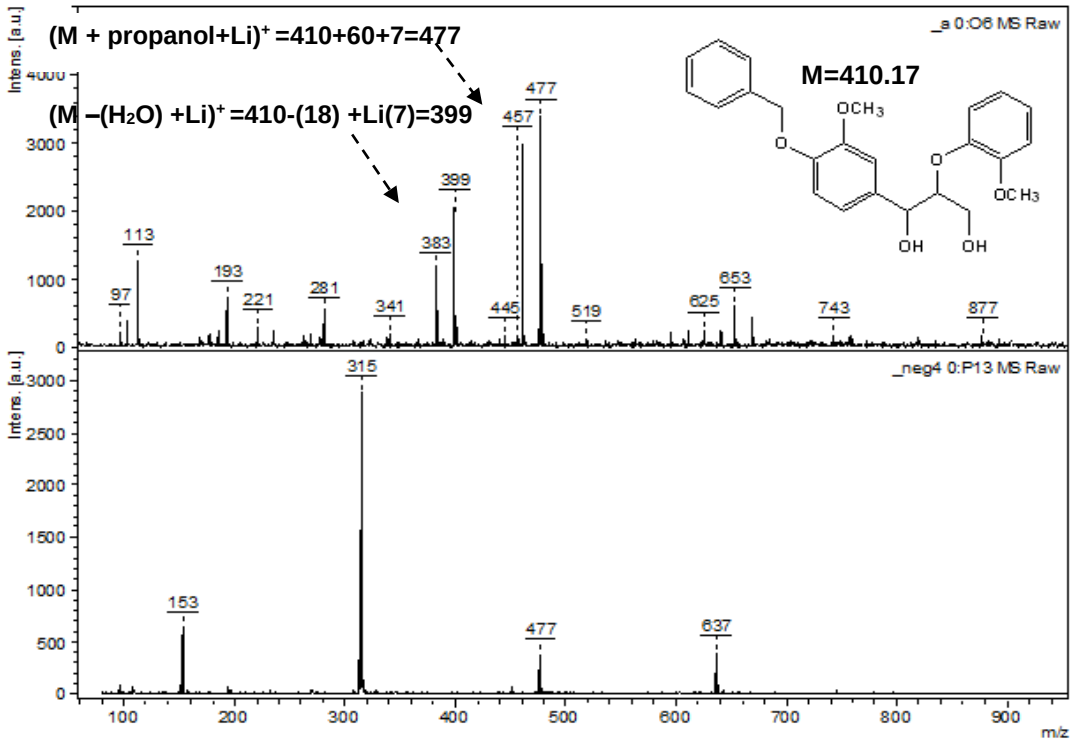

Figure 5.21 Spectrum MALDI TOF of 1-(4-(benzyloxy)-3-methoxyphenyl)-2-(2-methoxyphenoxy)propane-1,3-diol (3a) in positive (top) and negative (bottom) ionization mode

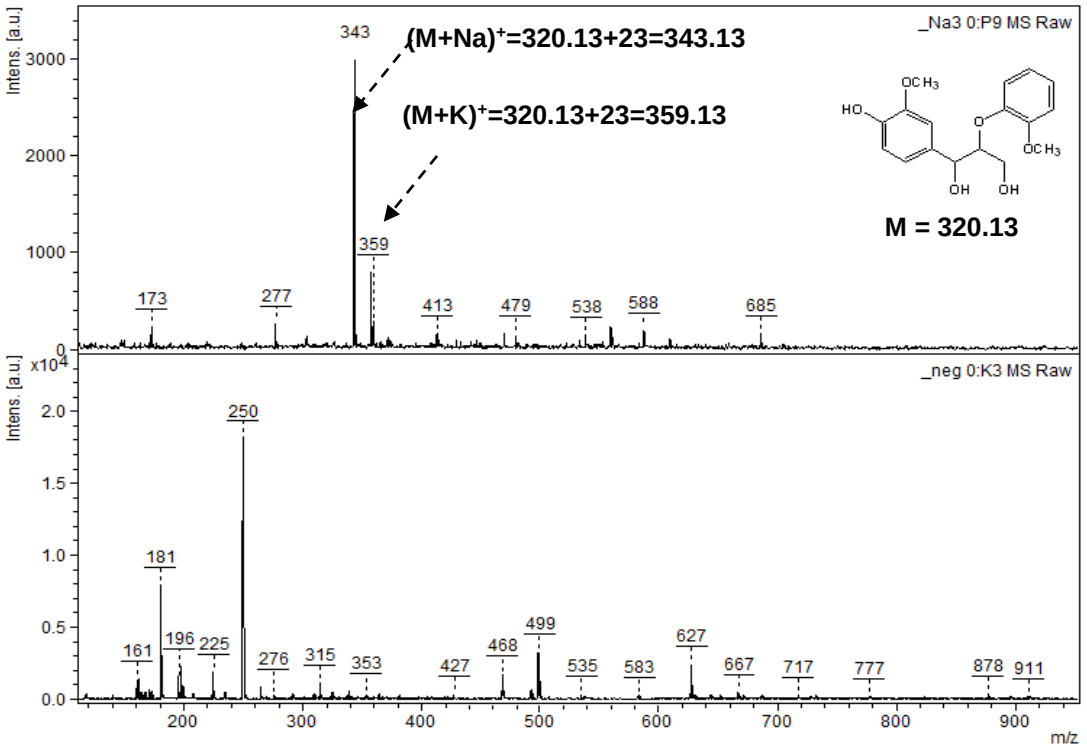

Figure 5.22 Spectrum MALDI-TOF of 1-(4-hydroxy-3-methoxyphenyl)-2-(2-methoxyphenoxy)propane-1,3-diol (4) in positive (top) and negative (bottom) ionization mode

5.2.3 Nuclear Magnetic Resonance (NMR)

Nuclear Magnetic Resonance (NMR) spectroscopy is a non-destructive analytical technique for the determination of the structure and purity content of the molecules.[10] It is a physical phenomena used to investigate molecular properties of matter by irradiating atomic nuclei in a magnetic field with radio waves.[9]

Among all offered spectral methods, NMR is the only technique to analyze and interpret a whole spectral range and determine the molecular composition.[10] The spectra are clear, distinctive, and often exceedingly predictable for small and pure molecules. Not only are the different functional groups easily identifiable but also the same functional groups with different neighbouring substituents give the unique signals. The working principle of NMR is related to the spins of the atomic nuclei of the sample. The spinning of proton in the nuclei generates a magnetic field which is aligned either in or out of the orientation of the external magnetic field when applied. If the proton positions itself in the direction of field, a lower energy orientation is achieved, called alpha spin state (α-spin) and beta spin (β-spin) for vice versa.[11] When the electromagnetic radiation of the right frequency is applied, the protons flip to from α to β or vice versa spin state. This flipping electromagnetic radiation is absorbed the nucleus that is oriented in the direction opposite to the magnetic field. Thus nucleus tends to be in the state of resonance which is revealed in the form of hyper fine spectral lines, detected by the NMR spectrometer. As the energy required to flipping the nucleus for all compounds vary, their resonance differs, giving details of the electronic structure. Therefore, highly characteristic spectral lines are obtained for each compound.[11]

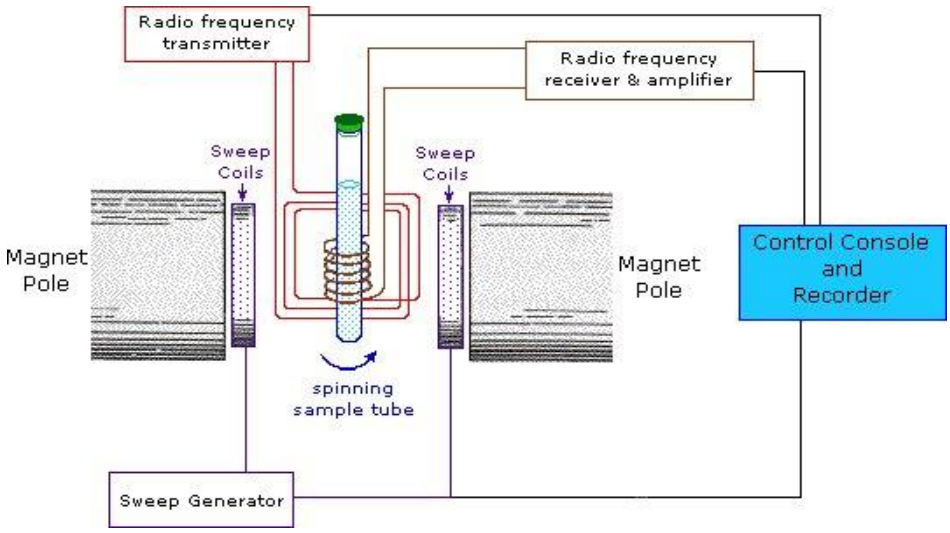

Figure 5.23 Schematic of nuclear magnetic resonance (NMR) [12]

5.2.3.1 NMR Analysis of Model Molecules

The ^{1}H and ^{13}C APT NMR were done on a Bruker 400MHz HD AVANCE III spectrometer with Bruker Smartprobe with two channels, ^{1}H and Broadband. For ^{1}H the hard pulse (90°) is 9.25µs for 40W and we use a 30° pulse with a D1 (relaxation delay) of 1s in 1D measurement. For ^{13}C the hard pulse is 9.90µs for 100W, frequency 100MHz. ^{13}C APT sequence show CH,CH_3 + and C,CH_2-.

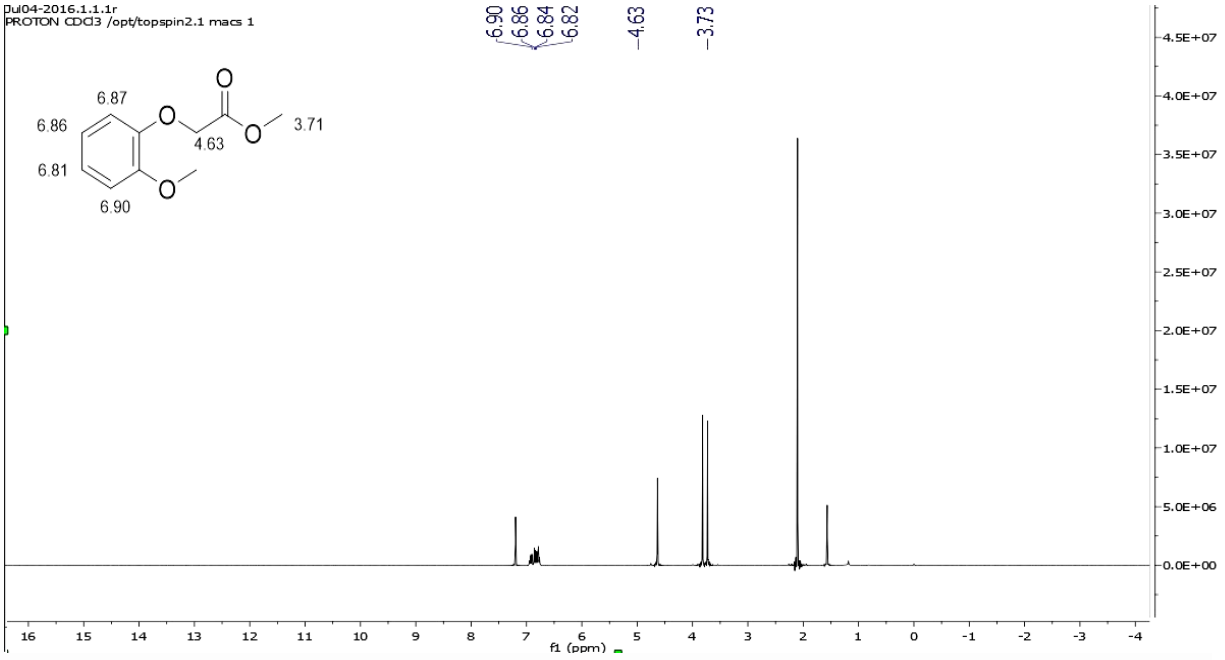

Figure 5.24 ^{1}H-NMR (400MHz, $CDCl_3$) of Compound 1a

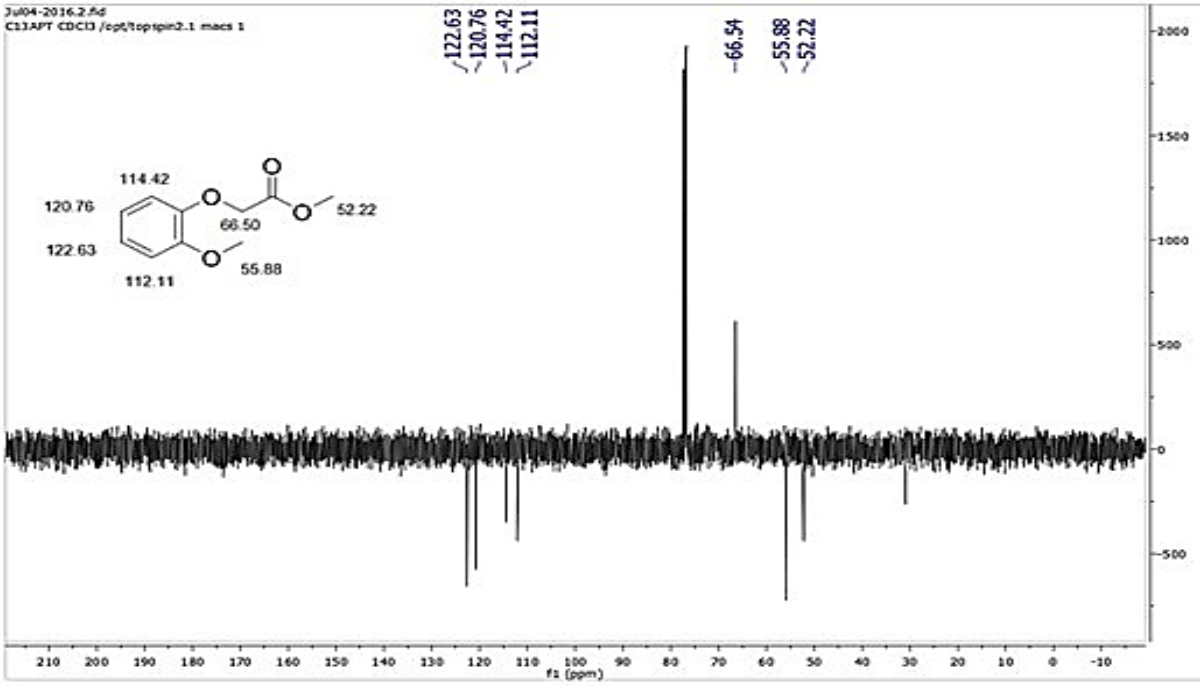

Figure 5.25 ^{13}C-NMR (100MHz, $CDCl_3$) of Compound 1a

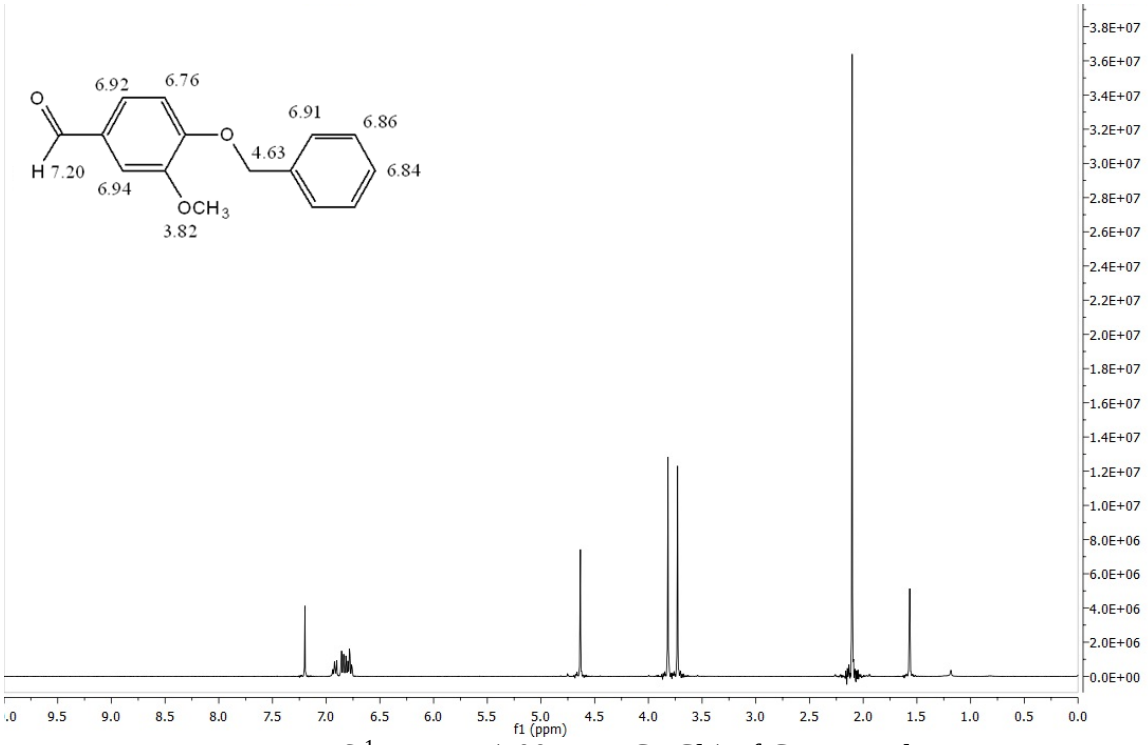

Figure 5.26 ^{1}H-NMR (400MHz, $CDCl_3$) of Compound 2a

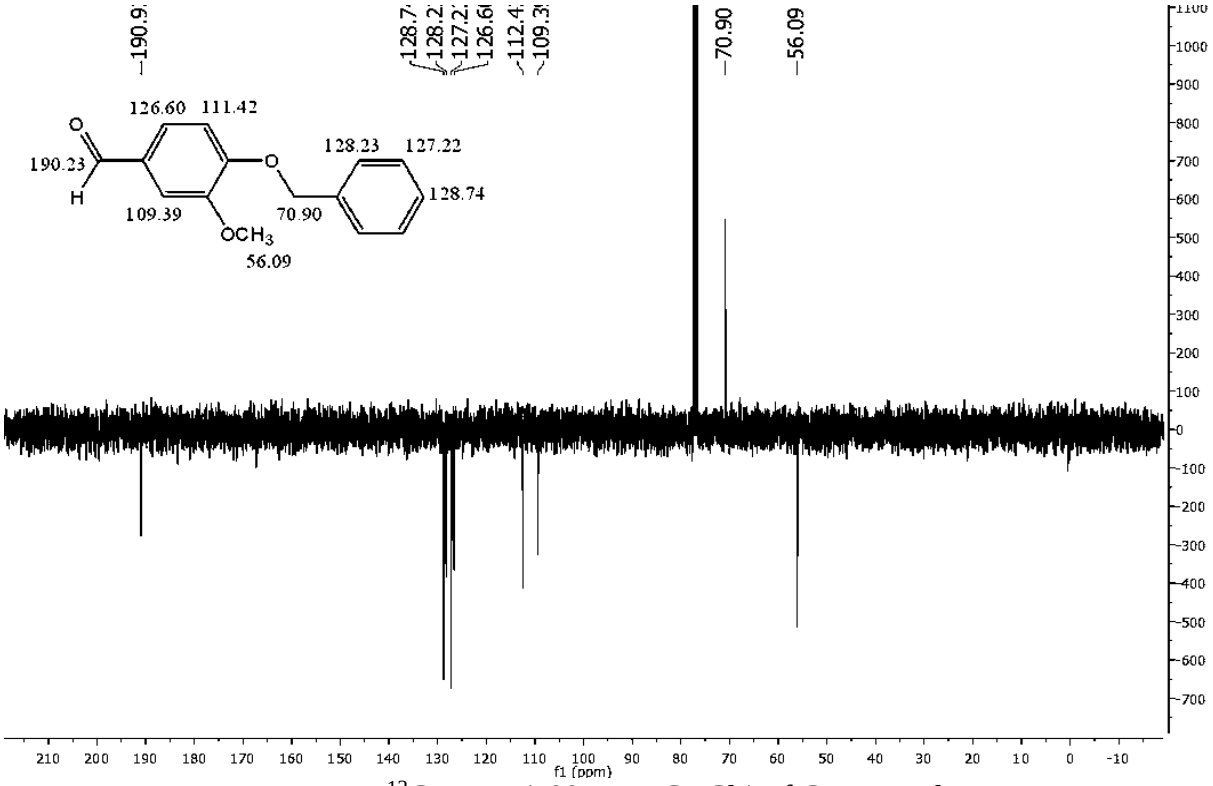

Figure 5.27 ^{13}C-NMR (100MHz, $CDCl_3$) of Compound 2a

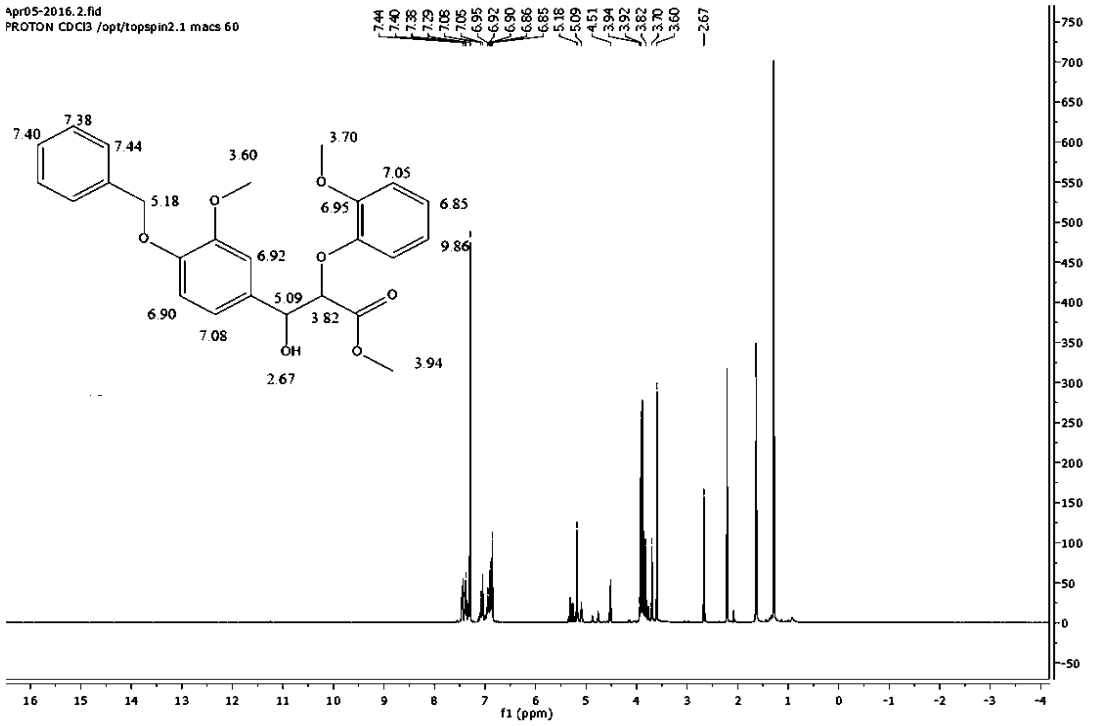

Figure 5.28 ^{1}H-NMR (400MHz, $CDCl_3$) of Compound 3

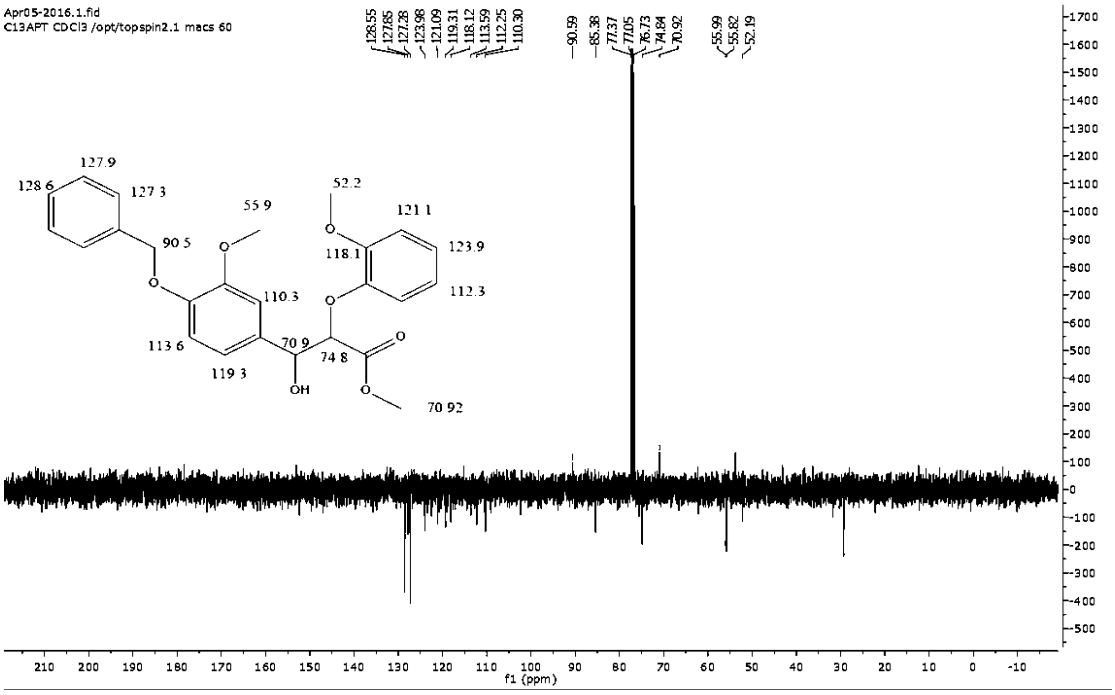

Figure 5.29 ^{13}C-NMR (100MHz, $CDCl_3$) of Compound 3

5.2.4 Elemental Analysis (EA)

Elemental analysis is an analytical tool to qualitatively and quantitatively characterize a sample composition by combustion.[13] In organic chemistry it generally refers to the carbon, hydrogen, oxygen, nitrogen and heteroatom (X) content of the sample. The technique is

useful to ascertain unknown compound synthesized composition. Moreover, it is the most convenient and inexpensive method to figure out impurities in the sample by comparing them with reference if available. The sample is burnt in excess of oxygen which produces combustion products like water, carbon dioxide, Nitric oxide (see Fig. 5.27). The masses of these substances, separated through gas chromatography, are used to calculate the average initial composition of the sample to derive its chemical formula.

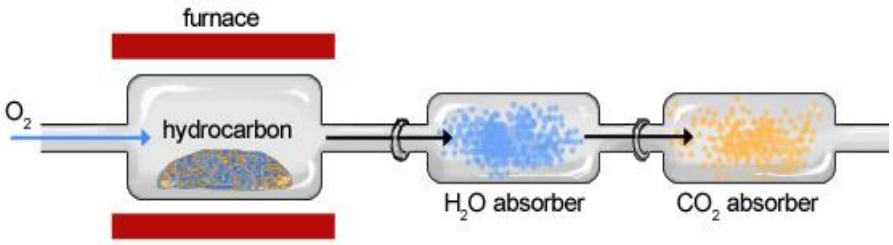

Figure 5.30 A typical combustion analyzer with a furnace.[14]

For determination of Carbon and Hydrogen: Elemental analysis was carried out on ElementarVario Micro Cube with a balance Mettler Toledo UMX5Comparator, accuracy 0.1µg. The sample (approx. 10mg) was prepared in a tin capsule which is introduced into a 120-position smother. The sample is sent in inert SAS (white zero) under helium gas flow. The catalytic combustion of the capsule and sample takes place at 1150°C in the first furnace. Reduction of gases is carried out on hot copper at 850°C in a second furnace. Hence, the gases formed, (CO_2, H_2O and SO_2) are mixed with the carrier gas Helium. This gaseous mixture is separated by the TPD (Temperature Programmed Desorption) column. The signals are detected by TCD Detection of the signal by a TCD catharometer (thermal conductivity detector).

For Oxygen: The sample is placed in a silver capsule and placed at 120-position smother. Under inert atmosphere (helium flow at 1050°C), pyrolysis. The pyrolysis gases products are converted to CO and separated by chromatographic separation followed by signal detection by TCD.

Elemental analysis data of the molecules have been reported along with the above mentioned protocols.

5.3 Conclusion

Successful synthesis and purification of four model molecules mimicking the α- and β-O-4 bonds present in the lignin models. The model molecule was used as a substrate for the catalytic hydrodeoxygenation studies aimed for the depolymerisation of lignin.

Unfortunately, we could not test all the molecules as substrate for HDO reactions due to time constraints but this work can be further pursued with the remaining model molecules.

References

[1]P.J. Deuss, M. Scott, F. Tran, N.J. Westwood, J.G. de Vries,, K. Barta, Aromatic Monomers by in Situ Conversion of Reactive Intermediates in the Acid-Catalyzed Depolymerization of Lignin. J. Am. Chem. Soc. 137 (2015) 7456−7467.
[2] S.C. Tsai, J.P. Klinman, De Novo design and utilization of photolabile caged substrates as probes of hydrogen tunneling with horse liver alcohol dehydrogenase at sub-zero temperatures: a cautionary note. Bioorg. Chem. 31, 2 (2003) 172-190.
[3]F. Nakatsubo, T. Higuchi, Synthesis of guaiacylglycerol-β-coniferyl and β-coniferyl aldehyde ethers. Wood research: Bulletin of the Wood Research Institute Kyoto University 66 (1980) 23-29.
[4] C.N. Njiojob, J.J. Bozell, B.K. Long, T. Elder, R.E. Key, W.T. Hartwig, Enantioselective Syntheses of Lignin Models: An Efficient Synthesis of β-O-4 Dimers and Trimers by Using the Evans Chiral Auxiliary. Chem. Eur. J. 22 (2016) 12506-12517.
[5] T. Ahvonen, G. Brunow, P. Kristersson, K. Lundquist, Stereoselective syntheses of lignin model compounds of the beta-O-4 and beta-1 types. Acta chemica Scandinavica. 37 (1983) 845-849.
[6] [http://www.bris.ac.uk/nerclsmsf/techniques/gcms.html] consulted on 14.09.2018
[7] [https://orgspectroscopyint.blogspot.com/2014/11/gas-chromatography-mass-spectrometry-gc.html] consulted on 14.09.2018.
[8]A.E. Clark, E.J. Kaleta, A. Arora, D.M. Wolk, Matrix-Assisted Laser Desorption Ionization–Time of Flight Mass Spectrometry: a Fundamental Shift in the Routine Practice of Clinical Microbiology, Clin. Microbiol. Rev. 26, 3 (2013) 547-603.
[9]Introduction B. Blümich (Ed.) in Essential NMR: for scientists and engineers. Springer Science & Business Media, Heidelberg, Germany (2005) 2.
[10][http://www.acttr.com/en/en-faq/en-faq-nmr/86-en-faq-what-is-nmr.html] consulted in September 2018.
[11] [https://socratic.org/questions/how-does-an-nmr-spectrometer-work] consulted in September 2018.
[12] [https://www.pharmatutor.org/articles/complete-review-on-nuclear-magnetic-resonance?page=1] consulted in September 2018.
[13] [https://en.wikipedia.org/wiki/Combustion_analysis] consulted in September 2018.

Results and Discussion

CHAPTER 6

From Layered Double Hydroxides to Mixed Oxides

Chapter Summary:

This chapter explains the calcination parameters opted for the transformation of layered double hydroxides to their corresponding mixed metal oxides (MMO). Characterization and evaluation of the phases present in the calcined catalysts was chiefly done by XRD. The data obtained show a clear distinction in textural properties, degree of crystallinity and crystalline phases evolved at each step of calcination temperature. Data from thermogravimetric analysis (TG/DTG) was also correlated to understand the decomposition pattern of house-of-cards assembly of the LDHs. It was observed that spinel formation begins at higher temperatre than the crystallization of divalent oxides. Upon calcination of Fe-containing as–synthesized catalysts, no Fe-phase was detected at calcinations temperature below 600°C. Late formation of a crystalline iron-bearing phase suggests a high stability of amorphous iron oxides. The quantitative estimation of phases was done by internal standard method using the Rietveld refinement. Surface area and pore volume of solids, measured by N_2-adsorption and analyzed by Brunauer-Emmett-Teller method, have also been studied. Among various catalysts synthesized, special emphasis has been given to those used in catalytic hydrodeoxygenation of lignin model.

Mixed Metal Oxides from LDH

As stated previously in chapter 2, mixed metal oxides (MMO) obtained by the thermal decomposition of LDH are favorable candidates as catalysts. In comparison to LDH, metal oxides own unusual properties like mechanical strength and resistance to leaching. Their metal sites are not obstructed by anions but their activity largely depends on the surface area, hence there is a trade-off between increasing stability and decreasing surface area with temperature of calcination. Thus, the temperature of calcination causes significant transformation to the morphology of the catalysts in terms of extent of crystallinity, phases present, crystallite size, surface area, and their efficiency for application as well. A few examples on this subject have been quoted below.

6.1 Fractional Crystallization of Oxide Phases

Elhalil *et al.* synthesized Zn-Al-CO_3 LDH nanoparticles by the co-precipitation method with Zn/Al molar ratios r = 1, 3 and 5 and calcined it in the temperature range from 300-600°C to be used for the removal of pharmaceutical pollutants.[1] At 300°C the characteristic XRD peaks of ZnO oxide were observed in all samples. As the calcination temperature was increased, characteristic reflections of the mixed composite ZnO-$ZnAl_2O_4$ appeared at 600°C. The optimum adsorption of 94.59% was achieved with Zn/Al (r= 3) catalyst, calcined at 300°C.Perez-Ramirez *et al.* explained the decomposition behavior and phase transition in Co/M^{3+} (trivalent cation (Al, Ga, Fe, and Cr)) through spectroscopic techniques.[2] For the Co-Al HTlc, calcination at 200°C brought to the collapse of the layered double structure and the formation of a spinel-like structure. A spectrum typical of a normal II–III spinel compound was already observed at 250°C, indicating the loss of lamellar arrangement in the layered structure and confirming that IR spectroscopy can detected local structure at temperature lower than the one required for extension of these structures in a crystalline phase. In Co-Fe HTlc, the layer decomposition was observed at even lower temperature of 200°C and finally leadto the oxidic phase. In case of Cr-Cr HTlc, spinel indicating doublet only appeared at 300°C, high stability and complete decomposition of the layers into oxidic phase only occurs at 350°C. Oxidic phase formation occurs above 300-350°C. In all cases, a well define crystallization is achieved upon calcination at 550°C for 3h yielding cobalt spinels. Kamanth and coworkers proposed a detailed formation mechanism of Co/Al LDH precursor to oxide with spinel structure caused by variation in basal spacing.[3] The studies were conducted in by in situ variable temperature XRD at 50, 125, 150, 145, 200, 225, 275, 600 and 800°C. Similarly, Kannan *et al.* contributed to the studies on the thermal decomposition pattern of

Co-Al LDH, synthesized by sequential precipitation and calcined at ≥400°C for 5h in air.[4] A spinel phase, solid solution of Co_3O_4, was observed at temperature as low as 200°C. The unusual low temperature of crystallization was considered specific to Co-bearing systems. In all the cases, however, spinel crystallinity varied with the atomic ratio of the cations. Increasing temperature improved crystallinity due to growth of spinel phase at sintering. The particle size grew at calcination temperature of 600°C.

It can be concluded that often precursors of catalysts generate different phases at a given temperature. Nevertheless, in most of the literature available, the percentage abundance of the phases as a function of temperature is not discussed. An interesting study is to correlate the thermal decomposition stages of the precursor with evolution and analysis of the quantitative transitions of the phases. In the present study, we have focused on the phase evaluation in a novel Cu-Ni-Fe LDH system (as uncalcined, discussed in Chapter 4) sintered at various temperatures and its comparison with the single precursor oxides and composition replicas with aluminum instead than iron.

In some cases, the XRD data do not provide clue about expected phases in the catalysts, particularly those calcined at lower temperature. At elevated temperature, the same catalysts clearly showed multi-phases. Thus, it was confirmed that transformation of LDH to mixed metal oxides is strictly dependent on the cation ratios and calcination temperatures.[2,3] It is verified that up to a certain range of temperature, a part of samples remains amorphous and hence undetected by XRD. The best possible way for calculating the amorphous fraction is by the internal standard method.[5] This provides a combined sumquantitative evaluation of well crystallized phases and the undetected residue of sample can be quantitatively evaluated as amorphous. This technique is not only efficient to determine the amorphous material in a polyphasic sample but can also assist in understanding the mechanism and differences in catalytic properties of catalysts.

6.2 Characterization of Mixed Oxides Catalysts

As described in the chapters 2 and 4, we will now focus our interest in formation and properties of mixed oxides as per modification in the cation nature, ratio and calcination temperature. These multiple factors allow the understanding of property modifications in the catalysts. Hence, here we report as typical catalyst Ni-Cu-Fe an example with Ni/Cu (1:1) and divalent/iron ratio 3. We will now discuss in detail the characteristic properties of this catalyst, which will be later compared with the rest of syntheses, keeping this as a typical catalyst.

6.3 Standard Catalyst Example: IZA 20 ($Ni_{0.37}Cu_{0.38}Fe_{0.25}$)

To determine the thermal stability and right temperature of calcination, the thermogravimetric analysis was carried out in air at 60mL/min, ramp=5°C, 40-900°C. The observed initial weight loss of 10.64% of the LDH around 150°C is attributed to the dehydration, caused by the loss of water molecules in the interlayer region. Later, the loss of hydroxyl groups linked with anions in the interlayer region is shows degrading 15.49% of the sample in 150-290°C. A complete collapse of the layer occurs when the carbonate anions in the interlayer are lost between 300-400°C with affective mass loss of 2.88%. In this sample IZA 20, the LDH is completely transformed into oxide phase after 400°C (Fig. 6.1). However, the loss of mass at a given temperature is also function of the time spent at that temperature and the loss of mass after several hours of calcination can be complete at 400°C also if it is not complete at the same temperature in the dynamic evolution of temperature of TG.

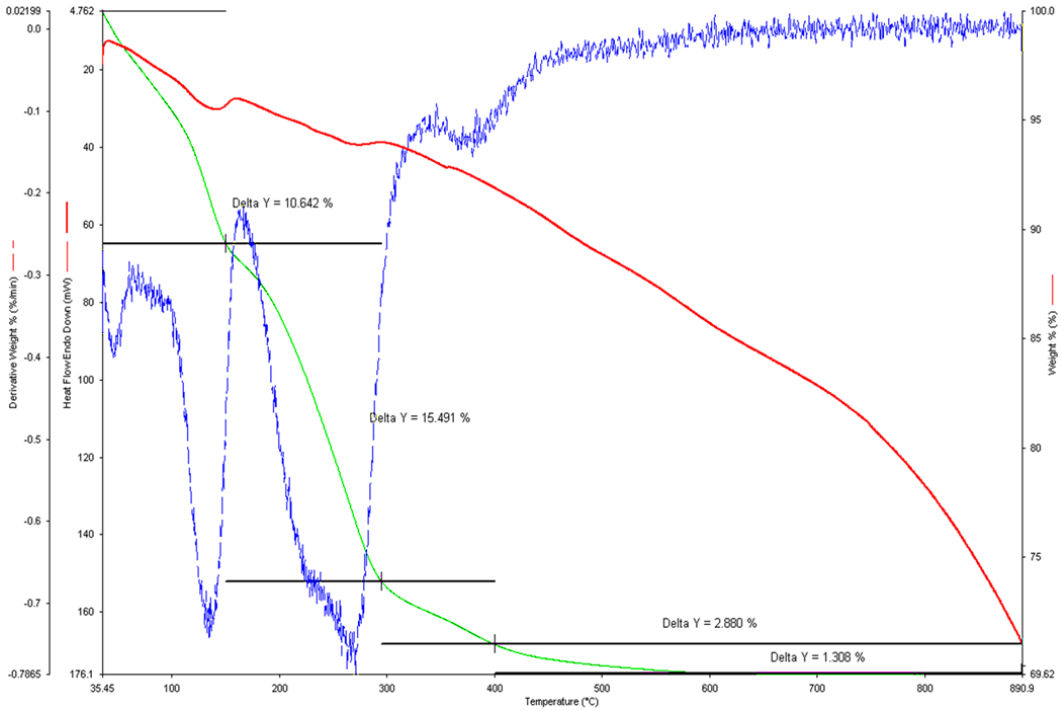

Figure 6.1 TG/DTG of uncalcined IZA20 ($Ni_{0.37}Cu_{0.38}Fe_{0.25}$) showing percentage loss of sample with increasing temperature

As the information provided by the TG/DTG, the loss of labile components of the uncalcined LDH is completeat 400°C and correponding formation of mixed oxides must have taken place. Therefore, we carried out the calcination at 400°C. However, the catalyst study by XRD indicated that the assumption of complete mixed oxide crystallisation just after 400°C was not factual, since only NiO phase was obtained, not well crystallized, and iron was

missing in the observed diffractograms. Further evidence was collected by calcining the LDH catalyst at even higher temperatures, 400-800°C, to study the evolution of phases.

Different crystalline phases obtained as a function of temperature (See Fig. 6.2) were identified by ICDD as: nickel oxide bunsenite-NiO, tenorite-CuO, spinel-M_3O_4 of mixed composition but surely including iron. The diffraction pattern, cell parameters and percentage of each phase, and evaluation of the amorphous fraction, have been indicated in the figure 6.2, annex A.1 and figures 6.3, 6.4 respectively.

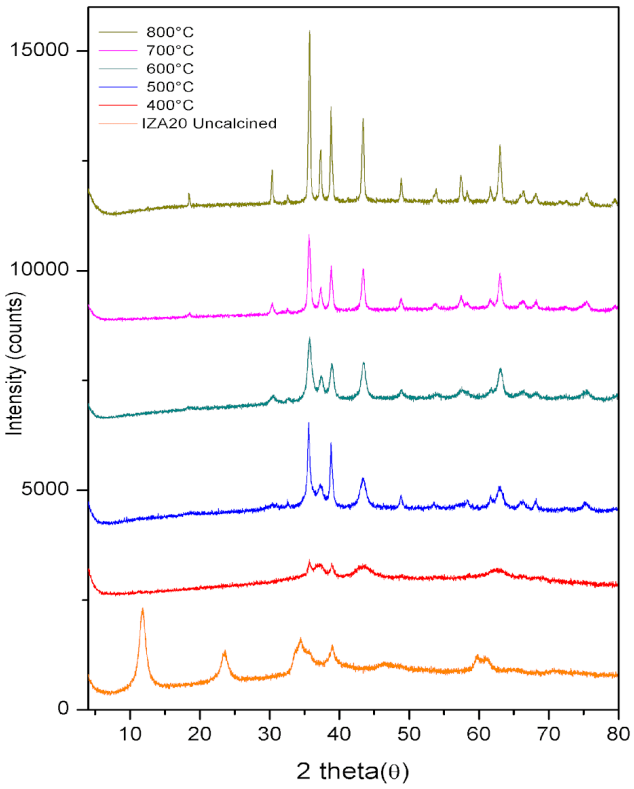

Figure 6.2 X-ray diffraction pattern of IZA 20 $Ni_{0.37}Cu_{0.38}Fe_{0.25}$ calcined at different temperatures

NiO and CuO phases are already present at 300°C. NiO phase is strongly prevalent at 300°C and 400°C, despite the equivalent amounts of Cu and Ni present in the sample. (see Fig. 6.3) Moreover, a spinel phase just appears at 500°C. Clearly the ratios between the XRD phases do not correspond to the composition of the sample. Some Cu and Fe are missing from the crystalline phase at low temperature and they can be considered as constituent of an amorphous material formed by the thermal decomposition of the LDH and coexistent with the crystalline phases observed. The presence of amorphous material can be confirmed by quantitative analysis of the XRD with internal standard.

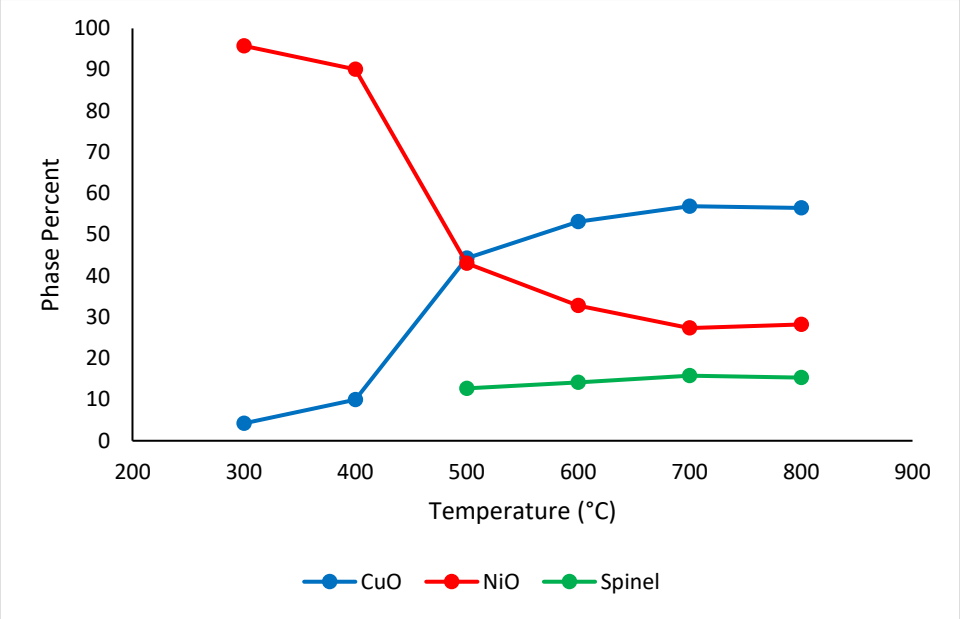

Figure 6.3 Change in percentage of crystalline phases in IZA20 $Ni_{0.37}Cu_{0.38}Fe_{0.25}$ at different temperatures

At the lowest temperature, the crystalline phases justify only the minor fraction of the sample. This confirms the presence of amorphous material, which amount decreases with the temperature of calcination. (Fig. 6.4) The ratios between phases changes as new fractions of amorphous material are selectively incorporated in crustalline phases, leading, between 400 and 600 °C, to the growth of CuO and spinel phases.

An open question is that at which point the composition of the amorphous material can be deduced by the internal standard analysis. It would be possible if the composition of the crystalline phases present could be surely known. However, it can be observed that, at increasing temperature of calcination, the CuO phase becomes predominant on the NiO phase despite the 1:1 ratio between Ni and Cu in the sample and that the spinel phase present is far from justifying the amount of Fe present in the samples. It can be safely assumed that the tenorite and bunsenite phases present are not pure CuO and NiO, respectively, but they are doped phases containing a significant amount of Fe. This can be confirmed by monitoring their cell parameters. The evolution of the cell parameters of the cubic bunsenite and spinel phase and the evolution of the cell size of the tenorite phase, reported in (Fig 6.5), clearly indicates a change of composition of these phases with the temperature of calcination. An increase of cell size of the divalent oxides with calcination temperature can easily be attributed to the incorporation of Fe^{2+} cations, larger (80 Å radius) than Ni^{2+} (72 Å) or Cu^{2+} (69 Å), incorporated from the amorphous material. The interpretation of the increase of cell parameter of the spinel phase is less easy to understand in terms of cation composition of the

phase. Indeed, the cell parameter of spinel, evolving fron 8.30 to 8.34 Å at increasing temperature,l are lower than the cell size of most expected phases, cuprospinel $CuFe_2O_4$ (8.369 Å), tenorite $NiFe_2O_4$ (8.355 Å), and even the cation-deficient γ-Fe_2O_3 maghemite (8.350 Å). It is clear that a solid solution between a ferrite and Co_3O_4 (8.08 Å) is present.[6] However, it is difficult to define a Vegard's law approach to the determination of the composition, as the increase of cell size with temperature is probably related to a decrease of the average oxidation state of the spinel. The loss of the cation vacancies in cation-defective oxidized spinel is expected to increase the cell size, going towards a correct M_3O_4 stoichiometry.[7]

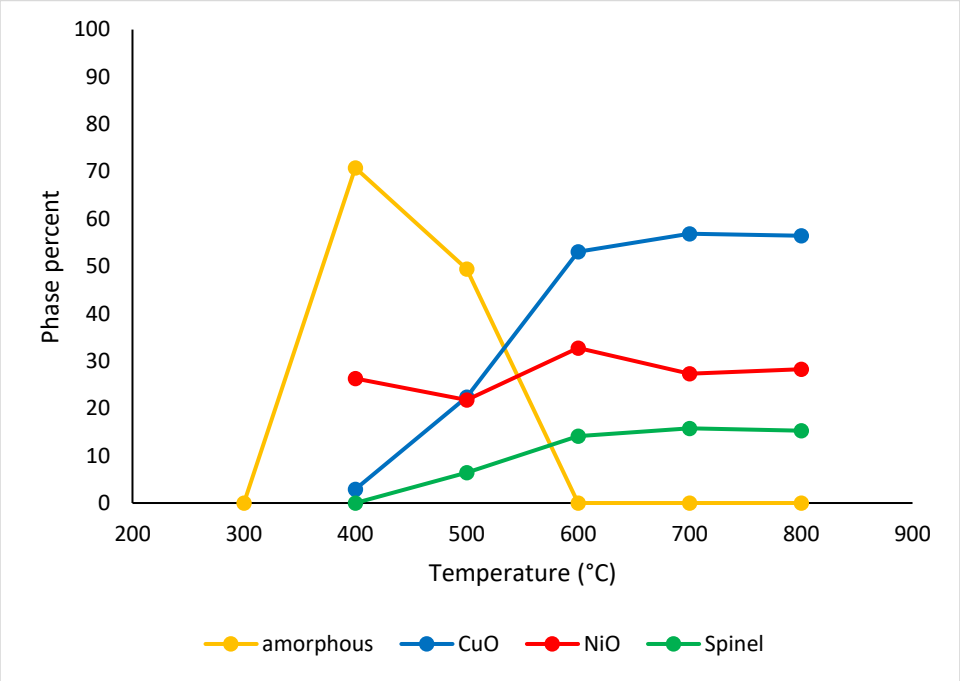

Figure 6.4 Mass fraction of phases and amorphous material in IZA 20 as a function of temperature by Rietveld analysis with internal standard. An inverse relation is observed between amorphous material and temperature (°C)

The N_2 physiosorption showed a type IV isotherm as classified by IUPAC. Fig. 6.5 shows the variation in *c* cell parameter with the rise of temperature. The surface area and pore volume calculated using BET method are indicated in Table 6.1.

Table 6.1: BET surface area and pore volume of IZA 20 uncalcined and calcined samples

Composition	Calcination Temperature (°C)	BET surface area (m^2/g)	Pore Volume (cm^3/g)
IZA20 $Ni_{0.38}Cu_{0.37}Fe_{0.25}$	-	109	0.253
	400°C	97	0.324
	500°C	32	0.164
	600°C	40	0.164
	700°C	18	0.015

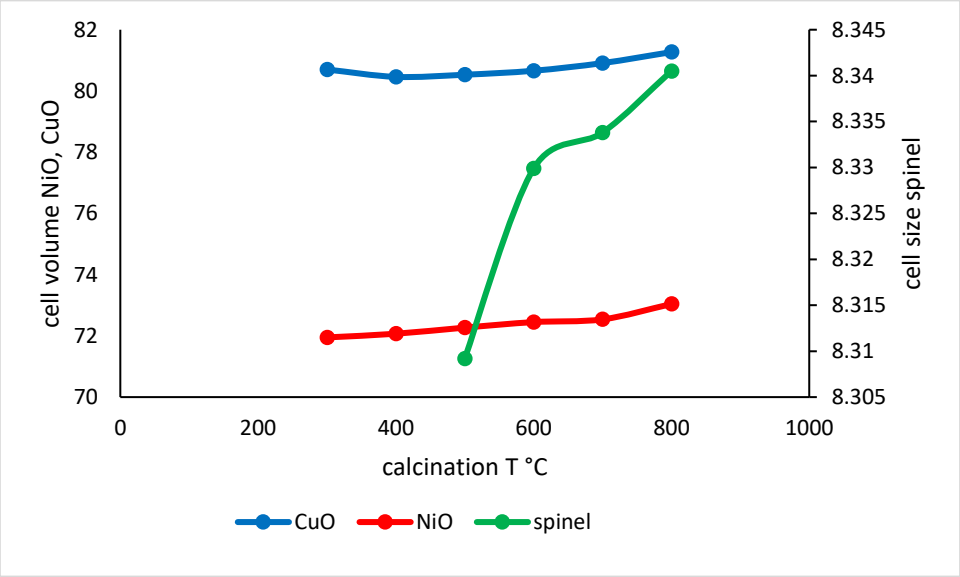

Figure 6.5 Cell Volume and size upon calcination of IZA 20 ($Ni_{0.37}Cu_{0.38}Fe_{0.25}$)

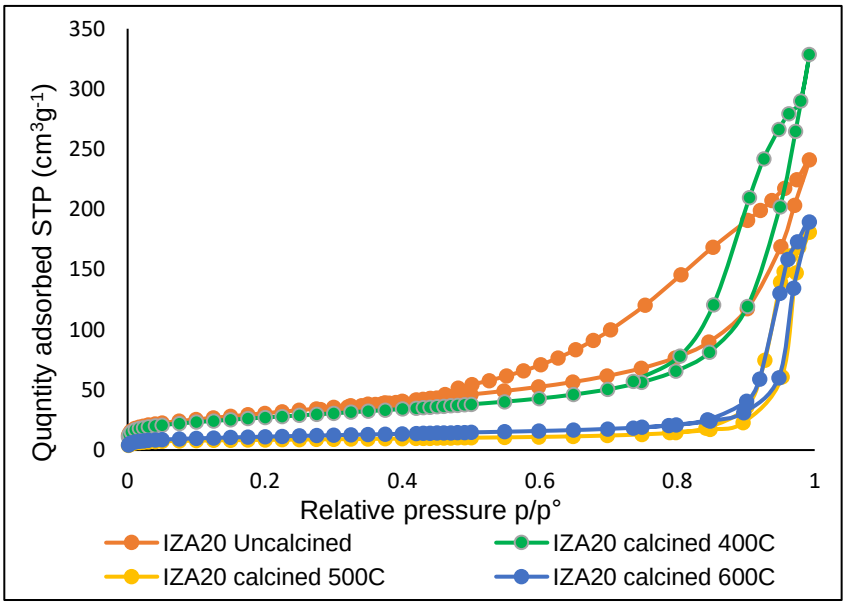

Figure 6.6 Adsorption-desorption isotherms of IZA20 ($Ni_{0.37}Cu_{0.38}Fe_{0.25}$)

6.4 Scheme series of Mixed Oxide Catalyst Synthesis

A scheme opted for the detailed exploration of the Ni-Cu-Fe system is the investigation of individual cations based catalysts such as Ni-Fe and Cu-Fe systems, their phase evolution and quantification of amorphous material along with variation in cell parameters. The calcination at 600°C was a standard temperature maintained for catalysts used in the HDO reactions. Now we will present the series of selected catalysts prepared in this range.

Table 6.2 List of mixed oxide catalysts in order of increase of Cu/Ni atomic ratio

Catalyst	Cu/Ni atomic ratio	Final Atomic Ratio (EDX)			Crystalline phase by calcination at (600°C)	Surface area (m^2g^{-1}) at 600°C
		Ni	Cu	Fe		
IZA 22	0	0.75	-	0.25	NiO, spinel	89
IZA 124	0.02	0.62	0.02	0.35	NiO, spinel	53
IZA147	0.04	0.72	0.04	0.26	NiO, spinel	71
IZA 123	0.2	0.55	0.17	0.27	CuO, NiO, spinel	55
IZA 20	0.38	0.37	0.38	0.25	NiO, CuO, Spinel	40
IZA 24	0.56	0.18	0.56	0.27	NiO, CuO, Spinel	53

Catalyst	Cu ratio	Final atomic ratio (EDX)		Crystalline phase by calcination at (600°C)	Surface area (m^2g^{-1}) at 600°C
		Cu	Fe		
IZA 31	0.47	0.47	0.53	CuO, Fe_2O_3, Spinel	-
IZA 23	0.65	0.65	0.35	CuO, spinel	25
IZA 42	0.79	0.79	0.21	CuO,Fe_2O_3	-

Table 6.3 List of Cu-Fe oxide catalysts in order of increase of Cu atomic ratio

The introduction of different metals in the structure could strongly influence the surface related properties of the catalyst such as dispersion, particle size and reducibility which eventually affect their catalytic performance. As in the above example, the increase in copper content visibly indicates the decrease in surface area of the catalyst, all calcined at same temperature, 600°C. However, all mixed catalysts retain a surface area higher than 50 $m^2 g^{-1}$, while the Cu-Fe oxides present a lower surface area.

From the previous results of TG/DTG, the corresponding temperature of calcination for each catalyst was initially set to 600°C.

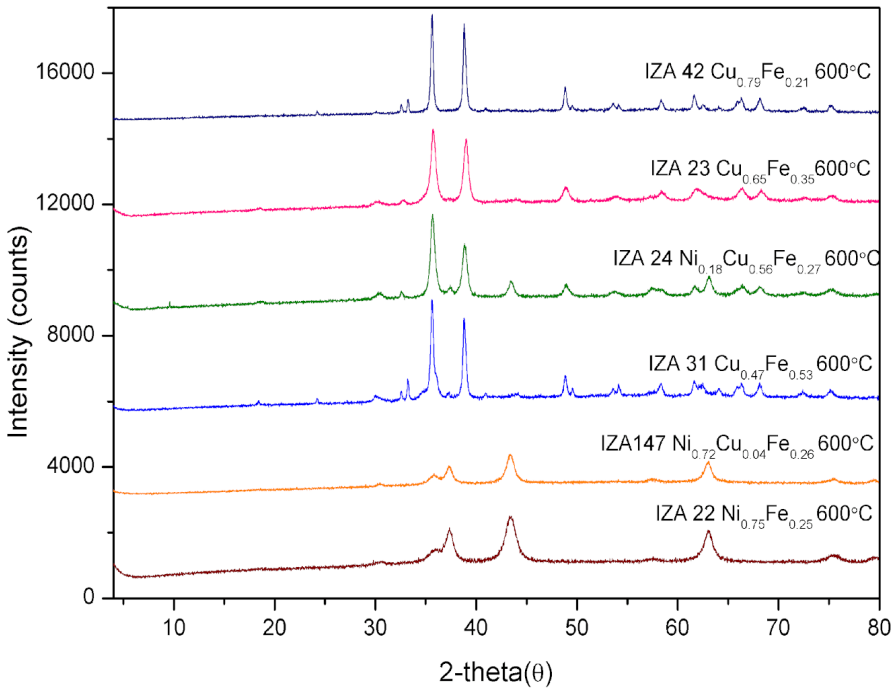

Figure 6.7 Diffractograms of mixed oxides catalysts calcined at 600°C

The TG/DTG was done for all the samples for which the graphs have not been shown here, nevertheless the data have been complied to evaluate the average loss at each step in the thermal decomposition. Though the decomposition trend is not accounted exactly as per the following temperatures. A variation of ±20°C for some samples is observed which could possibly be due to the synthesis conditions. Table 6.4 indicates the major steps of loss of LDH structure and the temperatures of transformation into mixed oxide for each catalyst.

Table 6.4 Percentage weight loss of sample upon thermal decomposition at each step

Sample	Type of Reactions	Dehydration	Dehydroxylation	Deanionization	Oxide formation
	Total loss (%)	100-200°C	200-300°C	400-500°C	>500°C
		Percentage weight loss/step			
IZA 22 $Ni_{0.75}Fe_{0.25}$	32.72	12.59	13.91	5.13	1.08
IZA 147 $Ni_{0.72}Cu_{0.04}Fe_{0.26}$	30.42	8.2	15	4.48	3.4
IZA 31 $Cu_{0.47}Fe_{0.53}$	28.6	5.85	15.06	6.23	1.46
IZA 24 $Ni_{0.18}Cu_{0.56}Fe_{0.27}$	24.05	6.56	9.93	4.42	3.14
IZA 23 $Cu_{0.65}Fe_{0.35}$	11.28	4.31	3.88	2.24	0.85
IZA 42 $Cu_{0.79}Fe_{0.21}$	30.59	2.07	24.30	2.85	1.37

The results clearly show that copper-rich LDH samples have relatively fewer total loss of total weight, particularly in the first step of dehydration. This effect could be related to the

decrease of c cell parameter with the Cu content observed in chapter 4, probably due to lower amount of water molecules in the interlayer region. On the other hand, Ni-Fe IZA 22 presents a typical LDH structure, where water of hydration is a key component for the structural stability. Layers accommodating the water of hydration show a sharp curve upon heating range 100-200°C, making this the most important step. It is interesting to observe, by comparison, the very high mass loss of IZA42, which at the origin presents not a LDH but a copper hydroxynitrate structure.

IZA22 ($Ni_{0.75}Fe_{0.25}$)

$Ni_{0.75}Fe_{0.25}$ (IZA22) mixed oxides obtained by calcination at 400-800°C, were compared with $Ni_{0.37}Cu_{0.38}Fe_{0.25}$ (IZA 20) to get understanding of the difference of evolution of phases in these systems. The crystalline phases is this case were Nickel Oxide-NiO (00-044-1159) 2θ: 37.2°,43.2°, 62.8°, 75.2°,79.4°; and spinel phase. 2θ: 18.5°, 30.1°,35.8°,57.3°,63.0°. The diffraction pattern, cell parameters and percentage of each phase have been indicated in the figure 6.7, annex A.2 and figures 6.8, 6.9 respectively. In this case, NiO is the only phase present at lower temperature whereas the spinel formation begins at T>500°C (Fig. 6.8). Calcination at 800°C presents very sharp peaks and indicates a significant decrease of crystal size.

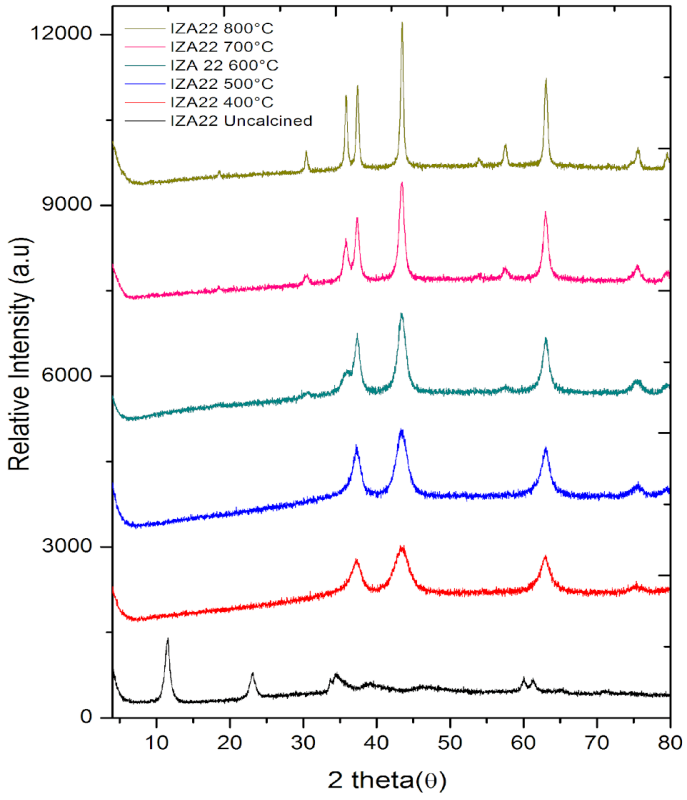

Figure 6.8 X-ray diffraction pattern of IZA22 ($Ni_{0.75}Fe_{0.25}$) calcined at different temperatures

With internal standard analysis, as done in the mixed catalyst system IZA 20, there was a clear presence of amorphous material in the catalyst calcined at low temperature. Bunsenite (NiO) was a prevailing phase until 700°C with a slow evolution of spinel phase. Clearly the amorphous material was crystallizing in both phases present. As the temperature increased further to 800°C, peaks sharpness increased to a great extent. Probably both the loss of amorphous material and the increase of crystal size have been contributing to the high surface area (Table 6.2) The decrease in amorphous material to zero at 700°C can be seen in (Fig. 6.9) The amount of spinel also after complete crystallization is too low to justify the amount of iron in the sample. Indeed, the cell parameter of bunsenite in the sample at 800°C, 4.189 Å, is much larger than the value for pure NiO, 4.176 Å, enough to justify the incorporation of a significant amount of iron.

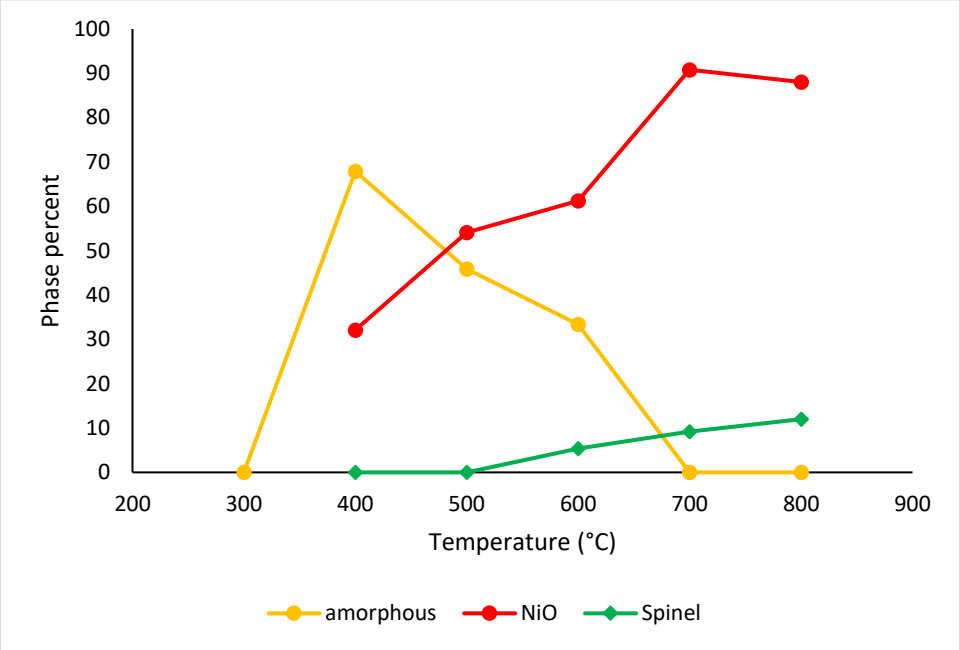

Figure 6.9 Change in percentage of amorphous and crystalline phases in IZA 22 at different temperatures (°C)

IZA 147($Ni_{0.72}Cu_{0.04}Fe_{0.26}$)

IZA147 is a sample with a very small copper content, with mixed oxide calcination data on 400-600°C. The diffraction pattern, cell parameters and percentage of each phase have been indicated in the figure 6.10(a), annex A.6 and figure 6.10 (b) respectively.

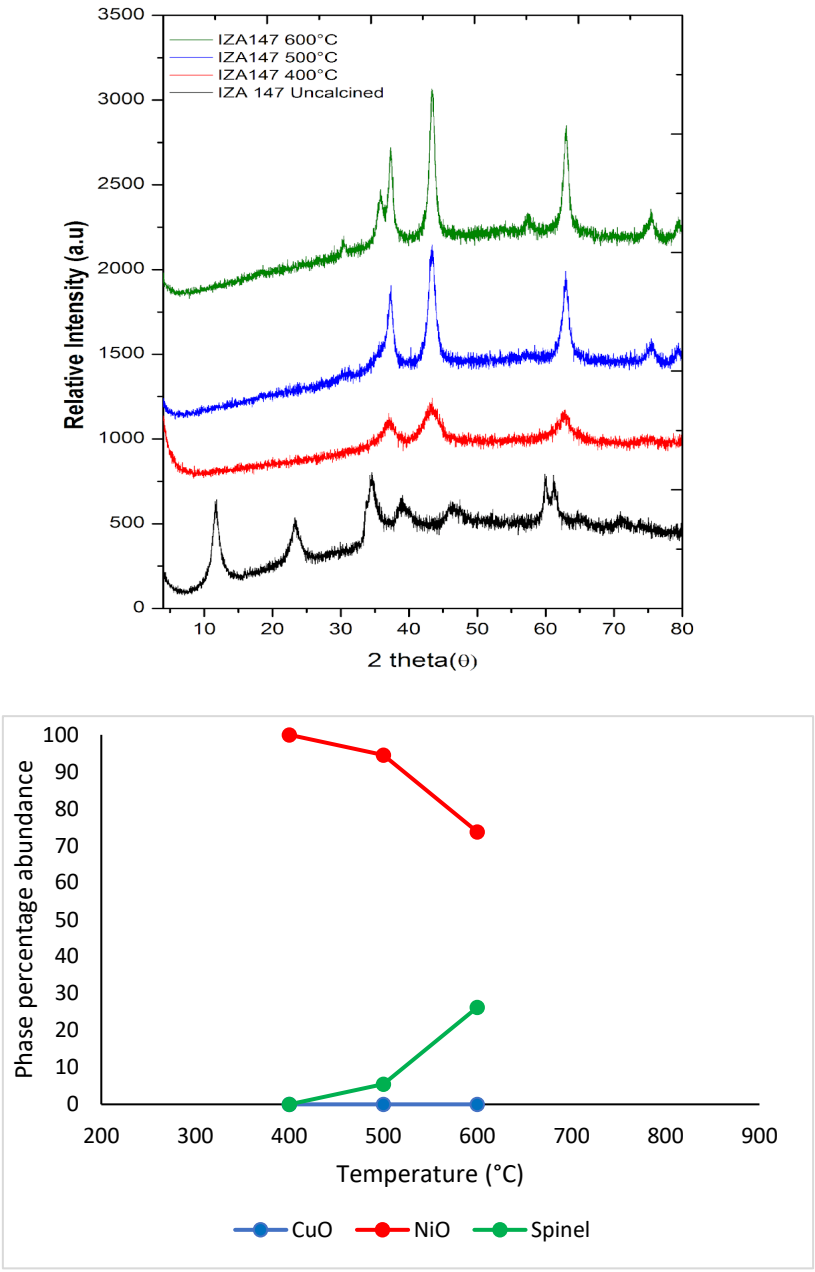

Figure 6.10 Change in percentage of crystalline phases in IZA147 at different temperatures (°C): a) diffractogram b) Phase percentage abundance

This system predominantly contains NiO and spinel phase with no presence of CuO throughout, even at higher temperature (Fig. 6.10). The presence of also a small amount of copper anticipates the formation of crystalline spinel at a lower temperature than in the pure Ni-Fe system.

IZA31 ($Cu_{0.47}Fe_{0.53}$)

In this sample, as the copper ratio (Cu/Fe) is increased in the uncalcined sample, copper hydroxy nitrate is formed with noticeable amount of amorphous material present as evident

from the baseline shift. At 600°C, CuO:2θ:32.7°,35.6°,38.8°,48.8°,53.3°,58.2°,61.7°,65.9, 66.2,68.0°; Fe_2O_3 :2θ: 24.2°, 33.2°, 35.2°, 49.6°, 54.1°, 62.5, 64.0°; Spinel: 18.3°, 30.30°,35.9°,37.3°,43.8° main peaks were identified. At 400°C, hematite Fe_2O_3 is the first phase crystalized with minor CuO.

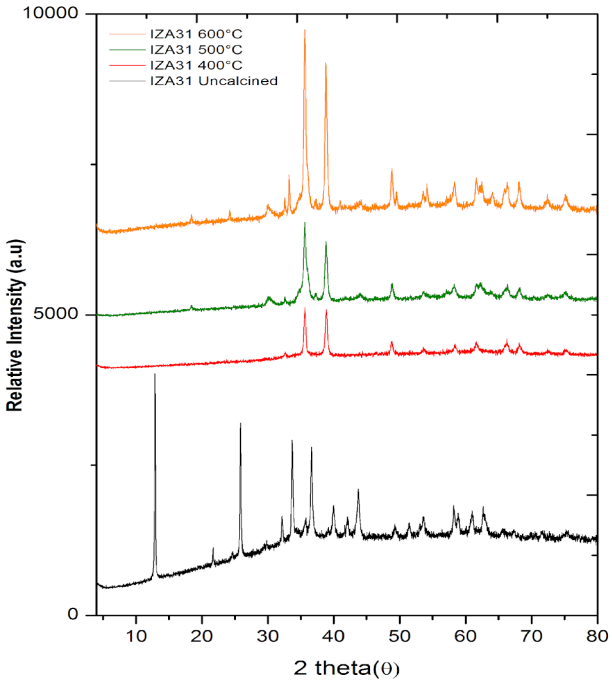

Figure 6.11 X-ray diffraction pattern of IZA 31 calcined at different temperature (°C)

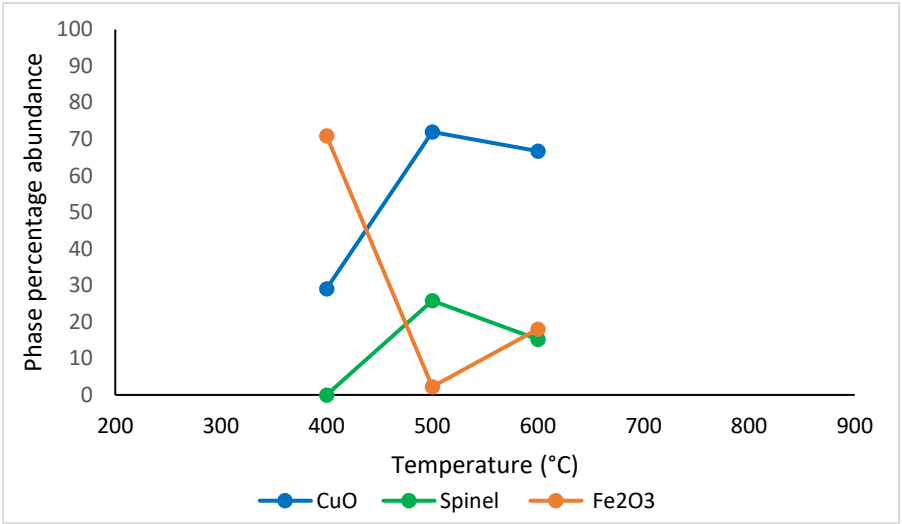

Figure 6.12 Change in percentage of crystalline phases in IZA31 at different temperatures (°C)

A drastic spinel formation, increase of CuO and decrease in Fe_2O_3 crystalline fraction occur at 500°C, probably due to the crystallization of Cu-rich amorphous material. The sharp peaks at 600°C are an indication of large crystals of CuO, which is the primary phase at this temperature. The diffraction pattern, cell parameters and percentage of each phase have been indicated in the figure 6.11, annex A.7, and figure 6.12 respectively.

IZA24 ($Ni_{0.18}Cu_{0.56}Fe_{0.27}$)

The influence of increasing copper content and decreasing nickel in the mixed oxide phases was studied through the catalyst where CuO, due to high copper content, has already started appeared in the uncalcined LDH phase. Upon calcination at 400°C, NiO and CuO are primary phases present whereas spinel formation begins at 500°C. As in the NiFe (IZA22) system, late spinel formation has been observed despite the same M^{2+}/M^{3+}ratio in both these system. However, as already observed in IZA 147, the presence of copper in the system leads to earlier spinel formation. CuO remains the most dominant phase throughout temperature range (400-800°C), followed by NiO and spinel. The system is characterized by an unusual persistence of amorphous material at a high temperature of 700°C. The ratio between CuO and NiO phases suggests the presence of a Ni-rich amorphous materials, which presence could only be understood by further characterisations. The diffraction pattern, cell parameters and percentage of each phase, amorphous material have been indicated in the figure 6.13, annex A.4. respectively.

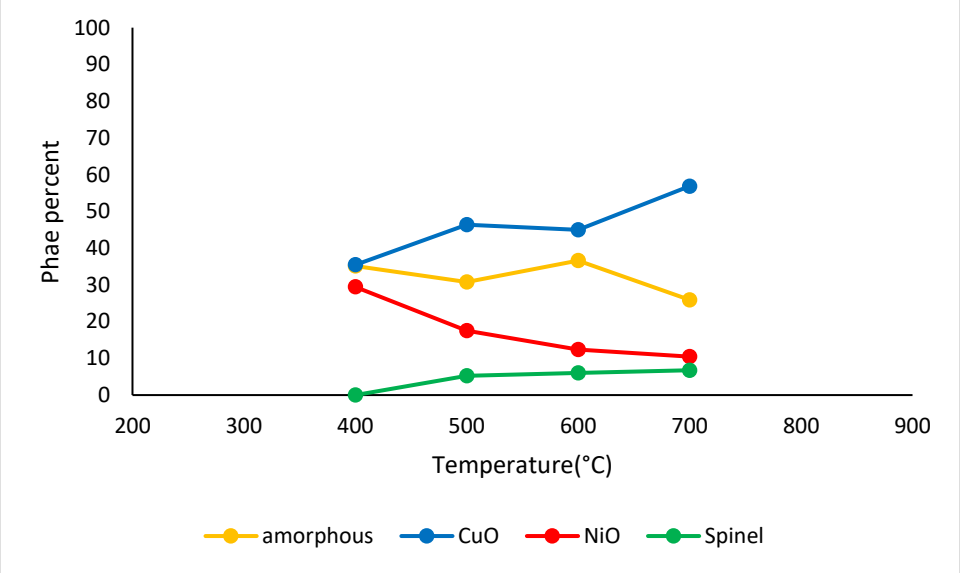

Figure 6.13 Change in percentage of amorphous and crystalline phases in IZA24 at different temperatures (°C)

IZA23 ($Cu_{0.65}Fe_{0.35}$)

The as-precipitated precursor just presents CuO diffraction peaks and no Fe-bearing phases are visible. A clear identification of amorphous material in the system under calcination is an indication of Fe-doped CuO system which gradually evolves as spinel phase at higher temperature.

Moreover, in comparison, the formation of hematite in IZA31 which is also a CuFe system with M^{2+}/M^{3+}=2 molar ratio indicates an important message. The difference lies in the initial

precursor which in case of IZA 31 is copper hydroxynitrate. This fact has also been proven with another sample IZA 42, which had a same molar ratio as of IZA 23 but a different pH. Also, in case of IZA 42, copper hydroxynitrate was the parent LDH as explained below. The cell parameters and percentage of each phase, amorphous have been indicated in the annex A.3 and figure 6.14 respectively.

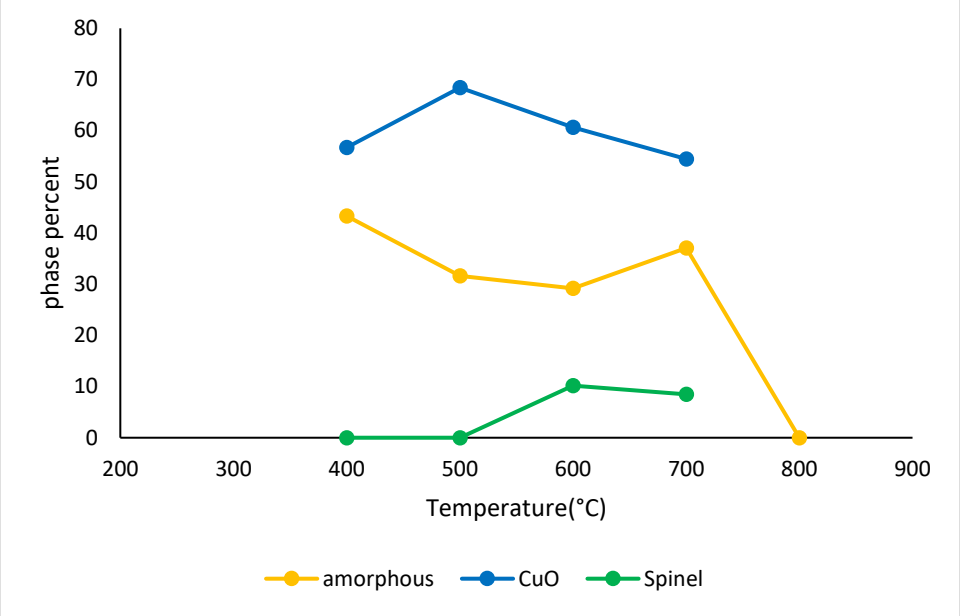

Figure 6.14 Change in percentage of amorphous and crystalline phases in IZA23 at different temperatures (°C)

IZA42 ($Cu_{0.79}Fe_{0.21}$)

IZA 42 is a replica of the synthesis of IZA 23 with the same molar ratios and just difference of 2 points in pH. Initial precursor synthesis pH was 8, instead than 10 for IZA23 and copper hydroxynitrate with prominent amorphous material was clearly observable. The diffraction pattern, cell parameters and percentage of each phase and amorphous material have been indicated in the figure 6.15, annex A.5 respectively.

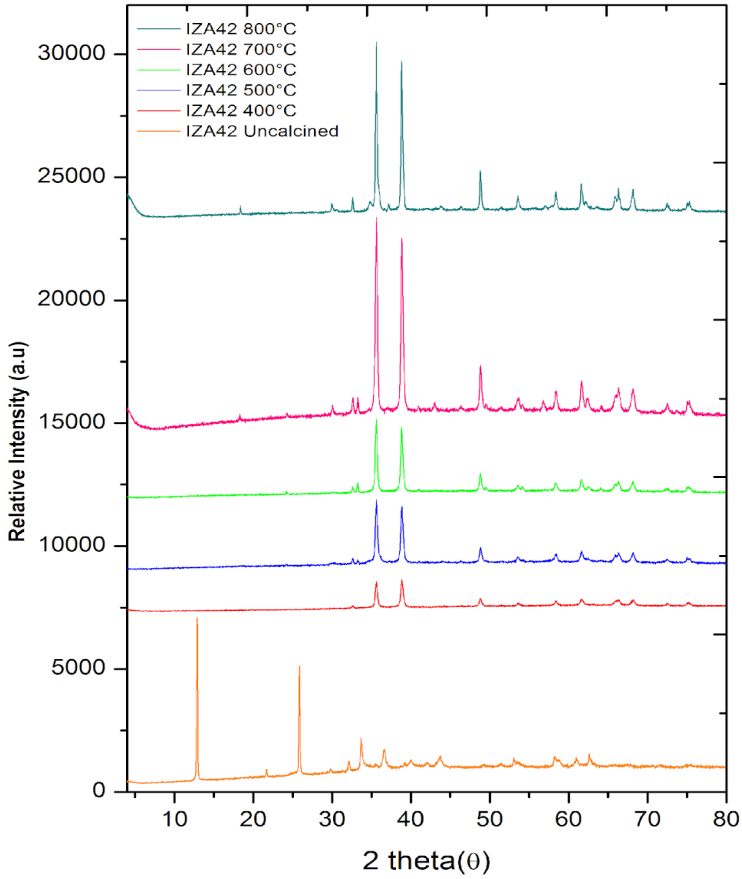

Figure 6.15 X-ray diffraction pattern of IZA 42 calcined at different temperature (°C)

Unlike, in all specimens calcined from 500°C upwards there are sharp peaks of hematite (for instance at 24 and 33 °) and irregular amounts of spinel. It is interesting to observe that in very copper-rich samples, like IZA23 and IZA42, the cell parameter of spinel is 0.39-8.41, much higher than the cell parameter of the spinel of previous described samples. It is indeed corresponding to the cell size of magnetite Fe_3O_4 (peak near 30°, a 8.395) suggesting that we are in presence of a pure iron spinel instead than of mixed spinels. It is important because this suggests than for forming mixed spinel we need to start from a precursor containing both cations, which is not the case for IZA42, when we start from Copper hydroxynitrate, or IZA23, where we start from CuO already in the precursor. In both cases it seems likely that iron in the precursor is an independent amorphous not containing copper. It is also remarkable that, at difference with copper-rich samples synthetized at pH 10, the amorphous material of IZA42, synthetized at pH 8, is not stable at high temperature. So it can be deduced that the pH (comparison of IZA 23 and 31) and molar ratio (comparison of IZA 23 and 42) of cation are the determinant factors in the phases evolution at high temperatures irrespective of the same cations distribution.

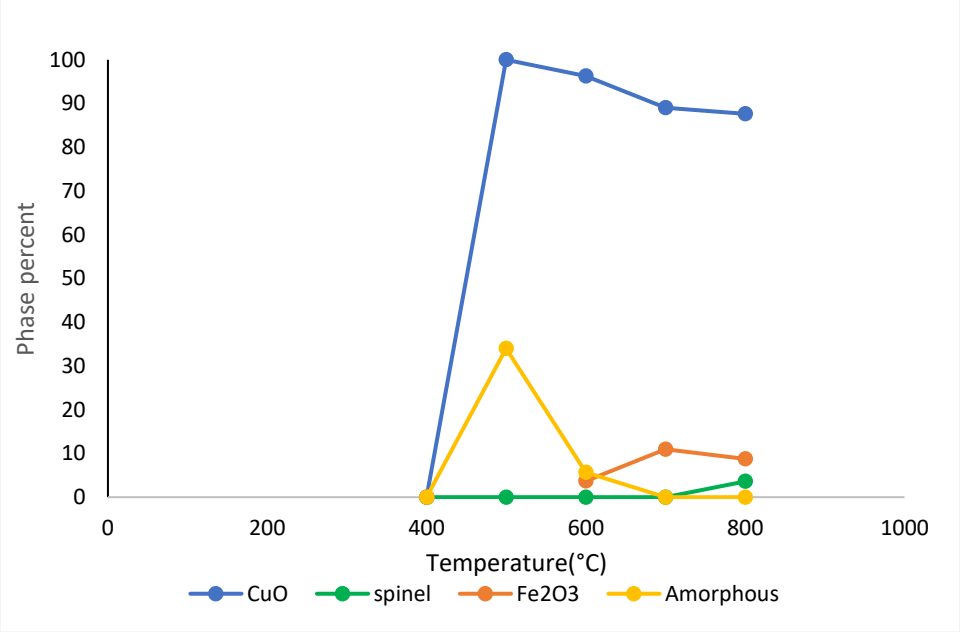

Figure 6.16 Change in percentage of amorphous and crystalline phases in IZA42 at different temperatures (°C)

There was no significant difference in the shape of the isotherm (Type IV) of these samples therefore the isotherms have not been shown here. A significant loss in surface area is observed by the thermal treatment of mixed oxides at high temperature.

Table No 6.5: Change in surface area as a function of calcination temperature (°C)

Sample	Surface area (m^2/g^{-1})			
	400°C	500°C	600°C	700°C
IZA 22 $Ni_{0.75}Fe_{0.25}$	114	113	89	48
IZA124 $Ni_{0.62}Cu_{0.02}Fe_{0.35}$	121	76	52	20
IZA 147 $Ni_{0.72}Cu_{0.04}Fe_{0.26}$	197	87	71	24
IZA 123 $Ni_{0.55}Cu_{0.17}Fe_{0.27}$	145	52	55	20
IZA 24 $Ni_{0.18}Cu_{0.56}Fe_{0.27}$	72	43	53	21
Cu-Fe system				
IZA 23 $Cu_{0.65}Fe_{0.35}$	57	44	25	11
IZA 42 $Cu_{0.79}Fe_{0.21}$	30	11	8	5

6.5 Single Oxides Catalysts

To understand the role of each oxide and study them as benchmark catalysts in the HDO, single/pure hydroxides were also prepared using exactly the same synthesis parameters used for the LDH synthesis leading to oxides as previously explained in chapter 4. The same

method was applied to them; calcination temperature was determined by TG/DTG analysis, later XRD was done for catalysts calcined at 400-600°C.

Single oxides catalysts were prepared from precursor IZA238-($Fe(OH)_3$ and Fe_2O_3)$_3$, IZA239-$Ni(OH)_2$, and IZA240-CuO. Since no carbonate ion was present in these samples therefore the decomposition temperature of the hydroxides was relatively low (Fig.6.25). It was therefore not seen useful to calcine them a very high temperature. A Pure Fe_2O_3, NiO, and CuO were obtained with no significant change in the cell parameters, upon calcination at high temperature except a slight decrease of the 'c' parameter of CuO at the beginning of calcination.

The interest in single oxides was, from the catalytic point of view, to understand the selectivity and conversion differences in H-transfer reactions. They served as a second- step standards following the blanks. The TG/DTG, diffraction pattern, cell parameters and percentage of each phase have been indicated in the figure [6.17-20], annex [A.11, A.12] respectively.

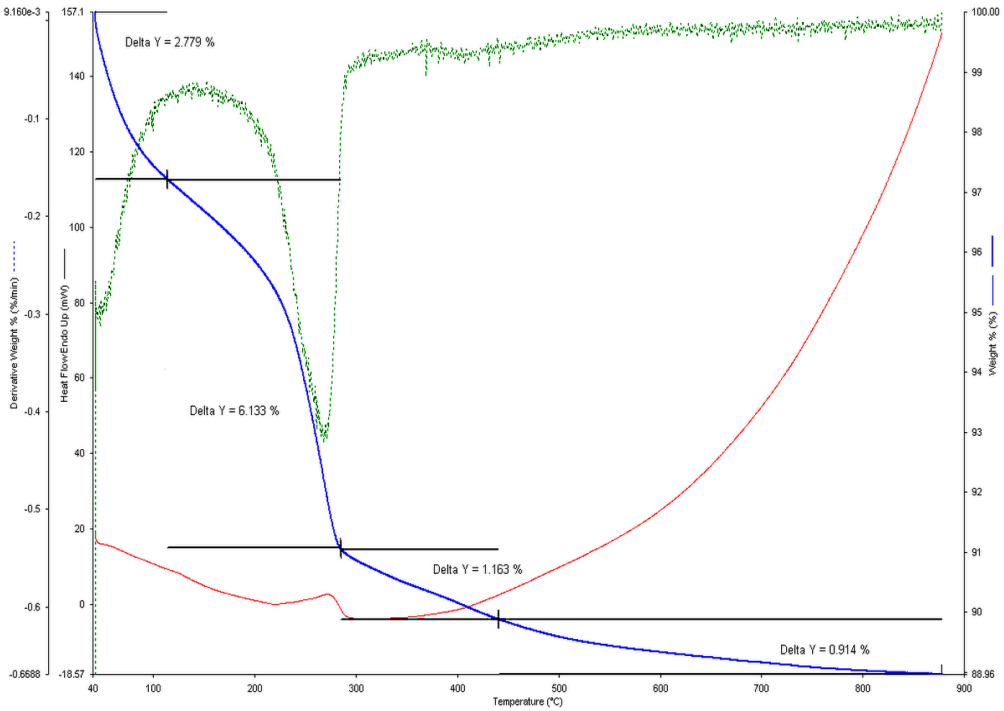

Figure 6.17 Thermogravimetric analysis of uncalcined IZA 238(Fe (OH)3) showing percentage loss of sample with increasing temperature [air 60mL/min, ramp=5°C, 40-900°C]

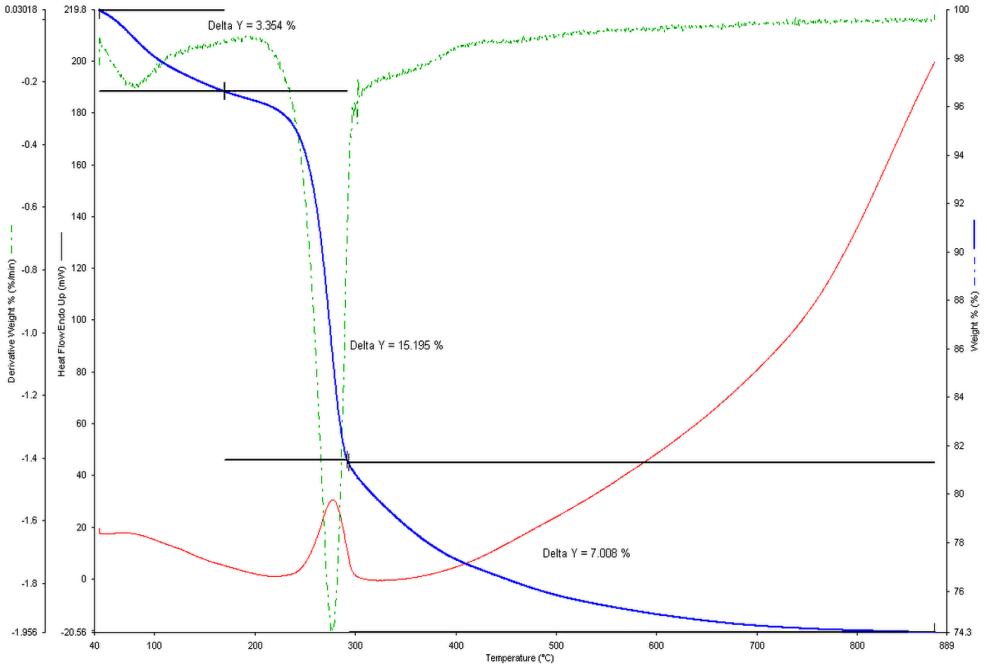

Figure 6.18 Thermogravimetric analysis of uncalcined IZA 239(Ni(OH)2) showing percentage loss of sample with increasing temperature [air 60mL/min, ramp=5°C, 40-900°C]

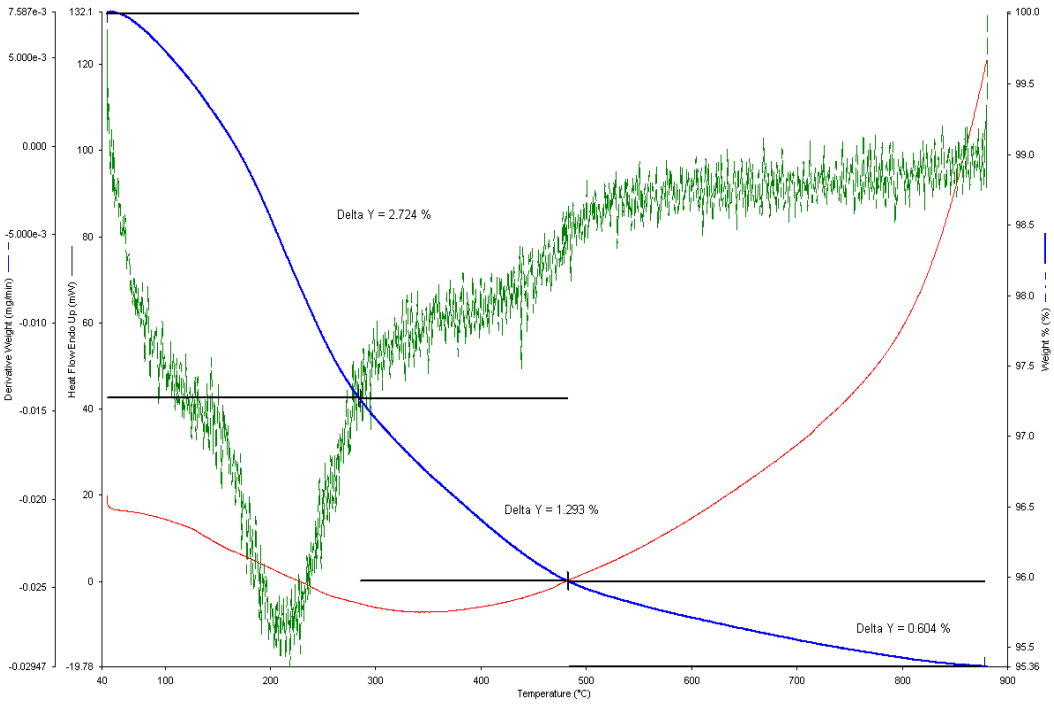

Figure 6.19 Thermogravimetric analysis of uncalcined IZA 240(CuO) showing percentage loss of sample with increasing temperature [air 60mL/min, ramp=5°C, 40-900°C]

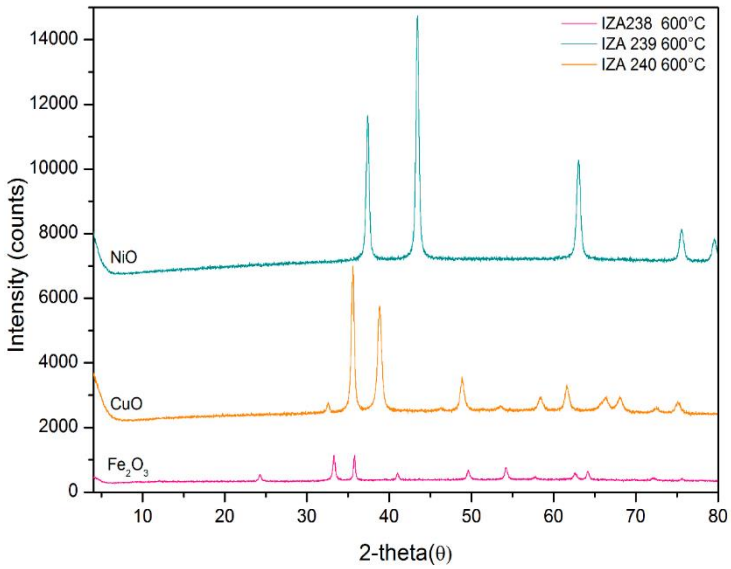

Figure 6.20 Diffractograms of single oxides catalysts at 600°C showing well-crystallized phases

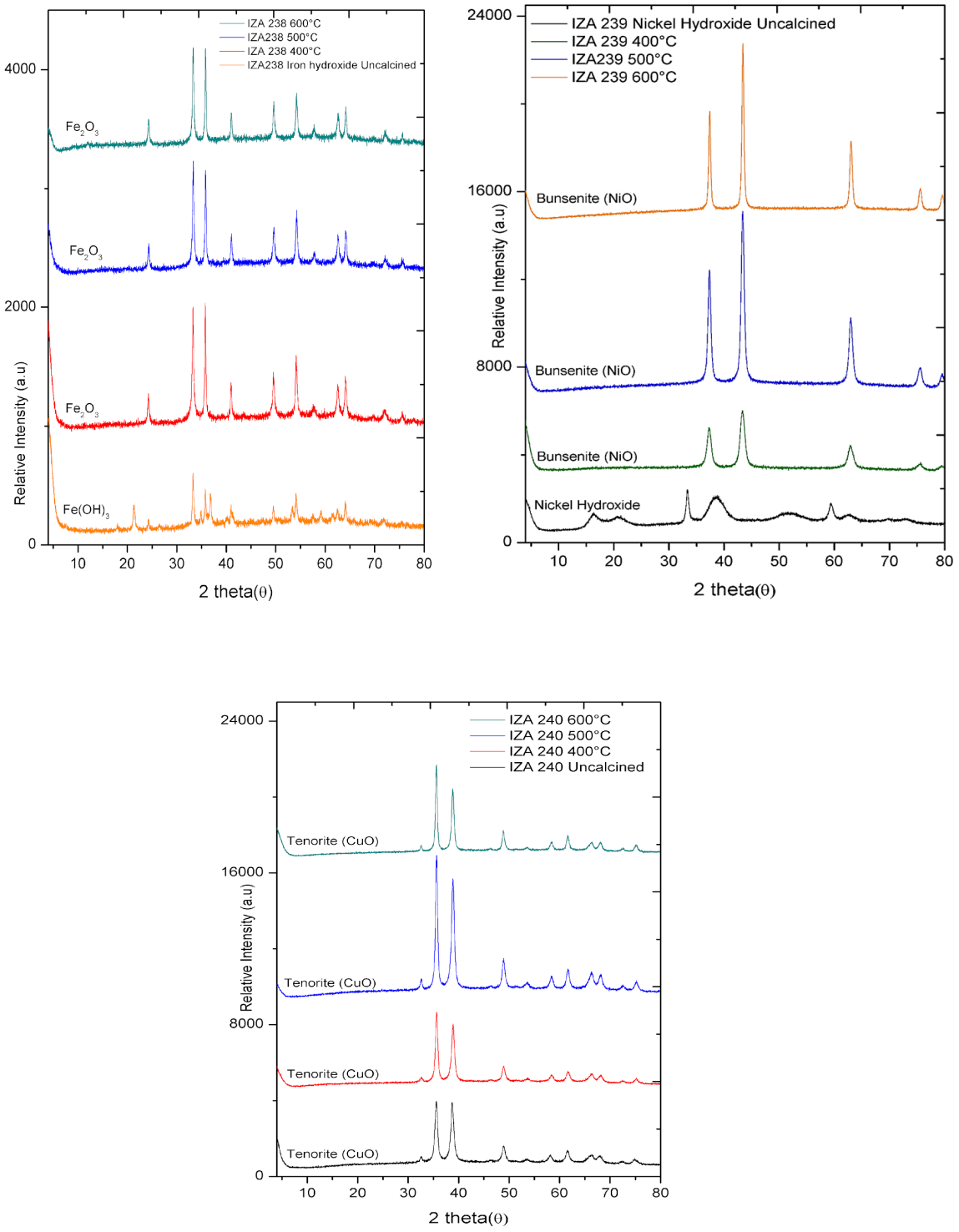

Figure 6.21 Diffractograms of single uncalcined and calcined oxides

Table 6.6 Surface area and Pore volume of single oxides calcined at 600°C

Sample	Calcination Temperature (°C)	Surface area (m^2g^{-1})	Pore volume (cm^3/g)
IZA238-$Fe(OH)_3$	600	38	0.208
IZA 239-$Ni(OH)_2$	600	24	0.141
IZA 240-CuO	600	13	0.04

6.6 Replicas of M-Fe in comparison to M-Al

To study the effect of iron in the prepared catalysts, ore classical analogues were synthesized in the same conditions. IZA 120,($Cu_{0.73}Al_{0.26}$), IZA126 ($Ni_{0.37}Cu_{0.37}Al_{0.25}$) and IZA 127 ($Ni_{0.74}Al_{0.25}$) were the Al analogues od respectively IZA23, IZA 20 and IZA22.

The comparative sample of IZA23 was initially synthesized with aluminium, to determine the structural constraints observed in Cu-Fe system as discussed in chapter 2 and 3. CuO was the only phase present in the system. Though the molar ratio analyzed by EDX well correspond to the syntheses, no indication of Al-containing phase was apparent between the temperature range 400-600°C. M^{3+} (Fe, Al) has always shown a late crystalline phase formation but this effect I especially pronounced when aluminium is used, to lower reactivity of aluminium oxides with comparison with iron oxides. The formation of amorphous alumina significantly contributed to the high surface area of the catalysts. The diffraction pattern and cell parameters have been indicated in the figure 6.28, annex A.10 respectively.

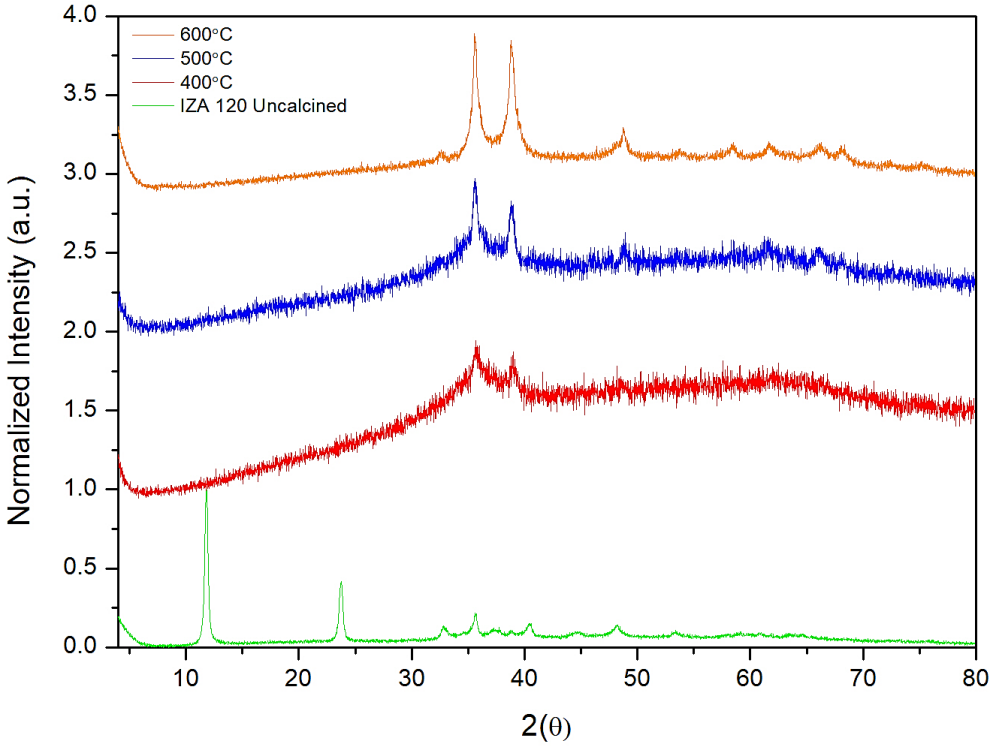

Figure 6.22 IZA120 ($Cu_{0.73}Al_{0.26}$) uncalcined and calcined at different temperatures

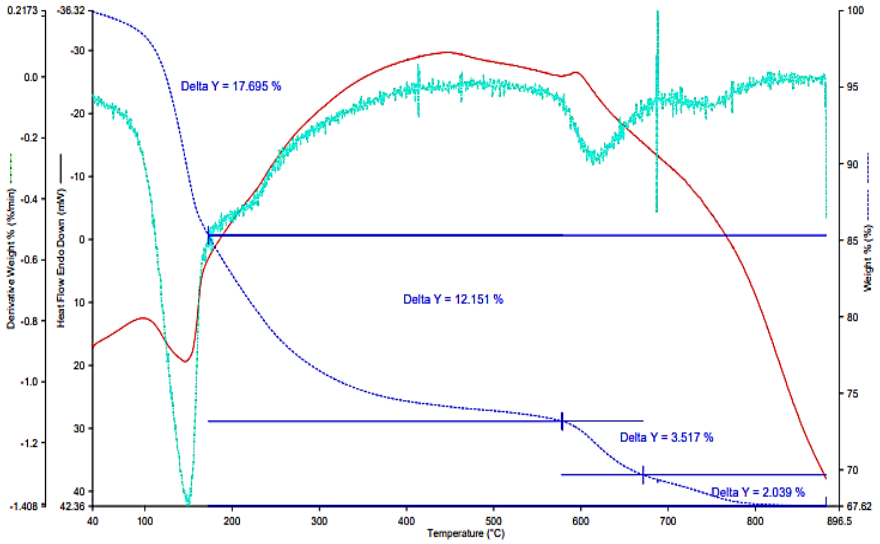

Figure 6.23 TG/DTG profile of IZA 120

Table 6.7 Surface area and Pore volume of single oxides calcined at 600°C

Sample	Composition			Surface area (m^2g^{-1}) at 600°C	Pore volume (cm^3/g)
	Ni	Cu	Al		
IZA 120	-	0.74	0.26	42	0.010
IZA126	0.37	0.37	0.25	121	0.325
IZA 127	0.74	-	0.25	191	0.568

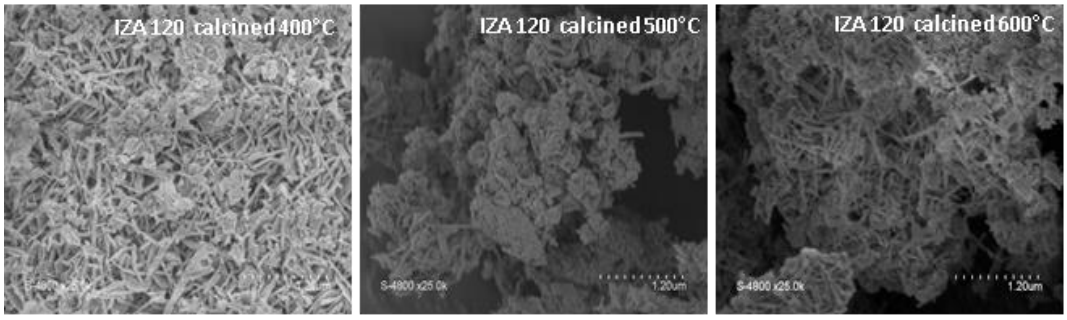

Figure 6.24 SEM images of IZA120 calcined 400°C (a) 500°C (b) and 600°C (c)

6.7 Conclusion

Mixed oxide catalysts are drastically temperature-dependent in terms of crystallinity and cation ratio of the trivalent cation plays a major role in the abundance of phases present. A compromise between temperature of calcination and surface area is important to reach for the catalytic applications of MMO.

As our catalysts are Ni-Fe based oxide, they typically stucked to the poles of the magnetic stirrer, due to magnetic properties that can be extremely useful in the easy separation of the catalyst.

Reference

[1] A. Elhalil, M. Farnane, A. Machrouhi, F.Z.Mahjoubi, R. Elmoubarki, H. Tounsadi, M. Abdennouri, N. Barka, Effect of molar ratio and calcination temperature on the adsorption performance of Zn/Al layered double hydroxide nanoparticles in the removal of pharmaceutical pollutants. JS: AMD. 3 (2018) 188-195.
[2] J. P. erez-Ramirez, G. Mul, F. Kapteijn, J.A. Moulijn A spectroscopic study of the effect of the trivalent cation on the thermal decomposition behaviour of Co-based hydrotalcites. J. Mater. Chem.11, 10 (2001) 2529-2536.
[3] A.V. Radha, G.S. Thomas, P.V. Kamath, C.A. Antonyraj, S. Kannan, Thermal decomposition of Co-Al layered double hydroxide: Identification of precursor to oxide with spinel structure. Bull. Mater. Sci. 33, 3 (2010) 319-324.
[4] S. Kannan, C.S. Swamy Catalytic decomposition of nitrous oxide over calcined cobalt aluminum hydrotalcites. Catal. Today, 53, 4 (1999) 725-737.
[5] F. Gualtieri, Accuracy of XRPD QPA using the combined Rietveld–RIR method. J. Appl. Cryst. 33, 2 (2000) 267-278.
[6] R.J. Hill, J.R. Craig, G.V. Gibbs. Systematics of the Spinel Structure Type. Phys. Chem. Minerals 4, (1979) 317-339.

[7] B. Lavina, G. Salviulo, A. Della Giusta, Cation distribution and structure modelling of spinel solid solutions. Phys. Chem. Minerals 29 (2002) 10-18.

CHAPTER 7

H-Transfer reaction of lignin model molecules over mixed metal oxides catalysts

Chapter Summary:

This chapter deals with the importance of Meerwein–Ponndorf–Verley (MPV) reaction chosen for testing the hydrodeoxygenation of lignin model molecules over mixed oxides catalysts. It summarizes the reaction pathways and choice of catalytic valorisation protocols developed for the employed reaction with interest in improved solvolysis. Several catalytic system containing different single and mixed oxide catalysts were used in the depolymerisation study of lignin model and related molecules at 160-200°C for 0.5-3hours in the presence of different hydrogen-donor solvents (methanol, ethanol**,** Isopropanol**).** The quantitative evaluation of results has also been outlined as yields per reaction type obtained by various types of cleavage occurring in the substrate molecule. The highest selectivity and conversion of 98% was achieved by a ternary Ni-Cu-Fe mixed metal oxide system, in the presence of MeOH at 200°C.

Methods for Reduction of Bio-oil

7.1 Hydrodeoxygenation (HDO)

Hydrodeoxygenation in chemistry is a term titled for the chemical conversion carried out at high H_2 partial pressures (100-200 bar) and high temperature (300-400°C) to remove oxygen primarily in the form of water.[1] Given that bio-oil or biomass-derived molecules are generally highly oxidized compounds, HDO methods are employed with the aim to reduce oxygen content particularly in aromatic hydroxyl and methoxy containing molecules and thus improving the H/C ratio and product heating value.[5]

7.1.1 Meerwein–Ponndorf–Verley (MPV) Reduction Reaction

Though for the reduction processes, catalytic hydrogenation is still a mainstream technique being used.[2] Nonetheless, the Meerwein–Ponndorf–Verley (MPV) reaction in organic chemistry deals with the reduction of ketones and aldehydes to their corresponding alcohols in the presence of alcohol and precious metal catalysts. The use of MPV reaction is advantageous for the reduction of carbonyl compounds due to its high selectivity for C==O double bond thus α,β-unsaturated carbonyl compounds can be selectively reduced leaving C==C bond intact.[8] In addition, a key interest in such methods other than direct hydrogenation is to save process economy and omit risks associated with safety and handling of H_2 gas. MPV reaction offers a practical approach for the chemoselective reduction of bio-oil, in which alcohol serves as an alternative hydrogen source. The reaction takes place with the catalytic transfer of hydrogen from alcohol to the carbonyl carbon [3,4]

7.1.2 Our Depolymerisation Approach

Organsolov pre-treatment is a pulping technique which solubilizes and separates the lignin fraction of the lignocellulosic biomass (lignin+cellulose+hemicelluloses). In this process, lignocellulosic feedstock is treated with aqueous organic solvents at temperatures 140-220°C. The hydrolytic cleavage of α-aryl-ether linkage breaks down the lignin into smaller solvent soluble fragments. Major advantages achieved through the process include a high quality lignin with low sulphate content and cost efficiency in the conversion. In this scenario, we implemented an early stage catalytic conversion on lignin model molecule having the following interests in this strategy: (Fig. 7.1)

1. Hydrogenation of a highest H/C component of lignocellulosic biomass (lignin is~26% phenols) is less challenging.
2. Improved solvolysis of lignocellulosic biomass to obtain selective hydrogenated products in one step from organosolv treated technical lignin at low temperatures.
3. Reduced solubility challenges in the presence of a green solvent.
4. Reasonably effective and economical reactivity could be achieved.

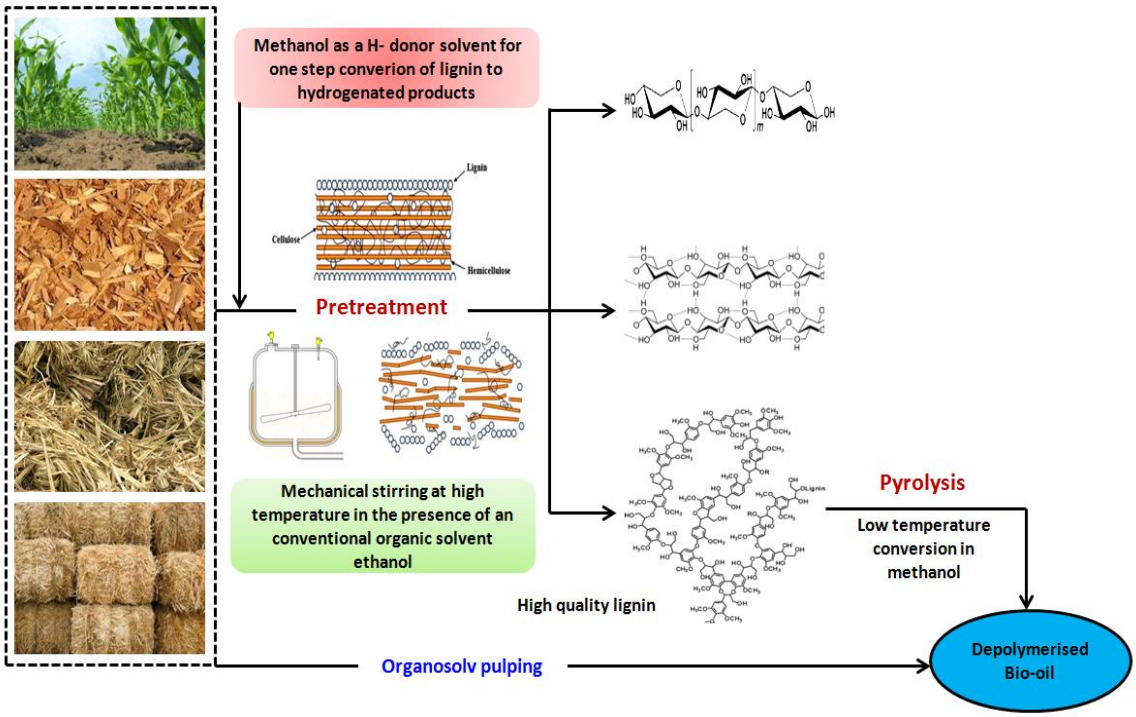

Figure 7.1 H-transfer pre-treatment from lignin for bio-oil

7.1.2.1 Method Development for catalytic test

Solvent: In this method, methanol serves as a H-donor solvent. The choice of methanol was made because its complete oxidation results in CO_2. The substrate molecule 4-(benzyloxy)-3-methoxybenzaldehyde and the products were completely soluble in methanol (>99.8%).

Temperature: The range of temperature (160-200°C) tested is much less severe than typical gas-phase hydrogen transfer reactions[5,6,7] and close to the conditions of organosolv pulping of lignocellulosic biomass. The lower temperature studies carried out assisted in identification of the intermediates and pathways of the reaction under different conditions.

Catalyst: As previously discussed in chapter 2, mixed oxide catalyst are effective and thermally stable enough to bear reactions carried out at elevated temperature.

Also, in this case, Fe in the catalyst, served as magnetic separator. After the reaction, all the catalyst was found attached to the magnetic stirrer and thus purification of the liquid phase was easier.

Autoclave Pressure Calibration: The HDO reactions are sensitive to oxidation at high temperature therefore for the complete removal of atmospheric oxygen from the autoclaves and purging of nitrogen gas, the autoclaves pressures were calibrated prior to begin the catalytic tests. A multipoint calibration method was performed. At room temperature, the pressure of nitrogen gas in all 6 autoclaves in a row was increased (0-15 bar) from the bottle of nitrogen gas fixed with the setup. (Fig. 7.2) The response of the measurement and autoclave control system pressure were noted down to see linearity or any technical fault and in pressure sensors. (Fig. 7.3)

Figure 7.2 Parr 5000 Automated 6-posts Multi Reactor stirrer System

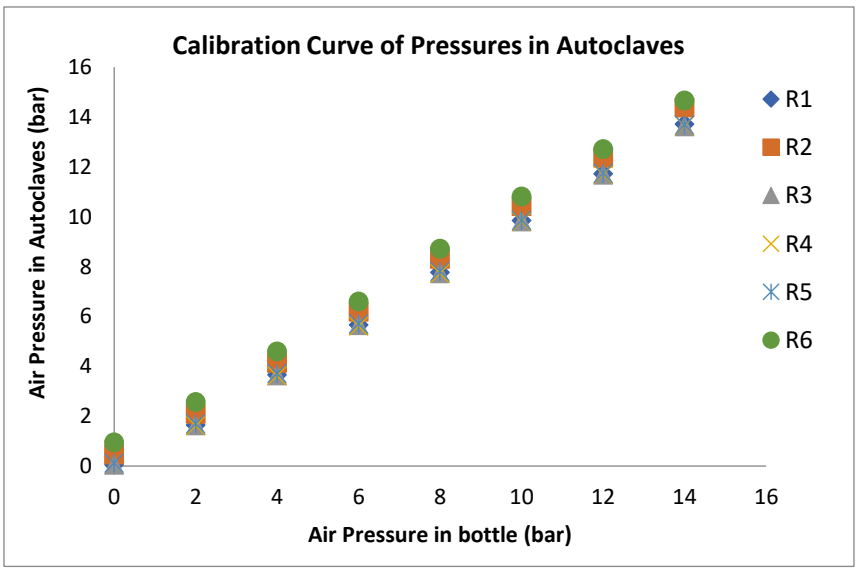

Figure 7.3 Pressure sensor calibration in each reactor/autoclave

The interesting questions to be addressed in the implication of this improved strategy were:

- Can hydrogen-donor solvents of organosolv treatments compete with hydrogenation of biomass by molecular hydrogen?

- Organosolv pre-hydrogenation of biomass can improve the economics of bio-oil production?
- Is the cost of a pretreatment worth the reduction of the hydrogen need for improvement of thermal bio-oil?

7.2 Procedure of the Catalytic Hydrodeoxygenation reaction

The catalytic activity of the catalysts was tested in batch liquid-phase reactors on the α-O-4 model 4-(benzyloxy)-3-methoxybenzaldehyde**.** The reactions were carried out in Parr 5000 automated 6-posts stainless steel 75mL multi reactor system equipped with a magnetic stirrer and thermocouple with pressure sensors. Several preliminary tests were carried out at different temperatures, using different solvents with varying reaction time to for the optimization of reactions.

In a typical experiment, the substrate, 4-(benzyloxy)-3-methoxybenzaldehyde (20mg, 0.082mmoles) was dissolved in 20mL of methanol and 20mg of catalyst was added in the stainless steel reactor. Prior starting the reaction, the autoclaves were flushed multiple times with 10 bar of N_2 gas to remove any air residual. After, at ambient temperature, the autoclave was purged with 5 bar of N_2 and the outlet vale was abruptly closed to maintain the pressure. The reactions were conducted at 160-200°C at heating rate of 2°C/min, for 0.5-3hours with a constant stirring speed of 500rpm. Blank tests were also done in the same conditions. As the reaction halted, the reactor was cooled down to room temperature. The catalyst was found stuck to the magnetic bars in the reactors, still the liquid was poured into the tubes and centrifuged at 1000rpm for 10 minutes at 20°C. The liquid phase was then filtered with syringe filters of 0.20µm mesh size and analyzed by a gas chromatograph–mass spectrometer (GC-MS) gas chromatograph-flame Ionization detector (GC-FID).

7.2.1 Configuration of GC-MS

GC: Column: ZB-5HT Length=15m, thickness=0.10um, diameter=0.25mm; Column oven temperature=40°C; Injection Temperature=250°C; Carrier gas: He, Column flow =1.21mL/min; Total flow =9.3mL/min; Split=5; Total program time=17min. (Table 7.1)

Table 7.3 GC-MS configuration used for the analysis of hydrodeoxygenation products

Method in GC		
Rate (°C/min)	Final Temperature (°C)	Hold time (min)
-	40	0
15	250	3

MS: Ion source Temperature=200°C; Interface Temperature=250°C; Solvent Cut time=1.5min

Method in MS			
Start time (min)	End time (min)	Start (m/z)	End (m/z)
1.5	17	19	750

7.2.2 Configuration of GC-FID

GC-FID: Column: ZB-5HT, Length = 15m, Diameter =0.32mm, Film thickness =0.10µm; Injector Temperature=250°C; Column flow: 1.5mL H_2/min; Split: 50; Detector Temperature: 280°C; Solvent: as in the reaction (no dilution), direct injection of 2uL of sample. (Table 7.2)

Table 7.4 GC-FID configuration used for the analysis of hydrodeoxygenation products

Method in GC-FID			
Temperature (°C)	Rate (°C/min)	Hold time (min)	Total (min)
40	-	1	1
100	8	0	8.5
250	15	7	25.5

7.2.3 Calibration Curve for HDO products

The standard solution of the substrate and some products in different volumes (10-150µL) were prepared. For solid products, the equivalent weight was calculated for each point using the mass/density formula. The standards were run in both GCMS and GCFID using the above mentioned conditions to obtain reliable calibration curve with high R-squared value that were used for the accurate and precise quantification of products corresponding to the peak area in GC-FID and TIC in GC-MS. The response factors of the instruments were duly checked. (Fig 7.4)

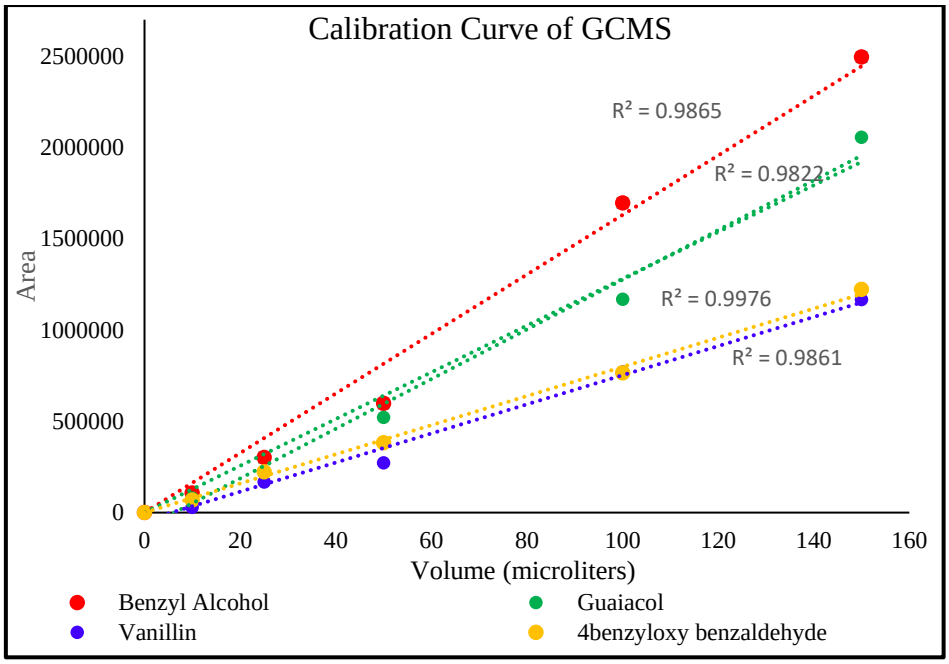

Figure 7.4 Calibration Curve of GCMS for the main products or intermediates of the reaction

7.2.4: Effective Carbon Number (ECN):

The fact that different detectors equipped with GC respond differently to the same compound for instance the MS detector records the response proportional to the fragmentation of the compound and spectral peaks are recorded in volts either by Selected Ion Monitoring (*SIM*) or total ion chromatograph (TIC), however the signals in FID are directly proportional to the number of carbon atoms present in the analyte.[9] Therefore for the meaningful quantitative analysis of the reaction mixture it is inevitable to alternatively correlate the response of these detectors. Calibration curve can be drawn for the compounds with available standards. The peak areas are then feasibly retrieved to estimate the unknown concentration in the reaction mixture and the quantitative analysis is thus very reliable.

As the instrumental response factor (RF) corresponds to the carbon number (CN) in the sample, thus a linear trend between the RF and CN can provide reliable quantification data for compounds that otherwise are unstable or lack the authentic standards.[10]

7.3 Reaction Mechanism

The use as a substrate of model molecules with aldehyde, methoxy and phenylether groups allowed modeling the effects of different catalysts on the reactivity of several functionalities of natural lignin.

If aldehyde functions were easily hydrogenated by a typical MPV mechanism, the breaking of phenylether bonds, mimicking the most frequent β-O-4 bonds of lignin, was only partial and probably followed several pathways. Deeper hydrogenation was observed, possibly due to H_2 issued from methanol reforming, with the formation of hydroxycresol by hydrogenation of C-OH bonds. Traces of guaiacol were sometimes observed, suggesting that also hydrogenation of C-C bonds is possible in our conditions.

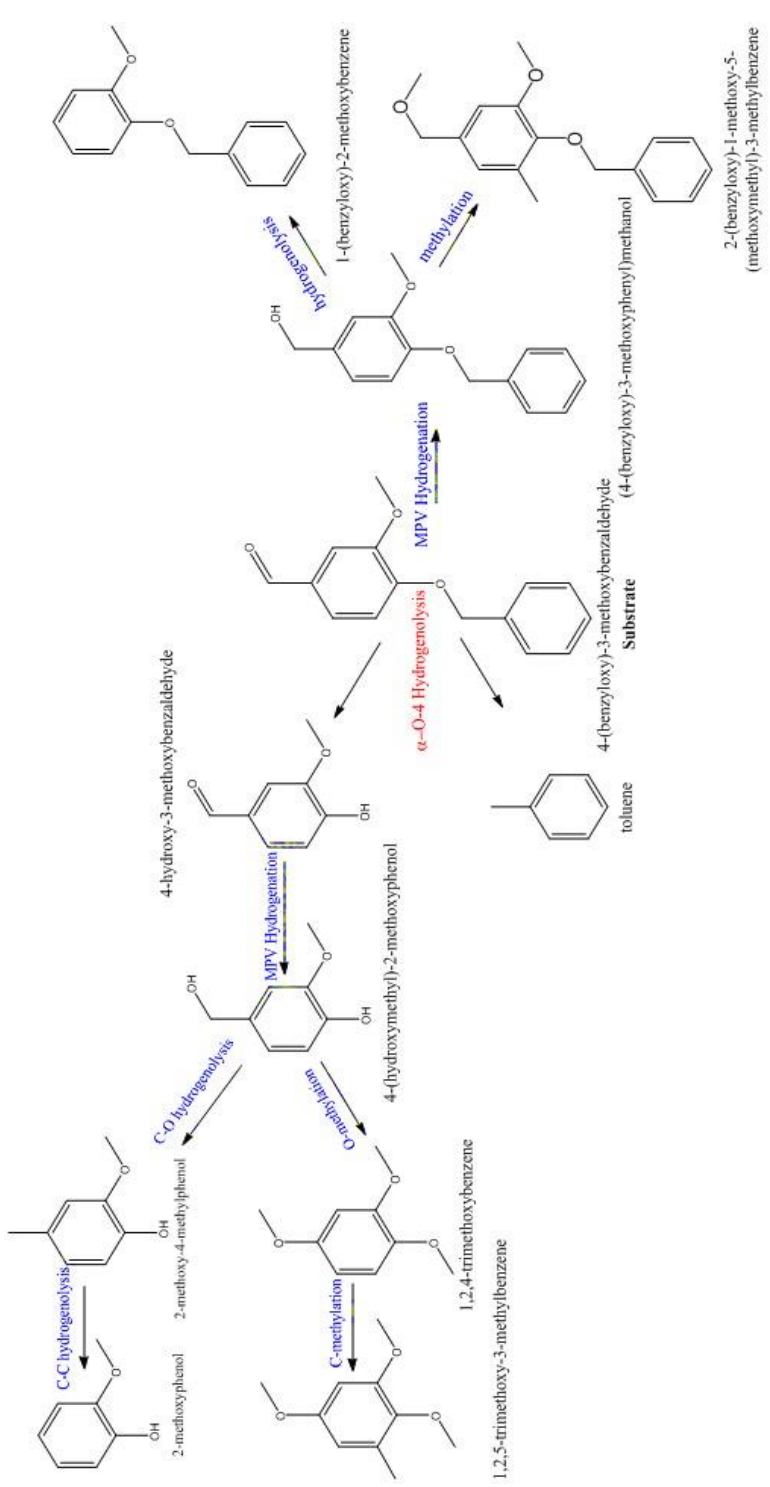

Figure 7.5 Main reaction pathways in the HDO reactionConditions: Solvent: MeOH; T: 200°C; Time: 3h; Stirring: 500rpm; Ni-Cu-Fe oxide catalyst calcined at 600°C

Beyond the hydrogenating activity, a significant factor in the reactivity of the aldehyde group of the model molecule used was the formation of hemiacetals and acetals. Stable cyclic acetals are desirable products of lignin depolymerisation in the presence of glycols.[11] However, acetals and especially hemiacetals of monoalcohols are unstable equilibrium products easily formed from aldehydes in presence of alcohols also at room temperature and without a catalyst.[12] Indeed, a standard 4 mM solution of the substrate at room temperature already presented traces of acetal and, after autoclave heating at 200 °C, 6 % acetals were detected. Due to the unstable nature of these compounds, generally reverting to aldehyde and alcohol upon concentration of the solution, we have not included them in the evaluation of the conversion, considering them as a reservoir of unreacted substrate.

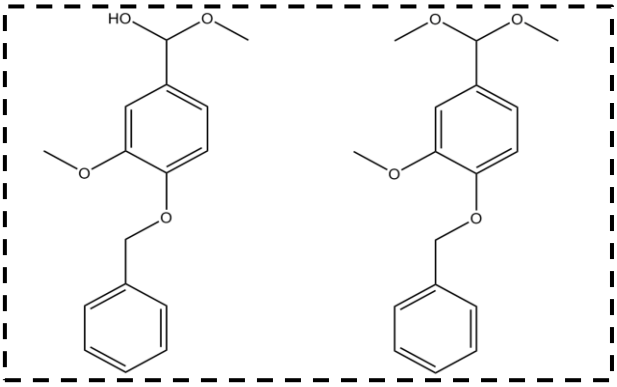

Figure 7.6 Hemiacetal (left) and acetal (right) of the substrate molecuele

7.4 Catalytic tests

Before testing the mixed oxides obtained from LDHs, the reactivity of single-cation oxides was tested (Table 6.6, annex A.10-11). In the standard conditions used (methanol, 200°C, 3 hours) on the IZA238 catalyst, formed of hematite (Fe_2O_3), the hydrogenating activity was limited. Less than 4% substrate was converted and the only measurable products were traces of veratryl alcohol, benzyl alcohol and toluene, none of them reaching 1% yield. Nickel oxide and copper oxide catalysts (respectively IZA239 and IZA240) were both more active than the iron oxide catalyst but oriented the hydrogenation in very different ways. Both catalysts provided nearly 16% yield of hydrogenation products but, in the case of the CuO catalyst, virtually no hydrogenolysis of the α-O-4 bond was observed and the only significant product was the alcohol formed by MPV hydrogenation of the aldehyde group. The benzyloxymethoxybenzyl alcohol was the main product also by reaction on NiO but, in this case, significant amounts of products of hydrogenation of the α-O-4 bond were observed. The

presence of veratryl aldehyde and benzylmethyl ether indicates some etherification activity of methanol.

In the case of the mixed Cu-Ni-Fe oxide catalysts, the conversion was always higher than for the single-component oxides but the reactivity was enormously influenced by the Cu/Ni ratio in the catalyst (Fig. 7.7). The conversion values of nearly 30% for the Ni-Fe catalyst rapidly rose to nearly complete conversion for Cu/divalents ratio of 0.4 or higher. With the increase of the conversion, the mass balance became rapidly unsatisfactory, very likely due to the formation of volatile non-analysed products.

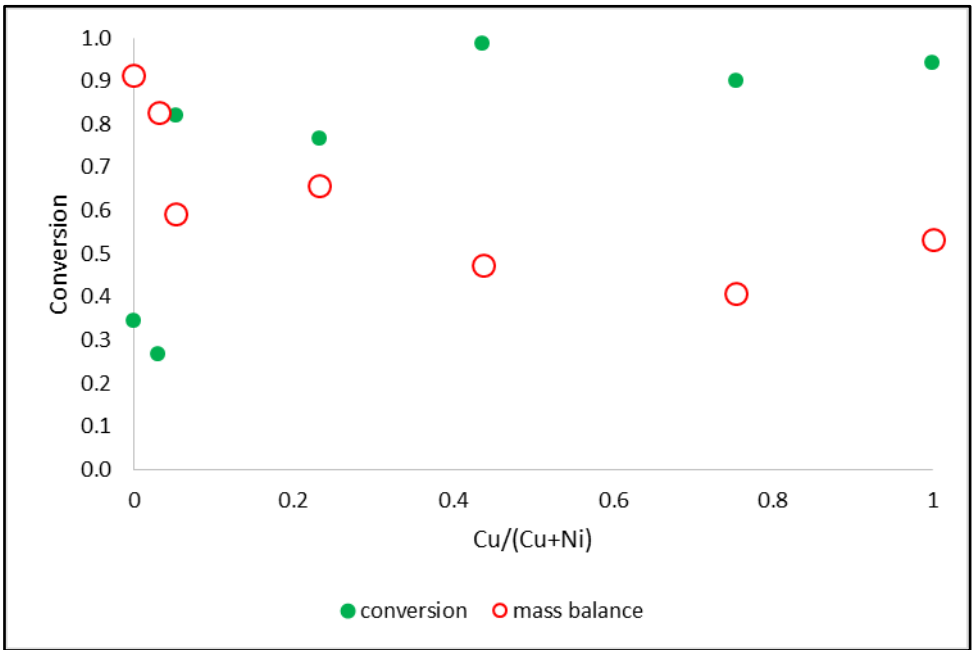

Figure 7.7 Evolution of the conversion (filled symbols) and the mass balance (void symbols) with the copper fraction of the Ni-Cu-Fe catalysts

The evolution of the main products reported in (Fig. 7.8) clearly indicates that deeper hydrogenation is reached at the increase of the copper content. For catalysts with low copper content, the main product is benzyloxymethoxybenzyl alcohol, *viz.* the first MPV hydrogenation product of the substrate. At increasing copper content, the main product becomes benzyloxymethoxybenzene, the product of successive C-O hydrogenolysis of the alcohol group of benzyloxymethoxybenzyl alcohol and C-C hydrogenolysis of the intermediate product. When the Cu/divalent ratio approaches 0.5, the presence of nickel oxide accelerates the α-O-4 hydrogenolysis, as already observed on the single-component oxides, and the main products become methoxycresol and toluene, respectively the C-O and C-C reduction products of the vanillic and benzylic moieties of the parent substrate.

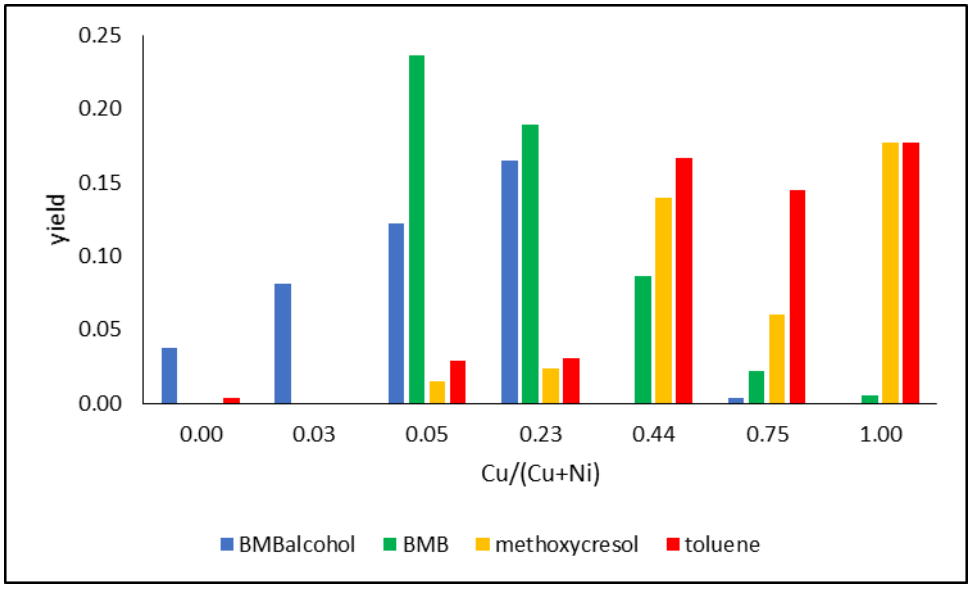

Figure 7.8 Yields of benzyloxymethoxybenzyl alcohol, benzyloxymethoxybenzene, methoxycresol and toluene with the copper fraction of the Ni-Cu-Fe catalysts

The relevance of benzyloxymethoxybenzene among the products clearly indicates that also aliphatic C-C bonds are hydrogenated. This suggests that benzene can be formed as hydrogenation product of toluene. Too short retention time of benzene made its measurement unavailable in our analytical system. No products of hydrogenation of the aromatic ring were observed.

Oxides were prepared by calcination of divalent-aluminium precursors to give hints on the role of iron in H-transfer catalysis. We have already seen that Fe_2O_3 (IZA268) itself is virtually inactive, however its presence affects in some way the activity of the catalysts (see annex table). The Cu-Al catalyst (IZA120) is much more active than the catalyst with CuO alone (IZA240), keeping the same product distribution oriented towards simple initial MPV reaction. This effect could be attributed to the higher surface area of the sample with amorphous alumina, however it is likely that the more important effect is the Scherrer size of CuO crystallite, 39 Å for IZA120 and 53 Å for IZA240. When compared with the Cu-Fe analogue IZA23, the CuO crystallite size (40 Å) is the same than for the Cu-Al catalyst. However, the activity of the Cu-Fe system is significantly higher and the distribution of products indicates a much deeper hydrogenation. It is likely that iron defects in CuO plays a significant role in catalysis.

In the case of the Ni-Al system, the presence of amorphous alumina seems to deactivate the catalyst (IZA127), which is less active than pure NiO (IZA239) and much less active than the

Ni-Fe catalyst (IZA22). Also in this case the promoting effect of iron is patent. More complex is the situation in the case of the mixed Cu-Ni systems in the presence of Al (IZA126) or Fe (IZA247). The conversion is nearly total and the level of hydrogenation is high in both systems but the distribution of products is very different, with the Al-bearing system presenting a less effective hydrogenolysis of α-O-44 bonds. It is likely that, in this case, the manin effect is due to a different distribution of defects between Cu- and Ni-bearing phases.

7.5 Conclusions

Oxides obtained by thermal decomposition of LDH precursors are effective catalysts for H-transfer reactions to lignin model molecules, also in absence of the basic properties induced by Mg^{2+} cations in the most usual catalysts ex hydrotalcites. The catalytic activity strongly depends on the presence of copper in the system but the presence of Ni2+ induces significant variations in the product distribution. The doping of CuO and NiO by iron undoubtedly affects the activity of the catalysts. The relative effectiveness of MPV hydrogenation and hydrogenolysis of phenylether bonds can orient the choice of the catalyst in a lignin organosolv environment towards the obtention of products with different molecular weight and level of functionalisation.

References

[1] M. Saidi, F. Samimi, D. Karimipourfard, T. Nimmanwudipong, B.C. Gates, M. R. Rahimpour, Upgrading of lignin-derived bio-oils by catalytic hydrodeoxygenation. Energy Environ Sci. 7, 1 (2014) 103-129.
[2] Y. Nakagawa, M. Tamura, K. Tomishige, Catalytic reduction of biomass-derived furanic compounds with hydrogen. ACS catalysis, 3, 12 (2013) 2655-2668.
[3] E.D. Williams, K.A. Krieger, A.R. Day, The Mechanism of the Meerwein—Ponndorf—Verley Reaction. A Deuterium Tracer Study. J. Am. Chem. Soc. 75, 10 (1953) 2404-2407.
[4] R.S. Assary, L.A. Curtiss, J.A. Dumesic, Exploring Meerwein–Ponndorf–Verley reduction chemistry for biomass catalysis using a first-principles approach. ACS Catalysis, 3, 12 (2013) 2694-2704.
[5] P.M. Arvela, Y.D. Murzin, Hydrodeoxygenation of Lignin-Derived Phenols: From Fundamental Studies towards Industrial Applications. Catalysts, 7, 9 (2017) 265.
[6] Y. Yunquan, H. Luo, G. Tong, K.J. Smith, C.T. TYE, Hydrodeoxygenation of phenolic model compounds over MoS2 catalysts with different structures. Chin. J. Chem. Eng. 16, 5 (2008) 733-739.
[7] M.M. Ambursa, P. Sudarsanam, L.H. Voon, S.B.A. Hamid, S.K. Bhargava, Bimetallic Cu-Ni catalysts supported on MCM-41 and Ti-MCM-41 porous materials for hydrodeoxygenation of lignin model compound into transportation fuels. Fuel Process Technol, 162 (2017) 87-97.

[8] A. Lolli, Y. Zhang, F. Basile, F. Cavani, S. Albonetti, Beyond H_2: Exploiting H-Transfer Reaction as a Tool for the Catalytic Reduction of Biomass in F. Cavani, S. Albonetti, F. Basile and A. Gandini (eds) Chemicals and Fuels from Bio-Based Building Blocks (2016) 353-378.
[9] The flame ionization detector,J. Chromatogr. Sci., 11 (1973), pp. 251-255
[10] Szulejko, J. E., & Kim, K. H. (2014). Re-evaluation of effective carbon number (ECN) approach to predict response factors of 'compounds lacking authentic standards or surrogates'(CLASS) by thermal desorption analysis with GC–MS. Analytica chimica acta, 851, 14-22.
[11] P.J. Deuss, C.S. Lancefield, A. Narani, J. G. de Vries, N.J. Westwood. K. Barta. Phenolic acetals from lignins of varying compositions via iron(III) triflate catalysed depolymerisation. Green Chem. 19 (2017) 2774-2782.
[12] J. Clayden, N. Greeves, S. Warren. Organic Chemistry, 2nd edition, UOP Oxford (2012) 340-347.

Annexes

Chapter 6-Annex 1: Fractional Crystallization of Oxide Phases

Table A.1: Index of phase percentage and cell parameters obtained by calcination of IZA20 at different temperatures

Sample	Composition	Composition and cell parameters as a function of temperature							
		Calcination temp (°C)	Identified Phases	Phase %	a (Å)	b (Å)	c (Å)	V (Å^3)	β
IZA20	$Ni_{0.37}Cu_{0.38}Fe_{0.25}$	400	NiO	26.29	4.161	-	-	72.07	-
			CuO	2.90	4.685	3.405	5.115	80.46	99.58
		500	NiO	21.76	4.1654	-	-	72.27	-
			CuO	22.40	4.6791	3.4078	5.1198	80.53	99.435
			Spinel Phase	6.43	8.3092	-	-	573.7	-
		600	NiO	32.75	4.1688	-	-	72.45	-
			CuO	53.09	4.6872	3.4032	5.1248	80.66	99.377
			Spinel Phase	14.15	8.3299	-	-	578.0	-
		700	NiO	27.33	4.1705	-	-	72.540	-
			CuO	56.88	4.6908	3.4139	5.1201	80.91	99.335
			Spinel Phase	15.78	8.3338	-	-	578.79	-
		800	NiO	28.24	4.1801	-	-	73.042	-
			CuO	56.46	4.6944	3.4176	5.1320	81.27	99.245
			Spinel Phase	15.28	8.3405	-	-	580.20	-

*Heating ramp = 2°C/min

* Bunsenite (NiO) = Cubic, Tenorite (CuO) = Monoclinic, Spinel= Cubic

Table A.2: Index of phase percentage and cell parameters obtained by calcination of IZA22 at different temperatures

Sample	Composition	Composition and cell parameters as a function of temperature							
		Calcination temp (°C)	Identified Phases	Phase %	a (Å)	b (Å)	c (Å)	V (Å^3)	β
IZA22	$Ni_{0.75}Fe_{0.25}$	400	NiO	32.10	4.1760	-	-	72.83	-
		500	NiO	54.10	4.1730	-	-	72.667	-
		600	NiO	61.27	4.1708	-	-	72.553	-
			Spinel Phase	5.34	8.3433	-	-	580.8	-
		700	NiO	90.80	4.18750	-	-	73.428	-
			Spinel Phase	9.19	8.3505	-	-	582.29	-
		800	NiO	88.00	4.1888	-	-	73.496	-
			Spinel Phase	12.00	8.3582	-	-	583.90	-

* Bunsenite (NiO) = Cubic, Spinel= Cubic

Table A.3: Index of phase percentage and cell parameters obtained by calcination of IZA23 at different temperatures

Sample	Composition	Calcination temp (°C)	Composition and cell parameters as a function of temperature: Identified Phases	Phase %	a (Å)	b (Å)	c (Å)	V (Å^3)	β
IZA23	$Cu_{0.65}Fe_{0.35}$	400	CuO	56.68	4.7278	3.3736	5.1274	80.52	100.086
		500	CuO	68.40	4.7196	3.3981	5.1361	81.17	99.813
		600	CuO	60.62	4.695	3.4127	5.125	80.97	99.525
			Spinel Phase	10.17	8.410	-	-	594.8	-
		700	CuO	54.47	4.6855	3.4130	5.1200	80.756	99.496
			Spinel Phase	8.48	8.422	-	-	597.3	-

* Tenorite (CuO) = Monoclinic, Spinel= Cubic

Table A.4: Index of phase percentage and cell parameters obtained by calcination of IZA24 at different temperatures

Sample	Composition	Calcination temp (°C)	Composition and cell parameters as a function of temperature: Identified Phases	Phase %	a (Å)	b (Å)	c (Å)	V (Å^3)	β
IZA24	$Ni_{0.18}Cu_{0.56}Fe_{0.27}$	400	NiO		4.168	-	-	72.42	-
			CuO	35.44	4.6734	3.4187	5.115	80.61	99.45
		500	NiO	17.54	4.1470	-	-	71.32	-
			CuO	46.40	4.6785	3.4242	5.1306	81.09	99.405
			Spinel Phase	5.25	8.397	-	-	592.0	-
		600	NiO	12.39	4.1783	-	-	72.946	-
			CuO	45.01	4.6943	3.4388	5.1387	81.85	99.361
			Spinel Phase	5.99	8.3415	-	-	580.40	
		700	NiO	10.46	4.1708	-	-	72.552	-
			CuO	56.86	4.6895	3.4295	5.1357	81.497	99.357
			Spinel Phase	6.76	8.3539	-	-	583.01	-

* Bunsenite (NiO) = Cubic, Tenorite (CuO) = Monoclinic, Spinel= Cubic

Table A.5: Index of phase percentage and cell parameters obtained by calcination of IZA42 at different temperatures

Sample	Composition	Composition and cell parameters as a function of temperature							
		Calcination temp (°C)	Identified Phases	Phase %	A (Å)	b (Å)	c (Å)	V (Å^3)	β
IZA42	$Cu_{0.79}Fe_{0.21}$	400	CuO	100	4.6901	3.4233	5.1324	81.27	99.510
		500	CuO	96.31	4.6875	3.4240	5.1295	81.200	99.493
			Fe_2O_3	3.68	5.0452	-	13.706	302.13	-
		600	CuO	89.03	4.6895	3.4263	5.1336	81.355	99.495
			Fe_2O_3	10.96	5.0400	-	13.7581	302.65	-
		700	CuO	87.65	4.6879	3.4248	5.1330	81.281	99.5027
			Spinel Phase	3.6	8.4341	-	-	599.95	-
			Fe_2O_3	8.74	5.0460	-	13.750	303.21	-
		800	CuO	89.10	4.6875	3.4234	5.1310	99.4779	99.4779
			Spinel Phase	8.96	8.396	-	-	591.9	-
			Fe_2O_3	1.93	5.0655	-	13.792	306.47	-

* Tenorite (CuO) = Monoclinic, Spinel= Cubic, Hematite (Fe_2O_3) = Trigonal

Table A.6: Index of phase percentage and cell parameters obtained by calcination of IZA147 at different temperatures

Sample	Composition	Composition and cell parameters as a function of temperature							
		Calcination temp (°C)	Identified Phases	Phase %	a (Å)	b (Å)	c (Å)	V (Å^3)	β
IZA147	$Ni_{0.72}Cu_{0.04}Fe_{0.26}$	300	NiO	100	4.227	-	-	75.53	-
		400	NiO	100	4.1828	-	-	73.18	-
		500	NiO	94.54	4.1767	-	-	72.861	-
			Spinel Phase	5.45	8.413	-	-	595.5	-
		600	NiO	73.72	4.17743	-	-	72.900	-
			Spinel Phase	26.27	8.3446	-	-	581.06	-

* Bunsenite (NiO) = Cubic, Tenorite (CuO) = Monoclinic, Spinel= Cubic

Table A.7: Index of phase percentage and cell parameters obtained by calcination of IZA31 at different temperatures

Sample	Composition	Composition and cell parameters as a function of temperature							
		Calcination temp (°C)	Identified Phases	Phase %	a (Å)	b (Å)	c (Å)	V (Å^3)	β
IZA31	$Cu_{0.47}Fe_{0.53}$	400	CuO	29.08	4.690	3.4202	5.130	81.14	99.542
			Fe_2O_3	70.91	5.25	-	12.8	305.5	-
		500	CuO	71.97	4.6892	3.4197	5.1267	81.11	99.393
			Fe_2O_3	2.24	5.057	-	13.732	304.1	-
			Spinel Phase	25.78	8.3766	-	-	587.8	-
		600	CuO	66.76	4.6892	3.4235	5.1298	81.236	99.446
			Fe_2O_3	18.00	5.0392	-	13.7454	302.28	-
			Spinel Phase	15.23	8.376	-	-	587.6	-

*Hematite (Fe_2O_3) = Trigonal, Tenorite (CuO) = Monoclinic, Spinel= Cubic

Table A.8: Index of phase percentage and cell parameters obtained by calcination of IZA124 at different temperatures

Sample	Composition	Composition and cell parameters as a function of temperature							
		Calcination temp (°C)	Identified Phases	Phase %	a (Å)	b (Å)	c (Å)	V (Å^3)	β
IZA124	$Ni_{0.62}Cu_{0.02}Fe_{0.35}$	400	NiO	100	4.1986	-	-	74.01	-
		500	NiO	100	4.1708	-	-	72.552	-
		600	NiO	82.64	4.1721	-	-	72.62	-
			Spinel Phase	17.35	8.337	-	-	579.5	-
		700	NiO	56.46	4.1775	-	-	72.903	
			Spinel Phase	43.54	8.3605	-	-	584.38	-
		800	NiO	63.85	4.17837	-	-	72.949	-
			Spinel Phase	36.14	8.3428	-	-	580.69	-

*Bunsenite (NiO) = Cubic, Spinel= Cubic

Table A.9 Index of phase percentage and cell parameters obtained by calcination of IZA123 at different temperatures

Sample	Composition	Composition and cell parameters as a function of temperature							
		Calcination temp (°C)	**Identified Phases**	**Phase %**	**a (Å)**	**b (Å)**	**c (Å)**	**V (Å^3)**	**β**
IZA123	$Ni_{0.65}Cu_{0.2}Fe_{0.33}$	300	NiO	100	4.1828	-	-	73.18	-
		400	CuO	100	4.1976	-	-	73.96	-
		500	CuO	9.16	4.766	3.425	5.031	81.04	99.30
			NiO	83.15	4.1788	-	-	72.971	-
			Spinal phase	7.68	8.3291	-	-	577.81	-
		600	CuO	23.86	4.689	3.3954	5.134	80.63	99.48
			NiO	69.83	4.1743	-	-	72.738	-
			Spinel phase	6.30	8.363	-	-	584.9	-
		700	CuO	18.64	4.7014	3.4356	5.1393	81.90	99.382
			NiO	66.28	4.1853	-	-	73.314	-
			Spinel Phase	15.07	8.3548	-	-	583.19	-
		800	CuO	16.53	4.6912	3.4224	5.1293	81.27	99.28
			NiO	68.72	4.1844	-	-	73.263	-
			Spinel Phase	14.73	8.3402	-	-	580.13	-

*Bunsenite (NiO) = Cubic, Tenorite (CuO)=Monoclinic, Spinel= Cubic

Table A.10: Index of phase percentage and cell parameters obtained by calcination of IZA120 at different temperatures

Sample	Composition	Composition and cell parameters as a function of temperature							
		Calcination temp (°C)	**Identified Phases**	**Phase %**	**a (Å)**	**b (Å)**	**c (Å)**	**V (Å^3)**	**β**
IZA120	$Cu_{0.73}Al_{0.26}$	400	CuO	100	5.2144	3.2700	5.4683	91.633	100.6633
		500	CuO	100	4.690	3.420	5.125	81.07	99.56
		600	CuO	100	4.6988	3.4062	5.112	80.65	99.651

*Tenorite (CuO) = Monoclinic

Table A.11: Index of phase percentage and cell parameters obtained by calcination of IZA238 at different temperatures

Sample	Composition	Composition and cell parameters as a function of temperature							
		Calcination temp (°C)	**Identified Phases**	**Phase %**	**a (Å)**	**b (Å)**	**c (Å)**	**V (Å^3)**	**β**
IZA238	$Fe(OH)_3$	400	Fe_2O_3	100	5.0338	-	13.759	301.93	-
		500	Fe_2O_3	100	5.0344	-	13.753	301.87	-
		600	Fe_2O_3	100	5.0342	-	13.749	301.77	-

* Hematite (Fe_2O_3) = Trigonal

Table A.12: Index of phase percentage and cell parameters obtained by calcination of IZA240 at different temperatures

Sample	Composition	Composition and cell parameters as a function of temperature							
		Calcination temp (°C)	**Identified Phases**	**Phase %**	**a (Å)**	**b (Å)**	**c (Å)**	**V (Å^3)**	**β**
IZA240	CuO	400	CuO	100	4.6836	3.4241	5.1285	81.126	99.471
		500	CuO	100	4.6828	3.4274	5.1294	81.206	99.463
		600	CuO	100	4.6844	3.4307	5.1313	81.334	99.501

* Tenorite (CuO) = Monoclinic

List of Scientific Activities and Trainings

CONFERENCES AND SEMINARS:

Oral Communications

- *Effective ways for the depolymerisation of lignin to produce functional aromatic compounds,* Third SINCHEM Winter School, Bologna, Italy (15^{th}-17^{th} Feb, 2016)
- *Catalytic valorisation of lignin model molecules with hydrotalcite-like catalyst.* Third SINCHEM Autumn School, Lyon, France (Nov, 30^{th}- 02^{nd} Dec, 2016)
- *Synthesis of Layered Double Hydroxides (LDHs) precursor catalysts for the depolymerisation of lignin model molecules*, 5th Young Mediterranean Researcher Days, Montpellier, France (12^{th}-13^{th} Oct, 2017)
- *Heterogeneous catalysts for the valorisation of renewable feedstocks by depolymerisation of lignins*, SINCHEM Autumn School Turin, Italy (22^{nd}-24^{nd} Nov, 2017)
- *Practical tips for a better characterization of materials through XRD*, SINCHEM Winter School, Bologna, Italy (15^{th}-16^{th} Feb, 2018)
- *Synthesis and limitations of Cu-Fe based novel Layered Double Hydroxides (LDHs) precursors of catalysts and their application for depolymerisation of lignin and its model molecules,* Catalyst Design: From Molecular to Industrial Level, Moscow, Russia (19^{th}-23^{rd} May, 2018)
- *Copper-bearing layered double hydroxides as precursors of heterogeneous catalyst for the oxidative depolymerisation of lignin models under mild reaction conditions,* 3^{rd} Green and Sustainable Chemistry conference, Berlin, Germany (13th-16^{th} May, 2018)
- *Study of the field of synthesis of Cu-Ni-Fe Lamellar Double Hydroxides and their transformation into mixed oxides for catalytic applications,* 55^{th} Annual Meeting of Clay Mineral Society, Champaign-Urbana, Illinois, USA (11^{th} -14^{th} June, 2018)
- *Relevance of Fe or Al-bearing amorphous oxides in catalysts from thermal decomposition of Cu-Ni-Fe Lamellar Double Hydroxides,* National Congress of the Chemical Society of France-SCF 2018, Montpellier, France (2^{nd}-4^{th} July, 2018)
- *Study of mild reaction conditions for the oxidative depolymerisation of Kraft lignin catalyzed by Cu-bearing Lamellar Double Hydroxide precursors of heterogeneous catalysts*. 7th EuCheMS Chemistry Congress, Liverpool, UK (26^{th} -30^{th} August, 2018)
- *Evaluation of the reduction of hydrogen burden in bio-oil production by hydrogen-transfer pre-treatment of lignin*, 7th International Symposium on Energy from Biomass and Waste, Venice, Italy (15-18^{th} October, 2018)

Poster Communications:

- 2^{nd} EFCATS-CNRS European Summer School on Catalyst Preparation, Vogüe, France (12^{th}-17^{th} June, 2016)
- 4^{th} Tailor Made Fuels from Biomass, Aachen, Germany (21^{st}-23^{rd} June, 2016)

- Green Chemistry Conference, Aachen, Germany (02nd-04th Feb, 2017)
- The International Symposium on Green Chemistry, La Rochelle, France (16th-19th May, 2017)
- 16th International Clay Conference, Granada, Spain (17th-21st July, 2017)
- EUROPACAT, Florence, Italy (27th-31st Aug, 2017)

Attended:

- Third International Conference, Catalysis for Renewable Sources: Fuel, Energy, Chemicals, Catania, Sicily, Italy (6th-11th Sept, 2015)
- French Conference on Catalysis (FC Cat 1), Frejus, France (23rd-27th May, 2016)
- ELITECAT School of Catalysis, CPE Lyon, France (03rd-06th July, 2017)
- PHOTOTRAIN Winter School, UNIBO, Bologna, Italy (12th-14th Feb, 2018)

TRAININGS/FORMATIONS:

- X-ray Diffraction: XRD (Bruker AXS D8 Advance diffractometer) 05th Sep, 2016.
- Thermogravimetry: TG (Perkin Elmer STA 6000/8000) 09th Sep, 2016.
- High Performance Liquid Chromatography: HPLC (Shimadzu UFLC), 07th Dec, 2016.
- Nuclear magnetic resonance spectroscopy: NMR (Bruker 400MHz HD AVANCE III spectrometer), 11th Oct, 2016.
- Gas Chromatography Mass Spectrometery: GCMS (Shimadzu GCMS-QP 2010 Plus), 10th April, 2016.
- Gas Chromatography Flame Ionization Detector: GCFID (Varian 3900), 09th Oct, 2017.
- UV-Visible Spectroscopy Solid state: UV-VIS (Perkin Elmer Lambda 40 UV/Vis Spectrometer) 09th May, 2017.
- N_2 Physiosorption: (Micrometrics Tristar-3000) 12th Sept, 2016.
- Mössbauer Spectroscopy (MBBC-HE0106 Mössbauer He / N_2 Cryostat), 10th April, 2017.
- Matrix Assisted Laser Desorption/Ionization: MALDI-TOF/TOF (Bruker RapifleX mass spectrometer) 02nd June, 2016.
- Autoclave reactor (Parr 5000 Automated 6-posts Multi Reactor stirrer System) 01st October, 2016.

*All trainings were carried out in Ecole Nationale Superieure de Chimie de Montpellier, Montpellier, France under the supervision of trained engineers and technicians (names mentioned on acknowledgment page)

COURSES:

- Materials for catalysis in MaMaSELF-M2, University of Montpellier (2016)
- Crystallography in MaMaSELF-M2, University of Montpellier (2016)
- French Language Course (A1), CIHEAM-IAMM, Montpellier (2017)

PUBLICATIONS:

Book Chapter:

Heterogeneous catalysis as a tool for production of functional aromatic compounds from lignin I.Z. Awan, N. Tanchoux, F. Quignard, S. Albonetti, F. Cavani, F. Di Renzo, in S. Albonetti, S. Perathoner, E. A. Quadrelli (Eds.) Horizons in Sustainable Industrial Chemistry and Catalysis, 178, Edition 1, Elsevier (in press) ISBN: 9780444641274, Chapter 13.